A Thesis entitled

"A STORAGE TUBE FOR THE OBSERVATION OF FAINT IMAGES OF LOW CONTRAST"

by

R.S. Filby, B.Sc., A.R.C.S., A.Inst.P.

Presented for the degree of

Doctor of Philosophy

in the

University of London

April 1967.

Department of Physics,
Imperial College of Science and Technology,
London, S.W.7.

ABSTRACT.

The problem of faint, low-contrast image detection is discussed in general terms. Factors which will determine the effectiveness of image detectors, applied to this problem are considered, and a figure of merit is proposed to enable a ready comparison to be made between various image detectors.

After reviewing image detectors, employing photographic storage media, the author considers, in detail, how charge storage may be exploited as an image detecting technique to achieve optimum results. A critical survey follows of existing charge storage devices and a new storage tube is described. This incorporates a spongy potassium chloride target layer which possesses exceptional gain and insulation properties.

An account of the development, design, construction, and processing of the new tube is given, and a demountable apparatus is described which enables spongy potassium chloride layers to be tested under signal generating conditions. The properties and signal generating mechanisms of the spongy potassium chloride target camera tubes are investigated, so that

the advantages and limitations of the device may be assessed, and suggestions are made for possible further development.

CONTENTS.

(Contents - contd.).

(Contents - contd.). PAGE

(Contents - contd.).

(Contents - contd.). PAGE

(Contents - contd.).

(Contents -- contd.).

(Contents - contd.). PAGE

CHAPTER 1

INTRODUCTION.

The observation of light images involves making a comparison between the numbers of photons arriving from different regions of an object under examination. Measures of the resolution and efficiency of a device, used to detect optical images, will be provided by how small a region on the object may be isolated, and how few photons are necessary for an intelligent observation to be made.

The human eye can claim to be a versatile and sensitive image detector, which compares very favourably with any man made device. Its superiority over other devices has been assessed by Rose[148] who has made a direct comparison between various image detectors for scene brightnesses ranging from 10^{-6} to 10^{4} foot-lamberts. Rose's curves indicate that the eye performs particularly well at low light levels. In order to make such a direct comparison, all the devices considered must be assessed for the same object size, lens diameter, scene brightness, image contrast, and exposure time. The latter must be 0.2 seconds, simce this is approximately the storage time of the eye. This restriction in the length of time for which the eye can integrate a light flux imposes a limiting scene brightness (10^{-7} foot-lamberts) below which the unaided eye is no longer capable of operating. Further limitations of the eye arise from the facts that it is only a qualitive detector, that the eye can only be used in locations, congenial to life, and that no scientifically useful, permanent record is derived from the visual process.

Other image detectors, while appearing to be inferior to the eye when compared under a specified set of conditions at which the eye performs well, may nonetheless prove more useful than the eye for many applications because they are not so severely restricted in the time intervals for which they are capable of integrating an incoming light flux, and because they may be used in environments where human observers cannot be located.

The photographic plate is such a device which has long been a useful tool in the detection of faint images. When exposed to a dim object for a long period, the weak light flux is integrated and stored as developable grains of silver halide. This property of being able to store and integrate incident radiation may be exploited more effectively if the photographic emulsion is used in conjunction with a photoelectric device, since photoelectric detection is much more efficient than direct photography. Much effort has therefore been channelled into combining the photoelectric and photographic processes to the best effect.

After development, the information contained on the photographic plate is readily interpretable by the eye, but if quantitative measurements are required, a detailed photometric study of the plate is necessary.

An alternative method of detecting faint optical images is to use a televison camera, capable of integrating and storing information[109,113]. Such a device is called a storage tube. A television camera has all the advantages afforded by the efficiency of photoelectric detection, while one has the choice of either making direct photometric measurements from the electrical signal generated, or of converting the signal into a picture on a monitor for easy visual interpretation. A further advantage of telemetry over photography is the ability to transmit data by radio. This is of great value in balloon borne astronomy[20,55] and essential in space research[3,27,103,134].

This thesis describes the work done by the author and his collaborators in producing and developing a storage tube which may be used as a photometer, capable of measuring the intensity distribution of low contrast images, e.g. faint stars, superimposed on the sky background, or faint spectral lines, superimposed on a continuum.

CHAPTER 2

PROPERTIES OF IMAGE DETECTORS.

2.1. Cameras used for non-scientific applications.

The function of all image detectors is to convert the intelligence conveyed by a photon flux into a more conveniently observable form. For non-scientific applications, this usually involves presenting to the eye of an observer in a location, remote from the original object, another photon flux which creates the illusion that the original scene is being observed. The reproduced image may take the form of a moving picture displayed on a television monitor or a cinema screen, or it may be in the form of a still photograph, providing a permanent visual record or evidence of an item of interest. The important properties of such image detectors will clearly be those which indicate how successfully the attempted illusion is accomplished. The observer will be satisfied if :-

(a) a picture is presented, containing detail just beyond the resolution capability of the eye.

(b) faithful picture geometry is achieved.

(c) continuous motion is simulated without introducing the sensation of flicker.

(d) the brightness variations in the picture correspond to those present in the original scene.

(e) noise or graininess is unobtrusive.

(f) the picture is presented within an area which can be viewed comfortably, i.e. head movement is not required by a properly located viewer to enable the whole picture to be observed[155].

The degree to which these specifications may be realised depends upon properties of image detectors, considered in greater detail below, resolution, quantum efficiency, storage capacity and picture lag. The limitations of the eye provide a limit, beyond which, further development of the properties of image detectors to be used for entertainment purposes is unnecessary. It is debatable whether the additional sophistication of picture generation to provide colour reproduction, panoramic viewing and stereoscopic vision really adds sufficiently to the entertainment value to fully justify the expense and effort involved.

2.2. Cameras used for scientific applications.

The scientific application of image detectors does not necessarily require that the input information derived from the primary photon flux under examination should be converted into a secondary photon flux to provide a facsimile of the original. Processing of the signal need continue only so far as to enable quantitative measurements to be made. Thus, a negative or the raw video signal from the head amplifier of a pick-up device are often, scientifically more useful than a positive photographic print or a picture displayed on a television monitor.

It follows, too, that the standards of performance demanded for entertainment purposes do not necessarily coincide with the properties required of a device used for a specific scientific application.

In order, therefore, to make an assessment of a scientific measuring instrument, it is desirable to avoid the practice of automatically describing its performance when used under conditions corresponding to entertainment standards. (e.g. for television-type storage tubes, these would be 405 or 625 lines at 25 frames per second). Such standards could be quite irrelevant to the application in view and might represent quite an inefficient use of the instrument in question. A much better guide to the value of a detector to be used as a scientific measuring instrument will be provided by giving the properties of the device when used under conditions which enable optimum performance to be realised.

2.3. Image Information Recording Efficiency, a Figure of Merit for an image detector.

In order to facilitate comparison between image devices, it would be useful if a unique figure of merit could be assigned, which could be quoted when the device is operated with parameters, corresponding to the best performance of which it is capable, i.e. conditions for which the figure of merit is maximized.

It must be emphasised, however, that a single figure of merit cannot uniquely provide a measure of the usefulness of a device since, in practice, one is always dealing with a special rather than with a general application. The application will invariably weight the properties included in any suggested figure of merit. Further, so many and varied are the properties of a complex device like a television camera, that it is difficult to know which properties may be neglected when compiling a figure of merit, e.g. the physical size of a camera and the length of time for which a device is capable of integrating an image are clearly both important properties which are bound to receive consideration for a particular application. However, they are difficult properties to accommodate when making a general assessment.

Having said this, it is clear that a 'figure of merit' will always tend to be an artificial concept, and have little use, other than in making a purely academic comparison between various devices. A well chosen 'figure of merit' may, nonetheless, still serve to embrace a number of properties common to all image detectors and so provide some indication of the relative performance capabilities of various image detecting devices. In order then to make such an academic comparison between devices used as image detectors, let us consider how a figure of merit might be defined.

The quantity of information which a camera is capable of providing in a given time could be taken as a measure of its utility. The ability of a camera to record information may be considered as the number of co-ordinates available to define the image under consideration. Thus, if the image device is capable of providing an output picture which can be sub-divided into 'n' separate, resolvable units of which, each may contain 'h_o' definitely discernible half tones, the information carrying capacity can be represented by the product of $n \times h_o$.

The figure for h_o will, in general, be less than the number of discernible half tones, h_i, inherently present in the input photon flux, which could be discriminated by a perfect detector. A real detector may thus be considered to be inferior to a perfect detector by a factor $\frac{h_o}{h_i}$.

A figure of merit, F, which the author has called the Image Information Recording Efficiency of an image detecting device may thus be defined by:-

$$F = n \frac{h_o}{h_i} \qquad (2.1)$$

n and the factor $\frac{h_o}{h_i}$ are, in general, not mutually independent. To enable a quantitative assessment of the value of F to be made, more precise definitions will be assigned to the concepts of number of resolvable picture elements and to the concept of a definitely discernible difference in half tones. A discussion will then follow on the factors affecting these parameters.

2.4. Resolution and total number of resolvable units.

A common method of specifying resolution is to quote the finest detail a system can resolve. Such a specification, while useful, cannot completely represent the ability of a device to portray detail[145]. The value of a single figure to represent resolution serves to do little more than to provide a memorable number which may be associated with a particular detector to enable a rough comparison to be made with kindred devices.

Resolution should not be considered as an independent property of a system, divorced from the concept of perceptible contrast differences. If the performance of a device is limited by the scarcity of input photon information, the ability to perceive given contrast differences may often be maintained at the expense of resolvable detail[148]. If adequate input photon information is available, the ability of a device to discriminate detail may be expressed in terms of the output picture contrast produced by a fully modulated input picture of a spatial frequency corresponding to the detail in question. Thus, the modulation transfer response characteristic provides one of the best representations of the overall resolution properties of an image detector. This is the image modulation, produced by a square wave light pattern, plotted as a function of image detail when the detector is used under conditions of optimum light level.

The modulation, M_m, may be defined by:-

$$M_m = \frac{I_{max} - I_{min}}{I_{max} + I_{min}} \qquad (2.2)$$

where I_{max} and I_{min} are the signal levels or intensities of the image in the regions corresponding to the whites and blacks of the original object. This definition which gives the modulation as the signal amplitude, expressed as a fraction of the mean signal level is based on Michelson's definition of the visibility of optical fringe patterns[39].

Image detail may be expressed in terms of line pairs per mm., but a convenient method of describing the resolution of a pick-up tube is in terms of the equivalent number of television lines. If the resolution is quoted as 'm' television lines, 'm' represents the number of horizontal scanning lines which correspond to the same detail as that observed along the direction of a scanning line, i.e. if the picture in a system of aspect ratio (width/height) A_r may be sub-divided into p units of perceptible detail across the frame, the resolution expressed as 'm' television lines will be given by :-

$$m = \frac{p}{A_r} \qquad (2.3)$$

Thus, if we consider systems in which the number of scanning lines actually used is the same as the value of m, given by Eqn.(2.3), the total number of separable picture elements will be given by:-

$$n = mp.$$

$$\therefore n = A_r m^2. \qquad (2.4)$$

A_r will usually take the value $\frac{4}{3}$, since an aspect ratio of television picture height to width to diagonal, originally chosen as 3 : 4 : 5 for entertainment purposes, has become an almost universally accepted constant in television-type pick-up tubes.

2.5. Minimum detectable contrast, and the number of discernible half-tones, inherent in a primary photon flux.

(a) Criterion for defining discernible differences in brightness.

Having specified a definite picture element, the image detecting process may be regarded as estimating the number of photons, falling on to a given picture element, and comparising this with the numbers of photons, estimated to pertain to neighbouring picture elements. Distinct differences in half-tone may be discerned when significantly different numbers of photons are counted in neighbouring picture elements. The criterion by which a significant difference is judged to exist between the relevant numbers of photons, requires that this difference should exceed the r.m.s. random noise fluctuations present by a factor, known as the coefficient of certainty, K_c.

Thus, if the mean number of photons observed to fall on one picture element in an exposure time T_e is $\overline{P}_1$, with a root mean square fluctuation, $\overline{\Delta P}_1$ and the mean number falling on a neighbouring element in the same time is $\overline{P}_2$, with a root mean square fluctuation of $\overline{\Delta P}_2$, then these picture elements may be perceived as separate half tones if

$$|\overline{P}_1 - \overline{P}_2| \geq K_c \sqrt{\overline{\Delta P}_1^2 + \overline{\Delta P}_2^2}$$

For just discernible differences, $P_1 \approx P_2$, so that $\overline{\Delta P}_1^2 \approx \overline{\Delta P}_2^2$. Hence

$$|\overline{P_1} - \overline{P_2}| \geq \sqrt{2}\, K_c \overline{\Delta P} \qquad (2.5)$$

(b) Minimum detectable contrast.

A particular problem, involving the discernment of small differences in half-tone is that of observing a faint object against a relatively strong background. If the numbers of photons, seen to arrive at an array of picture elements during a period of observation, fluctuate in a random fashion about a mean, $\overline{P}$, with a root mean square deviation, $\overline{\Delta P}$, and if the total number of photons, arriving during this period on a single picture element, observed as a highlight in the array, is P', then the contrast of that highlight against the background is defined as

$$C = \frac{P' - \overline{P}}{\overline{P}} \qquad (2.6)$$

P' is considered to be significantly different from the background if

$$P' - \overline{P} \geq K_c \overline{\Delta P} \qquad (2.7)$$

This is similar to the test applied to define discernible brightness differences in two neighbouring picture elements (Eqn.2.5).

This criterion for deciding whether or not an observation deviates significantly from the mean of a series of readings is encountered in textbooks dealing with the assessment of measurements, subject to random errors. Braddick[22] has provided a table for measurements whose fluctuations follow a Gaussian distribution, from which may be read the probability for the occurrence of an error in the measurement of P', exceeding $K_c\overline{\Delta P}$, for various values of K_c. A suitable value to assign to the coefficient of certainty, K_c, in problems involving the detection of optical images is 5[149].

Eqns. (2.6) and (2.7) yield for the least detectable contrast, C^i_{min}, inherently discernible in an image whose picture elements include a mean number of photons per picture element, equal to $\overline{P}$:-

$$C^i_{min} = \frac{K_c \overline{\Delta P}}{\overline{P}} \qquad (2.8)$$

$$\therefore \quad C^i_{min} = \frac{K_c}{(S_i / N_i)} \qquad (2.9)$$

where (S_i/N_i) is the signal to noise ratio in the input photon flux.

It is convenient at this stage to introduce the concept of an ideal detector of images. This is a hypothetical image detector, in which every photon is unequivocally detected. Thus, unlike a real detector of images, discussed below (§ 2.6), in which the statistical fluctuations of observed events are degraded during processing, a perfect detector of images would yield a value for $\overline{\Delta P}$, equal to the root mean square fluctuation, inherent in the primary photon flux. The fact that these photons occur randomly in time leads to the conclusion that the distribution of the number of photons, arriving in consecutive time intervals of specified duration,is Poissonian[104]. This enables us to write :-

$$\overline{\Delta P} = \sqrt{\overline{P}} \tag{2.10}$$

Hence, Eqn. (2.7) becomes

$$C'_{min} = \frac{K_c}{\sqrt{\overline{P}}} \tag{2.11}$$

This is a fundamental limit, and represents the ultimate in the detection of perceptible contrast differences. From this, it follows that the larger the value of $\overline{P}$, i.e. the greater the capacity of the postulated ideal detector to accept photon information, the smaller will be the minimum detectable contrast.

The condition necessary for a highlight to be just perceptible against background picture elements is illustrated diagrammatically in Fig.2.1.

(c) Number of discernible half-tones.

To the number of photons, P, which may be observed in a picture element, let us assign a suffix h to represent the number of discernible half-tones which this input photon flux is inherently capable of accommodating. Then if P_{h_i} is the maximum number of photons which may be observed per picture element, h_i will be the maximum number of discernible half-tone steps which may be accommodated. h_i may be ascertained by determining the number of times it is necessary to subtract the successively decreasing value of $\sqrt{2}\ K_c\ \overline{\Delta P}_h$ (given in Eqn.2.5 as the least detectable brightness difference) from P_h, starting at P_{h_i}, and continuing to P_1, the ultimate number of photons which can be detected in isolation.

FIG 2.1 MINIMUM DETECTABLE CONTRAST

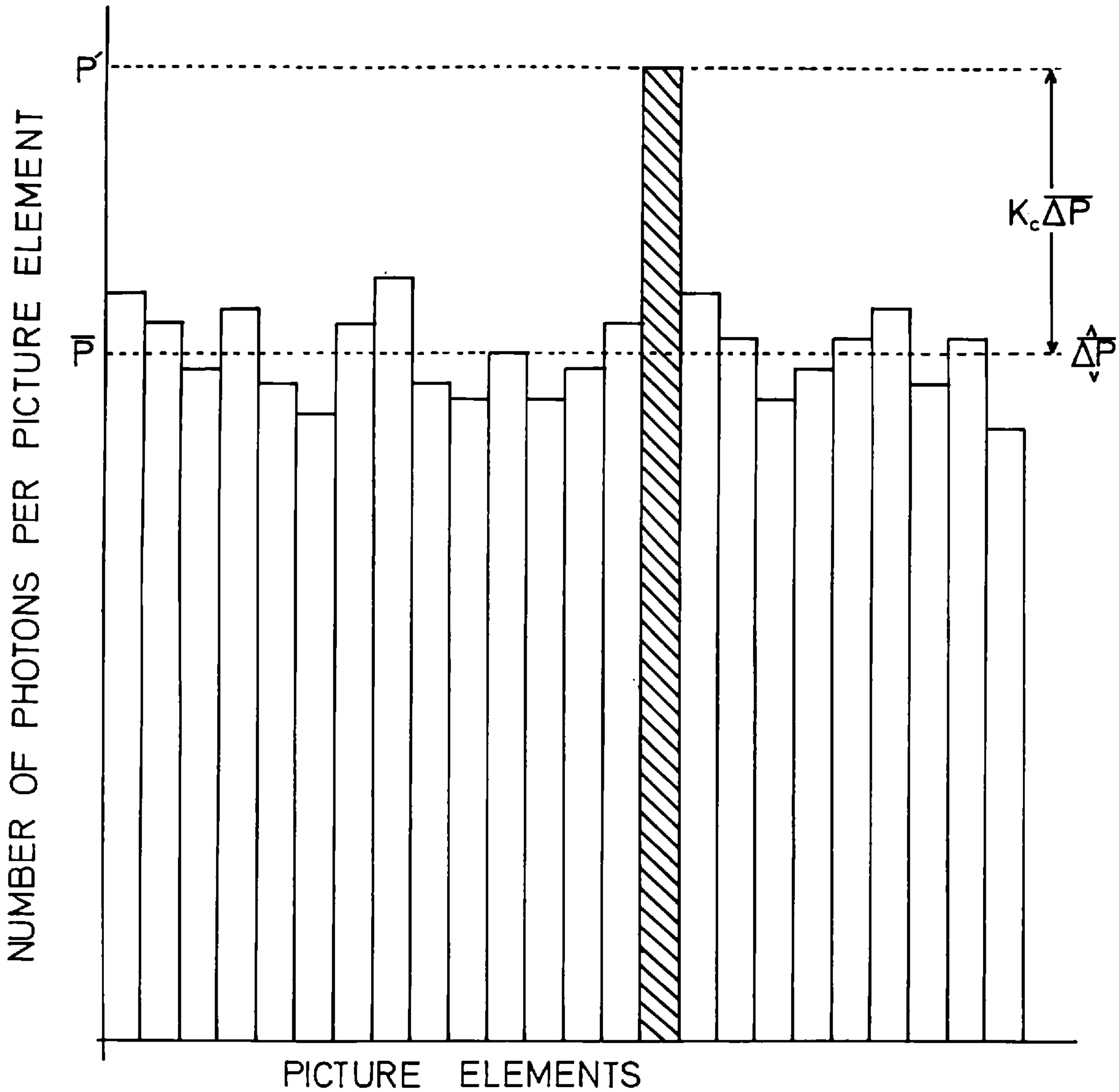

IF $P' - \overline{P} \geq K_c\overline{\Delta P}$, A PICTURE ELEMENT IN WHICH P′ PHOTONS HAVE BEEN OBSERVED BY A PERFECT DETECTOR OF IMAGES IS CONSIDERED TO BE SIGNIFICANTLY DIFFERENT FROM THE NEIGHBOURING PICTURE ELEMENTS. THUS THE CONTRAST OF THE HIGHLIGHT, REPRESENTED BY THE SHADED AREA, AGAINST BACKGROUND IS SAID TO BE JUST DETECTABLE.

The criterion for a discernible difference in the brightness of two picture elements given in Eqn. 2·5 holds strictly, only for large values of P_{h_i}, where the approximation

$$\overline{\Delta P}^2_{h_i} \approx \overline{\Delta P}^2_{(h_i-1)} = \overline{\Delta P}^2 \quad \text{(say)}$$

may be made. This condition no longer applies for small values of P_{h_i}. In the analysis on page 31, a definite half-tone difference in two picture elements has been assessed by using the value of $\overline{\Delta P}$ $(=\sqrt{\overline{P}})$ which corresponds to the fluctuation in the brighter picture element, providing a rather stricter criterion for definitely discernible brightness differences at low light levels, than that given by the equation at the foot of page 25.

This process of successive subtractions is illustrated diagrammatically in Fig.2.2, but may be treated analytically as follows.

From Eqn.(2.5),

$$P_{h_i} - P_{(h_i-1)} = \sqrt{2}\,K_c\sqrt{P_{h_i}}$$

$$\delta P_{h_i} = \sqrt{2}\,K_c\sqrt{P_{h_i}}$$

$$\frac{\delta P_{h_i}}{\sqrt{P_{h_i}}} = \sqrt{2}\,K_c$$

Similarly

$$\frac{\delta P_{(h_i-1)}}{\sqrt{P_{(h_i-1)}}} = \sqrt{2}\,K_c$$

$$\sum_{n=0}^{h_i}\frac{\delta P_n}{\sqrt{P_n}} = h_i\sqrt{2}\,K_c$$

$$\int_0^{P_{h_i}}\frac{dP}{\sqrt{P}} = h_i\sqrt{2}\,K_c$$

$$h_i = \frac{1}{\sqrt{2}K_c}\int_0^{P_{h_i}}\frac{dP}{\sqrt{P}}$$

$$= \frac{2\sqrt{P_{h_i}}}{\sqrt{2}\;K_c}$$

$$h_i = \frac{\sqrt{2}}{K_c}\left[\frac{S_i}{N_i}\right] \qquad (2.12)$$

FIG. 2.2 NUMBER OF DISCERNIBLE HALF-TONES

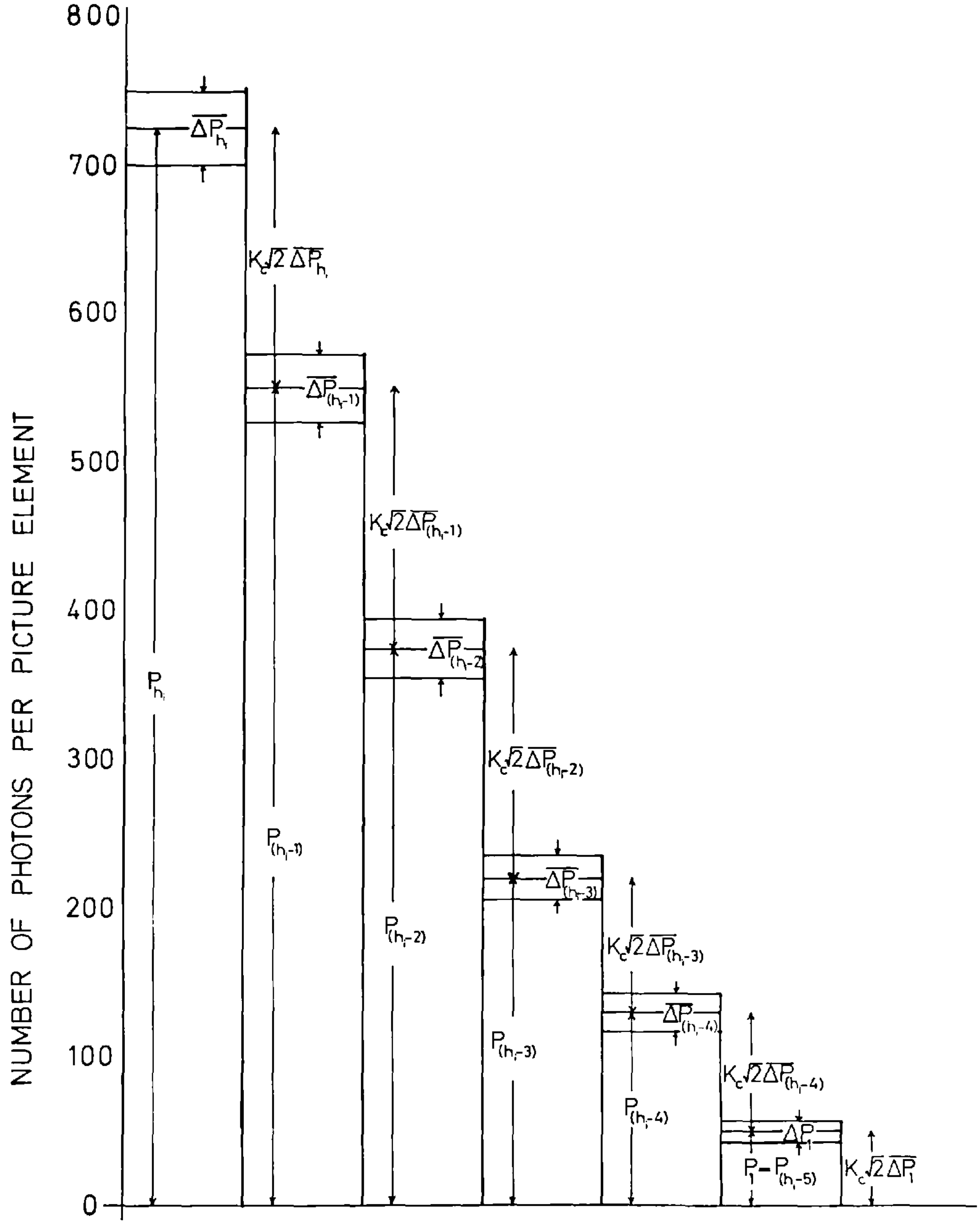

THE DIAGRAM ILLUSTRATES THE NUMBER OF DEFINITELY DISCERNIBLE HALF-TONES, h_i, THAT MAY BE PERCEIVED BY A PERFECT DETECTOR OF IMAGES, CAPABLE OF STORING UP TO P_{h_i} PHOTONS PER PICTURE ELEMENT. THE NUMBER OF PHOTONS OBSERVED IN SUCCESSIVE PICTURE ELEMENTS DIFFER BY $K_c\sqrt{2}\,\overline{\Delta P}$, CONSTITUTING A HALF-TONE DIFFERENCE THAT IS SAID TO BE JUST DISCERNIBLE.

FOR $P_{h_i} = 725$ AND USING $\overline{\Delta P}_{h_i} = \sqrt{P_{h_i}}$ & $K_c = 5$, $\underline{h_i = 6}$

2.6. Minimum detectable contrast and number of half-tones, discernible in an image after the input photon flux has been processed by a real image detector.

(a) Observation of photons as 'stored events'.

When the P photons per picture element of a primary image are processed by an image detector, they are usually converted into static form where they may be observed as 'q stored events'. These may be developed grains on a photographic plate, or electron charges, stored on an insulating target.

The measurement of q will be subject to an error $\overline{\Delta q}$, where $\overline{\Delta q}$ is equal to the root mean square fluctuation in the number of events observed to be stored per picture point.

(b) Minimum detectable contrast.

The minimum contrast, C^{o}_{min}, which may be perceived by means of a device, capable of storing up to q events per picture element may be calculated by the same method as that used to determine the minimum detectable contrast, inherently discernible in the input photon flux. §2.5 (b).

$$C^{o}_{min} = \frac{K_c \overline{\Delta q}}{q} \qquad (2.13)$$

$$C^{o}_{min} = \frac{K_c \overline{\Delta q}}{(S_o / N_o)} \qquad (2.14)$$

where (S_o/N_o) is the signal to noise ratio at the output. In all real detectors, the signal to noise ratio present initially in the input photon flux will be degraded through processing. The expressions for minimum detectable contrast given in Eqns.(2.8) and (2.9) therefore lead to the expected conclusion that:-

$$C^{o}_{min} > C^{i}_{min} \qquad (2.15)$$

(c) Number of discernible half-tones.

The maximum number of events which may be stored by an image detector is known as its total storage capacity, Q. It is also convenient to define an elemental storage capacity, namely, the maximum number of events which may be stored within a picture element. Now if the charge stored in a picture element is written as q_h, where h represents the number of distinct half-tones which may be accommodated by this quantity of charge, then, using this notation, the elemental storage capacity will be represented by q_{h_o}. h_o represents the maximum number of half-tones which can be discerned in the output signal for a particular device, for a specified picture element. (§ 2.3).

From the definition of n, given in § 2.3, we may relate Q and q_{h_o} by :-

$$Q = nq_{h_o} \qquad (2.16)$$

h_o is associated with a property of the image detector, known as its dynamic range, and may be estimated in an analogous way to that by which h_i was calculated, i.e. by determining the number of successive subtractions of $\sqrt{2}\,K_c\,\overline{\Delta q}$ which may be made from q_h.

Whereas this process was straightforward in the case of primary photons, where the mean square fluctuation in the photons was simply related to the total number of photons, it cannot be so readily applied to the general image detecting device. The calculation of the fluctuations encountered in q is discussed in detail below in §s 5.4–5.10 and in appendices A.2, A.3, A.4 and A.5. It may generally be expressed in the form :-

$$\overline{\Delta^2 q} = \overline{N_n^2} + F_1(\overline{g_P}, \overline{\Delta^2 P}) + F_2(\overline{P}, \overline{\Delta^2 g_P}) \qquad (2.17)$$

where $\overline{N_n^2}$ = mean square background noise of the detector expressed in terms of an equivalent No. of stored static events per picture element.

$\overline{P}$ = mean number of photons being detected per picture element.

$\overline{\Delta^2 P}$ = mean square fluctuation in P.

$\overline{g_p}$ = mean factor by which $\overline{P}$ is multiplied in the process of storing the photon flux as $\overline{q}$ static events.

$\overline{\Delta^2 g_p}$ = mean square fluctuation in g_p.

While Eqn.(2.17) in its general form is cumbersome to deal with, there are many image detectors for which the constant background noise of the detector predominates, and the expression for the mean square fluctuation in q reduces to :-

$$\overline{\Delta^2 q} = \overline{N_n^2} \qquad (2.18)$$

This means that the root-mean square fluctuation in the number of stored events per picture element is a constant and independent of q_h. The total number of discernible half tones in the output, h_o, will therefore be given by :-

$$h_o \sqrt{2}\, K_c \overline{\Delta q} = q_{h_o} \qquad (2.19)$$

$$h_o = \frac{q_{h_o}}{\sqrt{2}\, K_c \overline{\Delta q}}$$

$$h_o = \frac{1}{\sqrt{2}\, K_c} \left[\frac{S_o}{N_o} \right] \qquad (2.20)$$

Bearing in mind that, while this result holds for many devices, it is not universally true, the author will proceed to use Eqns.(2.12) and (2.20) to express a relationship between h_i and h_o in terms of a concept which finds considerable application in the field of image detection, namely that of equivalent quantum efficiency.

2.7. The equivalent quantum efficiency of an image detector.

The concept of quantum efficiency is much used in describing processes involving interactions of fundamental particles. Quantum efficiency may be defined as the probability that an input quantum should produce a secondary output quantum in a specified interaction. In the specialised field of photo-electronics, the most important direct application of this concept occurs in the interaction of primary photons at a photo-cathode to release free electrons. From the definition, it follows that P input photons, falling on a cathode of quantum efficiency σ will produce n_e output electrons, given by

$$n_e = \sigma P \qquad (2.21)$$

For a photocathode interaction, where it may be assumed that there is zero probability of more than one electron being emitted by an incident photon, it may be readily shown that the photo-electrons obey a Poissonian distribution as do the primary photons. (See appendix A.2). Therefore, if S_i/N_i and S_o/N_o represent the signal to noise ratios in the input photon and output electron fluxes respectively, we may write :-

$$S_i/N_i = \sqrt{P} \tag{2.22}$$

$$S_o/N_o = \sqrt{n_e} \tag{2.23}$$

These equations, together with Eqn.(2.21), enable us to write as an expression for quantum efficiency

$$\sigma = \left[\frac{S_o/N_o}{S_i/N_i}\right]^2 \tag{2.24}$$

This indicates that the quantum efficiency, σ, may be regarded as representing the factor by which the signal to noise ratio, inherent in the input photon flux, is degraded through the interaction occurring at the photocathode. Hence Rose[147, 148], Fellget [52,53], and Jones[78] evolved a concept of 'equivalent quantum efficiency', which could be applied to a general image detector, where the complete processing of the primary photoelectrons involved many more stages than the single interaction for which quantum efficiency, σ, was originally defined. (see Eqn.(2.21)). The equivalent quantum efficiency, E, of a complex image detector, in which the complete processing of an input photon flux of inherent signal to noise ratio S_i/N_i, gives rise to an output with a signal to noise ratio of S_o/N_o, is defined by an equation analogous to Eqn.(2.24) : -

$$E = \left[\frac{S_o/N_o}{S_i/N_i}\right]^2 \qquad (2.25)$$

Equations (2.22) and (2.25) show that E may be regarded as the reciprocal of the factor by which it is necessary to increase an input photon flux which could produce a signal to noise ratio of S_i/N_i in the output of a perfect detector, in order to produce the same signal to noise ratio in the output of the given detector.

Now it will be shown below (§ 5.8) that the signal to noise ratio in the output of a complex image detector such as a television camera is strongly dependent on the conditions under which the device is operated. In applications where it is not necessary to operate the device under conditions chosen for compatibility with some external system, e.g. a broadcasting network, various operating parameters may be adjusted to optimize the signal to noise ratio in the output, and so enable the maximum equivalent quantum efficiency to be realised. However, even when operating under ideal conditions, a unique value for equivalent quantum efficiency E cannot be assigned to any image detecting device, since E will always be dependent on the spatial frequency of the image being detected. If a single figure is quoted as the value of the quantum efficiency of a device, this will usually refer to the value E_o, corresponding to a low spatial frequency, where the efficiency is at a maximum. To compute the value of quantum efficiency at some definite spatial frequency, m television lines say, it is necessary to know, in addition to E_o, the ordinate of the modulation transfer characteristic, M_m, and the noise spectrum of the detector. If the noise is uniformly distributed throughout the power spectrum, it is said to be 'white'. For devices subject to white noise, it follows from the definition of modulation (Eqn.2.2) that the signal, and also the signal to noise ratio in a region of spatial frequency m, will be reduced by a factor M_m to that received in a similarly illuminated region of low spatial frequency. Hence, using Eqn.(2.25) we may write the following relationship

$$E = M_m^2 E_o \qquad (2.26)$$

2.8. Relationship between image information recording efficiency, F, resolution, m, and equivalent quantum efficiency, E, of a device.

The following relationships have been established above.

$$F = n \frac{h_o}{h_i} \qquad (2.1)$$

$$n = A_r m^2 \qquad (2.3)$$

$$h_i = \frac{\sqrt{2}}{K_c} \left[\frac{S_i}{N_i}\right] \qquad (2.12)$$

$$h_o = \frac{1}{\sqrt{2} K_c} \left[\frac{S_o}{N_o}\right] \qquad (2.20)$$

$$E = \left[\frac{S_o/N_o}{S_i/N_i}\right]^2 \qquad (2.25)$$

These equations enable us to write :-

$$\frac{h_o}{h_i} = \frac{1}{2}\sqrt{E} \qquad (2.27)$$

$$F = \frac{1}{2} n\sqrt{E} = \frac{1}{2} A_r m^2 \sqrt{E} \qquad (2.28).$$

Taking into account the dependence of E on spatial frequency Eqn.(2.26), we may write thefollowing expression for F, for a device in which the noise spectrum is white :-

$$F = \tfrac{1}{2} A_r m^2 M_m \sqrt{E_o} \qquad (2.29)$$

For all image detectors, M_m decreases towards zero with increasing m, and F will therefore adopt a maximum value at some definite spatial frequency m. While it would be interesting to calculate F_{max} for all the devices considered in the reviews of image detecting techniques, following in Chapters 4 and 6, this has not always been possible, since essential data in the form of modulation transfer characteristics is not readily available for some image detectors. The prevailing practice in the field of image intensifiers remains to specify the tube properties in terms of single figure parameters such as maximum quantum efficiency and limiting resolution.

CHAPTER 3

THE DETECTION OF LOW CONTRAST IMAGES

3.1. Minimum detectable contrast.

Having discussed the properties which may be used to specify the performance of an image detector, we may now consider how a knowledge of these parameters enables an assessment to be made of the ability with which a device may detect low contrast images.

It was shown above (Eqns.(2.8), (2.10)), that the minimum detectable contrast that can be perceived with a perfect detector, used to make observations of an image for which the average photon flux per picture element is $\overline{P}$, is given by :-

$$C^i_{min} = \frac{K_c}{(S_i/N_i)} \tag{3.1}$$

$$= \frac{K_c}{\sqrt{\overline{P}}} \tag{3.2}$$

The minimum contrast that can actually be perceived by a real detector was given in Eqn.(2.14) as:-

$$C^o_{min} = \frac{K_c}{(S_o/N_o)} \tag{3.3}$$

From Eqns.(3.1) and (3.3), it can be seen that C^o_{min} and C^i_{min} may be related by:-

$$C^{o}_{min} = C^{i}_{min} \left(\frac{S_i / N_i}{S_o / N_o} \right) \quad (3.4)$$

From the definition of equivalent quantum efficiency, expressed above by Eqn.(2.25), we may write :-

$$C^{o}_{min} = C^{i}_{min} \frac{1}{\sqrt{E}} \quad (3.5)$$

Using Eqn.(3.2), this may be expressed as:-

$$C^{o}_{min} = K_c \sqrt{\frac{1}{PE}} \quad (3.6)$$

3.2. <u>The contrast of faint stars against sky background</u>.

A problem of low contrast image detection of particular interest is the perception of faint stars with a terrestial telescope. The presence of the atmosphere presents two main difficulties to ground based astronomers. These arise from turbulence and from sky background.

Atmospheric turbulence sets a minimum to the angular subtense of a star, viewed by an earth-bound observer. Under good seeing conditions, this angle is one second of arc, which corresponds to an image diameter of 0.1 mm. at the prime focus of the Palomar 200 inch telescope. This is well outside the optical resolving limit of the telescope, and it is convenient to use this area to define a picture element when considering the use of the telescope in conjunction with an image detecting system[9, 10, 114].

Around the star exists a uniform sky background against which the star image must be detected. The intensity of this background is such that the light from the sky, falling on a picture element (i.e. an area equal to that occupied by a star image in good seeing conditions) is equivalent to the light that would be received from a 22nd magnitude star[9, 10 114].

The description of the visual brightness of a star in terms of stellar magnitude is based on a standard introduced by Pogson[139]. An increase in stellar magnitude of unity corresponds to a reduction in stellar intensity by a definite factor, r, say. Thus, if I_N represents the intensity of a star of magnitude N,

$$\frac{I_{N+1}}{I_N} = r$$

$$\therefore \quad \frac{I_{N+M}}{I_N} = r^M. \qquad (3.7)$$

A decrease in brightness by a factor of 100 is taken to correspond to an increase in stellar magnitude of 5. Therefore, from Eqn. (3.7), it can be seen that r will be given by:-

$$\frac{1}{100} = r^5$$

$$r = 10^{-2/5} \qquad (3.8)$$

Eqn.(3.7) may now be written as

$$\frac{I_{N+M}}{I_N} = 10^{-\frac{2}{5}M}. \qquad (3.9)$$

$$\therefore \log_{10} \frac{I_{N+M}}{I_N} = -\frac{2}{5} M$$

$$\therefore M = 2.5 \log_{10}\left[\frac{I_N}{I_{N+M}}\right] \qquad (3.10)$$

Eqn.(3.10) gives the magnitude of a star of intensity I_{M+N}, relative to a star of intensity I_N. The figure quoted in isolation as the magnitude of a star is its magnitude, relative to a bright star chosen to provide a reference. Aldebaran with magnitude unity is a commonly accepted reference star, but Vega as a zero magnitude reference star gives an almost identical standard. Thus, if the intensity of Vega is I_o, Eqns. (3.9) and (3.10) may be written as

$$I_M = I_o \; 10^{-\frac{2}{5}M} \qquad (3.11)$$

$$M = 2.5 \log_{10}\left[\frac{I_o}{I_M}\right] \qquad (3.12)$$

where M is the figure that would be quoted as the stellar magnitude of a star of intensity I_M.

If sky background corresponds to a 22nd magnitude star, it will follow from the definition of contrast given by Eqn.(2.6) that the contrast C_M of a star of magnitude M against sky background will be:-

$$C_M = \frac{I_M}{I_{22}}$$

$$= \frac{I_o}{I_{22}} \cdot \frac{I_M}{I_o}$$

$$\therefore \quad \log \; C_M = \log \frac{I_o}{I_{22}} - \log \frac{I_o}{I_M}$$

$\therefore$ From Eqn.(3.12)

$$\log C_M - \frac{22}{2.5} = - \frac{M}{2.5}$$

$$\therefore \qquad M = 22 - 2.5 \log C_M \qquad (3.13)$$

3.3. The magnitude of the faintest detectable star.

Using Eqn.(3.6) minimum detectable contrast C^o_{min} may be plotted as a function of the number of observed quanta, for various values of equivalent quantum efficiency, E. (see Fig.3.1). Using Eqn.(3.13), magnitudes of definitely discernible stars may be associated with values of minimum detectable contrast plotted

FIG. 3.1 MINIMUM DETECTABLE CONTRAST C°_{min} AND MAGNITUDE M OF FAINTEST DETECTABLE STARS PLOTTED AS A FUNCTION OF NUMBER OF OBSERVED QUANTA FOR DETECTORS OF VARIOUS EQUIVALENT QUANTUM EFFICIENCIES E

COEFFICIENT OF CERTAINTY $K_c = 5$

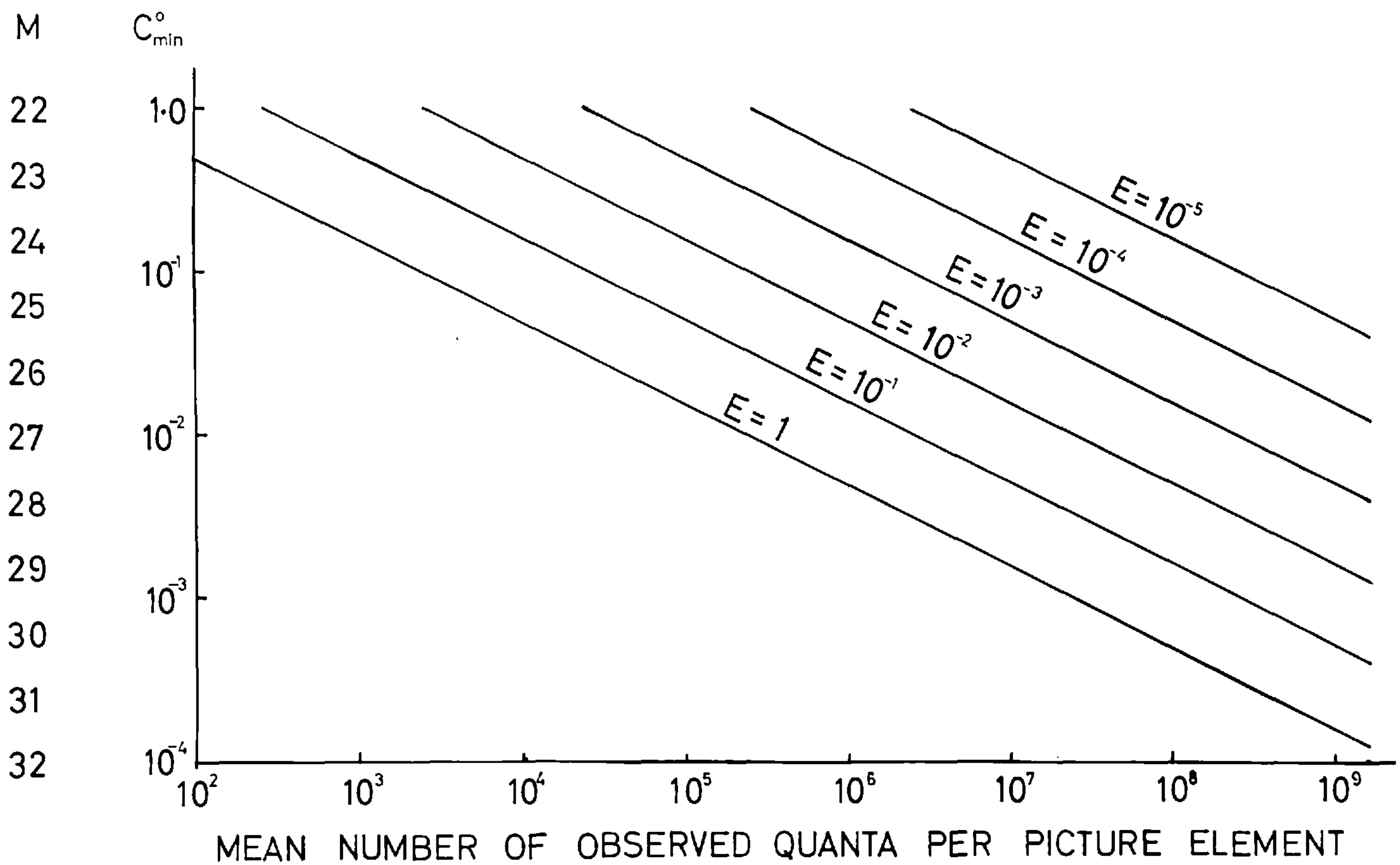

along the ordinates. If the observed quanta, plotted along the abscissae are considered to be the input photons, then the parameter, E, associated with each curve represents the overall equivalent quantum efficiency of the device, but the observed quanta may be identified with the electrons emitted from the photocathode, when E may be interpreted as the photo-electron recording efficiency of the device.

From the curves in Fig.3.1, it would appear that a star of indefinitely high magnitude could be perceived, even with a relatively inefficient detector, provided that enough input quanta may be observed. In practice, there is a limit to the number of quanta which may be assimilated by an image detector in a single exposure which is set by the mechanics of the device. This limit, known as the storage capacity of the detector, was defined above in § 2.6(c). For example, Baum[19] estimates that sensitive photographic plates like Eastman Kodak 103-a-O may be exposed to the night sky at the prime focus of the 200" Palomar telescope for a maximum useful time of half an hour, when the storage capacity of the plate of 5×10^6 grains per cm^2, sets a limit of 23.5 to 24 for the magnitude of just detectable stars.

3.4. The importance of the storage capacity of a detector of low contrast images.

In the previous chapter, a figure of merit for an image detector was derived, in which the maximum number of events which may be stored by a device was considered only as a ratio to the number of input photons (§s. 2.3, 2.5(c), 2.6(c)). The above discussion on limiting detectable magnitude would suggest, however, that the storage capacity of a device is an important parameter, deserving independent consideration in assessing a figure of merit for a low contrast image detector since, even if a device is very inefficient in its use of input photons, provided its storage capacity is adequate, a long exposure will enable more information to be rendered about a low contrast image than would be yielded by a more efficient but less capacious device. This conclusion would be valid, only if a single exposure represented an absolute limit to the information that a device may acquire about the object under examination. This, of course, is the case when moving objects are being observed, but in scientific applications involving the examination of static images, it is usually possible to superimpose the information contained in successive frames. This may be done by transferring the data stored in successive frames of a detector exposed to full capacity to a suitable secondary store of indefinitely large capacity, where the accumulated data may be integrated.

While, in principle, this procedure is always feasible, some devices are much more amenable to this practice than others. For example, if an image were stored on a series of photographic plates, exposed to optimum density, (see below §4.1), the data from the films could be analysed by means of a suitable scanning micro-densitometer[35], and the densities measured at corresponding picture elements added up. While a serious effort to push to the limit the information that can be obtained photographically about low contrast images could involve adopting such an arduous procedure, the work involved may tend to prove prohibitive. On the other hand, the electrical output from a telemetric device may either be recorded on tape, which acts as a secondary store[6, 20], or may be fed directly to the store of a suitably programmed computer[103].

CHAPTER 4

COMPARISON OF DETECTORS EMPLOYING PHOTOGRAPHIC OR NUCLEAR EMULSIONS AS A STORAGE MEDIUM.

Although this thesis is principally concerned with the application of charge storage to the observation of faint optical images, a brief review of photographic image detectors is included here, for while telemetric devices are by far the most advantageous instruments to use in space research, in the field of ground based astronomy, telemetry and photography closely compete.

4.1. Direct Photography.

The oldest way of overcoming the limited integration time of the unaided eye is the well established method of direct photography. A difficulty in exploiting a photographic plate to the full in the detection of faint images, lies in the fact that the exposure time, necessary to make best use of the storage capacity of the plate, conflicts with the exposure for which the quantum efficiency is highest. This arises from the fact that as the exposure of a plate is increased, enabling more information to be stored in the form of photographic grains, the overlapping of the developed grains causes a drop in equivalent quantum efficiency.

Thus, exposing plates, until further exposure does not result in the appearance of any new star image represents a use of the photographic plate which fully exploits its storage capacity, but does not correspond to the highest achievable equivalent quantum efficiency. For this reason, a figure for the equivalent quantum efficiency of photographic emulsions of 0.1 per cent, which used to be favoured by early workers(77), based on observations of plates exposed to full storage capacity, was perhaps rather low.

Felgett(52) and Jones(78) have independently calculated the equivalent quantum efficiencies of four types of plate over a range of exposures from data supplied by the Eastman Kodak Company, and their results are in good agreement. The four films considered were Eastman Kodak Royal-X, Plus-X, Tri-X, and Pan-X, (full names are given in Fig.4.1), and of these, both workers estimate that Kodak Royal-X Pan film has the highest quantum efficiency of 0.9%, when exposed to a density of 0.1 above fog at 430 mμ. For each of the emulsions, Felgett(52) gives curves of the equivalent quantum efficiency, and of the equivalent number of stored photons as a function of exposure which clearly indicate

FIG. 4.1 IMAGE INFORMATION RECORDING EFFICIENCY, PLOTTED AS A FUNCTION OF IMAGE DETAIL, FOR FOUR PHOTOGRAPHIC EMULSIONS

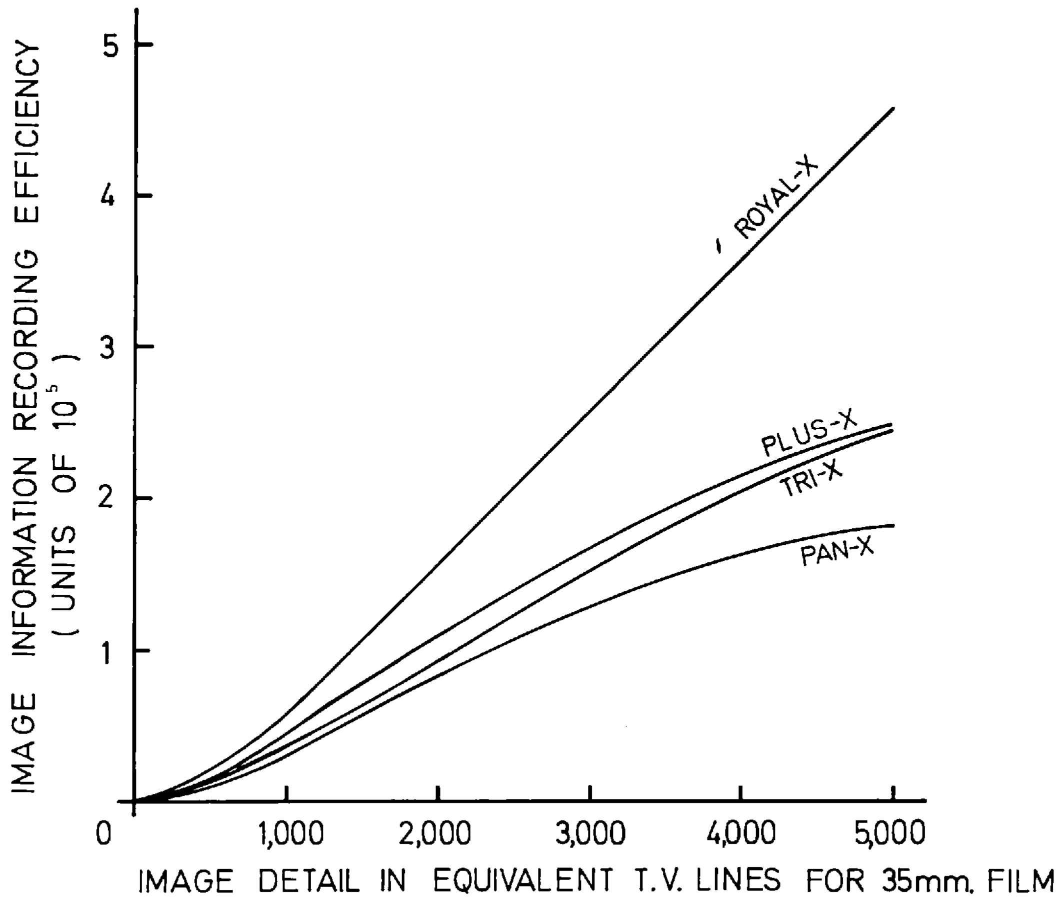

	TYPE OF FILM	E_0
ROYAL-X	KODAK ROYAL-X PAN FILM	0·9 %
PLUS-X	EASTMAN PLUS-X PANCHROMATIC NEGATIVE FILM TYPE 4231	0·7 %
TRI-X	EASTMAN TRI-X PANCHROMATIC NEGATIVE FILM TYPE 5233	0·5 %
PAN-X	KODAK PANATOMIC-X FILM	0·3 %

that maximum storage occurs when the equivalent quantum efficiency has dropped well below its peak. This would suggest that in order to derive the maximum information from a limited photon flux, photographically, it is better to make a series of exposures up to maximum quantum efficiency, rather than to fully utilize the available storage on a plate in a single exposure. The data from the films used in the series of exposures could be analysed and superimposed by the method described above (§ 3.4). However, not only is the integration of a series of photographic exposures an arduous procedure, but the interpretation of the results is made more difficult by the fact that the transfer characteristics of a photographic plate are non-linear.

A further disadvantage of the photographic process which limits its usefulness in the detection of faint images, lies in the fact that it is subject to a defect, known as long exposure reciprocity failure, that is, at low light levels, a reduction of light intensity must be accompanied by a disproportionately longer exposure time, in order to produce the same number of developable grains. This represents a reduction in the equivalent quantum efficiency at low light levels.

For photographic emulsions which obey Selwyn's law of granularity, the noise will be 'white', and the information recording efficiency of photographic emulsions as a function of image detail may therefore be calculated by direct application of Eqn.(2.29). The results of such calculations for four photographic emulsions are illustrated graphically in Fig.4.1. The values of equivalent quantum efficiency, determined by Felgett[52], were used in conjunction with modulation transfer characteristic data, supplied by Kodak[43]. The high resolution capabilities of photographic films enable very high image information recording efficiencies to be realised, even though the equivalent quantum efficiencies are relatively low. The data available enabled calculations to be made, up to definitions of just beyond 100 line pairs per mm., that is, before the image information recording efficiencies of the emulsions considered had adopted maxima. The abscissa in Fig.4.1 is labelled in terms of equivalent T.V. lines for 35 mm. film to facilitate direct comparison between films, and the television and storage tube type devices, considered below (Figs.6.10, 11.2).

In using Fig.4.1 and the similar curves, given below, to compare detectors considered for astronomical observations, it must be borne in mind that if a 35 mm. photographic film is placed at the prime focus of a large telescope, e.g. the Palomar 200 inch reflector, seeing will limit the useful definition to 270 equivalent T.V. lines, and for observations on faint stars, reciprocity failure will depress the value of image information recording efficiency given in Fig.4.1, derived from data for films used at optimum light levels.

4.2. Image Tube Photography.

(a) Advantages to be derived from the photo-emissive effect.

Many of the shortcomings of direct photography may be overcome by suitably exploiting the photo-emissive effect to achieve an improvement in the efficiency of detection of faint optical images. The principle advantages of this photo-electric effect over photography are as follows.

(i) Photocathodes have high quantum efficiencies which may surpass even the most sensitive emulsions by more than an order of magnitude[169,174].

(ii) The photo-emissive effect is linear with light intensity.

(iii) It is not subject to reciprocity failure.

(iv) Various photocathodes may be selected for use over a much broader spectral range than can be covered by photography.

(b) Single stage image intensifier with phosphor output.

(i) Essential features of a single stage intensifier

In this type of device, a faint image, focused on to the photocathode liberates photo-electrons which are in turn, electron optically focused on to a phosphor screen, included within the same evacuated envelope. Such a tube may achieve a light gain at the phosphor of the order of 100[117], and these photons may be used to produce a permanent record on a photographic plate. There are two ways in which this may be accomplished, but each method involves a serious loss in information.

(ii) Photographic recording of the tube output with transfer optics.

The use of conventional transfer optics preserves the resolution of which the tube is capable, (see appendix A.1) but is accompanied by a light loss of at least a factor of 10. The overall light gain of the system is thus less than an order of magnitude. This low gain, together with the accompanying statistical degradation of picture quality, produced through the photon and electron interactions involved in the intensifying process, mean that the device is of very limited use.

(iii) Contact photographic recording of tube output.

The light loss introduced by transfer optics may be avoided at the expense of image definition, by constructing a tube in which the phosphor screen is deposited on to a suitably mounted 12–15 μm. mica end window[115,119,192]. This is sufficiently thin to enable a contact print to be made by pressing a photographic film on to the end window. While this method of contact recording enables the full light gain of 100 to be realised, it is accompanied by a loss in image detail, and the limiting resolution which has actually been recorded with such a device is only 19 line-pairs per mm.[119].

(c) Multistage image intensifiers.

(i) Essential features of multistage intensifiers.

In order to ensure that each electron emitted from a photocathode may be recorded photographically, use is made of multistage intensifiers. A multistage intensifier basically consists of a photocathode, followed by a series of multiplying membrances and an output phosphor. Electrons from the photocathode are accelerated and focused on to the first multiplying membrane where a larger number of daughter electrons are generated. These are focused in turn upon the second multiplying membrane with further electron gain. This is repeated at each stage and electrons from the final membrane are focused on to the output phosphor, producing an intensified image which may be photographed in the normal way.

There are two types of multiplying layer which may be exploited in this way in high gain intensifiers. The multiplying membrane may be a dynode, consisting of a thin layer of suitably supported secondary emitting material which enables the incident electrons to be multiplied by transmission secondary emission[98, 135], (T.S.E.) or, alternatively, multiplication is achieved by using a membrane, consisting of a phosphor and a photocathode, formed on opposite sides of a thin transparent sheet of glass or mica, about 5 microns thick.

The photons emitted from the phosphor by the action of focused primary electrons generate photo-electrons from the part of the photocathode in the immediate proximity of the incident primaries[138]. This latter type of tube is known as the cascade image intensifier.

Both T.S.E. and cascade image intensifiers have been developed at Imperial College by groups led by Dr. Wilcock*and Professor McGee.

(ii) T.S.E. Image Intensifiers.

Workers at the Westinghouse research laboratories reported image intensifiers of the T.S.E. type, in which aluminium backed potassium chloride dynodes were supported on nickel meshes[178]. The Imperial College team avoided the disadvantages arising from the use of meshes, by using aluminium oxide films, 500 Å thick, to support the layers. The layers were prepared by evaporating aluminium and potassium chloride on to the alumina support[190]. T.S.E. intensifiers of this type have been improved in England by 20th Century Electronics[46], and by the English Electric Valve Co.[8,166,167], and in America, by Westinghouse[179].

---

*Now Professor of Physics at the University of North Wales.

T.S.E. tubes are run with interstage voltages of 4 to 5 kV., enabling mean electron gains of 5 to 6 per stage to be achieved. Because of the relatively low stage gain, it is necessary to use five stages of multiplication to efficiently record individual photo-electrons, and such tubes may have a light gain of up to 10^6 and achieve a resolution of up to 30 line pairs per mm.

The statistics of the secondary emission processes have been shown to be exponential[45]. This, together with the low stage gain, results in the device possessing an equivalent quantum efficiency, which corresponds to a significant reduction of the photocathode efficiency. Workers who have used this type of tube for photographing Cerenkov radiation have reported a 30% photo-electron recording efficiency[18].

Mandel[105] has shown theoretically the importance of a high stage gain in order for the equivalent quantum efficiency of an intensifier to approach the responsive quantum efficiency of the photocathode. It therefore appeared that the discovery by Goetze[59] of a method by which a spongy potassium chloride layer could be fabricated and used to achieve a secondary emission gain of 50 to 100, would enable a T.S.E. image intensifier of high equivalent quantum efficiency to be constructed. Problems associated with layer charging arise with this type of dynode, however, and it is necessary to include auxiliary stabilising meshes into tubes, incorporating spongy potassium chloride dynodes(59,61). While a two-stage device of this type has been described by Goetze(59), no multistage spongy layer intensifier has yet been reported. An alternative method of exploiting the high gain associated with low density potassium chloride layers is dealt with below, in the main part of this thesis.

(iii) Cascade Image Intensifiers.

This type of tube exhibits the high stage gain necessary for good multiplying statistics, and has been made in various forms by a number of workers(26,51,58,124,131,142,170,191). Multiplications of 100 per stage have been achieved with tubes incorporating cascade screens, consisting of 4 µm micas with an S9 cathode on one side and a P11 phosphor on the other, this cathode-phosphor combination constituting a good spectral match. Three-stage tubes have been made with a blue light gain of 10^6, and with a limiting resolution of 35 line pairs per mm., when run at an overall operating voltage of 45 kV., and using two loop magnetic focusing[124]. Improved resolutions may be achieved at the expense of gain by using finer grain phosphors[124]. The photo-electron recording efficiency has been estimated to lie between 70 and 80%[124].

From these considerations of high gain, multi-stage intensifiers, it can be seen that the cascade tube, particularly, is able to effect a considerable improvement in the efficiency with which faint images may be photographed. However, a single photographic plate, used to store the output information from a tube, has only a limited capacity. The emulsion will thus become saturated for a fairly modest primary photon flux at the intensifier input. Application of multi-stage intensifiers to the problem of low contrast detection would thus require a series of exposures to be made to the light source under observation. The plates would then need to be analysed by the laborious method of micro-densitometry discussed above (§ 3.4) to integrate the information stored in successive frames.

4.3. Electronography.

Some of the problems associated with image intensifiers with a phosphor output can be avoided if the intensifier is designed in such a way that the phosphor screen may be replaced by an emulsion, capable of directly recording the photo-electrons emitted from the cathode of the device. This modus operandi is known as electronography and has the following advantages over conventional photography.

Each photo-electron, incident on the emulsion with an energy of about 30 keV may render several silver grains developable[(42)], enabling each photo-electron to be recorded with a high degree of certainty. Since, also, the fog level in electronographic emulsions is low, compared with optical emulsions, the equivalent quantum efficiency of electronographic devices may approach the responsive quantum efficiency of the photocathode.

Electronographic emulsions exhibit a linear response, and are not subject to reciprocity failure[(91)].

A further important property of electronographic emulsions is that their storage capacities are much higher than the capacities realised by photographic emulsions, e.g. Ilford G5 electron sensitive emulsion has an effective storage capacity twelve times better than Kodak 103a-O[84]. Thus, the minimum perceptible contrast that may be recorded in a single frame electronographically is much lower than that which could be obtained with a single photographic exposure.

The electronographic recording technique was pioneered by Lallemand[89-93]. A major problem experienced in exploiting electronography lies in the incompatibility of photocathodes and emulsions, existing in a common vacuum compartment. In spite of many ingenious precautions which Lallemand has incorporated into the design of his camera, he has only succeeded in extending the life of the photocathode which has to be periodically replaced.

Various modifications to this type of tube have been investigated, in which the photocathode and the emulsion are located in separate chambers[71,72,86]. These have enabled the life of a photocathode to be extended from a few hours to periods of the order of a month.

McGee has suggested a device for electronographic image recording known as the Spectracon, which enables the photocathode to be preserved indefinitely. It has been developed to its present form by a team, working under Professor McGee in the Applied Physics section of Imperial College[84,120,125,188].

Electrons from the photocathode of the Spectracon are accelerated through 40 kV, and focused on to a mica window, which may be only 4 μm thick, but is so mounted, that it is mechanically strong enough to withstand atmospheric pressure. The energetic electrons are able to penetrate the mica to be recorded on a nuclear emulsion, pressed in contact with the mica. The cathode is thus isolated in a sealed-off chamber under high vacuum, while the nuclear emulsion remains in the atmosphere where it may be conveniently manipulated.

The equivalent quantum efficiency of the device has been measured to be 60% of the photocathode efficiency and the resolution obtained has been better than 80 line pairs per mm.[85].

4.4. Conclusions.

In spite of the relatively low equivalent quantum efficiencies of photographic emulsions, the high resolution that can be achieved by direct photography makes this a very efficient method of recording information from optical images. Image intensifiers and electronographic devices have enabled the equivalent quantum efficiency of image recording on photographic emulsions to approach the fairly high responsive quantum efficiency of photo-emissive cathodes, but at the expense of some resolution. The high quantum efficiency and the freedom from reciprocity failure of the photo-emissive effect has made image intensifier photography a powerful method for observing faint images, but the moderate storage capacity of photographic emulsions limits the contrast that can be observed in a single exposure. The improved storage capacity of nuclear emulsions makes electronographic devices more suitable as detectors of faint low contrast images, the magnitude of stars which may just be observed against sky background with a single exposure being about 25[85], compared with 23.5 for direct photography[9]. The effective capacity of optical or nuclear films can be increased by superimposing successive exposures. The use of an emulsion as a storage medium represents a defect in the detecting system, since further processing of the film is necessary for superimposition of photographic information, and for transmission of the data from an inaccessible source. This further processing can be a cumbersome procedure, and an image detecting device which could provide an output in the versatile form of an electrical signal, while matching the performance of image intensifiers and electronographic cameras in quantum efficiency, integration time, and resolution, would indeed be an extremely valuable detector of faint low-contrast images.

CHAPTER 5

IMAGE DETECTION BY CHARGE STORAGE.

5.1. Essential features of charge storage camera tubes.

Image detection by charge storage consists essentially of exposing a device, called a charge storage camera tube, to an optical image, which the device converts into a charge pattern, retained on an insulating surface. The information contained in this charge image is extracted by a reading process, in which the charge pattern is scanned with an electron beam. This restores the surface to a uniform potential and at the same time, enables an electrical signal, called a video signal, to be generated. This video signal conveys in a coded form the required information, and is amplified by means of a suitably designed head amplifier, or by an electron-multiplier, built within the camera tube envelope. It may be further processed to simulate the original light image as a display on a monitor. Alternatively, the video signal may be displayed on an oscilloscope for measurement purposes, stored on a tape, or fed to a computer.

While this general description embraces all charge storage camera tubes, there are many methods of converting the optical image into a stored charge image, and of converting the stored image into a video signal. In this chapter, the various methods of generating a video signal from a charge storage camera tube will be discussed. This will be followed in Chapter 6 by a review of existing charge storage tubes, and their effectiveness as detectors of faint low contrast images will be considered.

5.2. <u>Scanning modes which may be used in the generation of video signals from stored charge images</u>.

(a) <u>Scanning with a high velocity electron beam</u>.

Early television cameras, the Emitron (iconoscope) and Super Emitron (image iconoscope)- (see below § 6.1) used a high velocity scanning beam to generate a video signal as it discharged the camera target to a fixed datum level, (the potential of the nearest positive electrode) between each frame. This process is called anode potential stabilisation. A fuller description of the mechanisms involved in signal generation by this method is not included here, but several detailed accounts of the complex processes occurring as a camera target is scanned with a high velocity electron beam are available in the literature(4,159,195). Spurious signals arising from so-called redistribution electrons are superimposed on the useful signal. Devices employing high velocity scanning beams are thus unsuitable for making scientific measurements unless special precautions are taken. The use of a barrier grid(86), or the technique of pulse-biassing the storage surface(67,172) can minimise these spurious signals by preventing the return of redistribution electrons to the target.

(b) Scanning with a low velocity electron beam.

The practice used in most modern television camera tubes is to scan the target orthogonally with low velocity electrons. These arrive at the target with insufficient energy to produce appreciable secondary emission, and are able to land on positive areas of the target, until these regions become charged to approximately the same potential as the cathode of origin of the scanning electrons. Further scanning electrons will then be repelled from the target. This process is known as cathode potential stabilisation.

In practice, targets operated under so-called cathode potential stabilisation conditions, become effectively stabilised at a slightly lower potential because the scanning electrons are emitted from the cathode with thermal energies, additional to the potential energy, represented by the gun cathode voltage.

Although the low velocity electrons prove more difficult to focus than the high velocity beams used in early television cameras, there are no redistribution effects and associated spurious signals, accompanying low velocity read out. The output signal can thus be used for scientific measurements, or to generate high quality pictures.

In order to derive the best results, it is important that the electrostatic capacity of the target of the camera should be optimized. In general, the more the charge that can be stored on the target, prior to scanning, the greater will be the information transmitted in the signal. However, there are upper limits to the voltage excursions that can be tolerated on a target, scanned by a low velocity electron beam.

The potential of the target must not be allowed to exceed the first cross-over potential, i.e. the potential above which the secondary emission coefficient exceeds unity. Otherwise, the operating conditions will revert from cathode to anode potential stabilization, with the strong possibility of damaging the target. However, an undesirable effect, known as beam pulling can occur at target potentials, well below the first cross-over point. This is an effect, by which slow scanning electrons are constrained by transverse fields, existing across the charged layer, to dwell for a disproportionate time on areas charged to too high a positive potential, and it gives rise to a distorted output picture in which the white areas appear very large. The potential excursions that can be permitted on the target before this effect becomes objectionable will depend on parameters such as scanning speed and the electric field, normal to the target. A typical figure is 4 volts[123]. A charge which raises the target potential to a level just below the potential at which appreciable beam pulling occurs, corresponds to what is known as a peak white signal. In order to store an adequate charge on the target and also avoid undesirable beam pulling effects, it is necessary to have a large target capacity.

Another factor, however, which must be considered in deciding the best value for target capacity is the importance of avoiding discharge lag, i.e. the inability of the scanning beam to neutralize all the stored picture charge in a single frame. Discharge lag may be minimized by the use of a low capacity target, by application of target bias, or by scanning the target with a low temperature beam[126]. Target bias may not always be conveniently applied, and beam acceptance curves, measured for targets, scanned with electrons originating from both thermionic[126,164] and photo-emissive[83] cathodes show that in either case, the minimum scanning beam temperature that can be realised in practical devices is about 1000°K. Discharge lag in cathode potential stabilized tubes is therefore usually avoided by arranging as far as possible for the target capacity to be sufficiently small, that a stored charge, corresponding to a peak white signal, may be reduced in a single exposure to the scanning beam, to a charge, commensurate with the noise level.

c. <u>Other potentials at which camera tube targets may be stabilized</u>.

For the sake of completeness, it should be mentioned that there are two other potentials at which a camera tube target may be stabilised by the action of the scanning beam.

A target may be stabilised at the second cross-over potential when scanned by energetic electrons, provided that the electrode in closest proximity to the target is held at a more positive voltage than the second cross-over potential. This mode of operation corresponds to poor beam acceptance, and to the best of the author's knowledge, no practical device has been made to operate under these conditions.

It is also possible to stabilise the targets of devices whose sensitivity is dependent on the voltage gradient maintained across the target at a potential, close to that of the signal plate on to which the target is deposited. This phenomenon arises from the fact that the current, flowing to the target from the scanning beam may balance the current created by the optical image when the target surface potential lies near the signal plate potential. The mechanism is described in detail by de Haan et al [32]. This mode of target potential stabilisation is encountered as an undesirable state in a tube, intended to operate under conditions of cathode potential stabilisation, and is not exploited in practical cameras.

5.3. Factors effecting the resolution that may be realised in a charge storage tube.

a. Light optics.

Lenses can be made to achieve limiting definitions far better than can be realised by any television camera but, if there is a serious limitation in the available light, it may be necessary to increase the lens aperture until this component begins to contribute significantly to the loss in definition of the system. In the immediately post-war period of commercial television, high aperture lenses, available for use with television cameras, had been found to cause a significant drop in signal amplitude at spatial frequencies as low as 15 to 20 line pairs per mm. Such lenses thus represented components which limited the definition attainable with television cameras[158].

b. Electron optics of the image section.

Many television cameras use an image section in which primary photoelectrons are accelerated and focused on to a target where the stored charge image is created. In calculating the loss in definition, due to imperfections in the electron optics of an electrostatic imaging system, account must be taken of the five Siedel aberrations, as well as of chromatic aberration (i.e. the aberration arising from the spread of energies with which electrons are released from the photocathode). However, it is usually practicable to electromagnetically focus the image section, when the only aberrations which need to be considered are chromatic aberration and spherical aberration, (i.e. the aberration arising from the different directions in which electrons may be liberated from the photocathode).

The literature contains various treatments of the problem of calculating the size of the disc of confusion, produced in systems, in which electrons emitted from a point on the photocathode are focused by superimposed uniform electrostatic and magnetic fields. De Vore[36] has calculated the electron discribution occurring in a plane corresponding to the best focus for electrons emitted from the photocathode with zero axial energy. An empirical law was used to give the energy distribution of the photoelectrons which were assumed to be emitted in a Lambertian fashion. The focal plane for which De Vore made his calculations does not correspond to the smallest disc of confusion and Beurle et al[16] have calculated the minimum mean square radial aberration. This minimum is realised at a plane just beyond that where electrons of zero axial energy come to a focus. Beurle also assumed Lambertian emission, but based his calculations on mono-energetic photoelectrons. Beurle et al[16] made a similar calculation for the focusing of secondary electrons, where a Maxwellian distribution was assumed for emission velocities. Papp[136] has also made a similar calculation of the minimum mean square radial aberration, assuming Maxwellian velocity distributions of emitted electrons in both axial and radial directions.

A more detailed investigation into the problem has been made by the author, who has programmed a computer to calculate the distribution of electrons, emitted from a point in a photocathode, at any plane, in a system employing uniform electrostatic and magnetic focusing fields. Any electron velocity distribution may be accommodated by including appropriate data cards in the deck. In the programmes run, the angular distribution used was Lambertian[75], but the programme could be easily modified to accommodate any other angular distribution of photoelectrons.

An account of the calculations used in devising this programme, together with examples of electron distributions derived, is given in Appendix A.1. The parameters used correspond to the design of a camera image section, described below. (§7.2). The photoelectron energy distribution used to obtain these results was based on measurements made by Shalabutov et al[162] on electrons emitted from an antimony-caesium cathode, illuminated with light, of wavelength, 456 mμ.

The results obtained show that for the parameters considered, it is theoretically possible to obtain resolutions of the order 250 line pairs per mm.

An additional factor which should be taken into account in considering the resolution attainable in the image section of the camera is cross-talk[54,97], the effect by which scanning fields in the gun section may leak into the image section, so influencing the motion of the primary photoelectrons. The importance of this will depend on the energy of the primary photoelectrons as they come under the influence of these fields. An account of a practical investigation of the importance of this effect in the camera described in the main part of this thesis is given below (§10.7).

c. Loss in definition due to properties of the storage target.

The porperties of the target which will affect the image definition will depend on the mechanism by which the charge image is formed. In tubes, such as the Emitron and C.P.S. Emitron (see below §s 6.1 and 6.2), where the target is a mosaic of insulated photoemissive elements, it is important that the size of the individual elements should be sufficiently small to avoid their contributing to any observed loss in definition. In tubes, incorporating targets of only moderate resistivity, e.g. soda glass targets, used in image orthicons, lateral leakage of charge during a frame period can reduce resolution[36]. Loss of resolution in photo-conductive targets can be caused by lateral spreading of the positive carriers as they migrate across the layer to build up the charge image on the scanned surface, and also by scattering of light within the layer[32]. Camera tubes, embodying targets which are charged by the action of energetic primary electrons may experience a loss in definition due to the scattering of electrons as they penetrate through the target layer.

(d) Electron optics of the scanning section.

A full analytical treatment of the resolution that can be realised as a narrow electron beam scans a charge pattern stored on a target would require lengthy calculations to be made, based on a knowledge of the intensity profile of the scanning spot, the energy distribution of the scanning electrons, and the beam acceptance function of the target in question. The problem is complicated by the fact that the beam acceptance of an insulating target changes continuously as it is discharged during scanning.

No attempt will be made in the following discussion to provide a mathematical derivation of the definition that may be achieved with a low velocity scanning beam, but mention will be made of some of the electron optical effects which influence the resolution limit, set by the scanning section of the tube, with a discussion of how this may be optimized.

The electron optics of a typical scanning section is shown in Fig.5.1. The low velocity gun is a triode system with a plane cathode, (2), modulator (3), and an anode or limiter electrode, constructed with two apertures known as the anode diaphragm (4) and the aperture diaphragm (6). The diameter of the latter

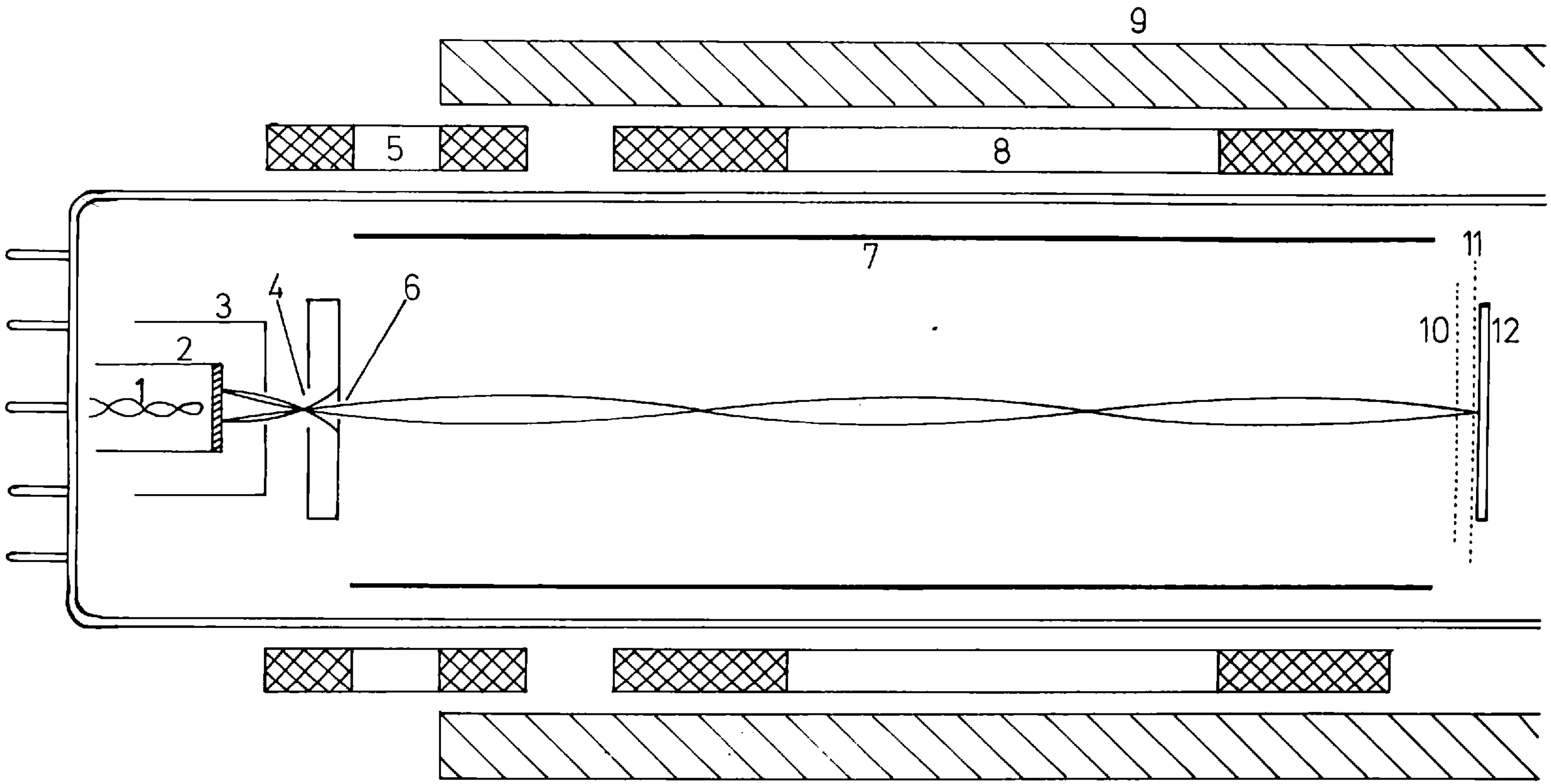

FIG. 5.1 SCANNING SECTION OF A TYPICAL TELEVISION CAMERA EMPLOYING LOW VELOCITY READ-OUT BEAM.

(not drawn to scale)

is about 30 μm, and serves to restrict the electron beam diverging from the crossover, so that the limiting trajectories of the beam which actually passes through the aperture make an angle of only about 20' with the axis of the system. The modulator potential may be varied between −10 volts and −150 volts, depending on the beam intensity requirements, while the limiter is held at a typical value of +300 volts. The anode diaphragm in the limiter electrode system serves to increase the field at the cathode, reducing the angular spread of each elementary beam, emerging from any point on the cathode surface, and improving the overall emission of the system by counteracting the limiting effect of space charge.

Alignment coils (5), mounted around the gun enable a small magnetic field to correct for any mechanical misalignment, introduced when sealing the electron gun pinch into the tube. It is difficult to maintain high mechanical tolerances during the glass blowing operation.

On emerging from the aperture diaphragm, the electron beam enters a field free region within a cylindrical wall anode, (7). The potential of the wall anode is adjustable within the range 100–300 volts, so that the axial magnetic field, provided by the solenoid (9) will constrain the electrons to complete an exact number of helices as they focus on the target (12).

By arranging for the emission system of the gun to protrude from the end of the focusing solenoid, and so to be located in a region of weaker magnetic field, demagnification of the aperture diaphragm by a factor of about two is effected, producing an electronic image on the target whose diameter is of the order 20 μm[176].

The beam is scanned laterally and vertically by the action of scanning coils, (8). It has been shown that it is desirable for the length of the scanning fields to be equal to the length of an integral number of focus loops, described by the scanning beam[144].

A few mm. from the target is mounted an ion trap mesh, (10), held at about the same potential as the wall anode. This eliminates an effect, known as ion spot[108]. In the absence of this mesh, the electrostatic fields would be such as to accelerate positive ions created within the wall anode towards the centre of the target, giving rise to a characteristic white spot in the centre of the video display. Lubszynski et al[100] have indicated that resolution can be improved by increasing the field between this mesh and the target. An improvement would therefore be effected if the potential of the mesh was raised, and its separation from the target reduced. These measures pose difficulties for tubes designed to have the mesh and wall anode connected to a common potential. Greater magnetic scanning and focusing power would be required and an increase would be observed in the port-hole effect, by which a variation in picture brightness occurs towards the edge of the picture. It is due to the non-orthogonal landing of the electrons at the edge of the target. The normal component of electron energy in the scanning beam is thus less at the edges of the target, giving rise to non-uniform stabilisation of the target surface potential. Connecting the mesh and anode as separate electrodes was shown to overcome these problems and to introduce further improvements in the electron optics of the scanning section[102].

It prevented the accumulation of ions which had been able to build up in the field free space defined by the commonly connected ion trap mesh and anode, and the electrostatic lens produced by the field between the wall anode and mesh when separately connected assisted corner focusing and orthogonal beam landing.

The stabiliser mesh[112],(11), shown in Fig. 5.1. has no electron optical function. It is included to limit the potential excursions of the target, only if there is any danger that this could rise beyond its first cross-over potential when overloaded. The stabiliser mesh has therefore to be maintained at a voltage, just below the first cross-over potential of the target. It consequently must be mounted very close to the target in order to maintain the strong field gradient normal to the target, necessary for good focusing.

While considering the resolution capabilities of a low velocity scanning beam, mention should be made of the effect known as beam pulling. This has been described above (§ 5.2(b)) and need not degrade definition, provided the target does not become charged to too high a voltage, through being over exposed.

From this discussion, it can be seen that there are several precautions which should be taken in designing a low-velocity, electron scanning system to optimize resolution. Definitions can now be realised with such systems which are as good as those obtainable with the high velocity guns, used in the obsolete tubes of the Emitron or iconoscope type(157). Weimer(187) has provided a characteristic for an image orthicon gun, delivering 10^{-7} amps, which shows a resolution limit of about 2,000 television lines per inch on the target.

(e) Overall resolution of a camera tube.

While it is often difficult to ascertain precisely the effect of the contribution to the resultant resolution, due to each image processing stage of a camera tube, an overall modulation transfer characteristic may be measured. Analysis on the performance of the tube may then be carried out by treating the tube as an electrical filter whose frequency characteristic may be inferred from its modulation transfer response. The output signal from the tube should be amplified by a device whose response is at least flat over the frequency range, accommodated by the tube itself. For entertainment purposes, aperture correction is employed by which high frequency signals are boosted in the amplifier to compensate for the attenuation arising in the camera itself.

5.4. Noise introduced in the creation of a charge image on a storage surface.

Fig.5.2 illustrates the processes occurring in a storage tube, in which the stored charge image is formed on an insulating surface, by secondary emission caused by the action of accelerated photo-electrons, focused on to the surface.

Let P = the number of photons incident per picture element.

n_e = the number of photoelectrons released per picture element.

n_s = the number of electron charges, stored per picture element.

n_t = the number of secondary electrons emitted per picture element.

σ = the photo-sensitivity of the cathode.

δ = the secondary emission coefficient of the storage layer.

g_e = the charge gain of the storage layer ($g_e = \delta - 1$).

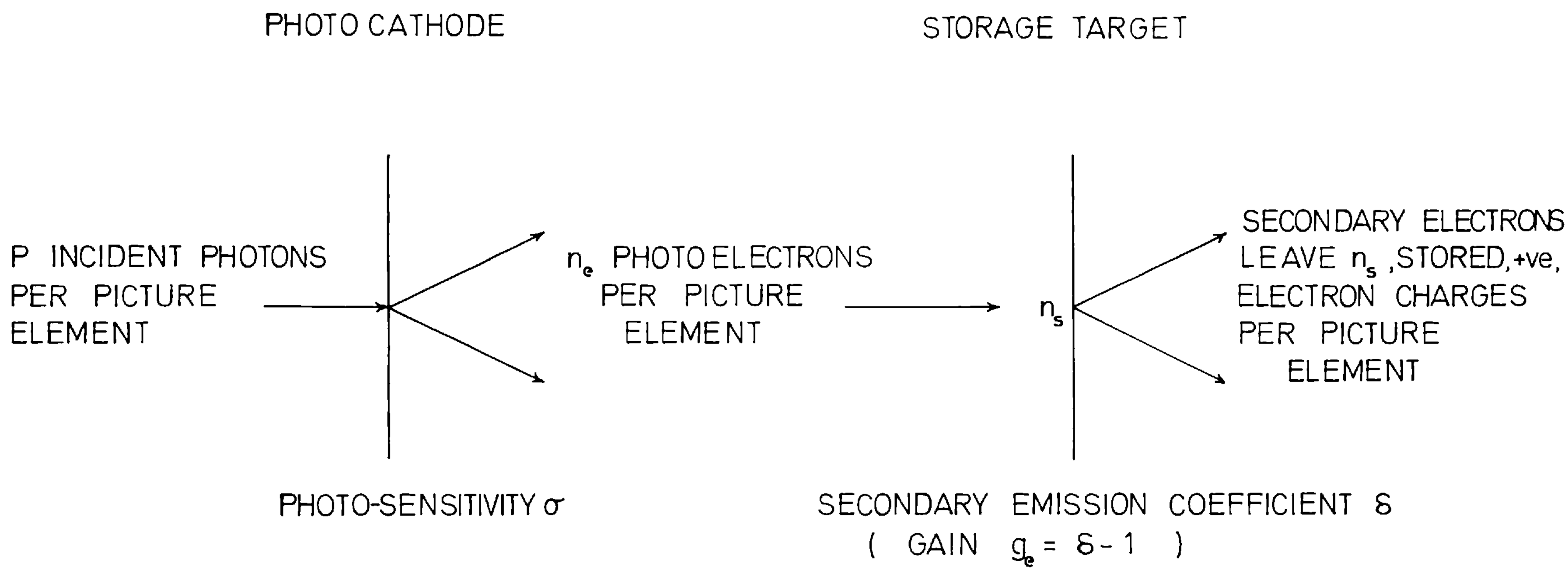

FIG. 5.2 PROCESSES OCCURRING IN A STORAGE TUBE IN WHICH THE STORED CHARGE IMAGE IS CREATED BY SECONDARY EMISSION

The noise to signal ratio in the stored charge $\left[\frac{N_s}{s}\right]$ has been calculated in appendix A.2.

For noiseless multiplication, or for multiplication obeying Poissonian statistics,

$$\left[\frac{N_s}{s}\right]^2 \approx \frac{1}{\overline{P}\,\overline{\sigma}} = \frac{1}{\overline{n_e}} = \frac{\overline{g_e}}{\overline{n_e}} \qquad (5.1)$$

For exponential statistics of multiplication,

$$\left[\frac{N_s}{s}\right]^2 \approx \frac{2}{\overline{P}\,\overline{\sigma}} = \frac{2}{\overline{n_e}} = \frac{2\,\overline{g_e}}{\overline{n_s}} \qquad (5.2)$$

5.5. Noise introduced in the discharging process.

The charge accumulated on the storage surface during exposure is discharged to gun cathode potential in the reading process by the action of the low velocity scanning beam (see §5.2(b) above). However, the target will never be restored to a perfectly uniform potential, and the final potential attained by each picture element will be subject to a fluctuation. Beurle(17) has provided a detailed analysis of processes involved, which show that this source of noise is negligible.

5.6. Noise introduced when the signal is processed by a thermionic head-amplifier coupled to the storage target.

As the storage target is discharged to gun cathode potential, by the action of the low velocity scanning beam, it produces an electrical signal, proportional to the stored charge. The storage surface can be capacitively coupled to a conducting signal plate, and the current from the signal plate can be amplified by a suitably designed head amplifier. Fluctuations present at the input of this amplifier (amplifier noise) set a limit to the minimum detectable signal from the camera tube. The amplifier should therefore be designed and operated in a way which will reduce the fluctuations as far as possible. At the time of writing, vacuum tube input circuits are believed to be still superior to transistor circuits for realising the best possible signal to noise performance(154), but the possibility of using field effect transistors in a low noise head amplifier is currently being investigated(175).

Fig.5.3 represents diagrammatically the arrangement by which a camera tube target is coupled to the input of a vacuum tube head amplifier.

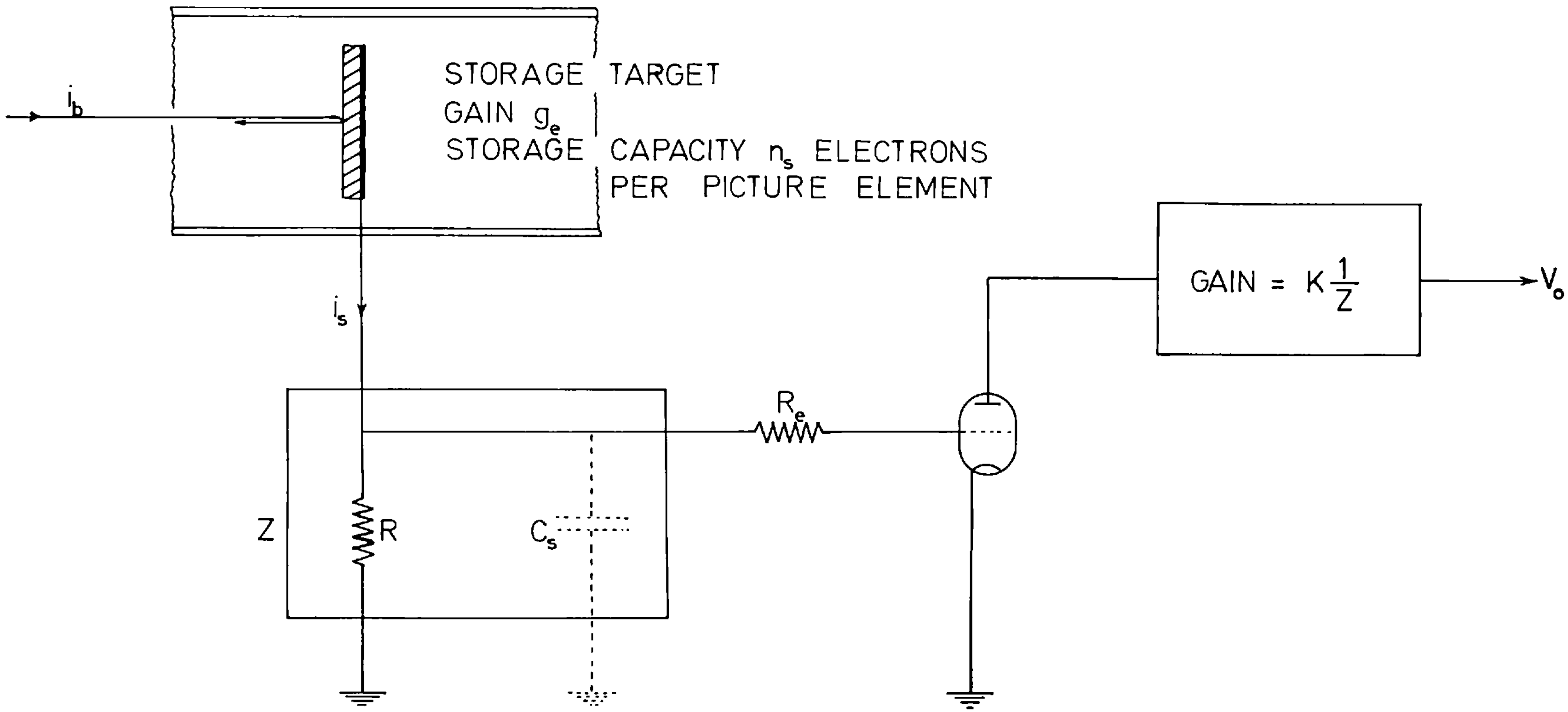

$$\frac{1}{Z} = \frac{1}{R} + j\omega C_s$$

FIG. 5.3 ARRANGEMENT BY WHICH THE CONDUCTING SIGNAL ELECTRODE OF A CAMERA TUBE MAY BE COUPLED TO A HEAD AMPLIFIER.

As the electron beam, i_b, scans the target, it neutralizes n_s equivalent positive electron charges, stored on a picture element, in a time ΔT, generating a signal current, i_s.

$$i_s = \frac{M_m n_s e}{\Delta T} \qquad (5.3)$$

M_m is the ordinate of the modulation transfer characteristic of the tube at a spatial frequency corresponding to m television lines. This factor is introduced to take into account the property of the tube, discussed above in § 5.5(e), by which it behaves as a low pass filter, attenuating signals corresponding to high spatial frequencies.

The current, i_s, flows through the input impedance, Z, of an amplifier, consisting of a grid resistance R, shunted by a stray capacitance C_s. The amplifier must have a minimum bandwidth, f_b, given by

$$f_b = \frac{1}{2\Delta T} \qquad (5.4)$$

and the attenuation of high frequency components in the signal, due to the capacitance, C_s, is compensated for by designing the amplifier to have a response of the form $\frac{K}{Z}$, where K is a constant.

White et al[189] have described a method by which frequency dependent feedback can be applied in a head amplifier to achieve the necessary equalization, and the advantages arising from the use of a cascaded input stage have been indicated by James[76] in a review of head amplifier designs. By minimizing the Miller effect, a cascode circuit effectively reduces the input capacity and hence the equalization required.

R_e, shown in Fig.5.3, is known as the equivalent noise resistance of the valve and is not a real circuit component. It is a device to enable the contribution to the total noise arising from anode current shot noise to be calculated by treating this as if it arose from the Johnson noise of a fictitious resistor, R_e, connected directly to the valve grid.

Beurle[17] has shown that the anode current shot noise of the first valve, together with the grid current shot noise of this valve and the thermal noise of the grid resistor, constitute the chief contributions to noise in the amplifier. The noise to signal power ratios arising from these sources has been calculated in Appendix A.3, where the following results are derived.

(i) Johnson noise $\left[\frac{N_R}{S}\right]^2 = \frac{kT}{M_m^2 n_s^2 e^2 f_B R}$ (5.5)

(ii) Grid current shot noise $\left[\frac{N_G}{S}\right]^2 = \frac{i_g}{2M_m^2 n_s^2 e f_B}$ (5.6)

(iii) Anode current shot noise $\left[\frac{N_A}{S}\right]^2 = \frac{4\pi^2 kTR_e C_s^2 f_B}{3M_m^2 n_s^2 e^2}$ (5.7)

The mean square noise to signal ratios represent a convenient form for expressing the various noise contributions. The total mean square noise to signal ratio under given conditions may be derived by simply adding the magnitudes of these expressions.

5.7. Noise introduced by the scanning beam.

The effect of beam current shot noise provides a major contribution to the noise generated in tubes using return beam multiplier read out. This is discussed below in §5.9. The fact that the scanning beam is composed of individual electrons can also introduce noise into tubes using signal plate and directly coupled head amplifier read out, for as the beam electrons not used in the discharge process approach and recede from the target, they induce charges in the signal plate. These charges will be induced with a statistical distribution with respect to time and so represent a noise contribution. Beurle[17] has shown that this source of noise is negligible in normal circumstances.

5.8. Optimum bandwidth and operating parameters for a charge storage tube using thermionic signal amplification.

While eqns.(5.1) and (5.2) indicate that high target gain, g_e, reduces the signal to noise ratio in a tube of given target capacity, these equations also show that the signal to noise ratio differs from that present in the primary photoelectrons by a constant, dependent on the statistics of multiplication alone, and not on the gain. A high target gain in itself therefore represents no degeneration to the value of signal to noise, fundamentally limited by the number of photoelectrons, n_e. The increase in the noise contribution due to the stored charge shot noise when the gain, g_e, is high is a desirable feature from the standpoint of making scientific measurements, since it represents an increase in the importance of a fundamental source of noise in comparison with instrumental noise introduced by the amplifier.

Examination of eqns. (5.5), (5.6) and (5.7) indicates certain obvious choices for operating parameters. We see from eqn.(5.7) that the stray input capacity, C_s, should be minimized. This may be done by locating the first valve of the head amplifier as close to the signal plate as possible, so reducing any capacity introduced by the coupling leads.

Eqns.(5.6) and (5.7) show that the input valve should have a low grid current, i_g, and equivalent noise resistance, R_e, properties that are often incompatible with a high mutual conductance, necessary to prevent the second stage of the head amplifier from contributing significantly to the noise. The E.M.I. R5559 is a suitable valve, having an equivalent noise resistance R_e of 145 ohms, a grid current, i_g, of 10^{-8} amps and an input capacity of 17 pF.

While Eqn.(5.5) indicates the desirability of a high input resistance, R, comparison with Eqn.(5.6) indicates that when :-

$$R > \frac{2kT}{ei_g} \qquad (5.8)$$

grid current noise will exceed resistance noise, thus setting a maximum useful value for the choice of R.

Eqns.(5.5), (5.6) and (5.7) indicate the importance of high modulation transfer characteristic, M_m.

Eqns.(5.1), (5.2), (5.5), (5.6) and (5.7) all show the desirability of high storage capacity to enable large values of n_s to be realised.

Properties, such as target gain, g_e, modulation, M_m, and storage capacity, n_s, are really properties dependent on the stage of development of the tube, rather than on operating conditions. However, the mechanism of signal generation in some tubes enables target gain to be varied, and it is possible to improve both M_m and n_s by operating at lower line standards. Nonetheless, this can only be done at the expense of definition, and thus improving on signal to noise by reducing the number of television lines can only be carried out to a limited extent if a good value for the image information recording efficiency (Eqn.2.29) is to be maintained.

The remaining parameter to be considered is bandwidth, f_B. Eqns.(5.5) and (5.6) represent sources of noise which decrease with f_B, while Eqn.(5.7) indicates that anode current shot noise becomes increasingly important as the bandwidth gets larger. Clearly, an optimum bandwidth exists for any set of operating conditions at which the total signal to noise is a minimum.

So many parameters are embraced by the signal to noise equations that it is difficult to present in a small number of curves, comprehensive data which enables the performance for any combination of operating conditions to be readily assessed and so allow an optimum bandwidth to be selected for a given system. A set of three diagrams is therefore provided in Figs.5.4, 5.5, and 5.6, which represent the variation with bandwidth of the contributions due to various noise sources, for camera tubes whose storage capacities correspond to 10^5, 10^6 and 10^7 electrons per picture element respectively. All curves are drawn for a head amplifier, using an E5559 input valve and a total stray input capacitance, C_s, of 50 pF. The values of other relevant parameters are marked on the graphs.

FIG. 5.4 CONTRIBUTIONS TO NOISE ARISING FROM VARIOUS SOURCES, PLOTTED AS A FUNCTION OF BANDWIDTH, FOR A STORAGE TUBE STORING 10^5 ELECTRONS PER PICTURE ELEMENT

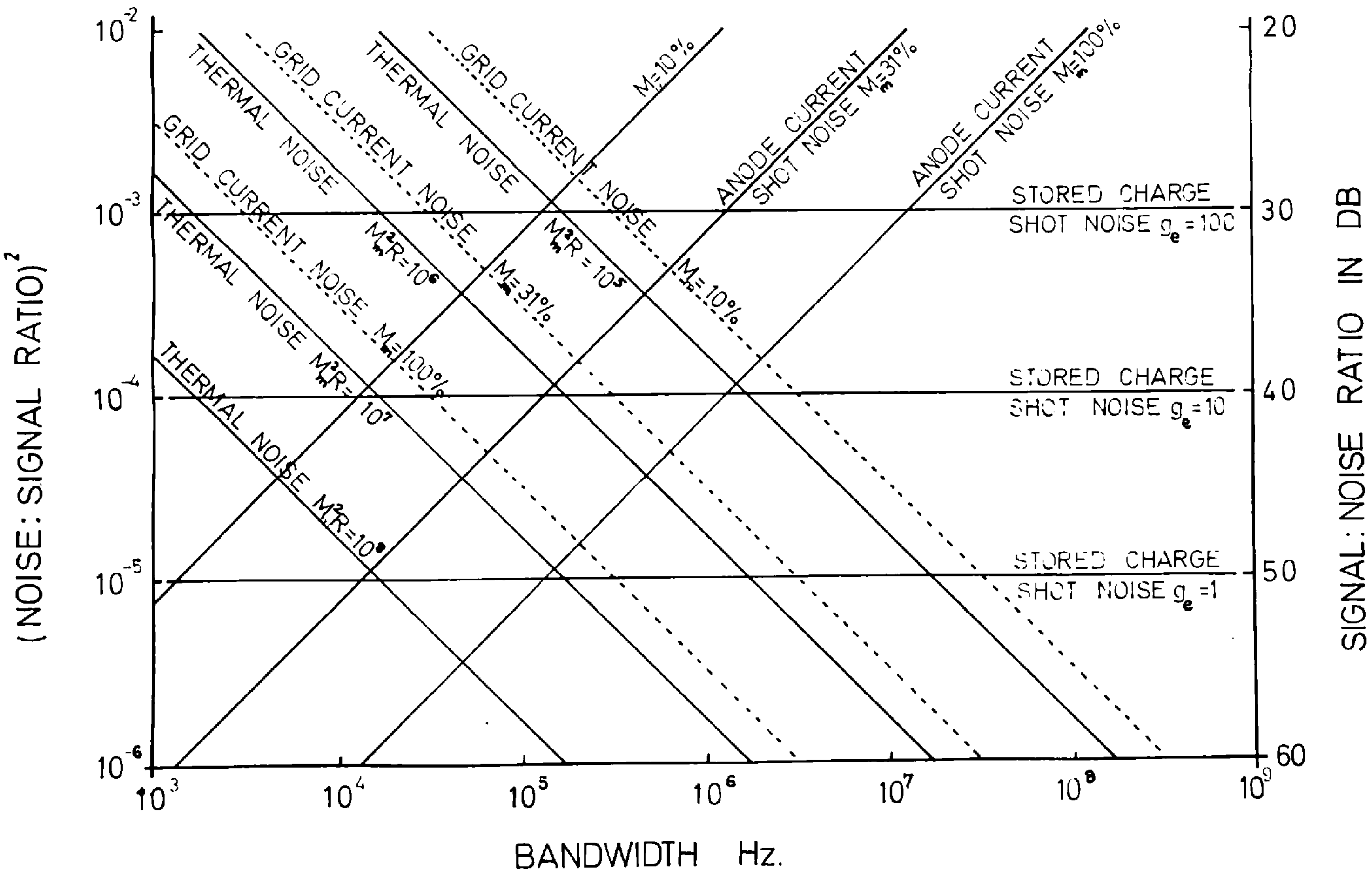

FIG. 5.5 CONTRIBUTIONS TO NOISE ARISING FROM VARIOUS SOURCES, PLOTTED AS A FUNCTION OF BANDWIDTH, FOR A STORAGE TUBE STORING 10^6 ELECTRONS PER PICTURE ELEMENT

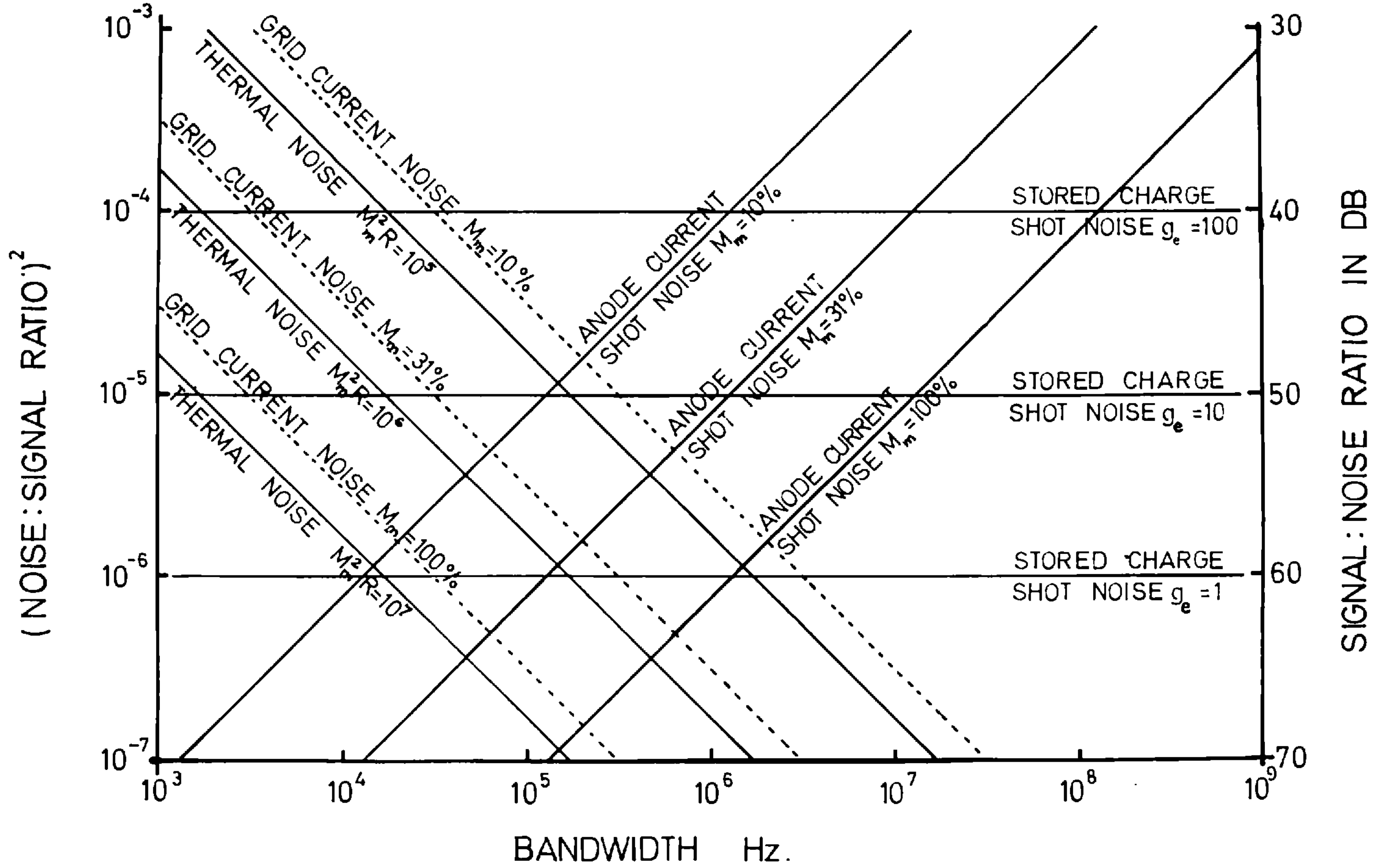

FIG. 5.6 CONTRIBUTIONS TO NOISE ARISING FROM VARIOUS SOURCES, PLOTTED AS A FUNCTION OF BANDWIDTH, FOR A STORAGE TUBE STORING 10^7 ELECTRONS PER PICTURE ELEMENT

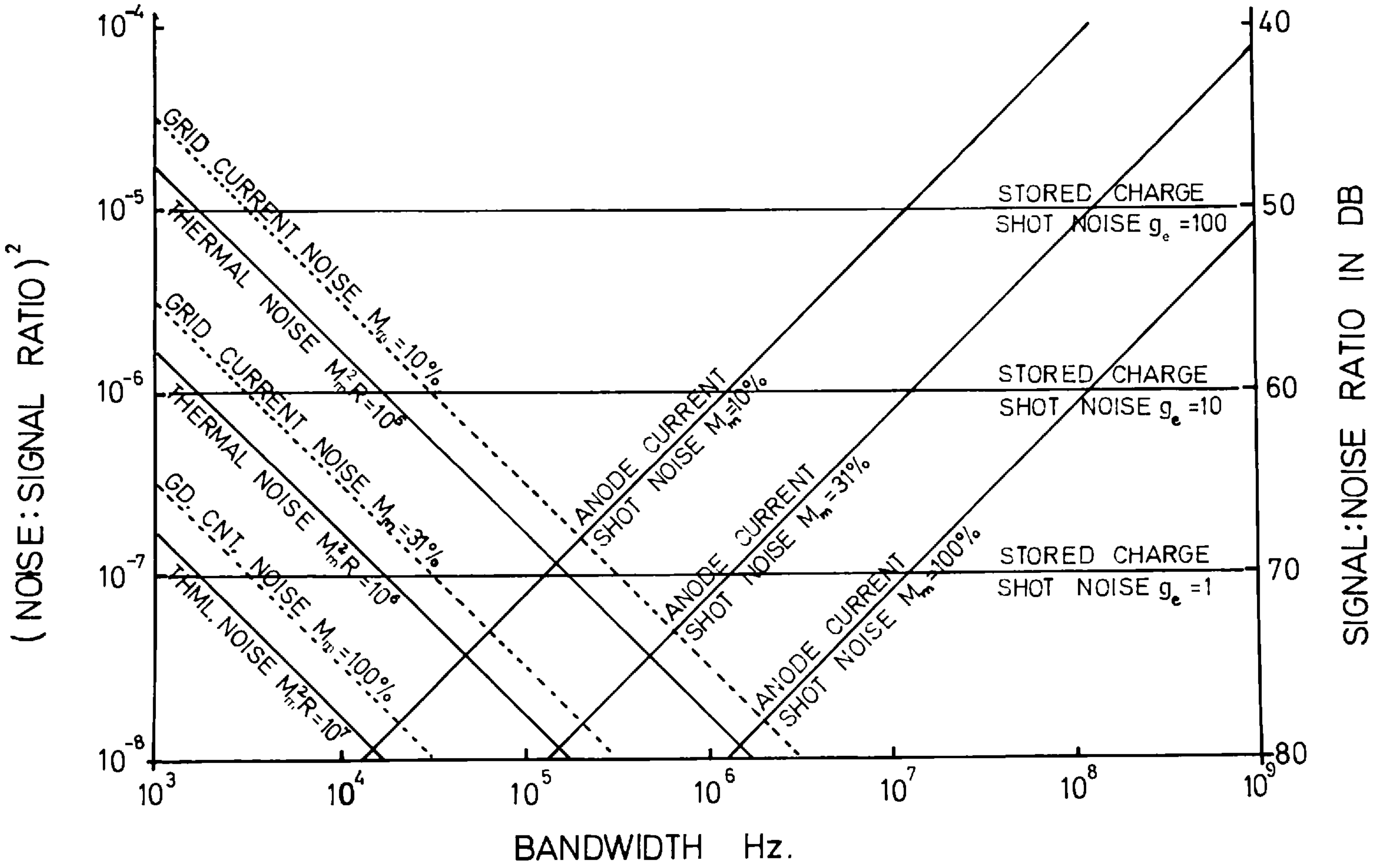

5.9. Noise in a camera in which the signal is derived from scanning beam electrons. reflected from the storage target and amplified by an electron multiplier.

This method of signal generation was first described by Rose et al[146], being one of the original features of the image orthicon camera tube (see below §6.3). A schematic illustration, representing this mode of signal generation is given in fig.5.7.

As the charge image on the storage surface of a target is scanned with low velocity electrons, the scanning electrons, not required to discharge the target will be reflected from the potential barrier, encountered at the target surface. They return towards the electron gun where they may be collected by the aperture of an electron multiplier. This amplifies the signal to give a current at the multiplier output, large enough to be further amplified electronically without increasing the noise.

Let $\overline{n_b}$ = the mean number of electrons, available in the scanning beam to discharge a picture element.

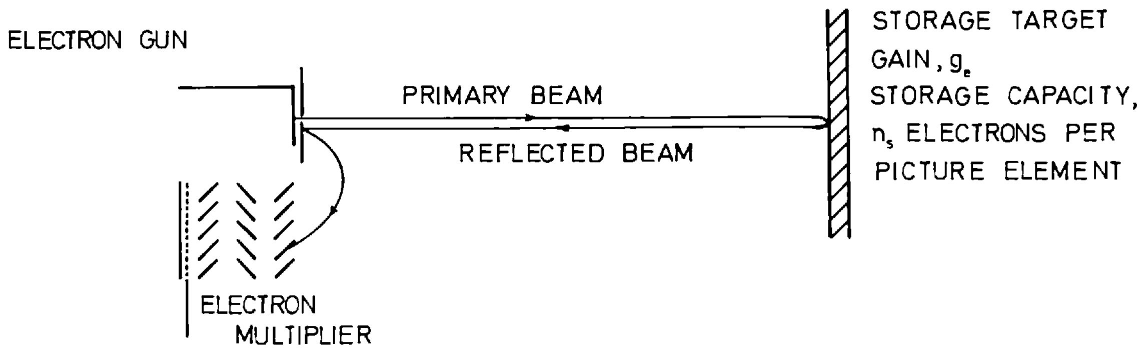

FIG. 5.7 SIGNAL GENERATION BY MULTIPLICATION OF SCANNING BEAM ELECTRONS REFLECTED FROM THE STORAGE TARGET

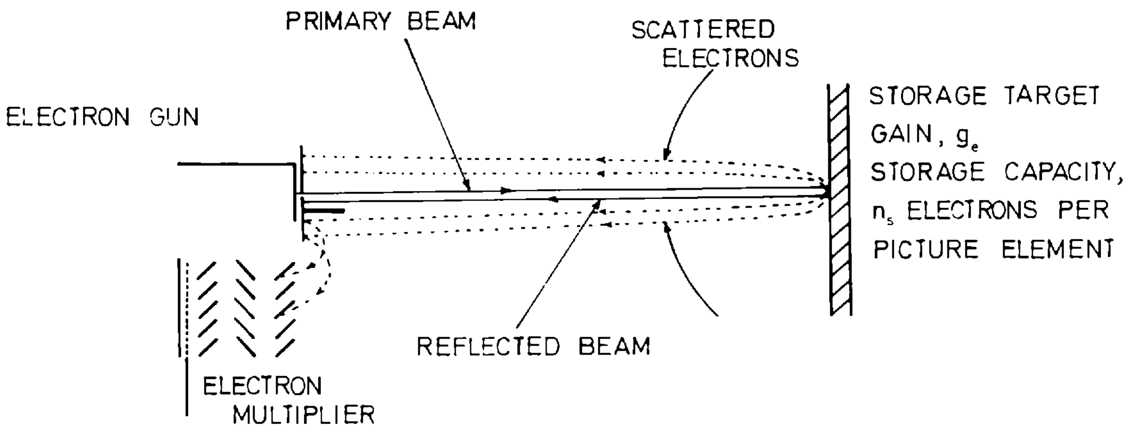

FIG. 5.8 SIGNAL GENERATION BY MULTIPLICATION OF SCANNING BEAM ELECTRONS NON-SPECULARLY SCATTERED FROM THE STORAGE TARGET

M_B = fractional depth to which the beam is modulated as it discharges a picture element. (This, of course, is not to be confused with the signal modulation, given by the modulation transfer characteristic).

The current received at the input of the photomultiplier is thus proportional to $(1 - M_B)\ \overline{n_b}$.

Using Eqn. [A2.8], we may write the following relationship to equate the stored charge on a picture element with the charge lost from the beam during read out

$$\overline{n_b}\ M_B = \overline{g_e}\ \overline{P}\ \overline{\sigma} \qquad (5.9)$$

This is the alternating component of the return beam current which may be amplified by a factor of the order of 10^3 by the multiplier to generate the video signal.

The noise to signal ratio $\frac{N_B}{S}$ in the output of a camera tube, using a return beam multiplier has been calculated in the appendix A.4 to be given by:-

$$\left[\frac{N_B}{S}\right]^2 = \frac{\overline{g_e} + 3 + \frac{1}{M_m^2 M_B}}{\overline{g_e}\ \overline{P}\ \overline{\ }} = \frac{\overline{g_e} + 3 + \frac{1}{M_m^2 M_B}}{\overline{g_e}\ \overline{n_e}} = \frac{\overline{g_e} + 3 + \frac{1}{M_m^2 M_B}}{\overline{n_s}}$$

(5.10).

Clearly, the greater the depth of beam modulation, M_B, that can be achieved, the more closely will the signal to noise ratio given by Eqn.(5.10) approach the fundamental limit of stored charge shot noise given by Eqn.(5.1). In practice, it is found impossible to fully modulate the return beam, and a good figure for M_B, measured at the B.B.C. Research Centre is 40%[143]. Livingstone[94] has obtained beam modulations of up to 65%.

An important property of the noise, generated in a camera using return beam read out is that it is 'white', i.e. the noise power is uniformly distributed throughout the frequency spectrum. On the other hand, the noise generated in systems using a head amplifier coupled to a signal plate and working at a bandwidth corresponding to a broadcast standard is 'peaked', i.e. the noise power increases with frequency. (See Eqn.(5.7)). Cameras using return beam multiplier read out thus enable the line standard, and hence, bandwidth to be increased, without the drastic reduction in signal to noise ratio which occurs in thermionically amplified systems. However, at moderate line standards, thermionic amplification can compete with multiplier amplification, since noise power, concentrated at the high frequency end of the spectrum provides the least objectionable form of noise from the standpoint of entertainment purposes. Schade[156] estimates that 10dB more peaked noise can be tolerated than white noise to give the same subjective picture quality.

For scientific applications where there is a free choice of the rate at which read out may be effected, better results may be obtained with a thermionic amplifier, than with return beam read out. This is because for a tube of adequate target capacity, a bandwidth may be selected to make the fundamental limit, arising from the contribution due to stored charge shot noise (Eqns.(5.1) and (5.2)) dominant, greatly exceeding the amplifier noise contributions (Eqns.(5.5), (5.6) and (5.7)), and there is no noise contribution arising from scanning beam current noise. The conclusion that optimum speed scanning and thermionic amplification is superior to return beam and multiplier read out is in agreement with Theile[173].

5.10. <u>Noise in a camera, in which the signal is derived from scanning electrons, scattered from the storage target and amplified by an electron multiplier.</u>

This method of signal generation was developed by Weimer[184] and incorporated in a tube known as the image isocon (see below § 6.4). Isocon scan was aimed at improving the modulation depth of the return beam, entering the electron multiplier, in a tube of the image orthicon type, and its principle is illustrated schematically in fig.5.8.

It must be appreciated that as well as the scanning electrons, specularly reflected from the storage target, some are elastically scattered in a non-specular fashion from the point of impact. The number of electrons thus scattered is approximately proportional to the localized target potential. Thus, if n_s is the number of electrons stored per picture element, and n_1 is the number of scattered electrons, n_s and n_1 are related by a constant of proportionality, R_s, which is of the order of unity.

$$n_1 = R_s n_s \qquad (5.11)$$

By suitable construction of the electron gun and multiplier, it is possible to arrange for a separation edge to shield the multiplier aperture from the reflected beam, so that a proportion of the scattered electrons only are sampled by the multiplier. A certain wastage of scattered electrons, carrying the signal current, occurs in this process, and thus, if A represents the fraction of useful scattered electrons, able to enter the multiplier, the number of electrons entering the multiplier to generate a video signal, n_v, will be given by :-

$$\overline{n_v} = M_m \overline{A}\, \overline{n_1}$$

from (5.11) $$\overline{n_v} = M_m \overline{A}\, \overline{R}_s\, \overline{n}_s \qquad (5.12)$$

from (A2.8) $$\overline{n_v} = M_m \overline{A}\, \overline{R}\, \overline{g}_e\, \overline{P} \qquad (5.13)$$

The factor M_m is introduced to take into account the modulation transfer characteristic of the tube.

Isocon read-out should theoretically enable a fully modulated electron beam to be received by the multiplier, enabling an improvement over the image orthicon to be realised in dynamic range (see §2.6(c)) as the noise component arising from the unused return beam is eliminated. In practice, this theoretical ideal has not yet been achieved, and a small, constant, background current, arising from stray electrons entering the multiplier, provides a small but significant source of spurious noise. The signal to noise ratio which may be achieved, using isocon read-out, has been calculated in appendix A5. to be given by:-

$$\left.\begin{aligned}
\left[\frac{N_T}{S}\right]^2 &= \frac{\overline{g_e} + 3 + \dfrac{1}{\overline{A}\,\overline{R_s}}}{\overline{g_e}\,\overline{P}} + \frac{\overline{B_n^{\,2}}}{M_m^2\,\overline{A}\,\overline{R_s}^2\,\overline{g_e}^2\,\overline{P}^2\,\overline{\sigma}^2} \\
&= \frac{\overline{g_e} + 3 + \dfrac{1}{\overline{A}\,\overline{R_s}}}{\overline{g_e}\;\overline{n_e}} + \frac{\overline{B_n^{\,2}}}{M_m^2\,\overline{A}^2\,\overline{R_s}^2\,\overline{g_e}^2\,\overline{n_e}^2} \\
&= \frac{\overline{g_e} + 3 + \dfrac{1}{\overline{A}\,\overline{R_s}}}{\overline{n_s}} + \frac{\overline{B_n^{\,2}}}{M_m^2\,\overline{A}^2\,\overline{R_s}^2\,\overline{n_s}^2}
\end{aligned}\right\} \quad (5.14).$$

Typical values of R_s, A, and B_n, given by Weimer[184] are 2, $\frac{1}{4}$ and $\frac{n_s}{20}$ respectively, where n_s is the charge stored by a picture element, giving a peak white signal. Substituting these figures in eqn.(5.14) enables a direct comparison to be made with the signal to noise ratio obtained with reflected electron return beam read-out, given in eqn.(5.10). It can be seen that for high gain targets, i.e. $g_e \approx 5$–7, a small improvement is obtained for the signal to noise ratio in the highlights by using isocon read-out, even when a good figure, e.g. $M_B = 40\%$, is used for the beam modulation factor with reflected beam read-out. In the lowlights, however, the reduction of the beam modulation, M_B, for reflected beam read-out, results in a much greater improvement being obtained by use of isocon scan, and a factor of four has been quoted[184] as the increase in signal to noise ratio that may be realised. A further advantage of isocon read-out over reflected beam read-out arises from the fact that scenes of very different light level may be observed in sequence without the beam current requiring adjustment.

While isocon scan was originally developed for use in tubes of the image orthicon type[184], Cope et al[24],[25] have reported the improvement in performance which may be realised when this type of read-out is used in tubes, incorporating photoconductive targets.

CHAPTER 6

A SURVEY OF CHARGE STORAGE IMAGE DETECTORS.

In the early days of television development, it was realised that a considerable improvement in sensitivity could be realised if, instead of sampling the signal from each picture element only once per frame, the signal from each picture element could be integrated and stored over a frame period, prior to read off. All sensitive television cameras, developed subsequent to the Farnsworth Dissector exploited this principle, and could therefore be described as charge storage image detectors.

The literature contains several excellent review articles, describing commercial television cameras[107, 111, 121, 122, 186]. The emphasis of these reviews tends to be on the application of these cameras to broadcasting. In this chapter, a discussion will follow on the performance of sensitive television cameras and other charge storage image detectors, when applied to the problem of observing faint images of low contrast.

6.1. The iconoscope and the image iconoscope.

These early television cameras[74, 107, 111, 186] employed charge storage, but the use of a high velocity reading beam resulted in only about 5% of the stored charge being used in the generation of a video signal. Degradation of the video signal by effects arising from redistribution electrons prevented these tubes from seriously competing with photography as image detectors when used under standard conditions. However, by using the technique of pulse biassing to avoid redistribution effects, and a scanning beam, generated by a flying light spot, focused on the photocathode, Heimann(67) was able to use an image iconoscope to integrate satisfactory pictures for periods of up to half an hour.

6.2. <u>The C.P.S. Emitron (Fig.6.1)</u>.

The tube(57, 112) consists of an envelope with a gun (1) at one end and a transparent photoemissive target, prepared in the form of a mosaic on a thin (0.003") glass target, (2), backed by a transparent conducting signal plate (nesa). The remainder of the tube is a low velocity scanning system whose essential features have been described above (§ 5.3(d)).

A charge image, created on the target by photoemission may be retained for a period, dependent on the insulation between mosaic elements. At room

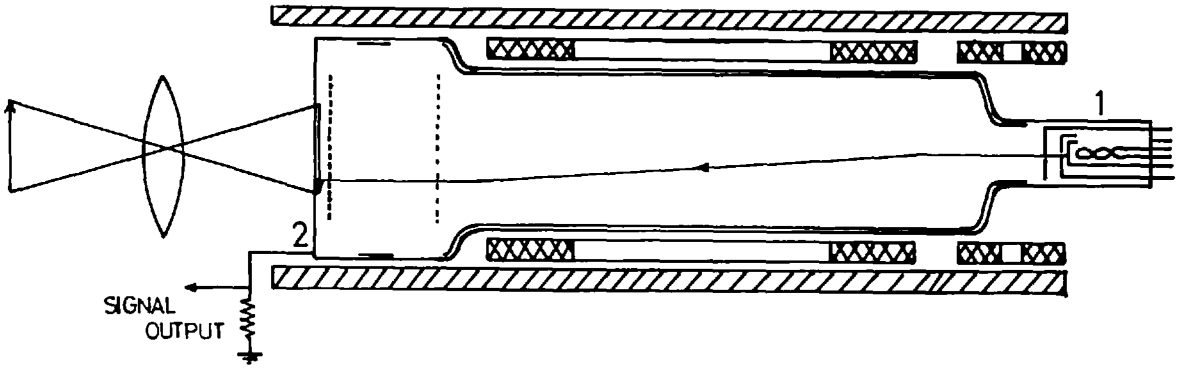

FIG. 6.1 THE C.P.S. EMITRON

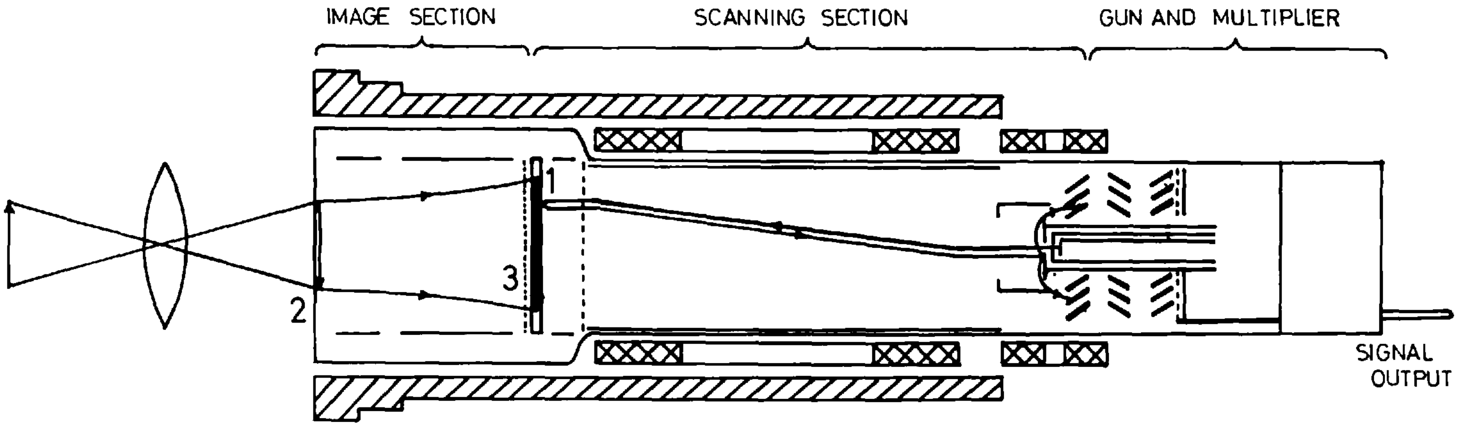

FIG. 6.2 THE IMAGE ORTHICON

temperature, this period is of the order of 30 seconds, but by cooling the target to -55°C., Randall[141] was able to extend the useful integration time to one hour.

The capacity of the target of a C.P.S. Emitron is 1,000 pF, and its response falls to about 55% at definitions of 350 T.V. lines[57]. The gamma of the tube is unity, which is of advantage for scientific applications, but gamma correction is required when the tube is used for entertainment purposes.

6.3. <u>The Image Orthicon (Fig.6.2).</u>

This camera tube[146] is constructed with a thin storage target, (1), mounted parallel to a photocathode (2). Electrons from the photocathode are accelerated to about 300 volts, and focused on to this target, causing reflected secondaries to be emitted. These are collected by a mesh, (3), spaced about 0.002" from the target, and held at about 2 volts positive with respect to the scanning gun cathode. The target is scanned from the reverse side, and the signal generated by the return beam mechanism, described above. (§ 5.9). Because the charge image is created on one side of the target, and is neutralized by scanning the other, it is necessary that the target should be sufficiently conducting to allow some charge exchange between the two surfaces, without appreciable lateral leakage taking place to degrade resolution.

The time constant, τ, of the target is independent of the geometry, but depends on the resistivity, ρ, and the permittivity, ε, of the target material. It is given by

$$\tau = \varepsilon \varepsilon_0 \rho$$

A modified form of soda glass, with a conductivity three orders higher than ordinary window glass has been widely used as an image orthicon target, this having a time constant, comparable with a broadcast frame period. However, the current carriers which transport positive charge from the photocathode side of the target to the scanned surface are sodium ions, which perform a one way transit only. Continued migration of these sodium ions results in a deficiency of sodium on the cathode side, creating a highly insulating layer in the target. This marks the end of the useful life of the image orthicon which is said to have become "sticky".

A search for new target materials, not subject to this defect, has led to the development of the

Elcon target[7]. This is a glass, containing substantial amounts of titanium oxide, prepared in a reducing atmosphere, so that a large percentage of the titanium is in a trivalent state. Such glass is unaffected by caesium vapour, used to process the photocathode, and is not subject to changes in properties due to ion migration, as conduction is due to electron transfer between the ambivalent titanium ions.

For long exposure storage applications, however, glass targets have too low a resistance to allow a charge image to be integrated in an image orthicon over an appreciable period of time, without excessive lateral leakage. As an alternative to glass, magnesia may be used as the image orthicon target material[30]. Use of this material does give rise to certain disadvantages and problems. Picture background can arise from the transmission through the target of primary photoelectrons, magnesium oxide has a granular structure which is apparent in pictures generated by tubes operating at high light levels[44], and it is difficult to prepare blemish free magnesium oxide layers.

Such defects have tended to disqualify magnesium oxide as a target material for image orthicons, used in entertainment[19], but it has found application in cameras, applied to scientific observation [37, 38, 95, 96]. Magnesium oxide targets have secondary emission gains of up to eleven, compared with about four or five for glass, and conduction is electronic rather than ionic as in soda glass[30]. Further, the crystal structure of the target is such that anisotropic conduction takes place, favouring the transfer of charge between the faces of the target, while restricting undesirable lateral charge leakage.

Image orthicons, incorporating magnesium oxide targets have enabled integration times of tens of minutes to be realised[38], and it was possible to extend this period to over an hour by cooling a selected tube to -100°C.[96].

The performance of the image orthicon is limited by just a few shortcomings to which the tube is subject.

First, beam shot noise, present in the incompletely modulated return beam, prevents high quantum efficiencies from being realised in the low-lights of a picture.

Secondly, redistribution of secondary electrons occurs around highlights, where the target has become charged to the same potential as the closely spaced collector mesh. This mesh potential (2 volts) defines the maximum voltage excursion of the target, and produces a discontinuity or knee in the transfer characteristic. This effect is undesirable from the stand point of using the tube as a scientific measuring instrument, and for such applications, the tube should only be exposed up to the knee. However, for entertainment applications the knee in the characteristic can be exploited to give a form of gamma correction. Also, the redistribution electrons can give a black border effect which enhances definition, but for strong highlights, the black border effect becomes objectionable. Miyashiro et al[130] have described a method of mitigating the effect by means of an additional collector mesh.

A third defect which may be encountered in the image orthicon is known as dynode spot. By this, a secondary emission image of the first dynode of the multiplier in a focal plane of the return beam becomes superimposed on the useful picture.

The fourth disadvantage of the image orthicon is its relatively small target capacity, which limits the signal to noise ratio which may be realised in the output signal, and hence, the minimum detectable contrast in a single frame. The target capacity of the three inch image orthicon is only 100 pF[122]. The development of the four and a half inch tube[69] doubled the target capacity.

Ingenious operating techniques have enabled astronomers to further increase the information that may be effectively stored by an image orthicon, in a single exposure. Livingstone[95] describes how the tube may be exposed with a high target to mesh voltage and then, after exposure, the mesh potential is lowered so that the maximum target potential, seen by the scanning beam is only two volts. A series of frames are then read out as the mesh potential is successively advanced in two volt steps.

Morton[133] gives an account of a method of increasing the capacity of storage tubes, used to observe faint, low contrast images, known as multiple storage. The camera is operated at a frame rate faster than the required integration period to discharge the target each time it charges to capacity. The lift control is set, so that the video signal contains the alternating part of the signal only, rejecting the d.c. component of the signal, corresponding to background. The video signal is stored on a second storage tube, this process of transfering the alternating part of the information stored in successive frames being continued, until the second storage device becomes charged to capacity. In this way, the useful integration time is extended. During the second charge storage, the noise from successive frames increases by the square root of the number of the frame, while the signal increases linearly.

Hynek et al[73] used a technique, known as hypersensitisation, which exploited the fact that a target, continuously scanned in the dark, adopts a potential 4 to 5 volts negative with respect to the gun cathode. Hence, when the tube is exposed to a low contrast image, a large amount of background is subtracted, enhancing the contrast that may be obtained on read out.

Gebel et al[56] have used a three inch, wide spaced image orthicon to photograph the planets in daylight, even recording the moons of Jupiter, without resorting to any of the methods described above to increase the effective storage capacity of the tube. Baum[10] estimates that the contrast of Jupiter's moons against daytime sky background is of the order, 10^{-2}.

Livingston[96] has evaluated the limiting resolution of an image orthicon under normal operating conditions as 22 line pairs per mm. This may be increased to 45 line pairs per mm. by photographic integration of many frames to reduce the noise.

6.4. <u>The Image Isocon. (Fig.6.3).</u>

This tube[23,184] is very similar to the image orthicon, but derives the signal from scanning electrons, elastically scattered from the target, rather than from the specularly reflected electrons, used in image orthicon read out. The mechanism of signal generation is described above, (§ 5.10), and the means by which this is accomplished in a practical device is illustrated in fig.6.3. A beam aperture (1),

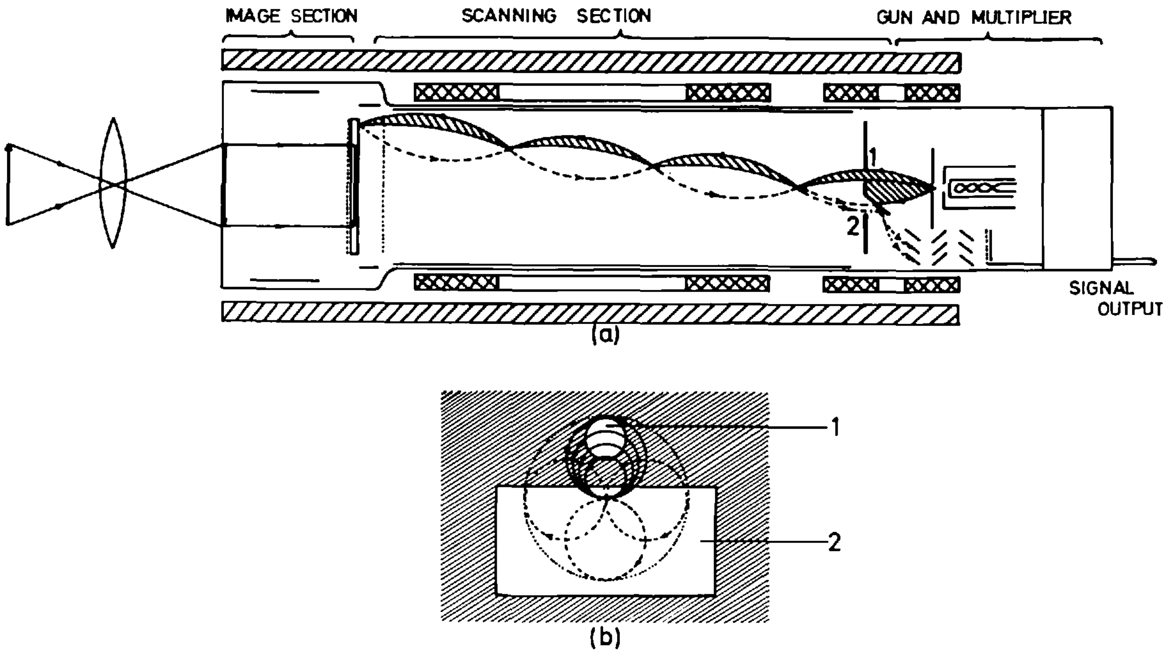

FIG. 6.3 THE IMAGE ISOCON

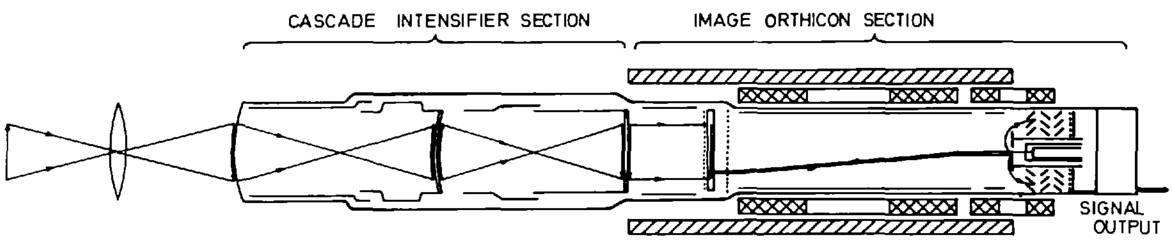

FIG. 6.4 THE INTENSIFIER ORTHICON

in front of the gun, and at an antinodal plane selects only those electrons with excess helical motion to provide the scanning beam. The scanning beam and the reflected beam are thus restricted to lie within the narrow pencil, shown shaded on the diagram.

A proportion of the scattered electrons which lie within the envelope shown by the dotted line are selected by means of another aperture, (2), mounted at the antinodal plane, whence they are fed to an electron multiplier. The number of scattered electrons is approximately proportional to the stored charge, and the video signal generated will therefore be of opposite polarity to that derived from a conventional image orthicon. Fig.6.3(b) represents the beam and multiplier aperture system, and illustrates the various electron trajectories in an equatorial plane.

The reduction of noise, especially in the blacks, enables the image isocon to realise a better equivalent quantum efficiency, and to obtain an order of magnitude improvement in dynamic range, over the image orthicon. Isocon beam current does not have to be adjusted (as in the image orthicon), to reduce the noise when dark objects are being observed, and dynode spot, a defect encountered in image orthicons (§ 6.3) is absent in isocons, because the return beam arrives at the multiplier, out of focus.

While superior in many respects to an image orthicon, the image isocon is still subject to certain disadvantages. The setting up and adjustment is very critical, and considerable skill is necessary to meet the close tolerances required for optimum operation. Slight misadjustment can lead to spurious side effects, and even to reversal of signal polarity, due to the reflected beam entering the multiplier. Even optimally adjusted tubes are inferior to image orthicons from the standpoint of definition and lag. This is because the scanning electrons to be focused are non-paraxial and more prone to aberration, and lag is increased because the beam aperture limits the amount of current, available to discharge the target. The limiting resolution of an image isocon is about 900 television lines.

6.5. The Intensifier Orthicon. (Fig.6.4).

This tube[106,132,137] consists of an image intensifier and an image orthicon, constructed within the same envelope. By achieving high gain, prior to read out, beam noise becomes relatively unimportant in comparison with the fundamental limit of photon noise, but an improvement in signal to noise and in dynamic range has been obtained by operating the tube in the isocon mode[106].

Intensifier orthicons can be constructed with up to three cascade stages of intensification, but at the expense of some resolution. With optimum illumination, the limiting resolution of a one-stage intensifier orthicon is 600 television lines. For a two stage intensifier, the limiting resolution drops to 450 television lines. Three stages of image pre-intensification are necessary however for single photoelectron scintillations to be readily observed[132]. The R.C.A., C74036 intensifier orthicon was able to operate at photocathode illuminations as low as 10^{-9} ft. cd., at which light level, the tube was able to resolve 100 television lines[106].

6.6. The vidicon and the plumbicon. (Fig.6.5).

These are two very similar tubes, incorporating photo-conductive targets. A field gradient is maintained across the photo-conductive layer (1) by means of a transparent conducting signal plate, (2) and a low velocity scanning beam (3). The charge image is created on the scanned surface as current is able to flow across the layer in illuminated regions.

The emergence of the vidicon[185] as a camera tube represented the advent of a sensitive, simple and compact television pick-up device. Early vidicons incorporated p-type amorphous selenium target layers[177], but the short life (300 hours) of such tubes led to the development of target layers, constructed from n-type semi-conductors, such as the sulphides and selenides of arsenic, antimony, cadmium, and lead.

Vidicons incorporating antimony trisulphide targets have under normal operating conditions, a gamma between 0.5 and 0.65 and an approximately panchromatic spectral response[101]. These are ideal properties for entertainment purposes, but for scientific applications, special photo-conductive tubes[28] have been developed with infra-red[68,171] and ultra-violet[181] responses.

Development of vidicons with a separately connected mesh enabled very good resolutions to be realised in this type of tube, giving modulations of up to 80% with 375 television line test patterns[102]. On the small target of the standard one inch vidicons, this corresponds to 40 line pairs per mm. An even more compact camera tube, the half-inch vidicon has been developed[29,182] which can give a modulation depth of 40% at 400 television lines.

While possessing so many excellent properties, the vidicon is subject to the defect of exhibiting lag, which can be due to both solid-state and discharge lag. Dresner[183] showed that discharge lag could be reduced by scanning the target with a high velocity beam, but this was accompanied by undesirable redistribution effects. The most successful method of combatting discharge lag is to prepare the target by evaporating the layer in an inert gas atmosphere. This enables a spongy layer to be produced which has a lower electrostatic capacity than the solid layer, because it is mechanically thicker and has a lower dielectric constant, but which is no more optically dense than the solid layer. Solid state lag, however, remains a serious defect, especially at low light levels when the lag current, arising from trapped carriers represents a significant proportion of the signal current. Solid-state and capacitive lag have been deliberately increased in the so called storage vidicons, where lag has been exploited to retain a display on a monitor[99,183]. However, a distinction must be drawn between this type of 'storage tube', and the type of camera with which this thesis is concerned, which integrates light images over long periods of time, converting them into the form of charge images, stored on an insulating target. The vidicon is not very satisfactory for this type of storage, because the resistivity of the photoconductive target is not particularly high, typical dark currents being of the order of 10^{-8} amps.

Many of the defects of vidicons, using impurity semiconductor targets have been overcome in the plumbicon[31,34], which incorporates a lead oxide photo-conductive target. The bulk of this target is prepared in a sufficiently pure state to be an intrinsic semiconductor, but the surface in contact with the signal plate is doped to be n-type, while the scanned surface is doped to become p-type. The absence of trapping centres in the intrinsic layer reduces solid-state lag to negligible proportions, and enables a strong internal field to be established in the layer with fairly moderate signal plate potentials, e.g. 30 volts. The establishment of a strong internal field in the layer enables carrier transit time to be reduced to less than carrier life time, achieving the condition necessary for saturated photo-current and high sensitivity. A typical figure quoted for target sensitivity is 210 µA/lumen, but sensitivities as high as 400 µA/lumen may be attained[34].

The gamma of the plumbicon is unity. This may be explained by the fact that when a tube is delivering a saturated photo-current, i.e. a current, independent of potential gradient in the target, the current will remain directly proportional to light level since it will be unaffected by small reductions of potential gradient, corresponding to high lights.

De Haan et al.[34] describe how layers may be prepared to be red or blue sensitive, or to have a panchromatic response. The colour response is strongly dependent on the impurity layers which sandwich the intrinsic lead oxide. These impurity layers also cause the target to behave as a reverse biased, PIN diode (p type-intrinsic-ntype) under normal operating conditions. This reduces the dark current encountered in plumbicons to much below that, occurring in normal vidicons, seldom exceeding 5×10^{-10} amps. Even this, however, is too large a leakage current to enable a plumbicon camera to integrate and store an image for more than several seconds.

6.7. The Intensifier Vidicon.

This type of camera may be regarded as the photo-conductive analogue of the intensifier orthicon, consisting of an image intensifier and vidicon, assembled within a common envelope. Tubes of this type were constructed and assessed at Imperial College by Enstone(50). The phosphor output of the intensifier and the photo-conductive layer were deposited on opposite sides of a thin mica sheet (5μm), enabling efficient coupling to be achieved without serious loss in resolution. These tubes were difficult to make with optimum performance of all photo-sensitive elements, as the processing of the second photo-surface can effect the properties of whichever type of photo-surface was prepared first, be this photo-emissive or photo-conductive. Successful highly sensitive tubes of this type have been constructed, but they are subject to the defects associated with photoconductive targets, discussed above (§ 6.6).

6.8. The Ebicon. (Fig.6.6).

Solid state conduction may be induced by the action of energetic electrons, as well as by photons. Electron bombardment induced conductivity has been studied by Ansbacher et al[5], who showed that under favourable conditions, it is possible for a single bombarding electron to excite as many as 10^4 electrons, into conduction bands. This phenomena suggests a method of constructing a sensitive television camera, and Schneeberger et al[160,161] describe such a tube, called the Ebicon, which is shown diagrammatically in fig.6.6. Essentially, it is similar to an intensifier vidicon (§ 6.7), except that the energetic primary photoelectrons (1) are focused directly on to an arsenic trisulphide target (2) instead of being first converted into photons by a phosphor. A field gradient is maintained across the target layer by means of an electron transparent, conducting signal plate (3) on one side, and a low velocity electron beam scanning the other (4). Thus, the electrons,

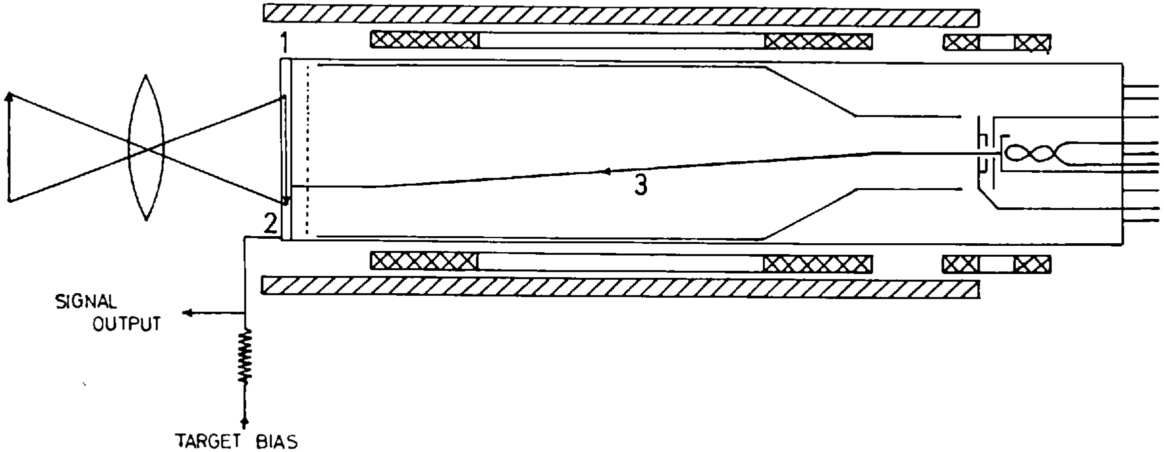

FIG. 6.5 THE VIDICON

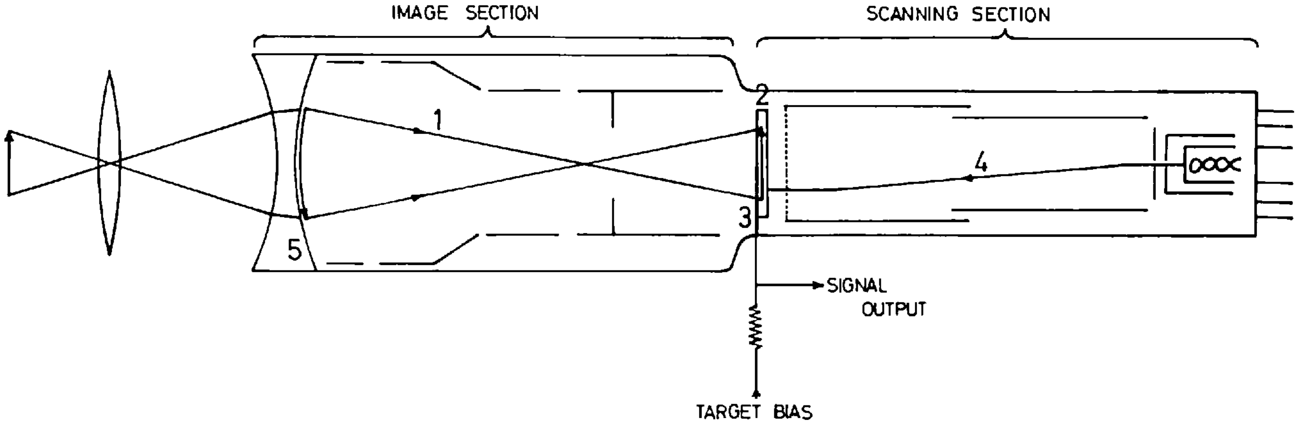

FIG. 6.6 THE EBICON

excited into the conduction bands by the energetic primaries, move under the influence of the applied field, creating a charge image in the target. Using accelerating voltages of the order 10 keV and biases of up to 40 volts, gains of the order of 500 have been obtained.

The camera was developed for space research, and is therefore focused and scanned electrostatically. A curved photocathode (5) is used to assist with the design of the electrostatically focused image section. The resolution obtained on such a tube is 8 line pairs/ mm., which corresponds to 500 television lines, but better definition could be achieved by using magnetic focusing.

Alexander et al[2] describe tubes, exploiting electron bombardment induced conductive targets which use return-beam multiplier read out. Targets fabricated from aluminium oxide, magnesium fluoride, and from zinc sulphide were used. The first two substances were sufficiently good insulators to enable faint optical images to be integrated, and storage periods of the order of days were reported.

The principle defect encountered in tubes, incorporating electron bombardment induced conductivity targets lies in the considerable solid-state and capacitive lag. The discharge lag arises from the fact that targets have to be thin, to enable good gains to be realised. A further disadvantage associated with the tube lies in the difficulty, experienced in manufacturing blemish free targets.

6.9. <u>Reversible Target Integrating Storage Tube. (Fig.6.7).</u>

Beurle and Slark[(15),(163)], working at Imperial College, constructed and assessed storage tubes of the type illustrated in fig.6.7. Photoelectrons are electromagnetically focused on to a dielectric target (1), where a charge image may be created by either reflection secondary emission, or by electron bombardment induced conductivity. Primary energies of 1 or 2 keV are used for the first signal generating mechanism, and 15 keV for the second. After creating a stored charge image, the target is rotated mechanically by means of a magnetic cross bar (2) and exposed to a low velocity scanning beam (3) which discharges the target, generating a video signal in the conventional manner.

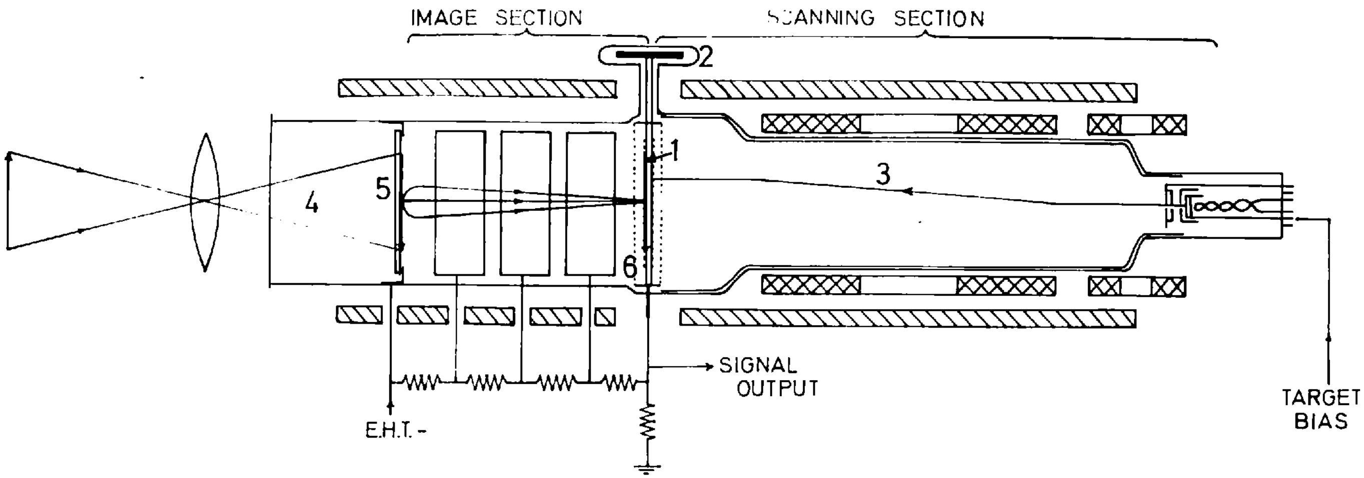

FIG. 6.7 REVERSIBLE TARGET INTEGRATING STORAGE TUBE

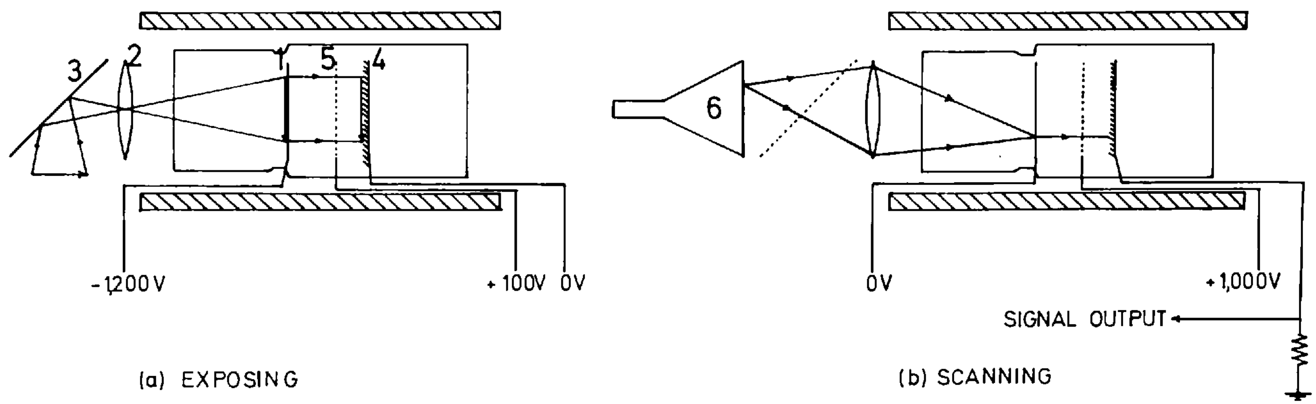

FIG. 6.8 OPTICALLY SCANNED INTEGRATING STORAGE TUBE

Various target materials were investigated, but the best results were achieved, using magnesium fluoride, evaporated to a thickness of 2 μm. on to a nesa substrate. Magnesium fluoride was found to be a sufficiently good insulator to enable charge images to be stored for days, without appreciable loss of intensity and definition.

By introducing a processing compartment (4) in which a photocathode (5) could be processed and then reversed, so that the sensitive surface faced the target, Slark was able to prevent the alkali vapours, used in processing, from entering the working part of the tube to create low work function surfaces and reduce the insulation of the target. In this way, background was reduced to a low enough level to enable integration periods of up to two hours to be attained.

Beurle and Slark investigated methods of increasing the storage capacity of the target, when used to observe low contrast images by compensating for the uniform background, so that only the variations in the high-lights are read off during scanning to provide a well modulated signal. A method of doing this, known as pre-exposure compensation, was devised in which the tube was exposed to a uniform background with the secondary emission collection mesh (6) held at a negative potential. In this way, a negative charge was deposited over the target to cancel the positive charge, corresponding to picture background, which is produced during the subsequent integration of a low contrast charge image. This method of background compensation was more effective than the simpler method of shifting the reading gun cathode potential, relative to the target, since it also provided a limited degree of compensation for non-uniformities in the photocathode.

While functioning well from the standpoint of integration and storage, certain problems and disadvantages were encountered in using this type of tube. Many troublesome features were associated with the moveable target assembly, besides the inconvenience imposed by making simultaneous exposure and read off impossible. Poor definition, discharge lag, and target blemishes all tended to detract from the tubes performance, which was operated at normal television scan rates, where amplifier noise and inadequate scanning beam current prevented optimum results from being obtained.

6.10. Optically-scanned Integrating Storage Tube. (Fig.6.8).

The shortcomings of the reversible target storage tube lead Beurle and Slark to the conclusion that further development of charge integrating storage tubes should be along the lines of the photocathode scanned storage tube, suggested earlier by McGee(110).

An investigation of tubes of this type was carried out by Khan(79) and Mende(127) at Imperial College, under the direction of Dr. Twiddy(129).

The optically scanned device is illustrated in fig.6.8. During exposure (fig.6.8a), an optical image is projected on to a semi-transparent cathode (1) via a lens (2) and a mirror (3). Photoelectrons liberated from the cathode are accelerated to about 1 kV, and focused by means of a strong uniform magnetic field on to a thin (10 µm.) magnesium fluoride target, deposited on a conducting signal plate (4). Secondary electrons are emitted from the target, to be collected by the mesh (5), leaving a positive charge image, stored in the target.

This charge image is converted into a video signal by scanning the target with a low velocity electron beam, derived by focusing the raster of a low persistence phosphor (P16) cathode ray tube (6) on to the photocathode (1). (fig.8.6(b)). Read out conditions are established by adjusting the photocathode voltage to be at signal plate potential and removing the mirror (3) to expose the photocathode to the cathode-ray tube.

Good results were achieved after certain precautions were taken to optimise performance. Slow speed scanning was employed to reduce amplifier noise and to give adequate beam current to discharge the high capacity (6,800 pF) target. Phosphor, photocathode and optical non-uniformities were compensated by a feed-back system between the photocathode and the cathode-ray tube modulator. A short working length between the cathode and target, 1.5 cm., facilitated focusing. The reversible photocathode assembly (see § 6.9) enabled background and target leakage to be minimized.

Under these conditions, it was possible to integrate for up to 3 hours, and to store images for days. Quantum efficiencies, approaching that of the photocathode were realised.

The photocathode scanned tube was found to be subject to certain defects. As in the case of the image orthicon (§ 6.3), there is a loss in primary photoelectrons due to the presence of the collector mesh,and also, redistribution effects occur. Setting up this tube can be tedious, since, like the reversible target storage tube (§ 6.9), it is impossible to expose and read-out simultaneously. The definition of the system is limited by the flying spot scanning mechanism. The photoelectrons used in read-out are spread over a 2π solid angle and are, therefore, much more difficult to focus, than the praxial electrons, selected by the limiter of an electron gun. The limiting resolution of the system is only about 400 television lines.

6.11. Comparison of the performance of charge storage image detectors, applied to the problem of detecting faint, low-contrast images.

Of the camera tubes surveyed above, most have been developed with broadcast applications in view, and the target insulation is often inadequate for long term exposure and storage. In some cases, this problem could be met by cooling the target(141), but this introduces an undesirable inconvenience. Magnesium-oxide target image orthicons have many properties which make them well suited for observing faint images, and they have actually been used in the field by astronomers(37,38,95,96). The relatively low target capacity represents the main disadvantage of the image orthicon when applied to low-contrast image detection.

While tubes, specailly developed for storage applications have high target capacities, such devices considered in this Chapter (§s.6.9 and 6.10) are much inferior to image orthicons from the standpoint of definition, besides imposing the serious inconvenience of making it impossible to simultaneously expose and read out.

Graphical comparisons of various storage tubes are provided by plots of equivalent quantum efficiency, E, (§2.7) and image information recording efficiency, F, (§2.3) as functions of image detail, given in figs.6.9 and 6.10. These curves were computed for

FIG. 6.9 EQUIVALENT QUANTUM EFFICIENCY AS A FUNCTION OF DETAIL FOR VARIOUS TELEVISION-TYPE CAMERA TUBES OPERATED AT OPTIMUM SCAN RATES IN A 405 LINE SYSTEM

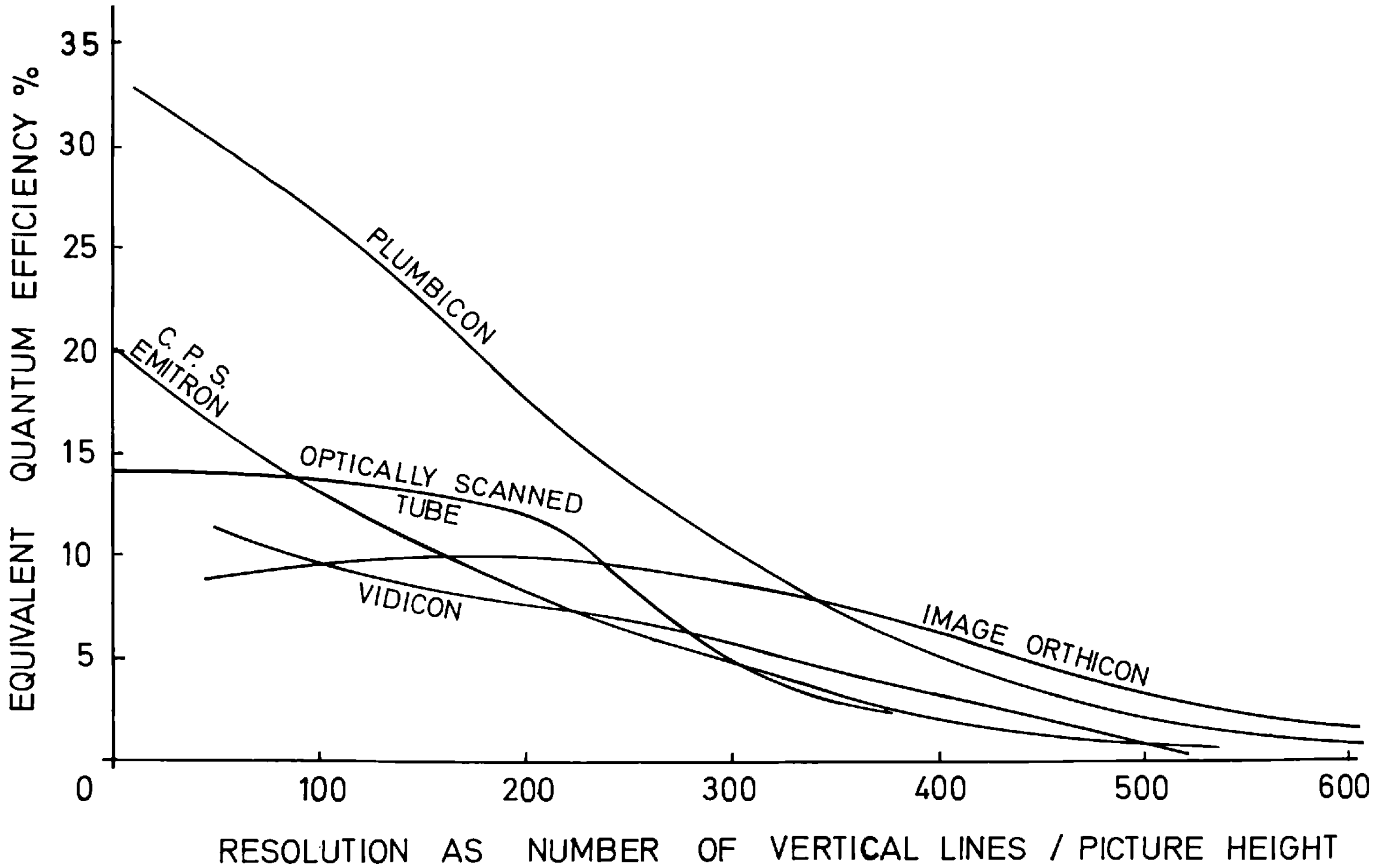

FIG. 6.10 IMAGE INFORMATION RECORDING EFFICIENCY AS A FUNCTION OF DETAIL FOR VARIOUS TELEVISION TYPE CAMERA TUBES OPERATED OPTIMUM SCAN RATES IN A 405 LINE SYSTEM

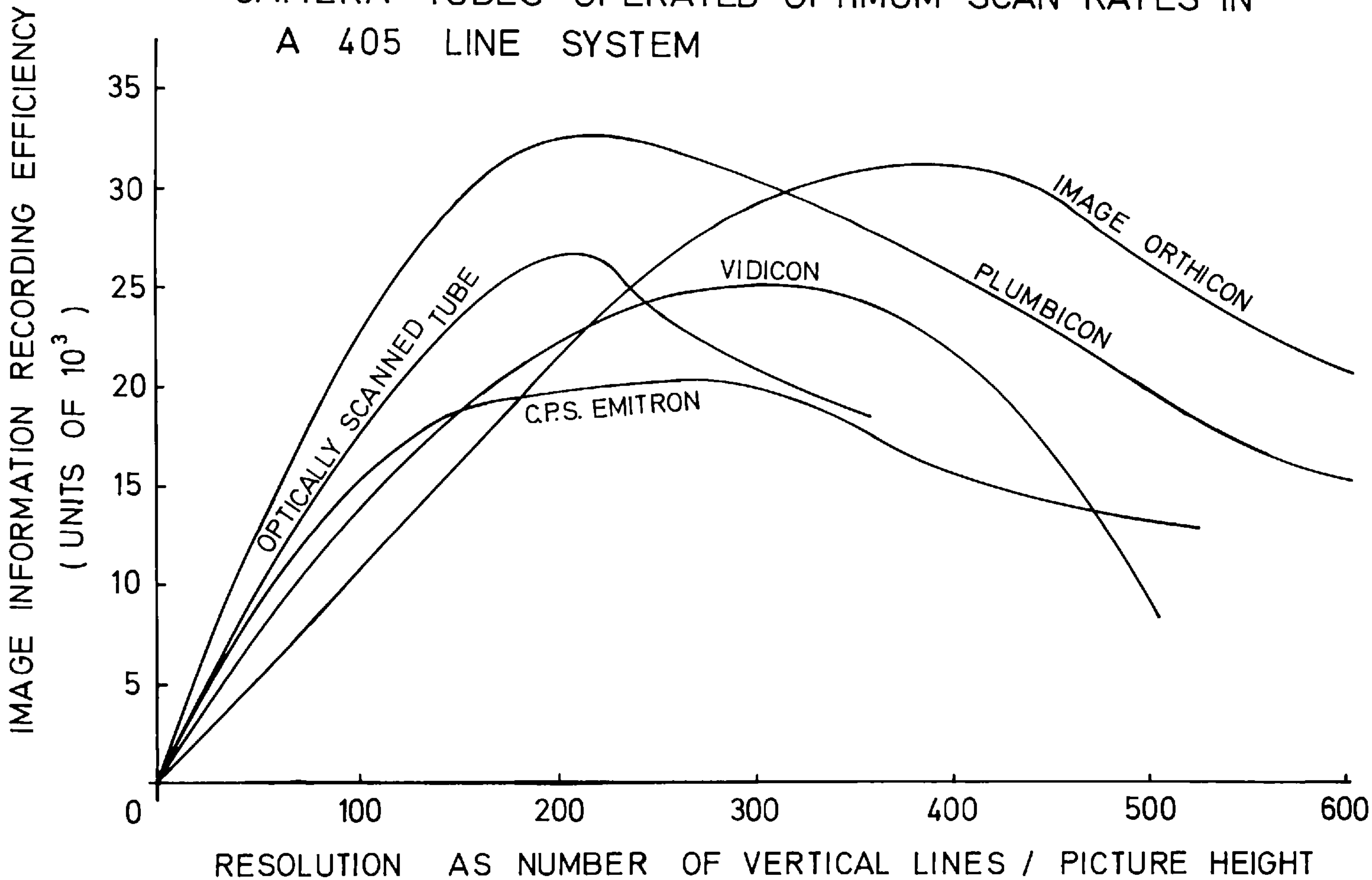

those camera tubes, for which the necessary data were available.

The calculations from which these curves are derived were based on the equations, defining E and F (Eqns.2.25 and 2.1) and used the appropriate expressions for noise, obtained in appendices A.2 to A.4. The number of television lines, represented along the abscissae defines the size of a picture element. For tubes using a head-amplifier, directly coupled to the target, the ordinate at each resolution was calculated, using a value for bandwidth, f_B, of 2×10^5 Hz. This corresponds to the picture elements being scanned at an optimum rate for a head amplifier with an R.5559 input value. (see § 5.8). Eqn.(A 4.6) was used to calculate the output signal to noise ratio for the image orthicon.

All tubes using photoemissive cathodes were assumed to incorporate trialkali cathodes of peak quantum efficiency, 20%. The remainder of the data, necessary to calculate the performance of each specific tube is as follows.

(a) <u>10764A. C.P.S. Emitron</u>.

The modulation transfer characteristic and the total storage capacity, Q, (see §2.6(c)) are given by Gibbons[57].

$$Q = 3.36 \times 10^{10} \text{ electrons.}$$

(b) E.E.V. 8540 Image Orthicon.

The modulation transfer characteristic was obtained from an English Electric Valve data sheet[49]. The curve supplied represented the modulation obtained for a tube exposed at half a stop above the knee, where redistribution effects give an apparent enhancement of definition. (§ 6.3). Thus, the results presented in figs.6.9 and 6.10 are somewhat misleading for this tube, giving rather favourable performance figures for the image orthicon considered.

The figure used for target gain, g_e, was 5 and the calculation was made, assuming a figure of 40% for beam modulation, M_B, in the peak white areas[143].

(c) E.M.I. High Resolution Vidicon, type 9677.

The modulation transfer characteristic and the total storage capacity, Q, were derived from an E.M.I. data sheet[48]

$$Q = 5 \times 10^{10} \text{ electrons.}$$

The sensitivity of the tube will depend on the operating conditions as the gammas is not unity.

For a tube, operating at a target voltage which gives 10^{-8} amps of dark current, and at a light level of 2 ft. cd., the target sensitivity is 77 µA/lumen [48,101]. For a panchromatic response, this corresponds to a peak quantum efficiency σ of approximately 13%.

(d) Plumbicon.

de Haan et al[34] provide a modulation transfer characteristic and give a figure of 210 µA/lm. as a typical target sensitivity. For a panchromatic response, the quantum efficiency of the target at the peak will be about 35%. The electrostatic capacity of the target is given as 1,500 pF., which corresponds to a total storage capacity, Q, of 5×10^{10} electrons.

(e) Optically Scanned Storage Tube.

Mende[127],[129] has measured the modulation transfer characteristic, the target gain, g_e, and the total storage capacity, Q.

$$g_e = 6.$$

$$Q = 17 \times 10^{10} \text{ electrons.}$$

CHAPTER 7

Design, construction, and processing of a new integrating charge storage tube, incorporating a spongy, potassium chloride, target layer.

7.1 Inception of the device.

The discovery by Goetze[59] of Westinghouse that potassium chloride dynodes exhibited remarkable secondary emission gains has been referred to above (§ 4.2). An independent investigation of these layers was undertaken at Imperical College by M.E. Rosenbloom[150], working under Dr. Wilcock. The initial objective of this project was to develop a dynode which could result in T.S.E. intesifiers of improved performance. However, in addition to their high secondary emission gain, these layers were found to possess exceptional insulating properties, which might be exploited with advantage in storage-type camera tubes. Work was therefore started by the author in collaboration with S.B.Mende and M.E.Rosenbloom, under the direction of Dr. Twiddy to construct a television camera tube, incorporating a spongy potassium chloride layer as target.

The first successful tube of this type was constructed at the end of 1962, and a reprint from 'Nature' describing the performance of this early tube is bound with this thesis.

At the time we were constructing the prototype version of this tube, it would appear that the Westinghouse workers were also working on a similar device. Allusions were made in the correspondence columns of scientific journals to a camera, described by Goetze and Boerio(60) at an 'Electron Devices Meeting of the I.E.E.E.', held in Washington. Later, descriptions of the Westinghouse camera appeared in the literature(62,63). More recent work performed by the Westinghouse team on camera tubes, incorporating spongy, potassium chloride targets was described in a series of papers, presented at the third symposium on photo-electronics, held at Imperial College(13, 14, 21, 40, 64).

7.2 Design and Construction of the prototype spongy potassium chloride target camera tube.

The prototype version of the spongy potassium chloride camera tube, constructed at Imperial College is illustrated diagramatically in Fig. 7.1, while Fig 7.2 is a photograph of the device.

An optical image is focused on to an end wall, semi-transparent photo-cathode, (1), where the photo-electrons liberated are electro-magnetically focused on to a spongy potassium chloride target, (2), creating within this layer, a stored charge image. The manufacture, structure, and mechanism of charge image generation of the target are discussed below. (§s. 7.7, 7.8, 10.2, 10.3, 10.4).

Rosenbloom's[150] work had indicated that a maximum in the secondary emission of spongy potassium chloride occurred for primary energies of 7 keV., so the image section was designed to give single loop electro-magnetic focusing for electrons, uniformly accelerated to 7 keV in a magnetic field of 4.5 milli tesla. This required a photocathode target separation of 19 cm.

While the discussion of methods of charge-image read-out, given above in chapter 5 indicated that the best performance from a camera tube may be realized by using

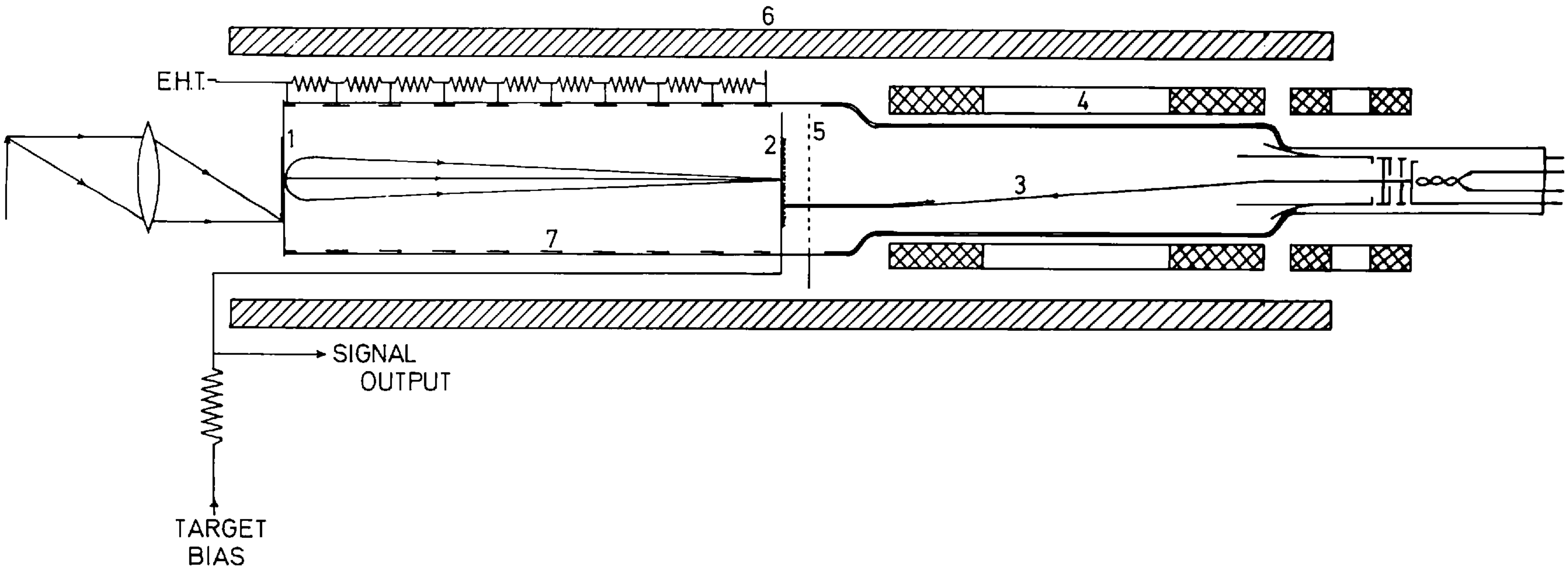

FIG. 7.1 PROTOTYPE VERSION OF SPONGY POTASSIUM CHLORIDE TARGET CAMERA TUBE

FIG. 7.2 PROTOTYPE VERSION OF SPONGY POTASSIUM CHLORIDE TARGET CAMERA TUBE

isocon scan (§5.10), the complexity of this system made it unsuitable for use in a prototype tube. Instead, signal extraction was effected by coupling the conducting backing of the target to a thermionic head amplifier. While this is by far the simplest method of signal extraction, it has been shown above (§s.5.6 and 5.8) that provided the scan rate is optimized, thermionic signal amplification is as goods as amplification by an electron multiplier.

The low velocity scanning section, (3), of the tube was made to be identical with the miniature C.P.S. Emitron, for which, scanning coils, (4), and circuits were available. The electron optical features of the gun section have been described above, (§ 5.3). The ion trap mesh (5) was taken to a separate connection from the wall anode, but no stabilizer mesh was incorporated into the proto-type tube.

The scanning system required a longitudinal magnetic field of the same strength (4.5 milli tesla.) as that to which the image section was designed, so that a single solenoid (6) could be used to apply a uniform magnetic field along the whole length of the tube.

The wall anode of the gun section consisted of platinum paint, fired into the pyrex glass at 600°C. This was protected from being scratched in regions where spring contacts were made from the elctron gun metal parts, by a coat of platinum paste, similarly fired into the glass. The electron gun used was a C.P.S. Emitron gun, whose kodial pinch was sealed to the main pyrex body of the tube by means of a graded seal.

The accelerating electrodes in the image section of the tube were platinum rings, (7), about 7 mm. broad, spaced at 2 cm. intervals, painted and fired on to the glass. Electrical connections were made to these rings by means of platinum tapes, sealed through the glass. These made contact with silver paste patches, fired on to the outside of the tube, to which soldered connections could be made.

The spongy target and the mesh were included together in a common assembly whose construction can best be explained with reference to Fig. 7.3 which represents a section through the assembly.

The electroformed 600 line per inch mesh, (1), was mounted by clamping it between two, stainless steel rings, (2)

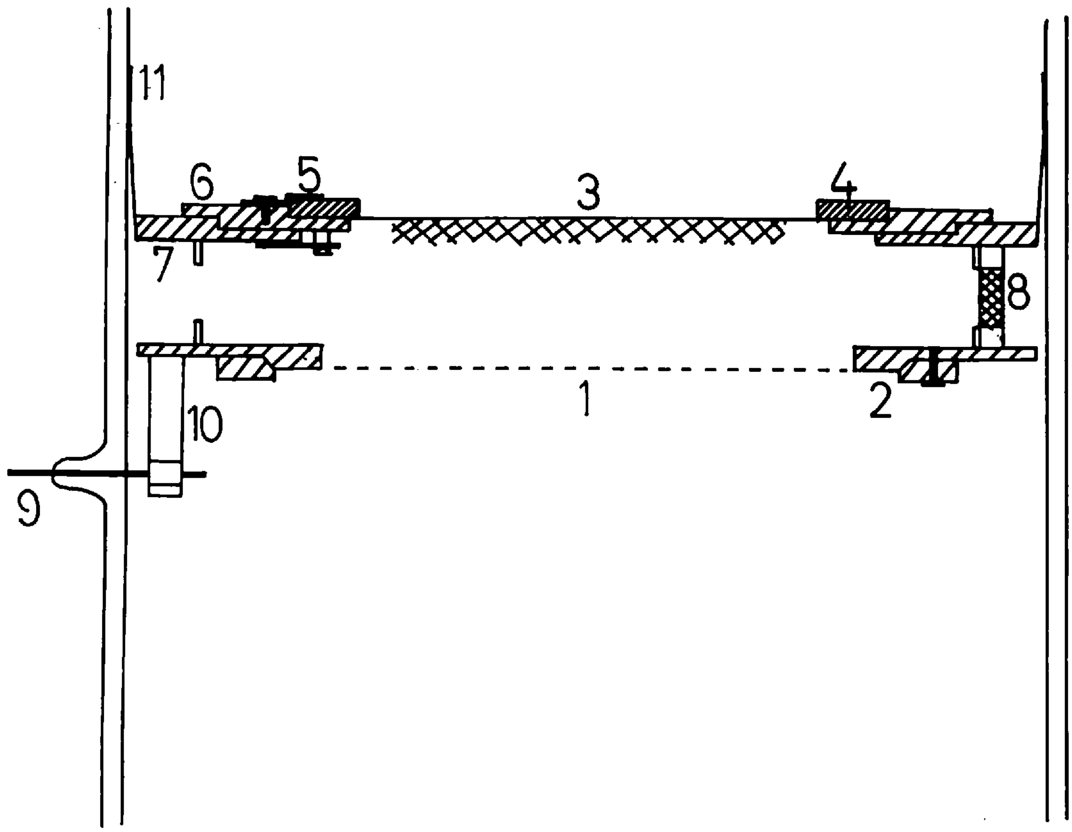

FIG. 7.3 CROSS-SECTION THROUGH TARGET & MESH ASSEMBLY OF PROTO-TYPE TUBE (not drawn to scale)

machined to mate into each other so that the mesh was stretched taut as the two rings were bolted together with 10 B.A. screws. The target (3) was prepared on a soda glass ring (4) by techniques, described below, (§s. 7.6 and 7.7), and secured by means of inconel clips (5) on to a stainless steel film holder, (6), which in turn, could be clipped on to another electrode, called the target mount (7). The target mount and the mesh electrode were fixed together by means of spot welded clips and ceramic rods, 1 cm. in length (8). The whole assembly could be clipped on to tungsten pins, (9), by inconel clips,(10), spot welded to the mesh electrode. Three tungsten pins were used, two of which were blind and one open, to enable electrical contact to be made to the mesh. Electrical contact to the target mount was made through a springy skirt, (11), welded on to the target mount and pressing against a platinum ring electrode, painted on to the tube wall with a platinum tape sealed through the glass. This skirt also served to isolate the gun section of the tube from the image section, protecting the scanned surface of the target from any adverse effects which might arise from the alkali vapours, liberated into the image section during photo-cathode processing.

Because the spongy potassium chloride target is rapidly attacked by water vapour[152], the target was assembled into the tube in a dry box, after the tube had been prepumped, baked to 300°C, and then let down to dry argon by means of a special gas admittance valve (Fig.7.4). The silver chloride sealed end plate was removed, and a long, specially designed tool was used to reach inside the tube to unclip and remove the empty film holder from the target mount. Fig 7.6 is a photograph of some of the long tools, used in tube assembly, which were designed to reach inside the tube and grip various tube parts. A film was clipped into the holder, and this was carefully replaced into the tube by means of the special tool. The end plate was resealed on to the tube which could then be removed from the dry box and resealed on to the pump. The well known magnetic ball valve[82], (Fig. 7.5), provided protection for the susceptible target from harmful atmospheric and glass-blowing vapours when the tube was removed from the dry box.

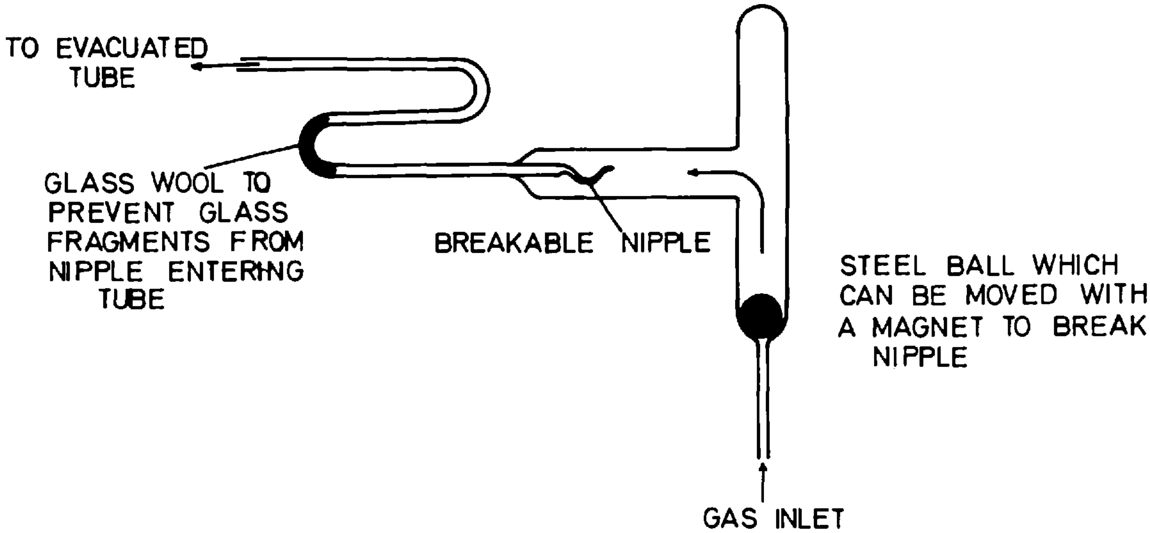

FIG. 7.4 GAS ADMITTANCE VALVE

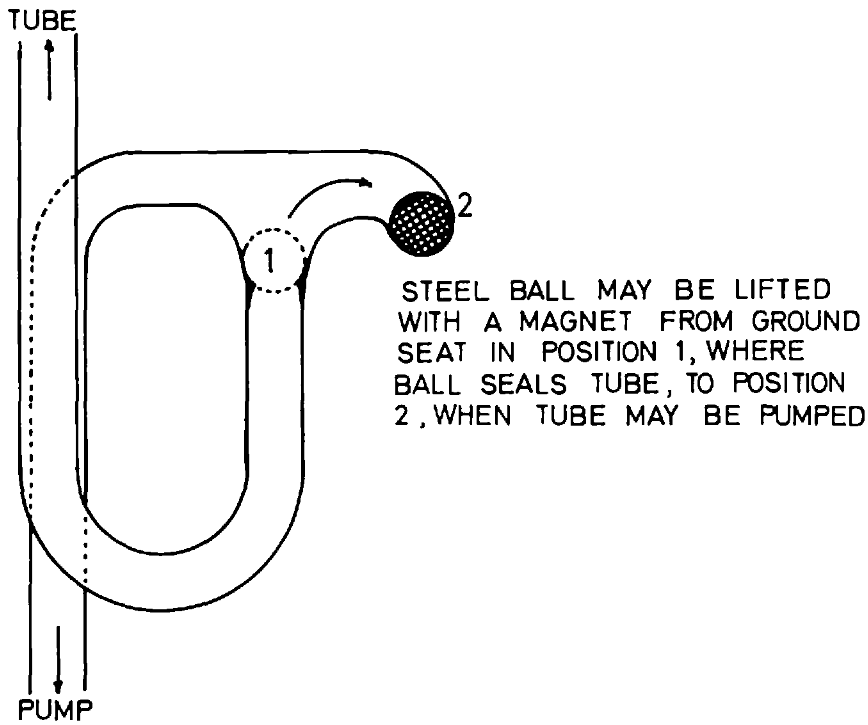

FIG. 7.5 BALL VALVE

FIG. 7.6 REACHING TOOLS USED IN TUBE ASSEMBLY

Initial pumping had to be carried out slowly through a constricted pumping line, to avoid rupturing the target. When a good vacuum had been achieved, the tube was rebaked, the electron gun and end wall photo-cathode processed, and the tube sealed off the pump. The cathode processing techniques used are discussed and described below (§7.9 and 7.10).

7.3 Design modifications introduced, after assessment of the prototype tube.

While the first successful camera tube enabled many of the characteristics of spongy potassium chloride layers to be investigated, (see chapter 10), the camera itself exhibited certain undesirable features for which remedial modifications were incorporated in subsequent tubes.

The insulation of the target proved high enough to enable a charge image to be retained for periods of several hours without appreciable loss in definition. However, this property could not be exploited to achieve long integration times in the proto-type tube, due to the fact that background limited useful exposure to periods of less than two minutes.

One source of this background was immediately evident. During the processing of the end wall photo-cathode, alkali vapours had been deposited on the walls of the image section, giving rise to low work-function surfaces which would contribute to background arising from thermal, photo-, and secondary emission.

Background was investigated by determining how the current reaching the target from the image section, with the applied electrostatic and magnetic fields. The photo-cathode was illuminated with a constant light, and the current reaching the target (to which the mesh and all the gun electrodes were strapped for this experiment) were measured with an electrometer. The target current was plotted as a function of electrostatic field for various fixed values of the magnetic field. A set of curves is provided in Fig. 7.7 showing the results of these measurements. For each magnetic field used, a maximum target current occurred for a definite value of electrostatic field. The electrostatic fields corresponding to maxima increased monotonically with magnetic field, and it was found that

FIG. 7.7 VARIATION OF TARGET CURRENT WITH ELECTROSTATIC FIELD FOR VARIOUS MAGNETIC FIELDS

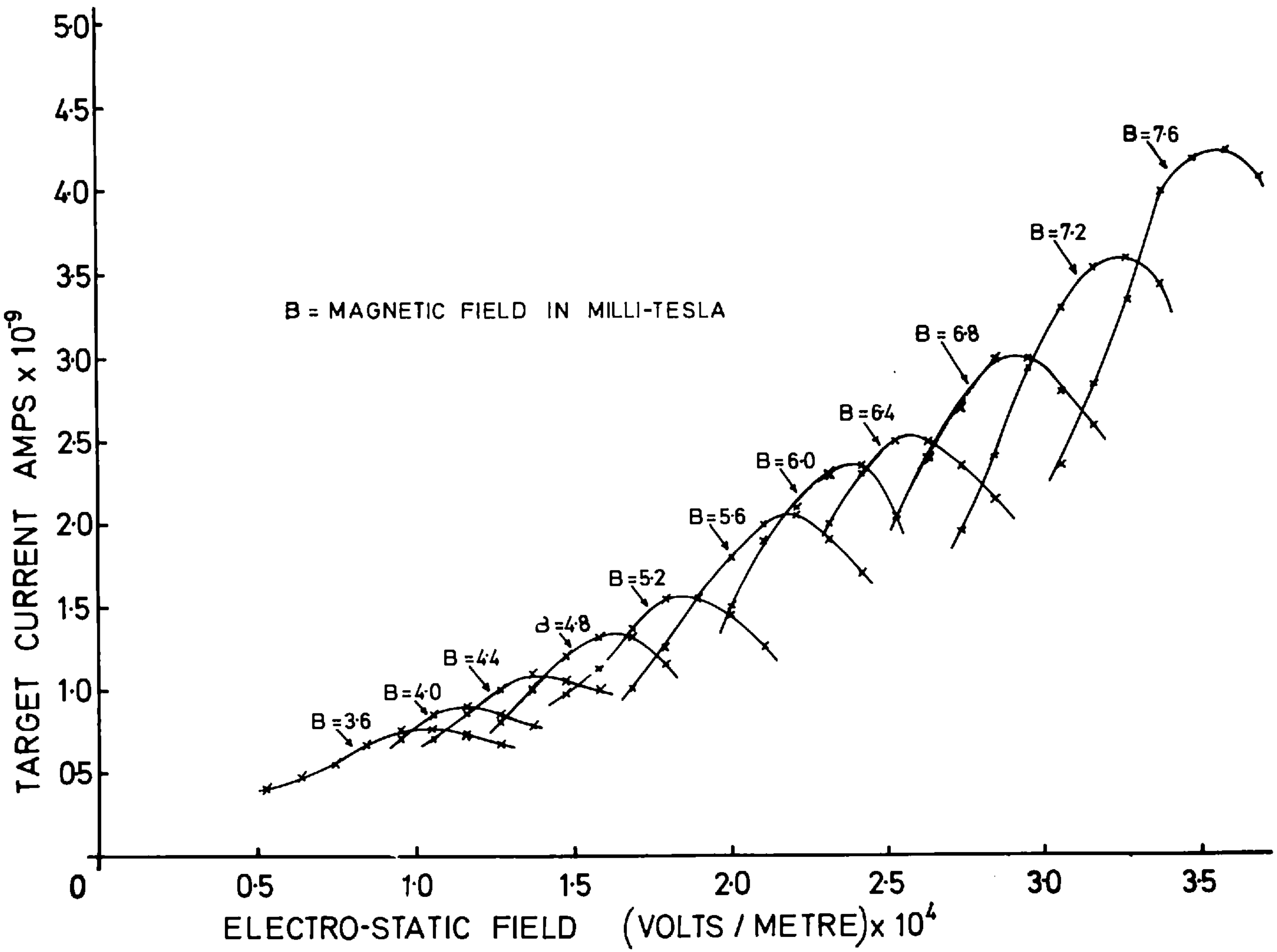

tube voltages for which maximum target currents occurred were approximately proportional to the square of the corresponding magnetic fields.

$$V \propto B^2 \qquad (7.1)$$

This is illustrated graphically in Fig. 7.8.

Now it has been suggested that a source of background in image intensifiers can arise from electron multiplication and ion emission from the glass walls of the tube[118, 193]. If this were to account for background in the image section of the tube under consideration, the combinations of magnetic and electrostatic fields, corresponding to maximum target current, might be expected to be related to a significant, preferred skip distance, travelled by an electron between collisions at the tube wall.

It is shown in appendix A.6 that a relationship of the type represented by Eq.(7.1) would be expected to hold if a definite, preferred mean skip distance for an electron emitted from the tube wall existed. (see Eq. A.6.4). Substitution of the operating parameters, used in the prototype tube in the equations derived in the appendix, yielded

FIG. 7.8 RELATIONSHIP BETWEEN ELECTROSTATIC AND MAGNETIC FIELDS FOR WHICH MAXIMA IN PRIMARY TARGET CURRENT OCCUR

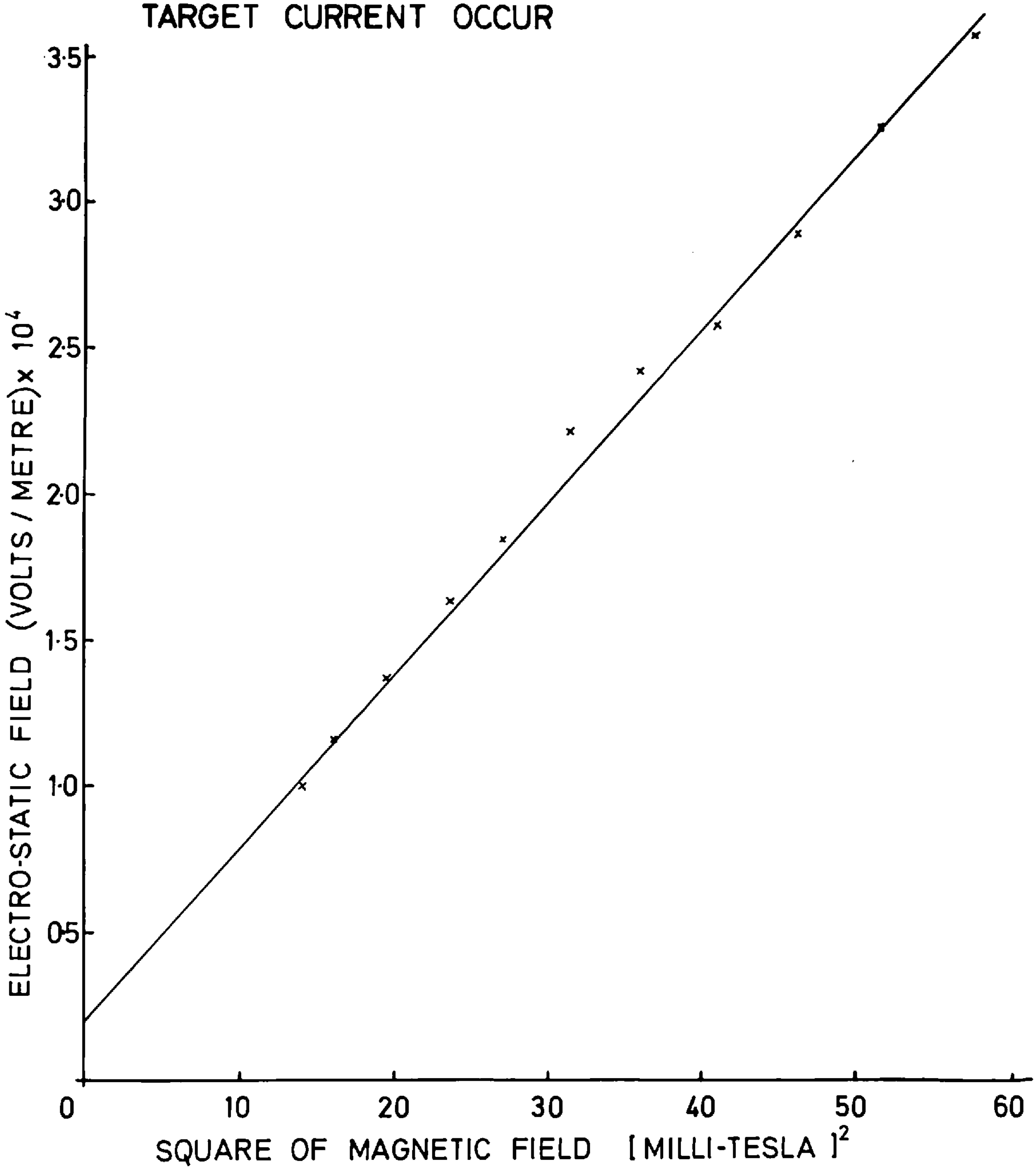

a value of about 2 cm. for this mean skip distance. The fact that this distance is the same as the separation of the platinized accelerating electrodes, painted on the walls of the tube, can be explained on the grounds that the insulating glass bands along the wall of the tube are better secondary emitters than the conducting platinized rings. A resonance thus occurs in the background current observed, when the fields are just right to accelerate and focus electrons from one region of unpainted glass on to the next, so giving rise to an electron cascade between the evenly spaced unpainted regions of the tube wall. This hypothesis is supported by the fact that shorting two adjacent electrodes to defocus one generation of secondary electrons considerably reduced the background current.

Three modifications were introduced into the design of the next tube (Fig.7.9) to reduce this background.

The cathode was processed in a separate compartment to prevent alkali vapours from entering the image section of the tube where the creation of low work function surfaces had to be avoided. This was achieved by making use of

FIG. 7.9 CAMERA TUBE INCORPORATING FIRST DESIGN MODIFICATIONS

a device, developed at Imperical College, which enables the processed cathode in the sealed off tube to be turned over in the processing compartment, so that its sensitive surface faces the working section of the tube(116, 165).

Secondly, the length of the image section was reduced from 19 cm. to 13 cm. This modification required that the applied magnetic field should be increased from 4.5 to 6.7 milli tesla, to maintain single loop focusing conditions for electrons accelerated through 7 kV in the image section. Operation of the prototype tube had indicated that the available scanning power was adequate for the target to be fully scanned in this increased magnetic field.

A third modification, aimed at reducing background was the replacement of the platinum ring accelerating electrodes by stainless steel annuli, clipped on to triads of tungsten pins, sealed into the tube at 2 cm. intervals. One pin of each triad was open, enabling electrical contact to be made to the annulus. The annuli acted as baffles, preventing electron multiplication along the walls of the tube.

The replacement of the platinum paint rings and tapes by annuli had the further advantage of avoiding lost contacts which could arise from the unreliability of platinum tapes. (A broken platinum tape had rendered one of the prototype tubes useless).

It was decided to avoid similar trouble through lost contacts occurring in the scanning section by replacing the platinum paint wall anode by one made from thin, stainless steel sheet. The method of mechnically locating the wall anode is illustrated diagramatically in Fig. 7.10., which shows the scanning section electrode assembly. The wall anode, (1), target mount, (2), and mesh electrode, (3), were assembled together by means of three ceramic rods, (4), glass separators, (5), and spot welded clips (6). The glass spacers, (5), were made from tubing which closely fitted the ceramic rods, by grinding down sections of this tubing in a jig, to lengths of less than 2 mm. Triads of equally sized spacers were selected for the assembly. This construction resulted in the mesh being located much closer to the target and aimed at improving the resolution

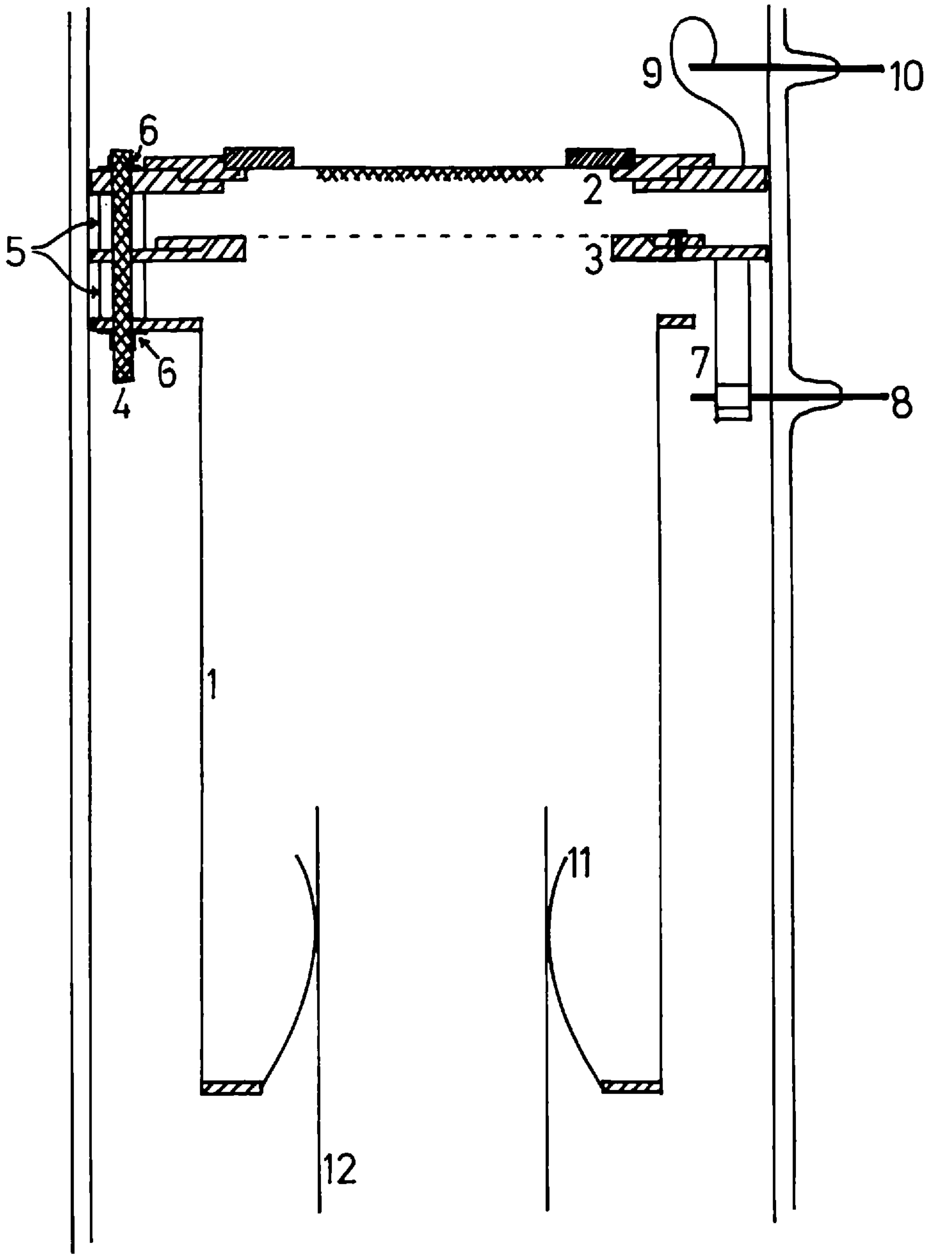

FIG 7.10 SECTION THROUGH WALL ANODE, TARGET & MESH ASSEMBLY OF CAMERA TUBE CONSTRUCTED WITH A STAINLESS STEEL WALL ANODE (not drawn to scale)

(see § 5.3 (d)) which was limited to only 10 line pairs per mm. in the prototype tube.

The whole assembly was anchored into the tube by means of inconel clips, (7), welded to the mesh electrode and attached to three tungsten pins (8), sealed into the glass, one of which was open to enable electrical contact to be made to the mesh. Electrical contact was made to the signal plate by means of a flying lead, (9), spot welded between the target mount and another open tungsten pin in the tube wall (10). No skirt was required around the target mount to protect the target surface from alkali vapours, as in the proto-type tube, because in this tube, a photo-cathode processing compartment was uded. The potassium chloride target layer was assembled into the tube by a method, similar to that used for the prototype tube (see § 7.2). Electrical contact was made to the wall anode, by means of spot welded inconel springs, (11), which bear against the wall anode of a standard vidicon gun, (12), sealed into the glass base of the tube.

Use of magnetic materials, such as nickel was avoided in all parts of the tube to prevent aberrations arising from magnetic field distortion.

These modifications resulted in a tube of much improved performance from the standpoint of background and resolution. Further modifications introduced into subsequently constructed tubes have resulted in additional improvements (§7.4), but the ovolution of tube design has been more gradual, following these initial drastic alterations.

7.4 Further modifications in the design of the storage tube and their effect on its performance.

(a). Screening of the glass walls of the image section.

While the use of annular accelerating electrodes enabled useful integration times of up to one hour to be realized and the limiting resolution was improved to 15 line pairs per mm., the images generated by the tube illustrated in Fig. 7.9 were badly distorted. (see fig. 7.11). This distortion was due to charging of the unscreened glass walls in the image section and the defect was overcome in subsequent tubes by welding metal

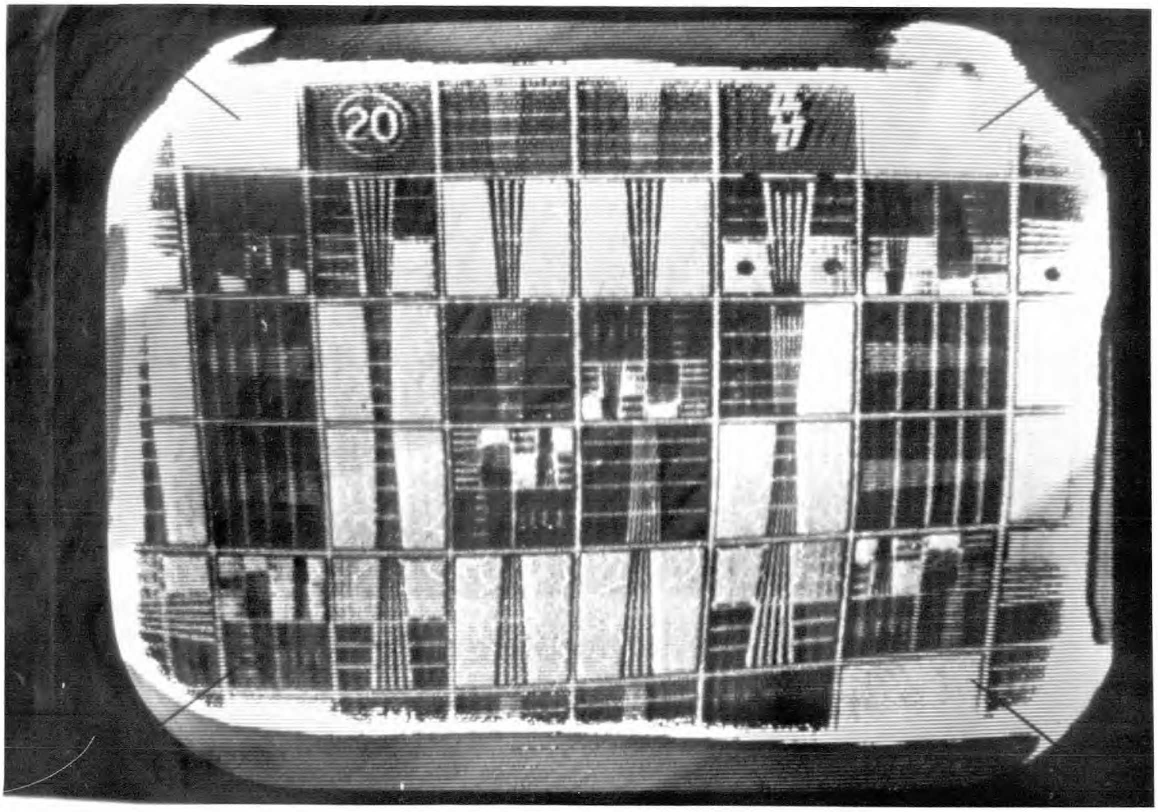

FIG. 7.11 DISTORTED PICTURE GENERATED BY TUBE INCORPORATING FIRST DESIGN MODIFICATIONS

skirts on to the annuli to screen the glass walls. This feature is illustrated in Fig 7.12 which shows a tube immediately before its final pumping to be processed. The gas admittance valve and ball valve described above in § 7.2 are also clearly shown in this picture.

(b). Modifications associated with tube processing.

Various photo-cathode processing techniques were adopted during the development of the tube, some of which involved modification to the processing compartment. These are described in the account of the photocathode processing technique, finally adopted, given below in § 7.10

(c). Internal mounting of resistor chain.

In the early tubes, the accelerating electrodes were held at uniformly increasing potentials by tappings from an external resistor chain, included in the tube mounting cradle. A separate connection was made to each electrode, via the open tungsten pin on which it was mounted.

This arrangement was improved upon by internally mounting the resistor chain, on to the accelerating electrodes, assembled together as a rigid unit. The method of construction

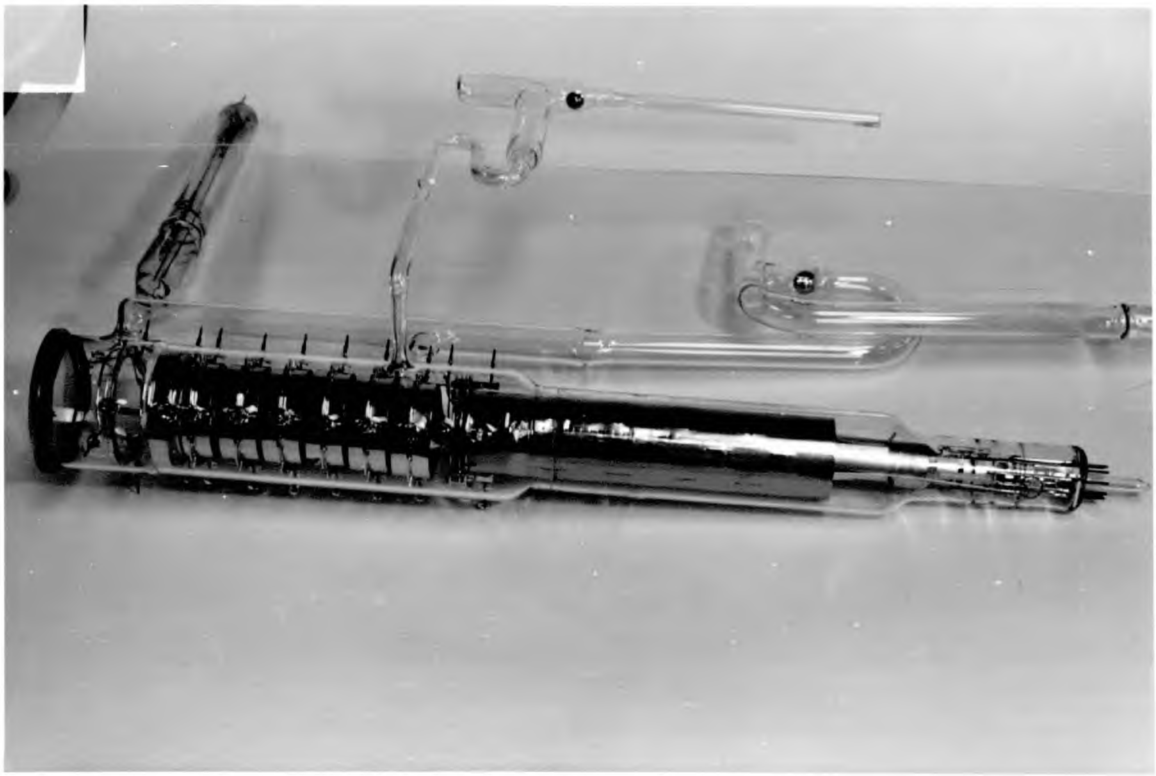

FIG.7.12 CAMERA TUBE ASSEMBLED WITH SKIRTED ANNULI, PRIOR TO BEING PUMPED AND PROCESSED

of this unit is illustrated in Fig. 7.13. The skirted annuli, (1), were attached to fused silica rods, (2), by means of clips, (3), spot welded round the rods at the positions where these passed through clearance holes in the annuli. Welwyn cracked carbon, 8.2 MΩ resistors, type C 82, from which the casing and paint had been removed, (4), were also mounted with spot welded clips, to connect adjacent annuli. These resistors could be baked to 300°C, without being adversely affected, and were run quite satisfactorily within the vacuum of the tube at twice their rating of 500 volts.

The advantages accruing from the introduction of this modification were threefold. First, only two electrical connections were required for the image section, enabling corona to be more easily prevented, as there were fewer external surfaces at high voltage. Secondly, the fact that only two electrical connections were required, enabled the risk of leaks to be minimized by allowing a considerable reduction in the number of tungsten pins, sealed in the glass. Thirdly, the construction of all the image section electrodes as a single unit, considerably facilitated assembly

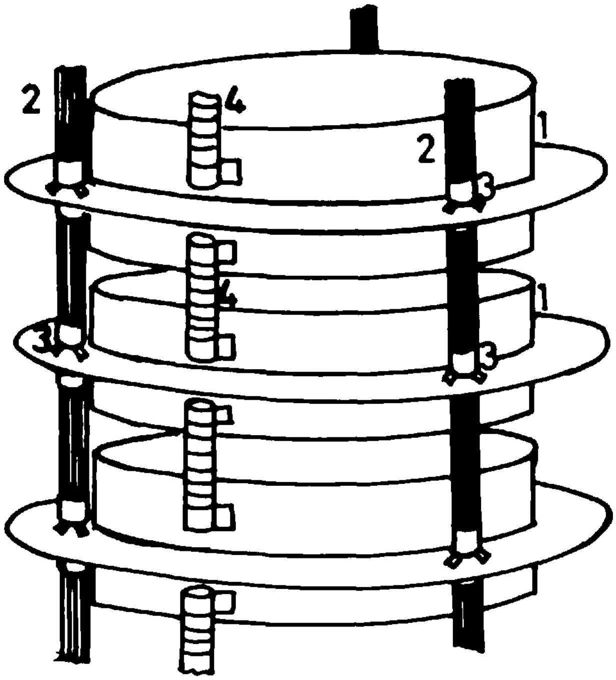

FIG. 7.13 CONSTRUCTION OF IMAGE SECTION ACCELERATOR ELECTRODES IN SYSTEM WITH INTERNALLY MOUNTED RESISTORS.

at the drybox stage (see § 7.2). Then, the annuli could be easily taken out of the pumped and baked tube as a unit, so enabling the removal of the target and mesh assembly. It was much less difficult to assemble the fragile target on to the target mount when this was outside the tube and then replace the whole assembly into the tube, than it was to manoeuvre and clip the target in position on to a mount inside the tube.

(d). <u>Modifications associated with target stabilization.</u>

One of the major defects of the spongy potassium chloride targets lay in their tendency to charge beyond the first cross-over potential in unscanned or overloaded regions. There was thus, always a risk of the target reverting from a cathode to anode potential stabilized state. This was accompanied by dielectric breakdown in the target, which became punctured during exposure to the energetic scanning electrons. Targets so punctured were permanently damaged, and pictures generated on restoration of cathode potential stabilized working conditions, exhibited prominent fixed white spots (see fig. 7.14).

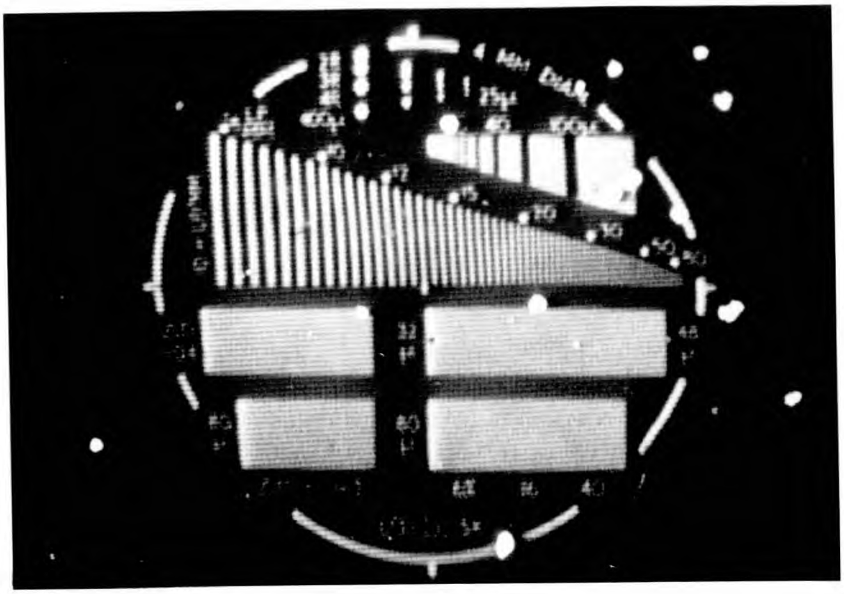

FIG. 7.14 PICTURE GENERATED BY A TUBE IN WHICH THE TARGET HAD BEEN DAMAGED BY OVERLOADING. V_{sp} = 10 volts. DIAMETER OF TEST PATTERN IMAGE ON TARGET = 8 mm.

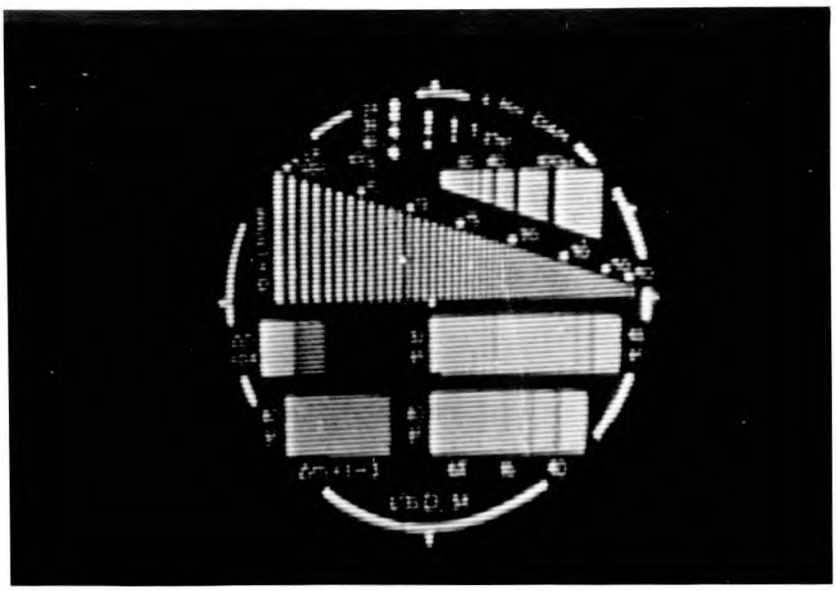

FIG. 7.15 TEST PATTERN GENERATED BY A TUBE INCORPORATING A STAINLESS STEEL WALL ANODE. V_{sp} = 10 volts. DIAMETER OF TEST PATTERN IMAGE ON TARGET = 8mm.

The problem was overcome in the most recently constructed tube by mounting a stabilizer mesh (see § 5.3 (d)) between the target and the field mesh, spaced at a distance of 0.020" from the target by means of mica washers.

Since targets in tubes without a stabilizer mesh had to be overscanned to maintain stability, the circular shape of the evaporated potassium chloride layers proved inconvenient. Various methods were tried of obtaining a useful picture from tubes without a stabilizer mesh, which completely filled the monitor while avoiding instability arising from unscanned areas becoming overcharged. Rectangular evaporated layers, or rectangular masks in front of either the photocathode side or the gun side of a standard layer were all tried. The best results were obtained by mounting rectangular masks each side of the target, the dimensions of the mask on the photocathode side being 1 mm. less than the mask on the gun side. This avoided any instability arising, due to the layers becoming overcharged under the edge of the gun side mask where it is not properly 'seen' by the scanning beam.

(e). Modification of the target mount.

The targets used in the early spongy layer camera tubes were one inch in diameter. It was considered desirable to increase the target diameter in order to improve resolution in terms of television lines. Now the first target membranes used were mounted on soda glass rings, which in turn, had to be mounted in a stainless steel film holder to enable the assembly to be clipped on to the target mount in the tube (see §7.2). This type of construction made it infeasible to increase the target diameter, without making a corresponding increase in all other image section dimensions, for the film holder had already been designed to occupy the minimum of annular space, consistent with satisfactory mechanical assembly to the target mount. A new method of mounting the film was therefore sought for, which could enable larger target areas to be used, without also necessitating the inconvenience of altering any other tube dimension. A solution to the problem would be the direct mounting of targets on to metal rings, so fashioned to allow them to be directly assembled on to the target mount without the use of an intermediate film holder. Experiments with stainless steel rings (expansion coefficient 11 x 10^{-6}) proved these to be unsatisfactory due to the 20% mismatch with the expansion coefficient of the aluminium oxide membrane being intolerable. Satisfactory rings were made however from titanium, whose linear expansion coefficient (9 x 10^{-6}) was sufficiently close to the hitherto used soda glass to enable the membranes to be stretched by just the right amount during layer preparation. (see § 7.6). Use of titanium film - mounting rings enabled targets with diameters of 1.5 inches to be included in tubes.

(f). Reversion to platinum painted wall anodes.

While good electrical contacts were always made to the stainless steel wall anodes, (see § 7.3), this type of anode did exhibit undersirable features. Power was absorbed from the scanning fields, resulting in eddy current heating of the anode and in distortion of the raster, scanning the target. (see fig. 7.15). Use of very thin (0.002") steel into which slots were cut (see fig. 7.12) failed to eliminate this effect, and it was decided to revert to the original method of using platinum painted wall anodes. Care was taken to avoid scratching the paint, and platinum paste was used over surfaces to which spring contacts were made.

The diagram in fig 7.16 shows the tube in its present state of development, showing processing compartment, (1), skirted annuli, connected by internally mounted resistors, (2), stabilizer mesh, (3), field mesh, (4), and gun section with platinum painted wall anode (5).

7.5 Preparation of metal parts, used in tubes.

(a) Copper meshed.

These were cleaned and relaxed prior to mounting, by vacuum stoving to 500°C.

(b) Stainless steel tube parts.

All the stainless steel tube electrodes were electropolished[168] by introducing them as the anode of an electrolyte consisting of 56% glycerol, 37% ortho-phosphoric acid and 7% water. After a current of density two or three amps per dquare inch of anode surface had passed for a few minutes, the tube parts became highly polished. After electropoloshing, the electrolyte was rinsed off with 3N hydrochloric acid and distilled water.

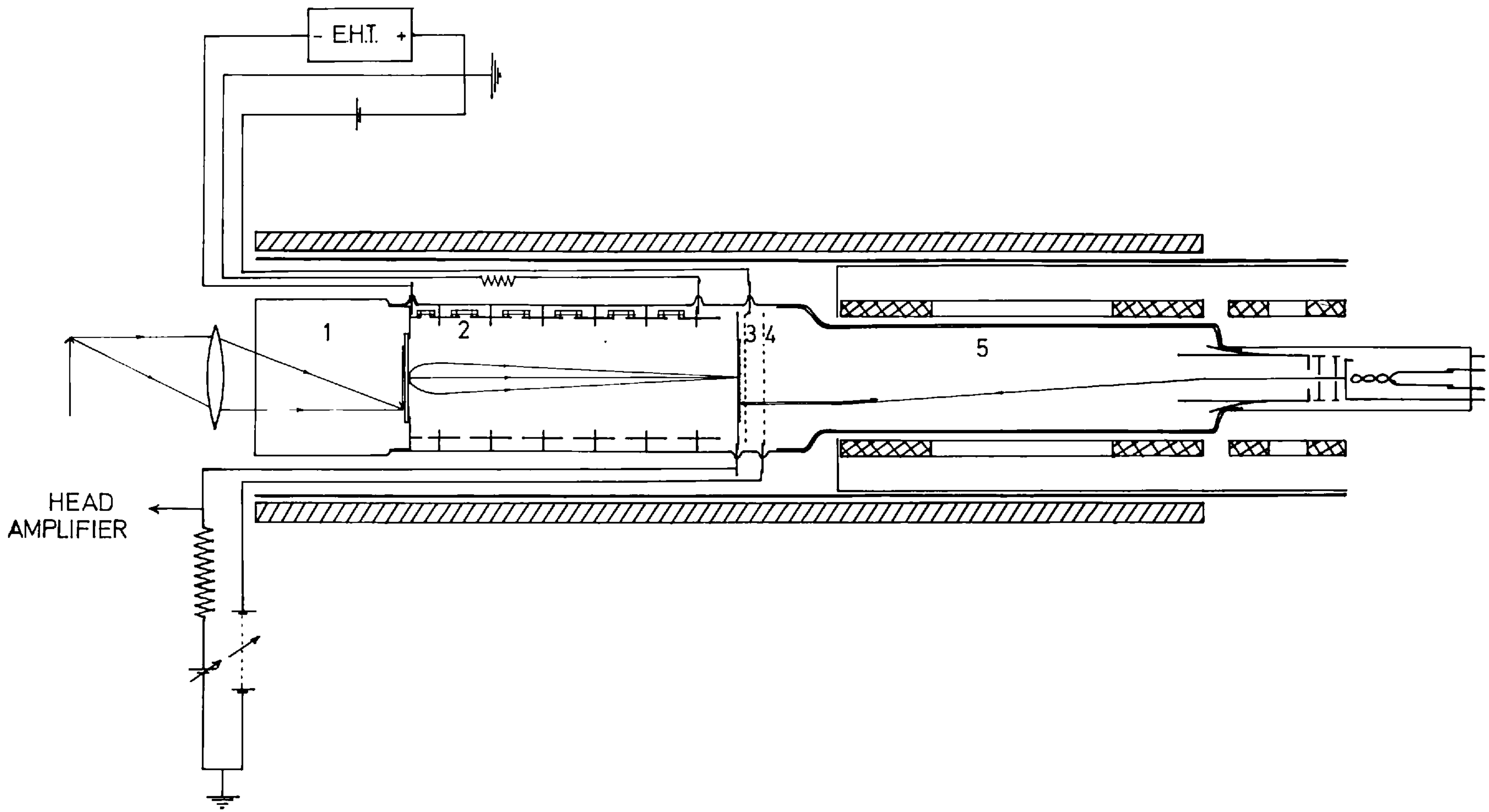

FIG. 7.16 SPONGY POTASSIUM CHLORIDE TARGET CAMERA TUBE AS DEVELOPED AT TIME OF WRITING

The electrodes were vacuum stoved to 1,000°C on the day, prior to tube assembly.

(c). Inconel springs and clips.

These were made by spot welding in pairs, and bending as required inconel strips which had been first crimped in a jig to enable the clips produced to positively locate on the 1 mm. tungsten pins, sealed in the glass walls. These clips were electropolished and rinsed in hydrochloric acid and distilled water, as were the stainless steel parts, but they were not vacuum stoved, because inconel losses its elasticity when annealed.

(d) Titanium rings.

After being turned and machined to shape, these were polished in a lathe with alumina powder.

7.6 Preparation of thin support film.

The thin films, used to support the spongy potassium chloride layers were made from aluminium oxide. Membranes of this type had been used to support image intensifiers dynodes by Emberson [47], whose method of preparation of alumina films was based on that described by Harris [65].

Clean, smooth, commercial aluminium foil (Starfoil) about 0.001" thick was stuck on to a tufnol ring with an acid resistant cement (bedacryl).

The front surface of the aluminium foil, was then cleaned with 6N caustic soda, applied with a brush, and rinsed off as soon as effervescence was observed. This surface was then anodized in a cell as shown in fig 7.17. Electrical contact was made to the aluminium by a metal pillar, (1), screwed into the tufnol ring, (2), through an aluminium tag which had been left for this purpose when the aluminium foil, (3), was trimmed to size round the tufnol mounting ring. The electrolyte, (4), was a 3% tartaric acid solution, buffered to a pH of 5.5 with 0.880 ammonia solution. The anodized layers produced were 13 Å thick per volt applied[66]. Thus, 500 Å membranes were prepared by the application of about 40 volts over a period of two minutes, the current flowing in the electrolyte dropping from the order of an amp to about 2 or 3 ma. as anodization reached completion.

After this, the anodized surface was washed clean with distilled water, and the atmospherically oxidised layer on the

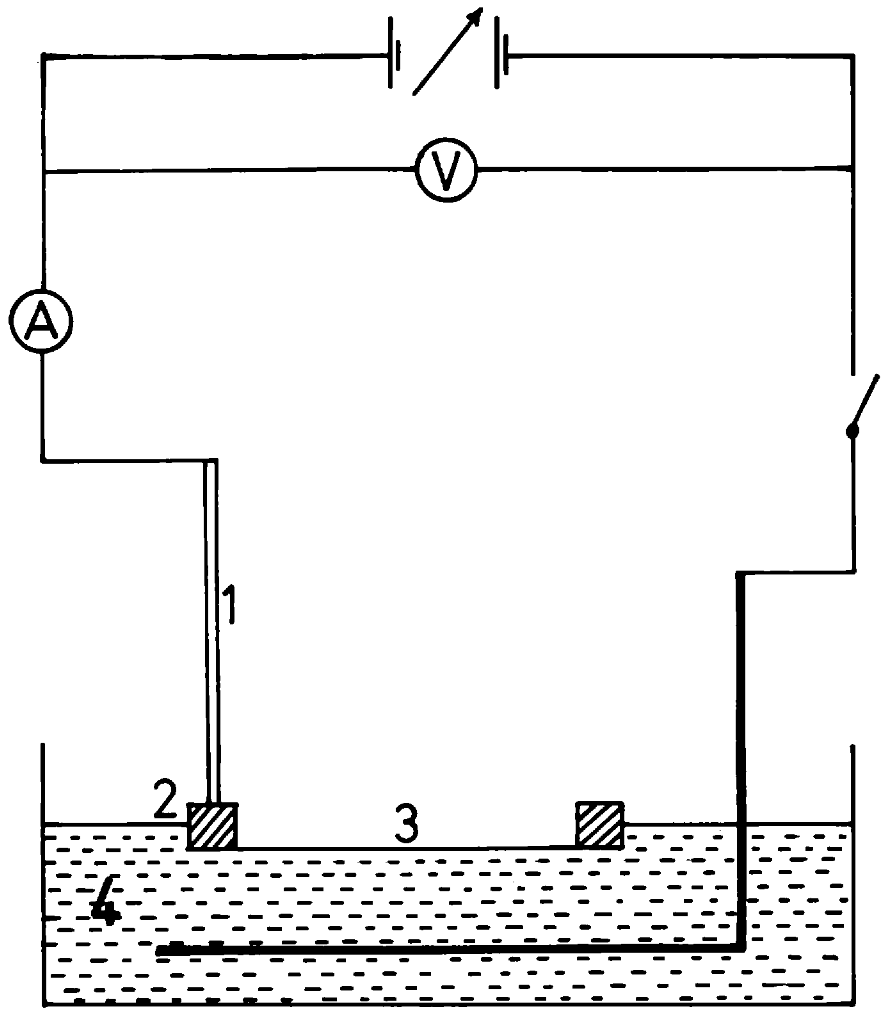

FIG 7.17 ANODIZATION OF ALUMINIUM FOIL

reverse side was removed by painting it with 6N sodium hydroxide solution until effervescence occurred. The caustic soda was then washed away with distilled water and the blank immersed vertically into an etching tank, containing about 400 ccs of 3N hydrochloric acid, to which, approximately 4 ccs of 0.1N cupric chloride and a couple of drops of detergent had been added.

Over the course of about ten minutes, the films became transparent as the aluminium dissolved away during etching, leaving a thin film of aluminium oxide. The cupric chloride aided the etching process by depositing traces of copper on the aluminium, to promote local electrolytic action. After etching, the acid was run slowly out of the bottom of the etching tank and the films washed.

The apparatus used to wash the fragile films in a way which kept turbulence to a minimum is shown in fig 7.18. The films were washed in succession with distilled water, nitric acid to remove electro-chemically deposited traces of copper, distilled water, and absolute alcohol, run in from dropping flasks.

The films were then mounted on conducting rings. Platinized soda glass rings were used in the early tubes, but for reasons explained above (§7.4 (d)), titanium rings were introduced as

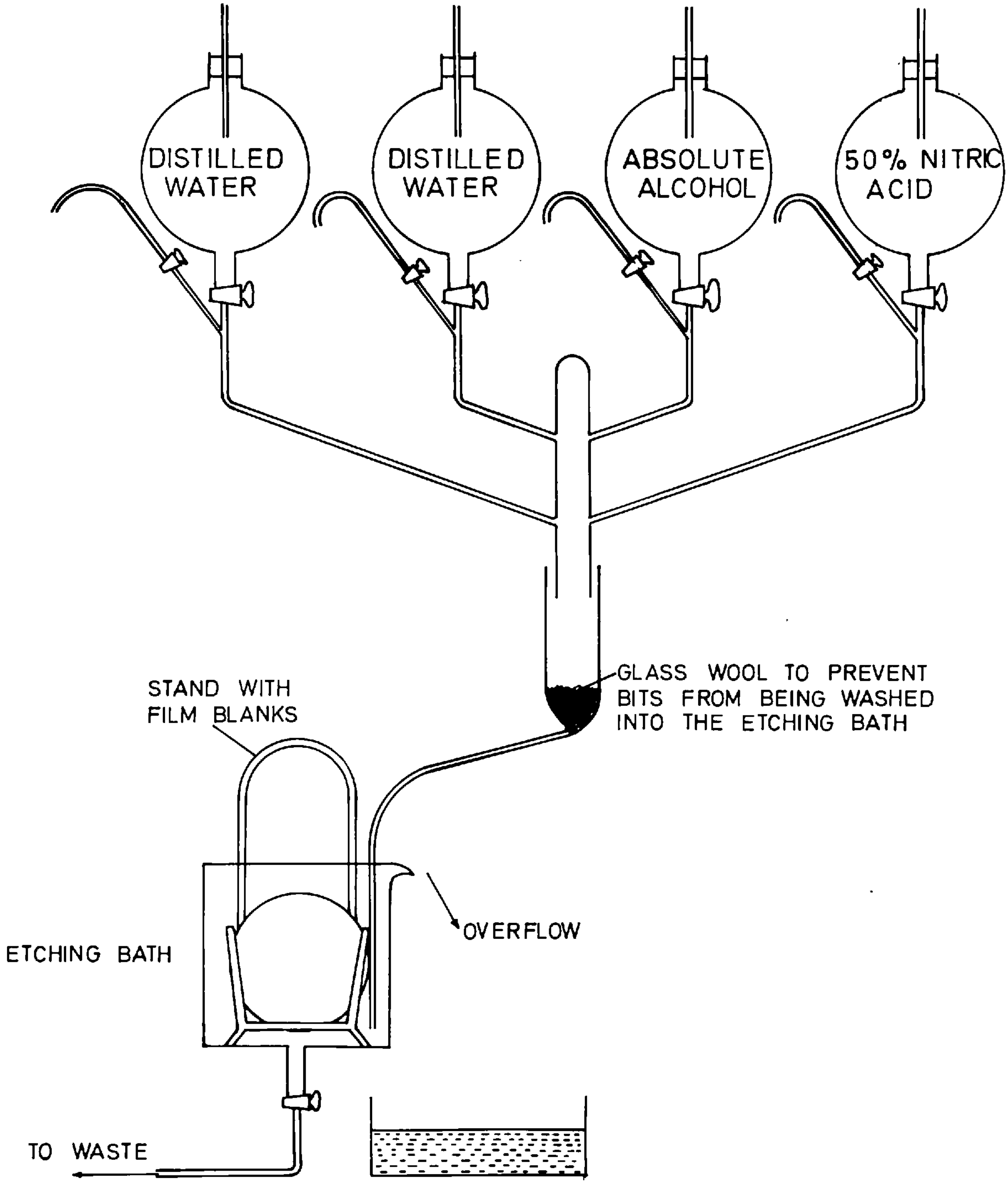

FIG.7.18 APPARATUS USED FOR ETCHING AND WASHING ANODIZED FILMS

film supports in later tubes. The mounting was effected by wetting the surface of the ring with a dilute solution of potassium silicate (0.1%), and offering the ring up to the film by means of a screw adjustable platform until surface tension forces pulled the film into intimate contact with the ring. After the film had stuck to the ring, the blank surrounds and tufnol ring were removed by trimming off with a wet paint brush.

The oxide film was then stretuched by heating it in air, up to 250°C. The expansion coefficient of the ring material (c. 9×10^{-6}) is just greater than that of aluminium oxide (c 8×10^{-6}), so producing the required stretching. During this stretching, the film underwent plastic flow, so that a slightly wrinkled film was left on cooling. This was able to take up strain induced by the annealing processes occuring in the layers subsequently evaporated on the film (aluminium and potassium chloride). Unstretched layers raptured during tube baking, but films which had been overstretched by preheating to 300°C produced targets with crazed surfaces. The crazing lines were visible in the pictures generated by a tube with such a target (see fig. 7.11).

7.7 Evaporation of aluminium and spongy potassium chloride layers on to the aluminium oxide film.

The evaporation techniques, used at Imperial College for preparing spongy layers were developed by Rosenbloom[151].

The demountable system, in which the evaporations were carried out is illustrated diagramatically in fig. 7.19 and pictorially in fig. 7.20. Prior to the introduction of the films, the open molybdenum boat, (1), was charged with finely ground, analar grade, potassium chloride, and degassed by heating the boat in the evacuated system. The films, (2), were then mounted on to a rotating film-holder, (3), and introduced into the demountable system. When the system had been re-evacuated, aluminium was evaporated on to the films from a triplestrand tungsten filament, (4). A lamp, (5), and a selenium photocell, (6), were used to monitor the evaporation until the film transmission dropped to 1%. This marked the production of a continuous , conducting, aluminium layer, 200 Å thick[180].

The system was then isolated from the pump by means of the butterfly valve, (7), and dry argon admitted through a needle valve (9), until a manometer, (10), indicated that the pressure had risen to two torr.

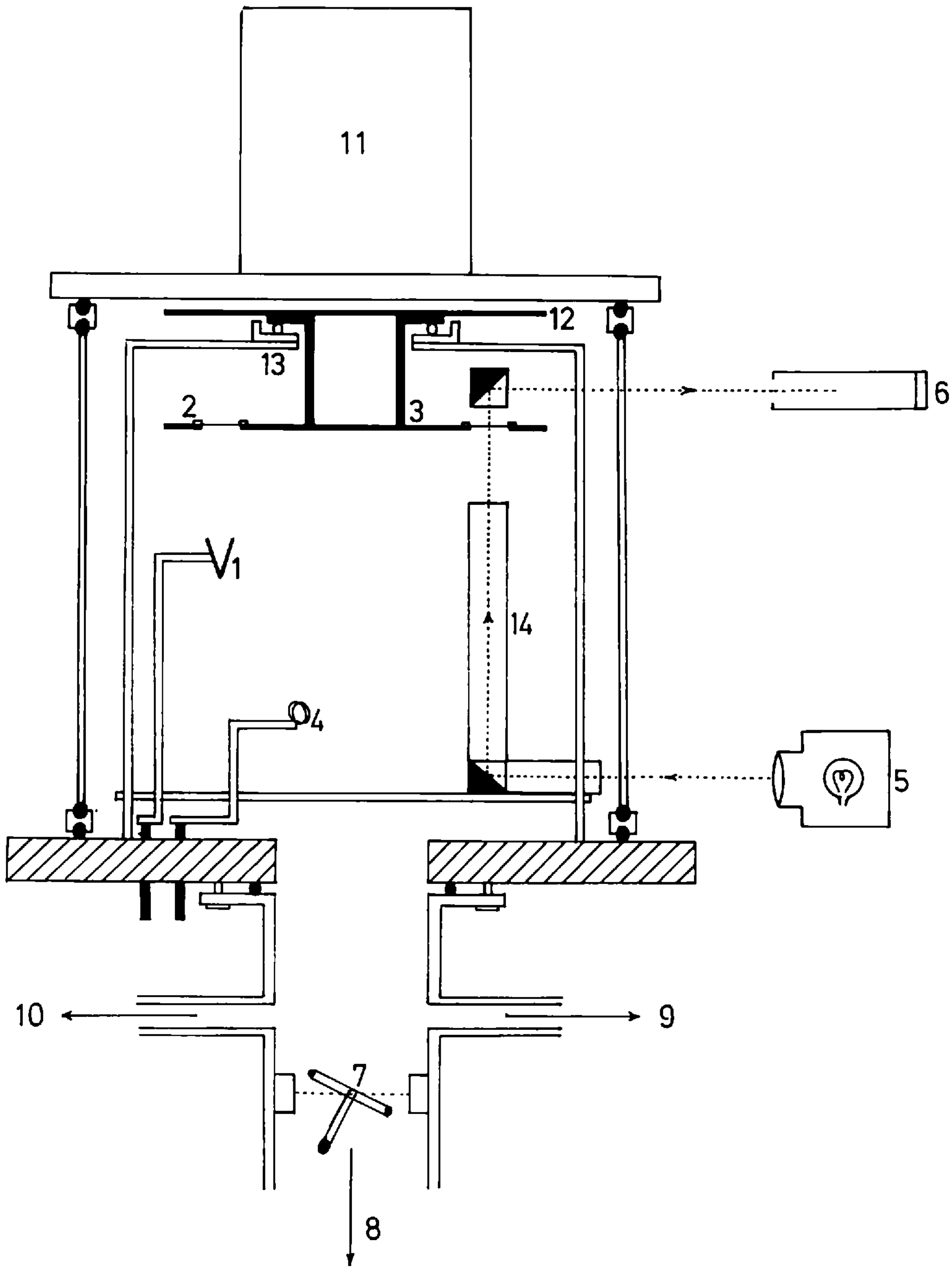

FIG. 7.19 DEMOUNTABLE EVAPORATION SYSTEM USED IN THE PREPARATION OF SPONGY POTASSIUM CHLORIDE TARGETS

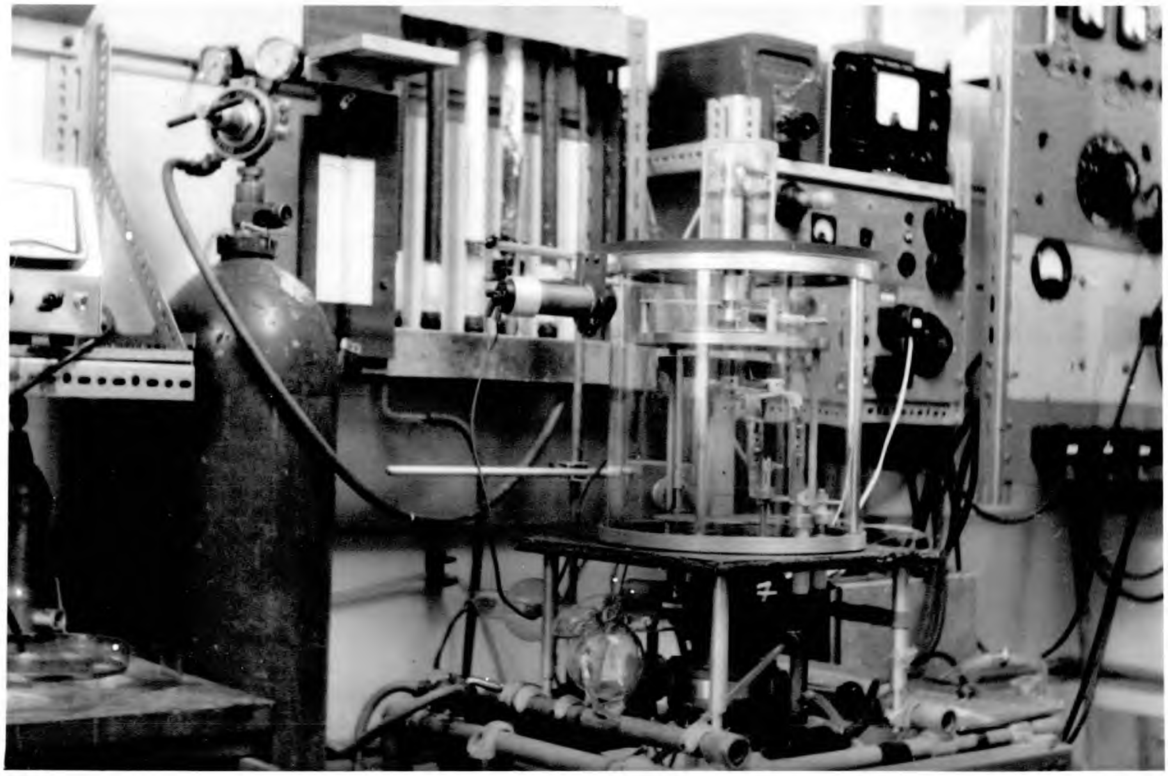

FIG.7.20 DEMOUNTABLE EVAPORATION SYSTEM USED IN THE PREPARATION OF SPONGY POTASSIUM CHLORIDE TARGETS

To ensure that the potassium chloride, evaporated from the boat held just two inches below the films should be deposited uniformly, the film holder was rotated during the evaporation. This was achieved by means of an external induction motor, (11), which acted on a copper plate, (12), fixed to the film mount, and supported by a free running thrust bearing, (13). The induction motor consisted of four relay coils, one pair of which was supplied through a large condenser, so that the currents flowing in adjacent coils were in phase quadrature. The supply to the motor was adjusted to keep the mount rotating at a rate of one cycle per second. The evaporation of the potassium chloride was monitored by observing for a 27% drop in the optical transmission of the film. The dropping effect of the rotating film holder necessitated the connection of a condenser across the galvanometer measuring the photo current delivered by the cell, (6), to increase the time constant of the circuit. This did not adversely effect monitoring, since the potassium chloride was evaporated slowly, the process being controlled to take, about ten minutes. An aluminium chimney[14] protected optical components in the monitoring system from deposition.

On completion of the evaporation, a dry box with glove ports was placed over the demountable vacuum chamber (see Fig. 7.21) and a desiccator was introduced into this through a side panel. The demountable system was let down to dry argon, and the dry box flushed with dry nitrogen. The film holder was then transferred from the demountable system to the desiccator, which in turn, was transferred to the large tube assembly dry box, which contained the tube and the necessary tools.

These precautions to ensure that the layers were exposed, only to extremely dry atmospheres, were taken in view of Rosenbloom's observations on the susceptibility of these low density layers to poisioning by the slightest trace of moisture[151].

7.8 Physical properties of the layers.

The mass of potassium chloride in the layers was determined by the conductimetric method described by Rosenbloom[151]. The potassium chloride on a layer was dissolved in a known quantity of water, and the conductivity of the solution obtained was measured under A.C. conditions to avoid polarization of the electrolyte. A standardization experiment had shown that over the range of concentrations used, a linear relationship existed between solution conductance and concentration.

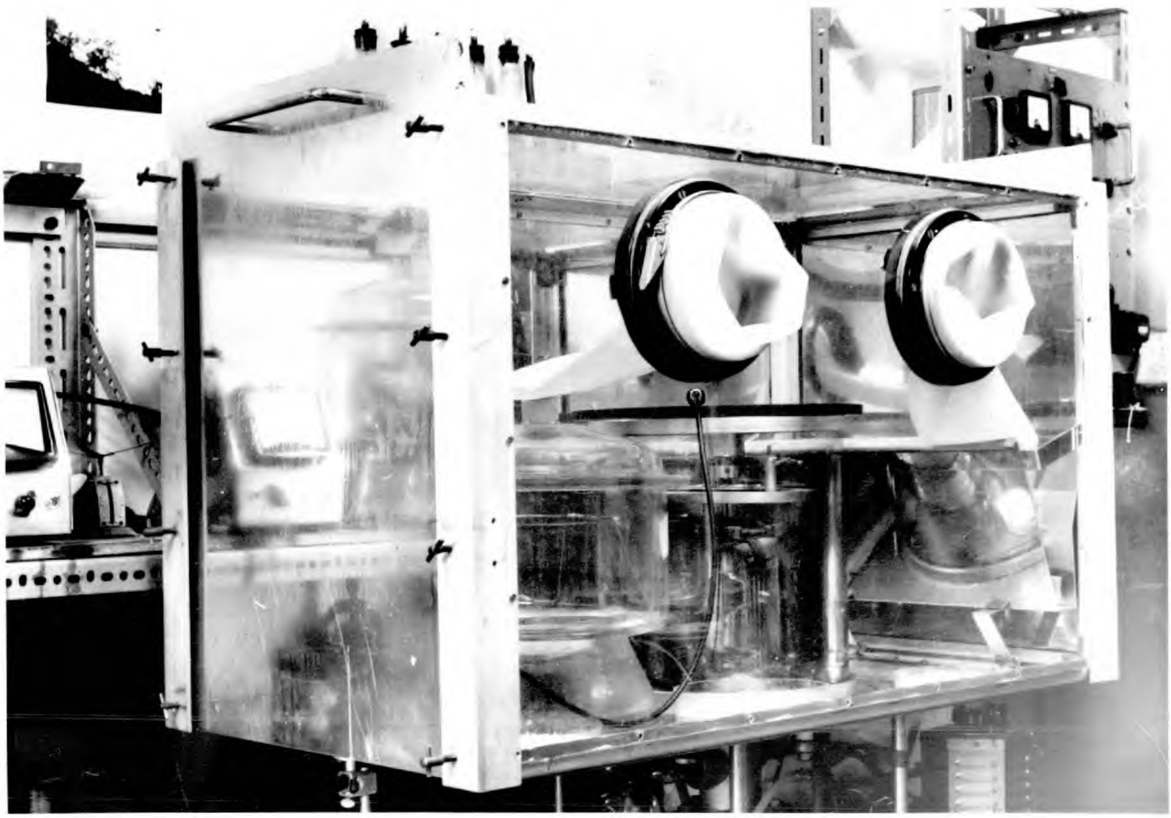

FIG.7.21 DRY BOX PLACED OVER THE EVAPORATION SYSTEM TO ENABLE THE NEWLY EVAPORATED LAYERS TO BE TRANSFERRED TO A DESICCATOR IN A DRY ATMOSPHERE.

The thickness of the spongy layers cannot be easily measured interferometrically, because of the uneven nature of the surface and Rosenbloom[151] concluded that the best method of determining the thickness was to observe under a microscope the cross-section of a flake from a punctured dynode. The flimsy nature of the layer made this difficult and the author measured layer thicknesses by making the microscope observation on broken sections of glass plates, which had been included with the films in the demountable system during the evaporation. The different substrates, represented by glass and aluminium oxide should not have affected the structure of the spongy layer produced, since an intermediate aluminium layer was deposited, prior to the potassium chloride evaporation. It was found that layers evaporated under apparently identical conditions had thickness ranging between 5 μm. and 20 μm. This is in agreement with Rosenbloom. A diagram of the cross-section of a typical layer is given in fig. 7.22, while fig. 7.23 shows a microscope photograph of a section through a potassium chloride layer, evaporated on to a glass plate.

The diffuse nature of the spongy potassium chloride is illustrated in fig. 7.24, which is an electron micrograph of potassium

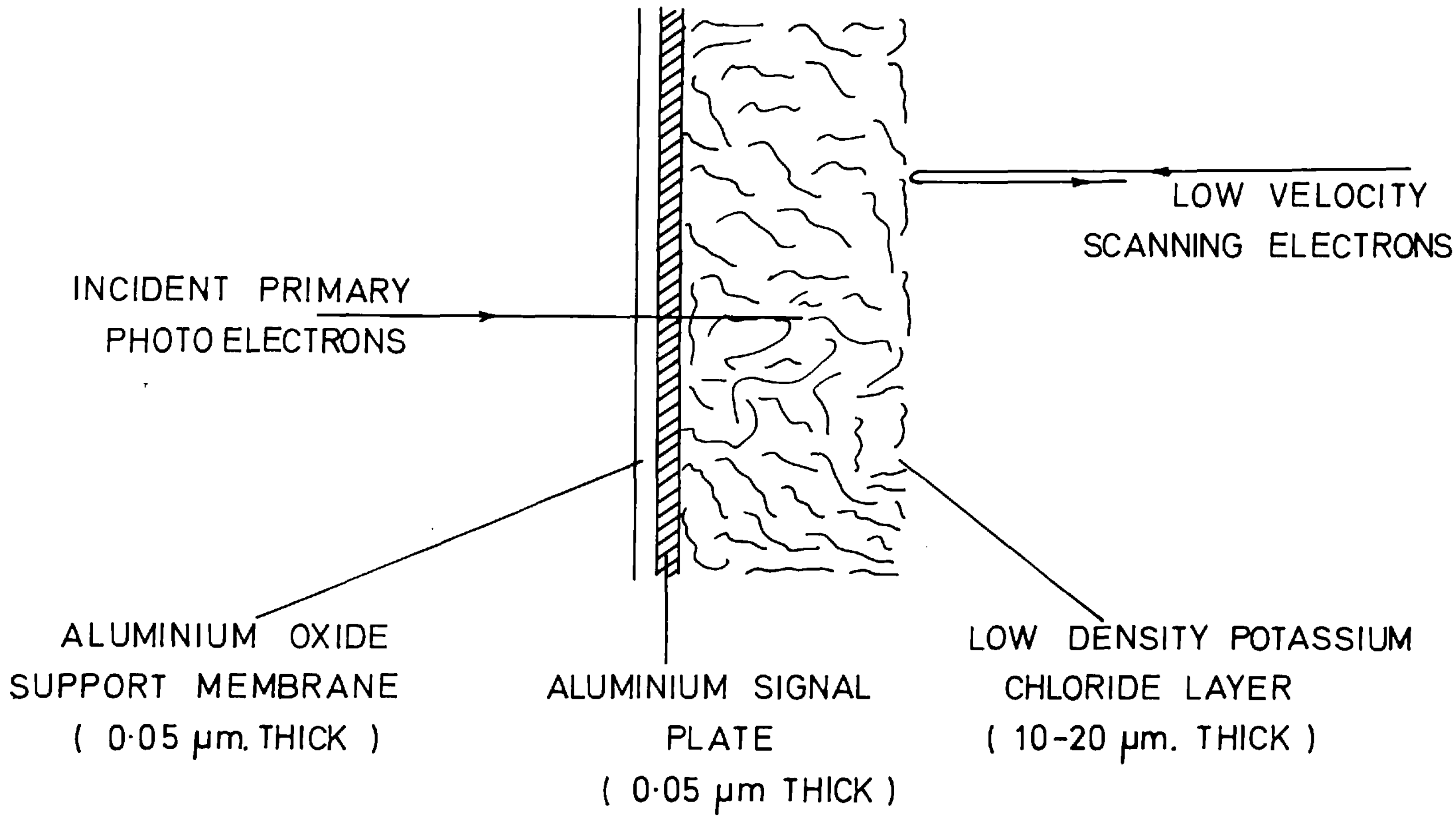

FIG. 7.22 SECTION THROUGH THE TARGET LAYER

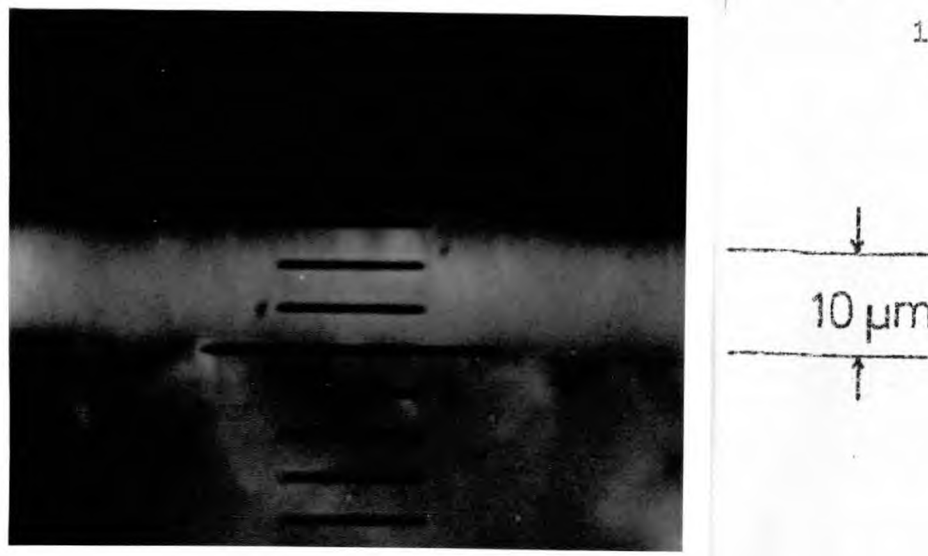

FIG. 7.23 CROSS SECTION OF A SPONGY LAYER OBSERVED THROUGH AN OPTICAL MICROSCOPE

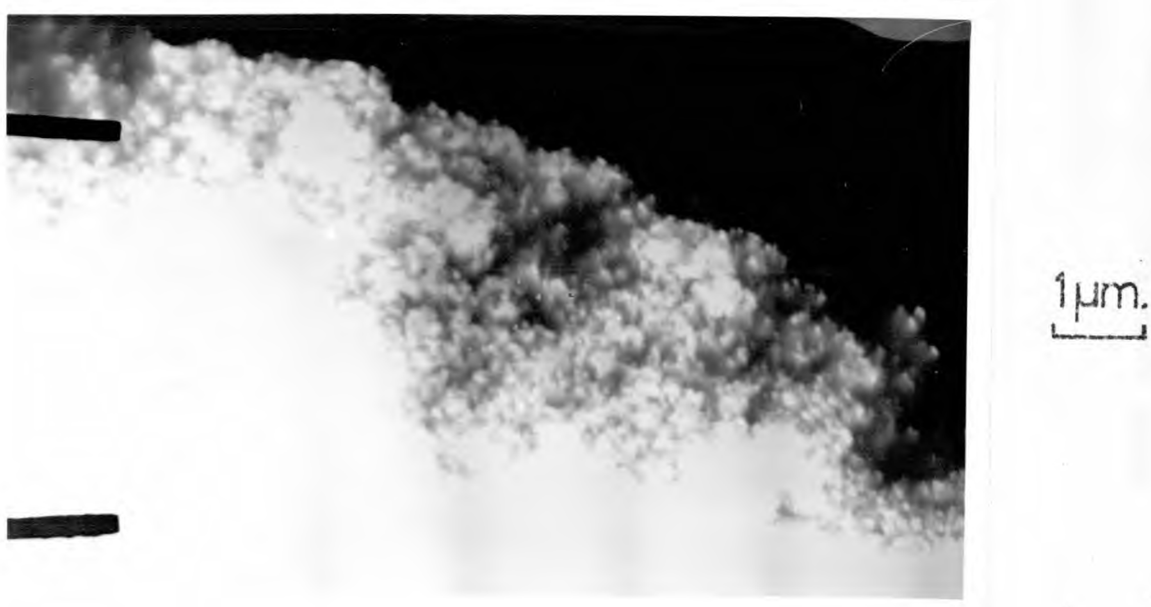

FIG. 7.24 ELECTRON MICROGRAPH OF DIFFUSE POTASSIUM CHLORIDE EVAPORATED ON TO A MESH.

chloride, evaporated on to a mesh in an argon atmosphere.

Mass and thickness measurements gave the layer density to be about 3% that of solid potassium chloride.

7.9 Formation of the thermionic cathode of the electron gun.

After the layer had been assembled into the tube in the dry box, the tube was re-evacuted (see §7.2), baked, and the gun electrodes degassed by eddy-current heating. The pressure was kept below 10^{-5} torr during this degassing procedure which was continued until the electrodes could be maintained at a dull red heat without the pressure rising above 5×10^{-6} torr. A smaller eddy-current heating coil was used to degas the getters, until on the point of firing.

After degassing the gun parts, the thermionic cathode was formed. The principles and chemical reactions involved in processing are described in detail by Herrmann et al[170]. Essentially, mixed barium and strontium carbonate crystals in the unformed cathode are converted into mixed crystals of the oxides of these metals, activated by small traces of metallic barium.

A processing unit was built, consisting of a power supply which enabled the filament voltage and electrode potentials to be independently varied and monitored over the ranges 0-10 volts and 0 - 500 volts respectively, while separate meters allowed the filament current and the emission current flowing to the limiter to be continuously observed.

With the limiter and the modulator held at zero volts, the filament voltage was gradually increased in half-volt stages to 8 volts, taking care that the pressure never rose above 5×10^{-6} torr. This precaution, besides ensuring that good vacuum conditions were maintained in the tube, minimized the risk of the cathode coating becoming cracked through over rapid heating at the processing stage. The filament was run above its rating of 6.3 volts during this processing procedure in order to take the temperature up to 1350°K, when the carbonates were completely reduced, not just to the oxides of barium and strontium, but to form crystals of the mixed oxide (Ba Sr) O.

When the filament was being run at 8 volts, the limiter potential was increased to 300 volts, and the emission current observed. A current in excess of 1 ma. indicated that the cathode had been satisfactorily processed by heating alone, sufficient metallic barium to produce the excess semiconductor structure which gives the required emission, being obtained through the reducing action of the cathode binder.

In cases where only a very small emission current was initially observed as the limiter was turned up to 300 volts, further processing was effected by leaving the filament set at 8 volts, and the limiter set at a voltage which drew a saturated emission current from the cathode. This emission current was then usually observed to rise over a period of up to one hour, as the necessary metallic barium was produced in the cathode through electrolysis and ion bombardment.

When fully activated, the emission current from the cathode remained in excess of 1 ma. as the filament was returned to its normal operating value of 6.3 volts. Afterthe cathode had been activated, the tube was rebaked and the getters fired.

7.10 Photo-cathode processing.

(a). Type of cathode used.

Early tubes incorporated antimony-caesium (S 9) photo-cathodes, prepared by standard techniques, used in this department. These have been documented by Khan[81]. Since the photo-cathode efficiency represents the maximum attainable quantum efficiency of any photo-electric detector, this should be made as high as possible, and therefore, the later tubes were made with trialkalim (S - 20) photo-cathodes since this type of cathode is the most sensitive semi-transparent photo-cathode for the visible region(169). Processing consisted essentially of evaporating an antimony layer of carefully controlled thickness on to a pyrex cathode plate, and activating this layer by exposing it to alkali vapours, when held at the temperature at which the most effective reaction occurs.

(b). Construction of the antimony evaporator.

An antimony bead was melted on to a platinum coated molybdenum wire in an argon atmosphere, and this was assembled into an evaporator whose construction is shown in fig. 7.25. Prior to processing, the evaporator rested in a side arm, blown on to the main pumping stem, (see fig. 7.12) but it could be manoeuvred into the processing compartment, by means of an external magnet, acting on the magnetic slug, and enabling the evaporator assembly to be slid along the tungsten rods through which the antimony heating current is introduced.

(c). Preparation of the alkali channels.

The alkali generating mixture consisted of alkali chromate, tungsten powder, and aluminium powder. Very pure reagents were used in each case, the metal powders being separately

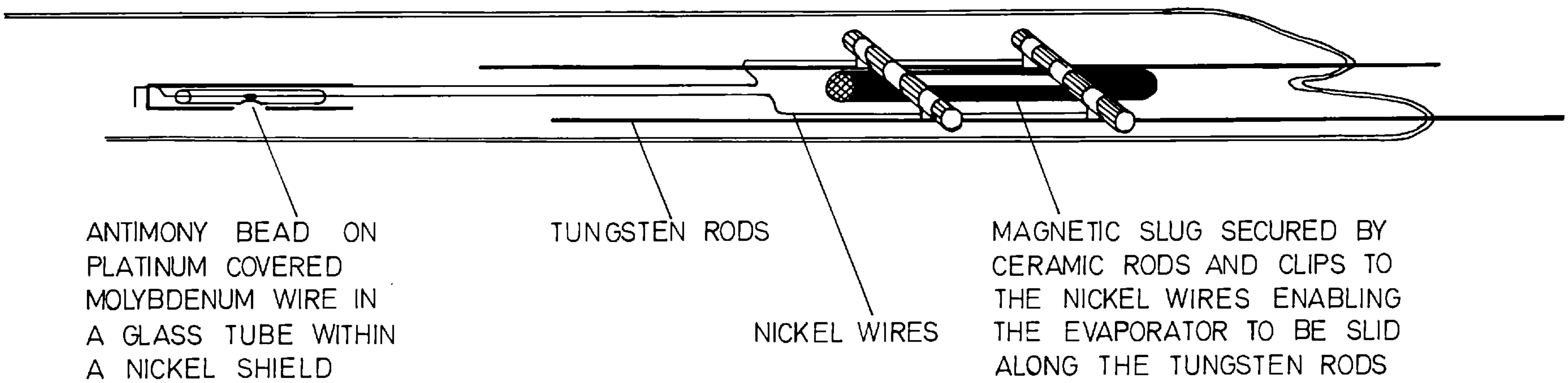

FIG 7.25 ANTIMONY EVAPORATOR

vacuum stoved before mixing with the chromate. The powders were mixed in the weight ratio of eight parts tungsten, to one each of aluminium and chromate for the caesium and potassium mixtures, but ten part of tungsten were used in the case of the sodium generating mixture. Alkali is liberated when these mixtures are heated through the aluminium reducing the chromate. Tungsten moderates this exothermic reaction by taking up excess heat. More tungsten was used for the sodium mixture as very careful control was required during the sodiation stage of processing.

The mixtures were transferred to nickel tubes of about 1 mm. in diameter. Slits were cut into these tubes by means of a razor blade, and they were cleaned by degreasing in trichloroethylene, boiling in caustic soda for ten minutes, soaking in cold dilute hydrochloric acid for another ten minutes, and then rinsing in distilled water and iso-propyl alcohol. They were finally cleaned by eddy current heating them up to red heat in a vacuum of 10^{-6} torr. After the tubes had been cleaned and filled with the mixtures, their ends were crimped, and they were assembled into the alkali generating chamber of the tube.

In the first tubes made with trialkali cathodes, the channels were welded on to tungsten pins in the walls of the processing compartment. This avoided the necessity of an extra seal-off when processing was completed, but introduced some disadvantages. Extra tungsten pins in the glass wall increased the risk of leaks, and, being located at the high voltage end of the tube, they provided extra sources of corona. Also, a certain amount of mixture invariably became shaken from the channels into the tube, during tube assembly. Therefore, when a method was devized of preventing the gas evolved during seal-off from entering the processing compartment, and poisoning the cathode, it was decided to mount the channels in a separate chamber, connected to the processing compartment by a side arm. The arrangement adopted is illustrated in fig 7.26.

The channels, (1), were welded on to tungsten pins in the walls of a chamber which was opened to the processing compartment during pumping and processing, by holding back a spring loaded flap, (2), by means of a hook on the end of the antimony evaporator (3). Magnetic manipulation of the evaporator, could either engage the hook to open the flap or release it, prior to seal off, when the flap would spring back to shut off the side arm. Another spring loaded flap, (4), sut off the other stem to be sealed off, and was pushed open

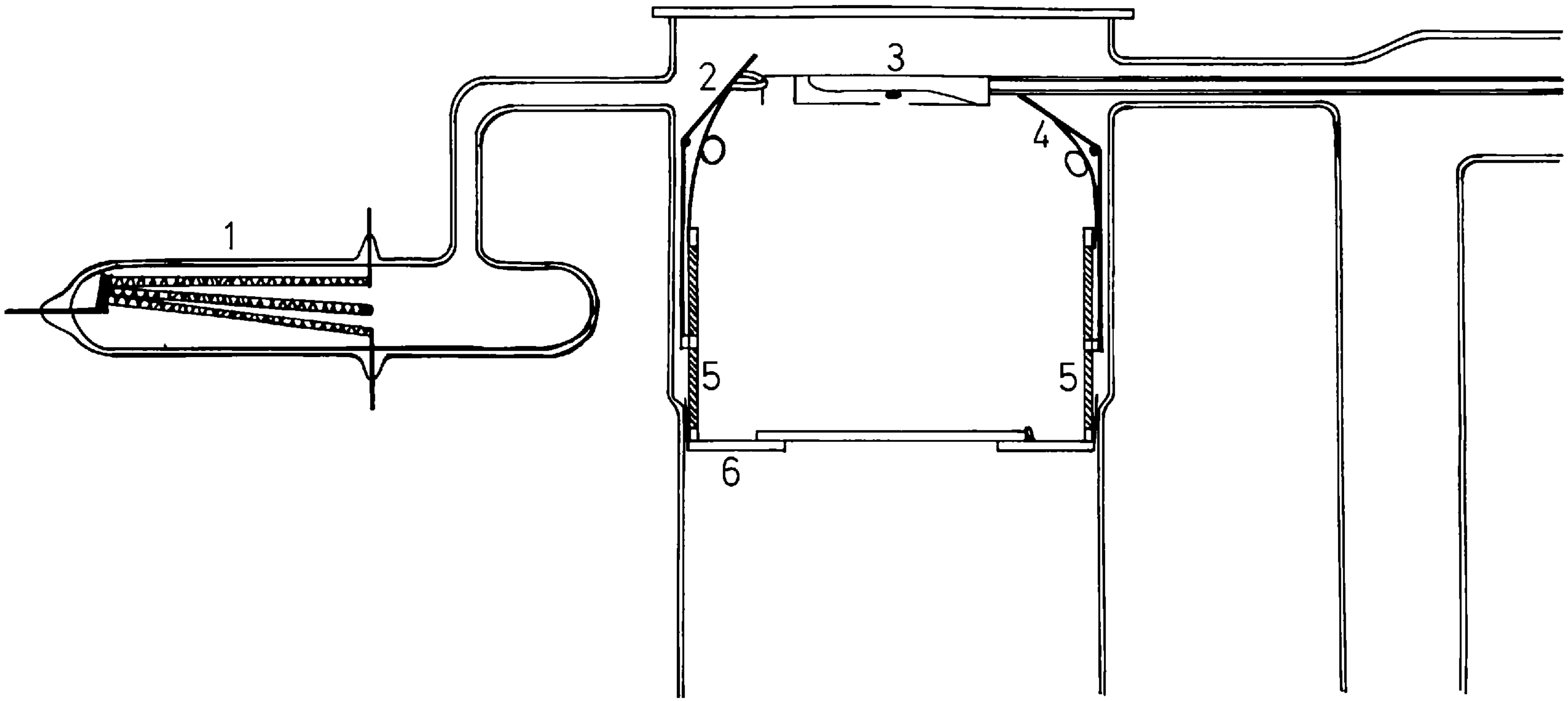

FIG. 7.26 PHOTOCATHODE PROCESSING COMPARTMENT

as the antimony evaporator was slid into the processing compartment, or spring back as the evaporator was withdrawn to its side arm. The spring loaded flaps were mounted on ceramic rods, (5), clip welded to the photocathode shelf (6).

As a further precaution against outgassing during seal off, the stems to be sealed off were degassed by flaming, prior to processing, and they were kept at 300°C during processing by heating coils.

The channels were degassed in situ, prior to processing, by passing currents through them, increasing the current as degassing proceeded until the channels were just observed to liberate alkali. At no time during degassing was the pressure allowed to rise above 5×10^{-6} torr.

(d). Antimony evaporation.

While still in the side arm, the antimony bead was cleaned by passing a current through the evaporator, increasing this heating current gradually, so that the pressure was maintained at a level below 5×10^{-6} torr. The current was noted at the point when the antimony started to evaporate, creating a metallic mirror below the antimony bead in the side arm. At this point, the heating current was turned off.

The evaporator was then manoeuvred into the processing compartment, opening the spring loaded flaps as described above (§7.10 (c)), and finally located in a position where the antimony bead stood directly above the centre of the photo-cathode plate.

A beam of light waa directed through the photo-cathode plate, to fall on to a barrier layer photo-ceil. This provided a means of monitorring the evaporation of antimony which was continued until the optical transmission of the photo-cathode plate had dropped to 65%.

(e). Setting up for activation.

A collimated beam of light, chopped at 1.4 K Hz was directed via a hole in the pump table and two prisms to pass through the photocathode plate.

The channels were connected to a supply, capable of delivering independent, metered outputs, variable from O to 10 amps.

A 150 volt supply was connected between the cathode shelf and a platinum ring which had been painted on the end of the tube for the purpose of silver chloride sealing, but which provided a convenient photo-electron collecting anode.

A screened lead was taken from the open pin on the cathode shelf to a sensitive amplifier, tuned to the lamp chopping frequency.

Thermocouples were arranged to monitor the temperature of the processing compartment and of the seal- off arms.

(f). Activation of the photocathode.

The oven was lowered over the tube, which was baked to 180°C and held at this temperature for 15 minutes. The current through the potassium channel was then slowly increased to the value at which it had previously been found to liberate alkali. At this stage, the chopper amplifier indicated a rise in photo-sensitivity which attained a maximum, and then began to fall as excess potassium was deposited on the cathode. The sensitivity was allowed to fall to about two-thirds of its peak before switching off the potassium channel. The tube was next baked to 220°C to drive off excess potassium. This was accompanied by the photosensitivity regaining its previously achieved maximum.

At this stage, the current through the sodium channel was increased to firing level and held there, the sensitivity rising as the sodium was generated. Immediately a new peak in sensitivity was attained, the sodium channel was turned off. This had to be done promptly, for unlike the other alkalis, any excess of sodium deposited cannot be baked off. The tube was then cooled back to 170°C by raising the oven slightly, when it was repotassiated to achieve a new peak in photo-emission.

The proportions of constituents, present in the cathode at this stage could be optimized by a procedure, known as the yo - yo technique, which involved alternately driving small amounts of potassium and antimony on to the cathode, until this could induce no improvement in sensitivity.

After this, the tube was cooled to 140°C, when caesium was introduced from the remaining channel to realize a new maximum photo-current. Caesiation was continued until a drop of about 30% in sensitivity occurred through over-caesiation. The tube was then allowed to cool to about 90°C, during which time, excess caesium baked off, restoring the photo-sensitivity to a typical maximum of 100 μA / lumen.

Once the tube had cooled to room temperature, the channel chamber was sealed off, and the antimony evaporator withdrawn to allow the tube to be sealed off the pump. The cathode was then turned over, putting the tube into the condition of an operational television camera.

CHAPTER 8

A demountable, continuously pumped, target testing apparatus.

8.1 The value of a demountable monoscope as a test apparatus.

It became clear that since the most important component of the new storage tube was the spongy target, development of the camera by the mere construction of a succession of tubes would be an inefficient approach to the problem. It was therefore decided to construct a layer testing device, in which the target could be exposed to energetic primary electrons, and scanned with a low velocity beam to generate a video signal, just as in a camera tube, but which provided the additional facility of being easily demountable to allow the target to be changed. Such an apparatus would permit the effect of varying target parameters to be readily assessed, as well as allowing experiments to be made on changing the design of the scanning section.

8.2 Design features of the demountable system.

The construction of the apparatus is represented diagramatically in fig. 8.1 and illustrated pictorially by the photograph, shown as fig. 8.2.

FIG. 8.1 DEMOUNTABLE TARGET TESTING APPARATUS

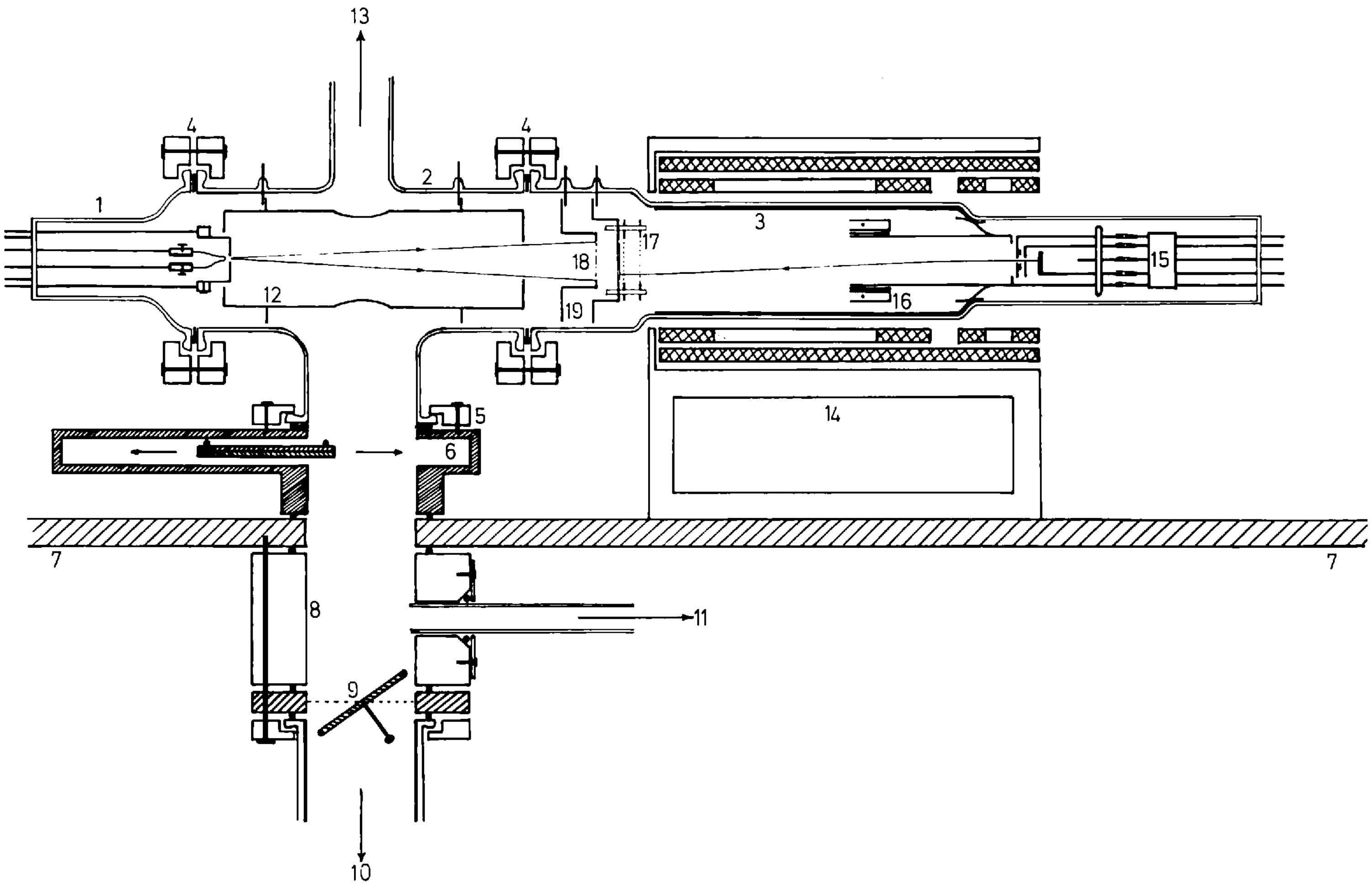

The device consisted basicly of threo separate sections, an E.H.T. flood gun, (1), a glass manifold, (2), and a scanning section, (3). The sections were held together by clamps, (4), assembled around flanges at the end of each section. A similar clamp, (5), held the whole system on to a gate valve, (6), which rested over the pumping port of a dural pump table, (7). Immediately under this pump table was a dural manifold, (8), which opened, either via a butterfly valve (9) to a mercury diffusion pump, (10), or to a roughing line, (11), which could be isolated by a stopcock. The roughing line could be pumped directly, or through a constriction when slow pump out was required to protect the layer.

The vacuum seals at all the ground glass faces of the flanges or at the various metal interfaces of the vacuum components were made by means of viton 'O' rings. Aluminium support rings were turned out to prevent the 'O' rings being sucked into the apparatus during pump down, in positions where an 'O' ring seating was not provided. The use of viton 'O' rings allowed the system to be baked up to 200°C, after which, vacuums of 5×10^{-7} torr could be achieved.

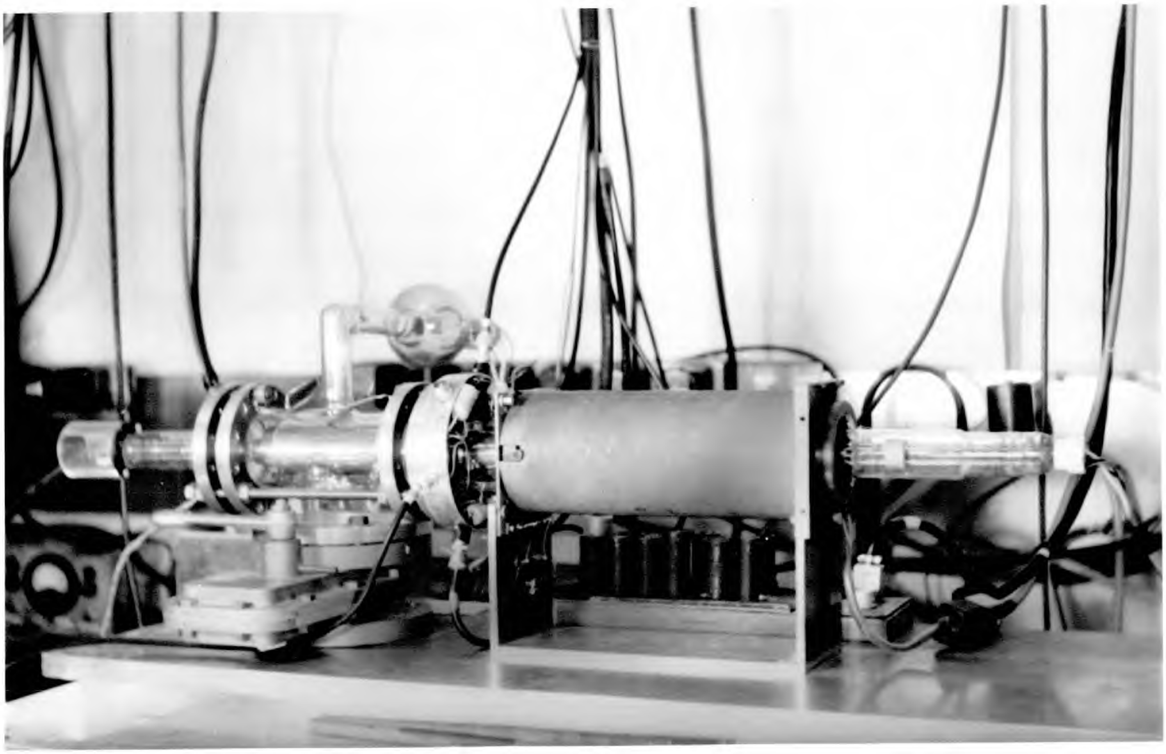

FIG.8.2 DEMOUNTABLE TARGET TESTING APPARATUS

8.3 The E.H.T. flood gun section.

The E.H.T. flood gun consisted of a 0.004" tungsten filament and a modulator. The modulator was retained in a seating by grub screws, and could thus be easily removed to allow the filament to be replaced in case of burn-out. The ends of the hairpin filament were clamped into two blocks by 10 B.A. screws. The flood gun was held at negative E.H.T. potentials, and the variable filament supply was derived from an emitter follower circuit, housed with its 6 volt accumulator supply in a perspex box.

8.4 The glass manifold.

A cylindrical, stainless steel, wall anode, (12), was mounted on tungsten pins, sealed through the walls of the glass manifold. This wall anode was earthed and had holes cut into it opposite the pumping port and a side arm, leading to a conventional ion gauge, (13). An aperture in the end of this wall anode defined the beam of energetic electrons which passed on to the scanning section where the target was mounted.

8.5 The scanning section.

The electron optics of the scanning section were based on the miniature C.P.S. Emitron system, used in the storage tubes described above, (chapter 7). Focusing and deflection were achieved by a standard solenoid and scanning yoke, (14).

The gun itself was an E.M.I., low-wattage, high resolution vidicon gun, which could be plugged directly into an internally mounted socket, (15). This allowed for easy gun replacement as the cathodes became poisoned.

In the region between the cylindrical, vidicon gun, wall-anode and the platinized continuation of this anode, painted on the glass wall, was mounted alow-velocity flood gun, (16), insulated from the wall anode by mica strips. This flood gun consisted of a circular, 0.001" tungsten filament, mounted within a low voltage annular cup, which served to direct the electrons forward when the normal H.T. was applied to the wall anode. Being located behind the vidicon wall anode, the low voltage flood gun was screened from the scanning beam, so avoiding any defocusing effects.

The mesh and target assembly, (17), was constructed as a unit with ceramic rods, glass spacers, and spot welded clips, by a similar method to that used in tube assembly (§7.3). The unit was clipped in position, on to tungsten pins, sealed in the glass walls of the tube.

Between the target and the E.H.T. flood gun was mounted a stencil test pattern, (18). This consisted of a 0.001" sheet of copper foil, through which a Baum test-pattern(12) enlarged to a diameter of 20 mm. had been etched by means of photo-resist techniques(87). The half tone features of the pattern were, of course, not reproduced in the stencil, but the detail achieved in the resolution wedge, almost reached the definition at the fine end of the master pattern, i.e. bars were etched through the copper, down to resolutions corresponding to 20 line pairs/mm.

The stencil was bolted into a stainless steel mount, (19), and clipped on to tungsten pins, sealed in the glass wall of the scanning section so that the stencil was located about 5 mm. from the target. The uniform beam of electrons from the E.H.T. flood gun passed through the stencil, before encountering the target, so that these primary, energetic electrons have impressed spatial information to simulate electrons from a pattern on a photocathode, coming to focus on the target.

8.6 Introduction of layers into the tester.

Whenever it was desired to change the layer in the test apparatus, the diffusion pump was isolated by means of the butterfly valve (9), and a stop-cock on the backing line, while the rest of the apparatus was let down to dry argon via the roughing line. When full of argon at atmospheric pressure, the layer tester could be sealed by the gate valve, (6), and transferred to a dry-box. Here, the scanning section could be unclamped, allowing the stencil, (19), and target assembly, (17), to be unclipped from their tungsten, mounting pins. The old target which was secured to its mount by three 10 B.A. screws through the titanium mounting ring could be easily removed and replaced with a new one. The target assembly and stencil were then reclipped into the scanning section, which in turn, was resecured to the main body of the layer tester. The layer tester was then replaced over the pumping port, the roughing line flushed with dry argon, the gate valve opened, and the system reevacuated.

8.7 Performance of the layer tester.

The layer tester proved to be straightforward to operate, and functioned much as anticipated. A picture, generated by the apparatus is given in fig. 8.3.

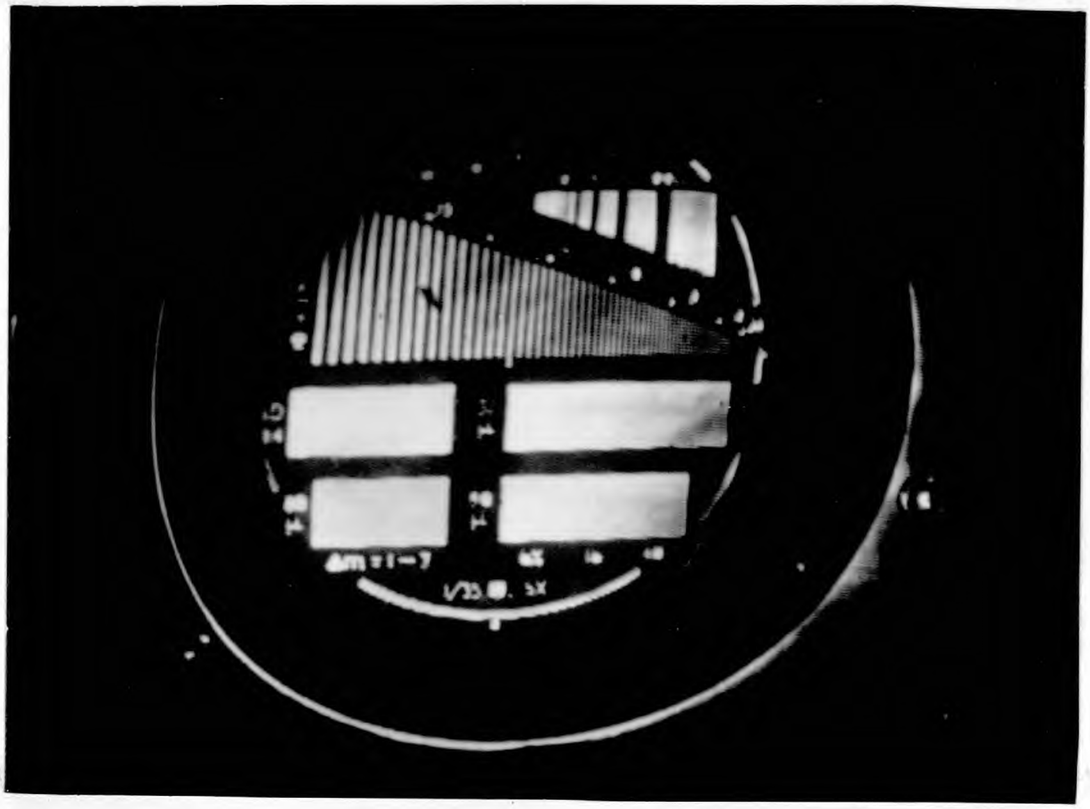

FIG. 8.3 PICTURE GENERATED BY TARGET TESTER OPERATED AT SLOW SCAN RATES.

It was possible to calibrate the primary current, reaching the target, in terms of current flowing to the stencil. This facilitated the measurement of target gain under operating, i.e. signal generating, conditions.

The low voltage, flood-gun filament in the scanning section could be biased to a potential, just below the first cross-over of the target. This provided a means of target stabilization which did not interfere with signal generation, and which allowed the reading beam to be zoomed to probe small areas of the target, without the surrounding areas becoming unstable. Examination of the high resolution end of the test-pattern in this way, enabled resolutions corresponding to the stencil limit, i.e. 20 line pairs / mm. to be displayed as the primary current from the E.H.T. flood gun was increased. This was better than the limiting resolution of 15 line pairs / mm. which could be achieved in tubes, or in the layer tester when the target was fully scanned. The implications of this are discussed below (§ 10.7).

The low-velocity, flood-gun also provided a method of measuring the potential excursions of the target. These could be determined by observing the low velocity, flood-gun, filament bias potential at which the video signal corresponding to a particular highlight of interest just began to reduce.

Although the target tester was essentially a monoscope, the primary image could be deflected across the target by means of a magnet, which gave an indication as to whether or not targets exhibited any appreciable lag.

It is hoped that more sophisticated stencils will be made, which will provide information about the ability of the target to enable discrimination to be made between half-tones.

CHAPTER 9.

Electronic equipment, used in conjunction with the storage tube and layer testing apparatus.

9.1 General.

Most of the experimental work was carried out, using a closed circuit industrial television channel, very similar to the E.M.I. Channel, type 10270-C. This provided television wave forms, corresponding to an interlaced 405 line system, running at 25 frames per second. The gun and scan supplies were fed from the industrial channel to the camera, mounted in a separate unit. The other voltages and currents, necessary to focus the tube, were fed to the camera unit from commercial stabilized power supplies, mounted in a separate rack. The overall system used, is illustrated in the block diagram, given in fig. 9.1.

A system working at slow scan rates was also constructed, and fig. 9.2 shows a block diagram of this apparatus. The camera and layer tester, featured in figs. 9.1 and 9.2 respectively could be fairly easily interchanged.

Much of the electronic equipment was inherited from previous workers in the applied physics section, and has been

FIG.9.1 BLOCK DIAGRAM OF CAMERA TUBE OPERATING WITH CONVENTIONAL SCAN-RATE EQUIPMENT

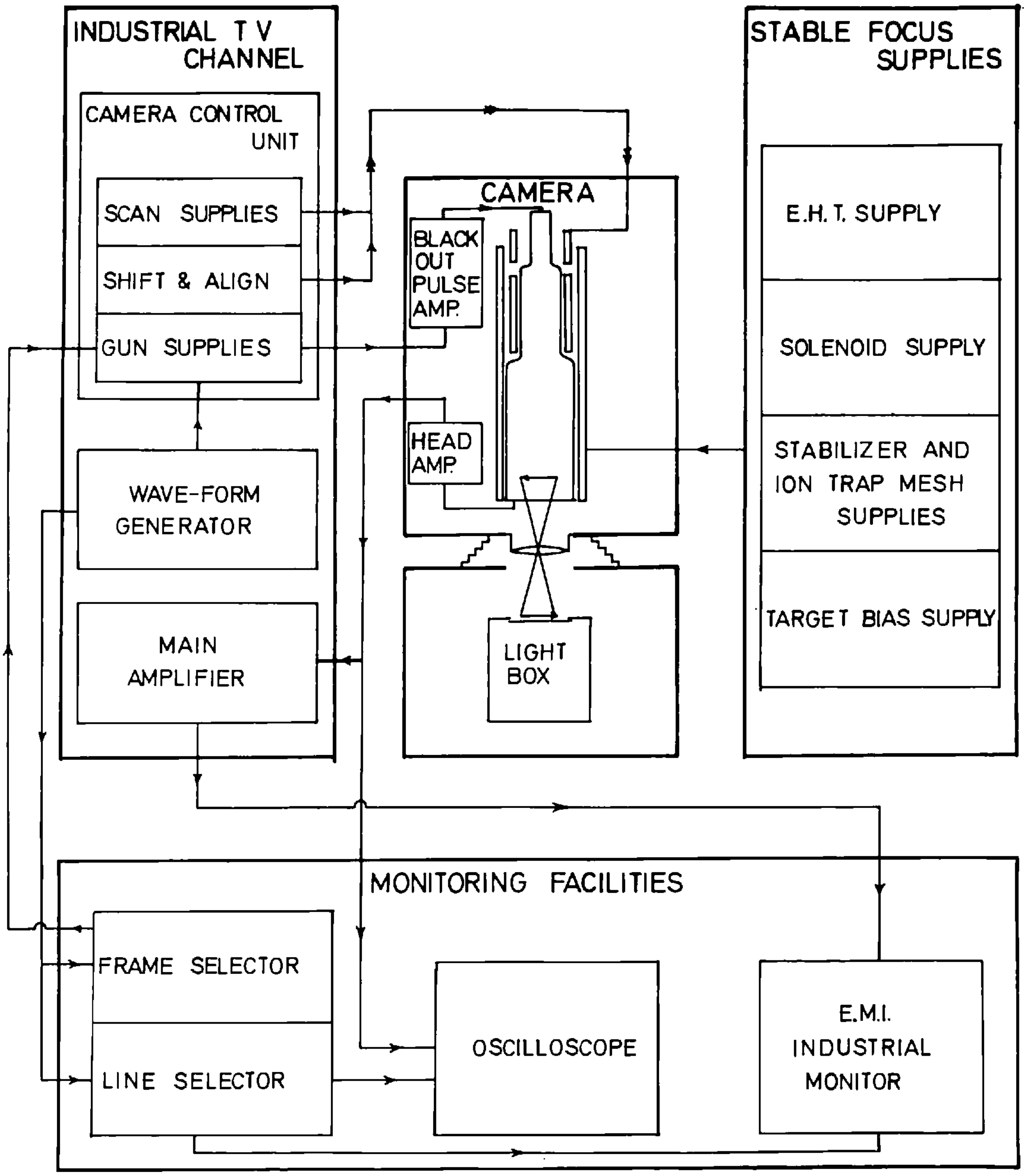

FIG.9.2 BLOCK DIAGRAM OF LAYER TESTER OPERATING WITH SLOW SCAN-RATE EQUIPMENT

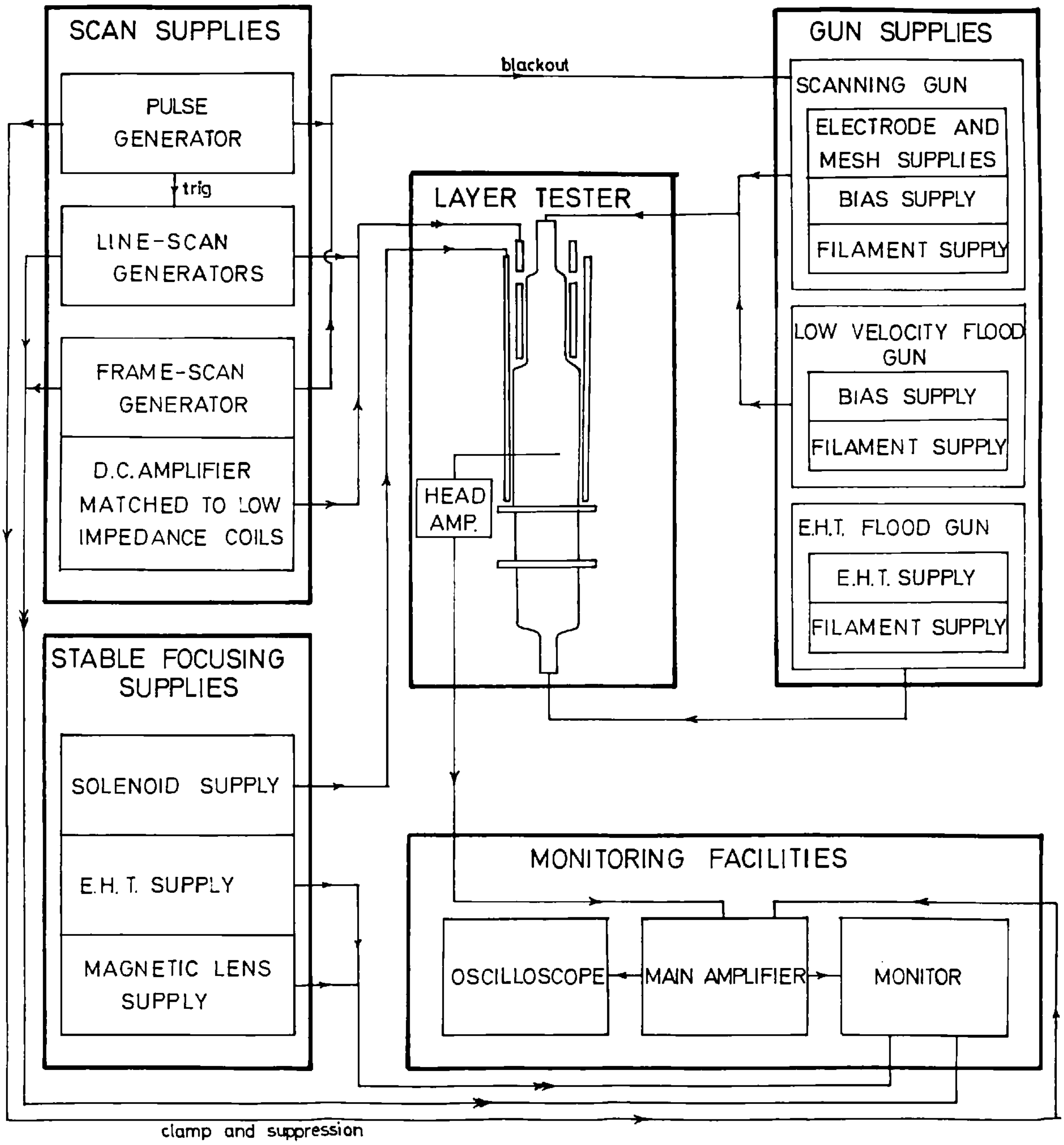

described in their various theses(80, 128, 140). A few additional units and modifications were required for the operation of the new camera tube and the layer testing apparatus.

9.2 Conventional Scan-rate Equipment.

The industrial channel, working at broadcast standards, provided an apparatus, generating an output video signal incorporating synch pulses. The video signal could thus be fed directly to a standard industrial monitor, without supplying separate synchronization. This ready-made equipment was of course, an invaluable piece of essential test gear, and it is perhaps looking a gift-horse in the mouth to suggest that the interlace and synch insertion features were unnecessary refinements and complications in an apparatus to be used for camera testing.

A line selector enabled the video signal, corresponding to any chosen line to be monitored on an oscilloscope.

A frame selector was built which provided a facility for switching off the scanning beam by applying a negative voltage to the modulator. After a predetermined number of frames, the modulator was switched on by the leading edge of a frame trigger pulse, for a period of one frame, allowing read-off of the charge image, integrated on the target. The frame trigger pulse, used to initiate the read off, could be gated by a manual control when it was required to integrate for more than 25 frames.

9.3 The Camera. (Fig. 9.3)

The storage tube was mounted in an obsolete C.P.S. Emitron Camera unit, donated to the department by the B.B.C. This was considerably modified to accomodate the spongy potassium chloride target tube. The solenoid was lengthened and provision was made to introduce and decouple the various focusing and bias supplies required.

The most useful feature of the precisely engineered B.B.C. camera box, retained after modification, was an optical focusing facility, provided by an external control, which allowed the solenoid complete with the tube and scanning yoke housed within, to be moved relative to the lens.

9.4 Light Source.

Test patterns in the form of 35 mm. transparent slides could be slipped into a slide holder, mounted at the front of a light-box, and uniformly illuminated from behind by a 25 watt tungsten filament lamp, located beyond a ground glass screen

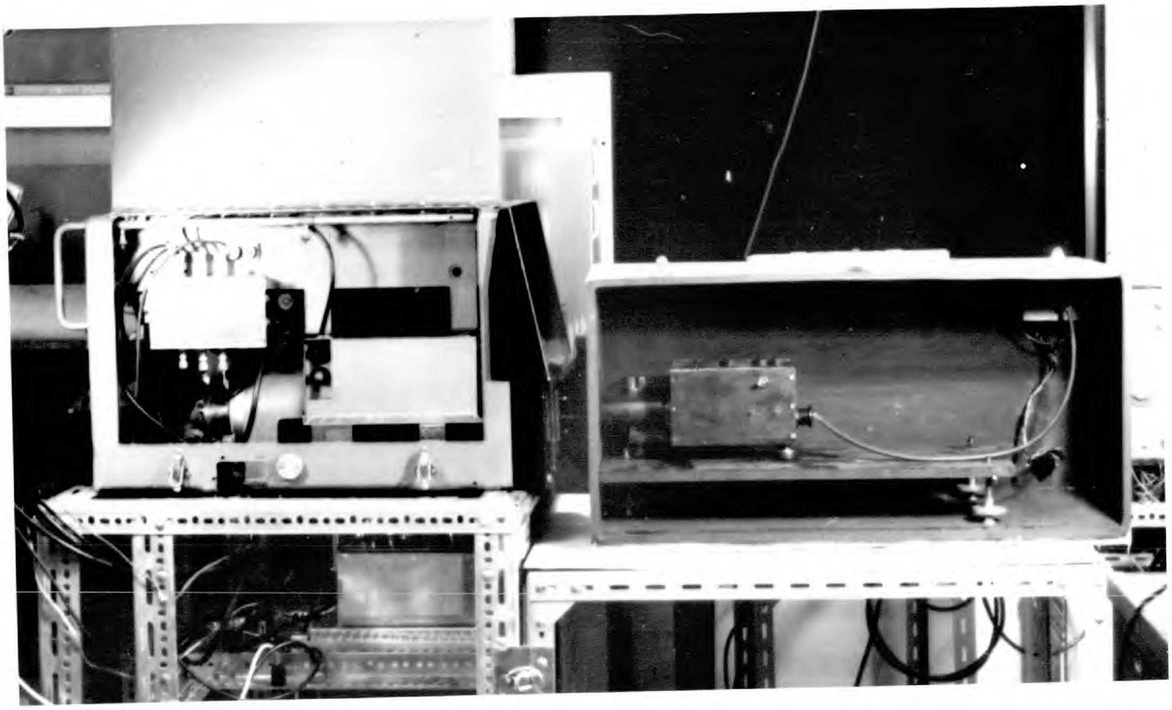

FIG. 9.3 CAMERA AND LIGHT BOX

in the light box. Adjustment of the light level could be made by means of calibrated neutral density filters, slipped into the slide holder, or by the relative rotation of two sheets of polaroid, mounted within the light box. The light box rested on a platform, whose height and level could be set by screw adjustments.

Recently, a light tight cabinet has been made, to provide a housing for the light-box. This cabinet contains a single aperture for the camera lens, and it may be butted against the camera and secured by case clips, so that the tube is exposed only to illumination from the light box within the cabinet. This enables low light-level experiments to be carried out, while maintaining a high ambient illumination in the laboratory. Access to the light box is provided by a hinged lid, at the side of the cabinet.

9.5 The slow-scan equipment.

The system employed, used a frame scan with an 8 second period, and a line scan of 50 Hz. This followed the practice adopted by Khan (80) and Mende (128), and some of the time base circuits and amplifiers, built by these workers were incorporated into the author's equipment.

Use of a 50 Hz line frequency enabled line scan circuits to be built, which were direct copies of frame scan units, used in the conventional video equipment. However, the bandwidth of 15 kHz differs from the optimum of 200 kHz, calculated above (§ 5.8) for a sytem, using a R 5559 valve as its first amplifying stage. The head amplifier was therefore designed around a different valve, the E 80 F, which is a very low noise pentode. The signal to noise in the output of this sytem was not amplifier limited, more noise being generated in the parts of the signal corresponding to picture whites.

A unit was built to generate the various 50 Hz pulses required, i.e. line trigger, clamp, suppression, and blackout pulses, synchronized with mains frequency. The frame blackout pulses were derived from the slow time-base unit. This consisted basicly, of a Miller integrator circuit, generating a linear ramp which was amplified to provide outputs, suitable for driving high impedance monitor scan coils and a low impedance camera yoke respectively. The monitor coils were supplied from the output, generated across the anodes of two power valves in a long-tail pair circuit, while a transistorized D.C. amplifier was used to drive the camera coils. The monitor was an old radar tube with a long persistance (P 26) phosphor.

9.6 Layer tester gun supply unit.

A unit was built to supply the scanning gun in the layer tester which provided facilites for adjusting and monitoring all the electrode potentials. Provision was also made for measuring the cathode emission current as the filament voltage was varied from zero to 8 volts, enabling the gun supply to be used as a processing unit. This facility was important, as guns needed to be reprocessed, each time the system was pumped down. A connection was made, direct from the evaporated aluminium signal plate of the layer to the imput of the head amplifier, so minimizing the stray capacity of the signal lead to earth. Bias across the target, which is set by the relative potentials of the scanning gun cathode and the signal plate, was varied by arranging for the complete gun electrode system to be adjusted by up to $\pm$ 40 volts, relative to earth, additional provision being made on the gun supply unit to control and monitor this adjustment.

The photograph in fig 8.3 shows a picture generated by the layer tester when operated at slow scan rates.

CHAPTER 10

Experimental work and results.

10.1 Early tests on the transmission secondary emission properties of spongy potassium chloride targets.

The author, working in collaboration with Rosenbloom, made measurements on the transmission secondary emission of potassium chloride films, using a gun tube whose construction is shown schematically in fig. 10.1. A beam of electrons from a hairpin filament gun (1), was accelerated and focused on to the film (2). A magnetically controlled phosphor plate, (3), was used to monitor the position and the sharpness of the electron image. When a sharply defined circle was observed on the phosphor, at about the centre of the target, the phosphor plate could be swung out of the beam, allowing the electrons to impinge directly on to the potassium chloride film, (2), where excited secondaries could be emitted and collected by the mesh (4). The accelerating and focusing electrodes, (5), and the guard rings (6) round the layer were platinum painted on to the glass, and electrical contact was made by means of platinum tape seals. A silver chloride sealed end plate (7), enabled the tube to be opened for the purpose of layer changing.

FIG. 10.1 GUN TUBE FOR TESTING TRANSMISSION SECONDARY EMISSION PROPERTIES OF SPONGY POTASSIUM CHLORIDE LAYERS

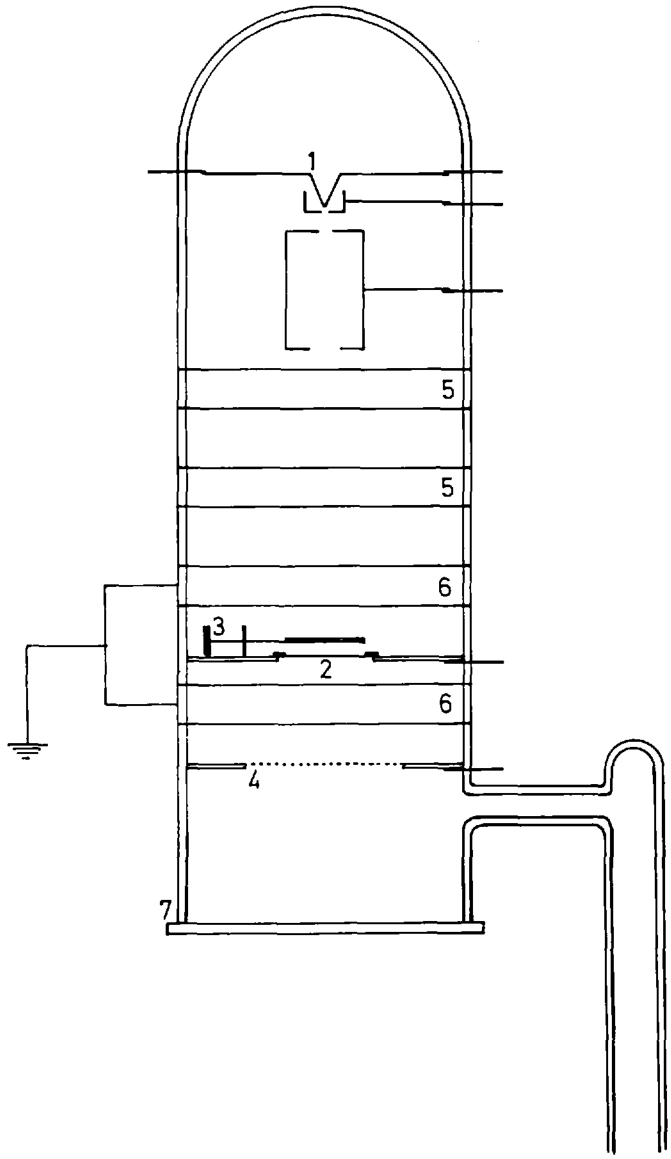

The currents flowing to the film were measured by means of an electrometer, and secondary emission was measured as a function of primary electron energy for various values of the mesh potential.

Essentially, the same experiment was repeated on the first camera tube constructed. The only differences in the experimental procedure, lay in that an electro-magnetically focused primary electron beam, derived from a light spot on the photo-cathode was used, and television monitoring replaced the swinging phosphor. The scanning beam was turned off when making measurements.

The results of the two experiments are shown in figs 10.2 and 10.3 respectively. The slight but definite differences in the two families of graphs cannot be readily accounted for, as both layers came from the same batch. The layer in the gun tube was baked to 200°C, while that in the camera tube experienced a photo-cathode processing baking cycle and this may account for the small differences in layer properties, observed, but a systematic investigation on the effects of baking targets has yet to be carried out.

FIG.10.2 T.S.E. GAIN CHARACTERISTICS OF A FILM MEASURED IN GUN TUBE

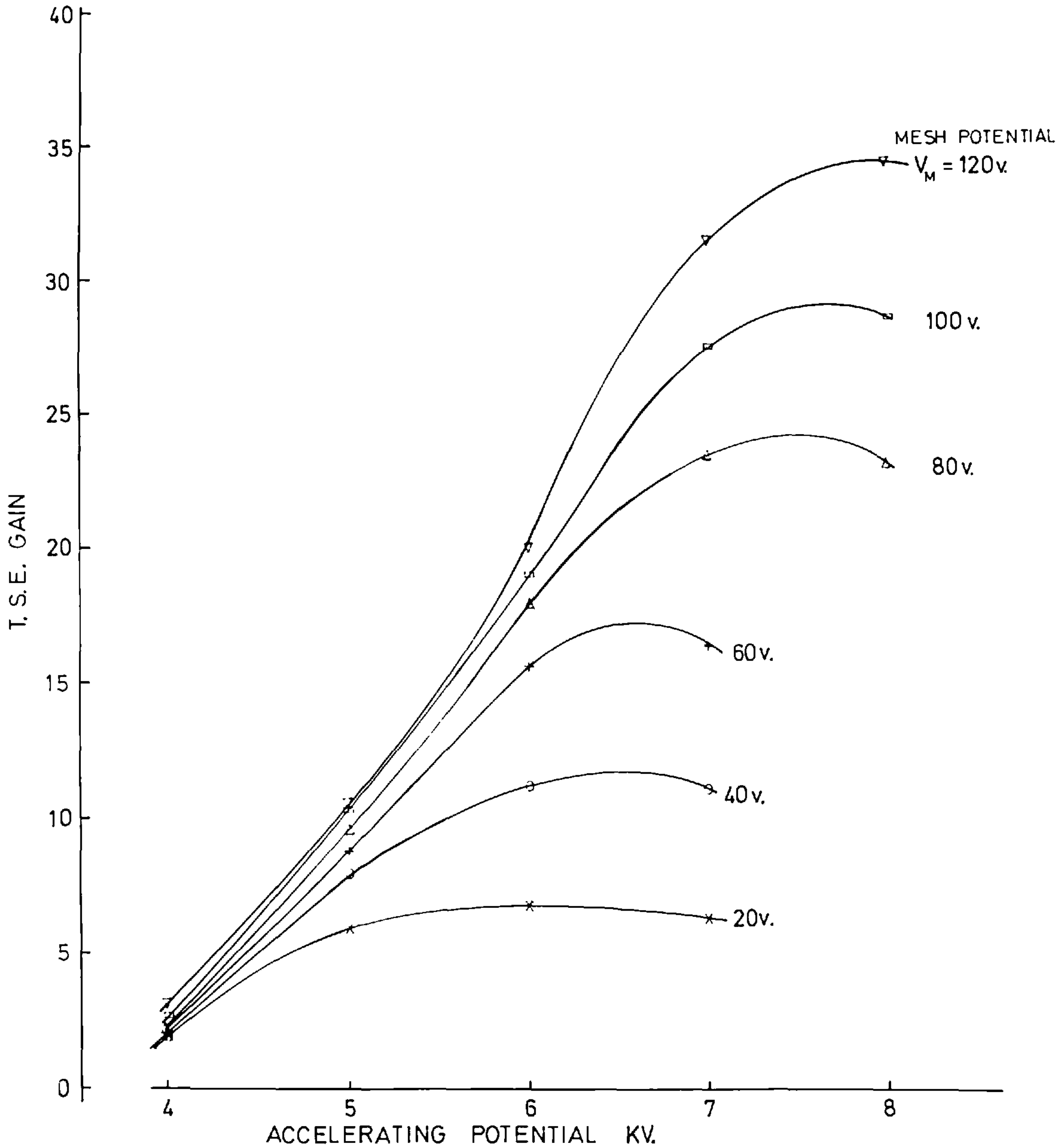

FIG. 10.3 T. S. E. GAIN CHARACTERISTICS OF A FILM MEASURED IN A CAMERA TUBE

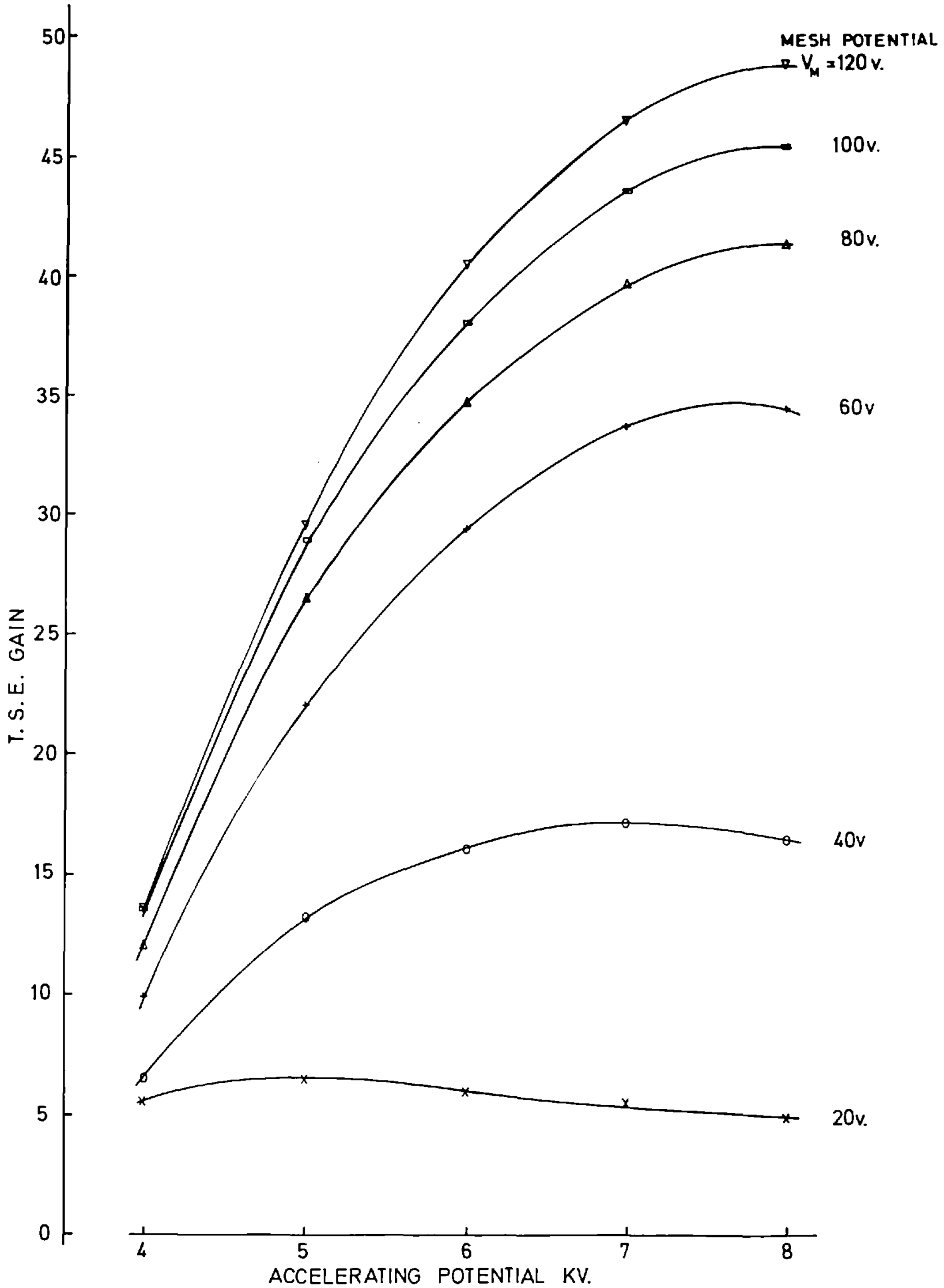

The curves in figs 10.2 and 10.3 illustrate that transmission secondary emission gain increases monotonically with mesh potential, V_M and adopts a maximum for primary electron energies of about 7 KeV. The dependance of secondary emission gain on mesh potential is an indication that the gain is strongly affected by field gradients, existing across the layers.

While the results indicate that spongy dynodes exhibit transmission secondary emission gains, of an order of magnitude higher than that of solid dynodes, it does not follow that a spongy layer will behave in the same way, when functioning as a camera tube target. In a pick-up tube, the field gradients which would build up across the insulating dynode as a result of secondary emission are countered by the stabilizing action of the scanning beam.

10.2 Measurement of the transmission secondary emission of a target, operated under video signal generating conditions.

In order to ascertain the transmission secondary emission gain of a spongy dynode, whose exit surface was stabilized by the action of a scanning beam, a pulsed light experiment was devized and set up as illustrated in fig. 10.4.

The pick up tube was exposed to the light patch on the phosphor of a defocused cathode ray tube, which was switched on, once a frame, for a period of 20 μ sec. ($<$ line period) by means of a delayed pulse, initiated by the line selector. Since the cathode ray tube used for this experiment had a low persistance (P 16) phosphor, the pick-up tube received a sharp light pulse, once per frame. The video signal, corresponding to the line, embracing this pulse, was monitored on an oscilloscope, triggered from the line selector, and the observed features of this signal are indicated in fig. 10.4.

The positive going pulse corresponded to the true video signal, resulting from the scanning of the charge image, stored on the target during exposure to the light pulse. The origin of the 'infra-black' pulse was the charging signal, generated by the pulse of electrons, arriving from the photo-cathode, and ejecting secondaries to the mesh from the reverse side of the layer. Overlapping of the two signals was avoided by appropriate positioning and timing of the light patch and pulse respectively.

The transmission secondary emission gain of the scanned target was measured by observing the charging signal pulse

FIG. 10.4 PULSED LIGHT EXPERIMENT TO MEASURE THE CONTRIBUTION TO SIGNAL GENERATION ARISING FROM T.S.E.

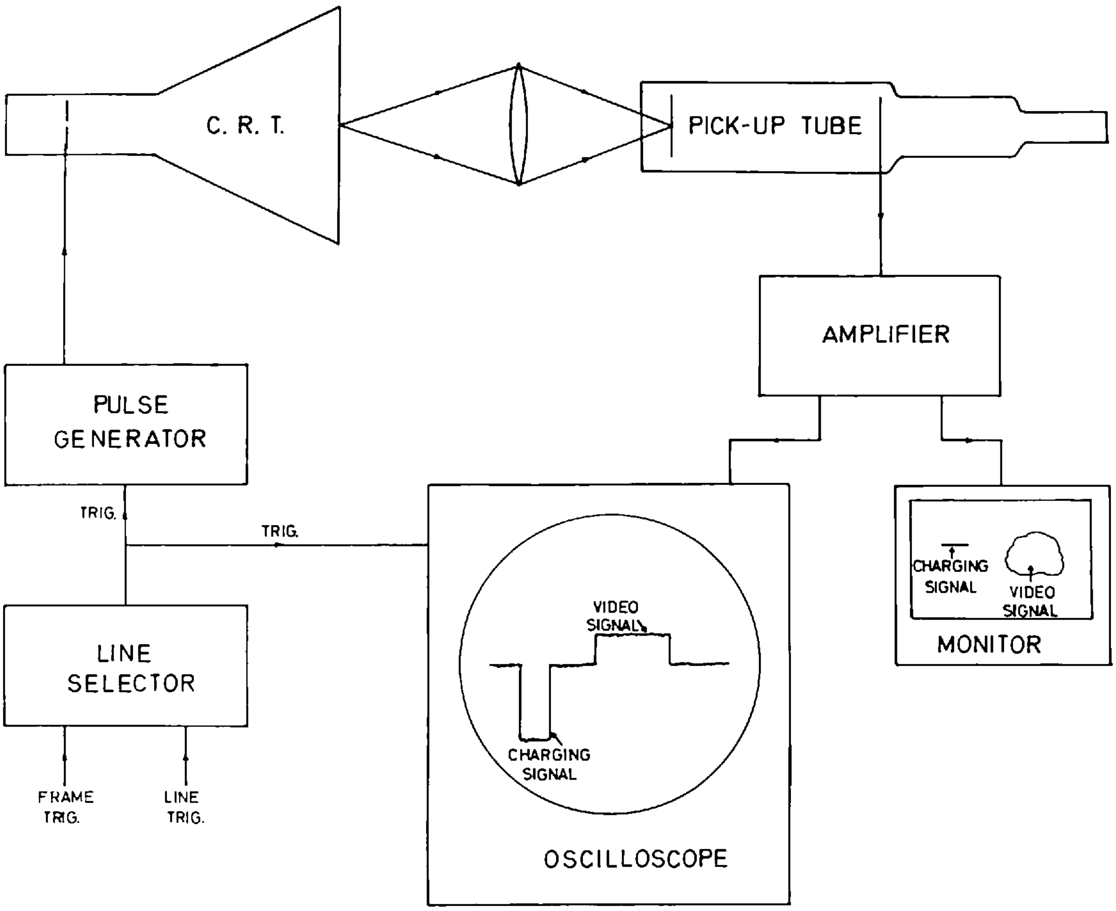

THE LINE SELECTOR IS USED TO PROVIDE TRIGGER PULSES FOR THE OSCILLOSCOPE AND PULSE GENERATOR, ONCE PER FRAME, AT A PRESELECTED LINE.
ON TRIGGERING THE PULSE GENERATOR INTRODUCES A DELAY OF 20μSECS. BEFORE SWITCHING ON THE C.R.T. FOR A 20μSEC. PERIOD.
THE OSCILLOSCOPE MONITORS THE LINE FROM THE VIDEO SIGNAL WHICH EMBRACES THE CHARGING SIGNAL PRODUCED BY THE LIGHT PULSE

height at various accelerating voltages. Reduction in the accelerating potential was accompanied by decreased secondary emission, and the video signal reduced to noise level, while the charging current pulse reversed in sign to become a positive pulse, whose height adopted a flat maximum over the range of primary voltages, 1-3 Kv. This positive pulse height was taken as a measure of the primary current, delivered by the photocathode. Thus, the transmission secondary emission gain could be calculated, and plotted as a function of primary electron energy.

It was possible to vary the potential gradient across the spongy layers, scanned with a low velocity beam, by altering the signal plate potential, V_{sp}, with respect to the scanning gun cathode potential.

A series of measurements of transmission secondary emission gain were made for various signal plate potentials, and the results obtained are illustrated in fig. 10.5. The curves exhibit a flat maximum for primary energies in excess of 7 to 8 keV. Fig. 10.6 illustrates the variation of T.S.E. gain with Vsp for 7 keV primaries.

FIG.10.5 THE VARIATION OF T.S.E. GAIN OF A SCANNED LAYER WITH PRIMARY PHOTO-ELECTRON ENERGY FOR VARIOUS SIGNAL PLATE POTENTIALS

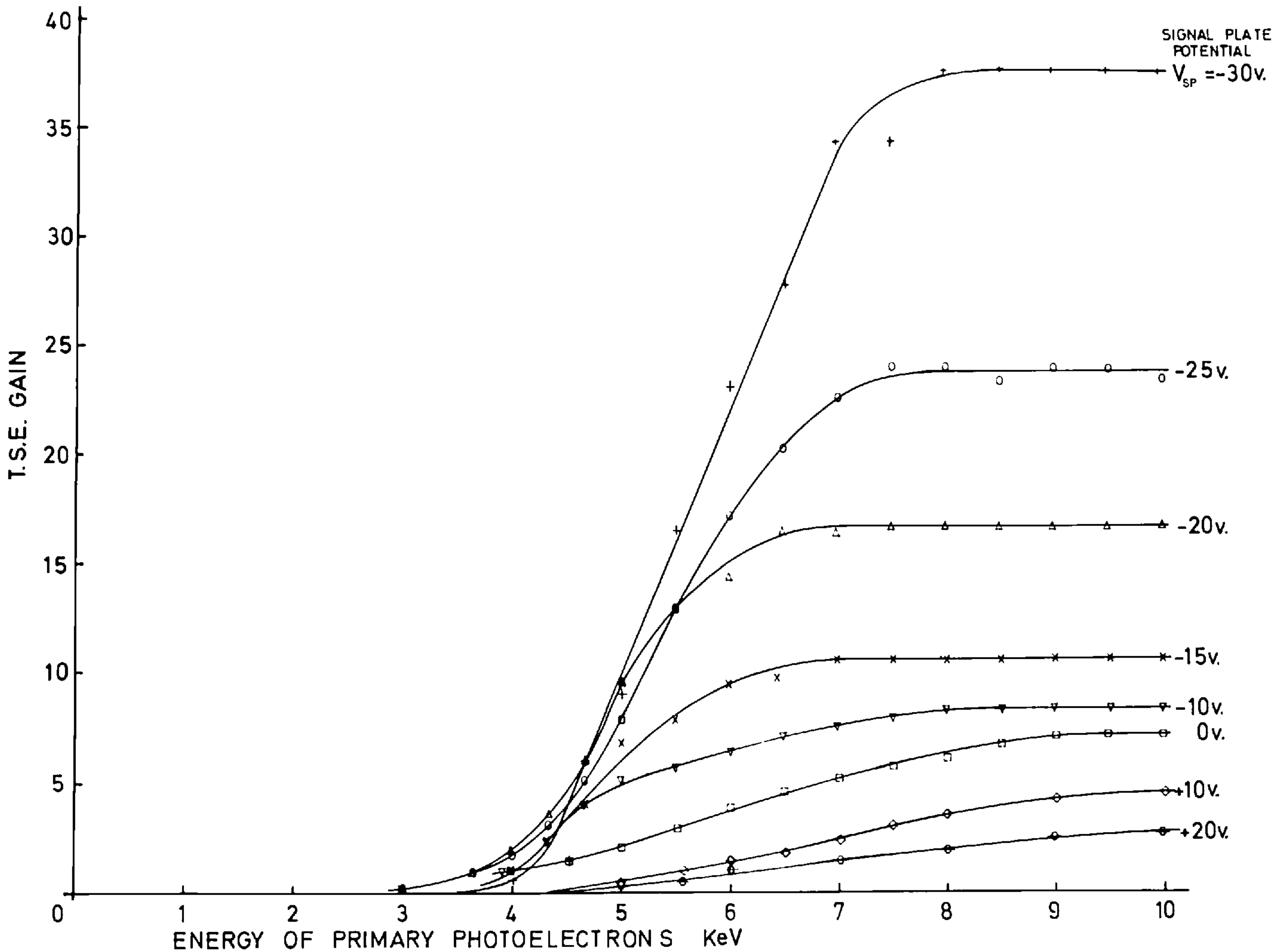

FIG. 10.6 THE VARIATION OF T.S.E. GAIN OF A SCANNED LAYER WITH SIGNAL PLATE POTENTIAL FOR 7KeV PRIMARY PHOTO-ELECTRONS

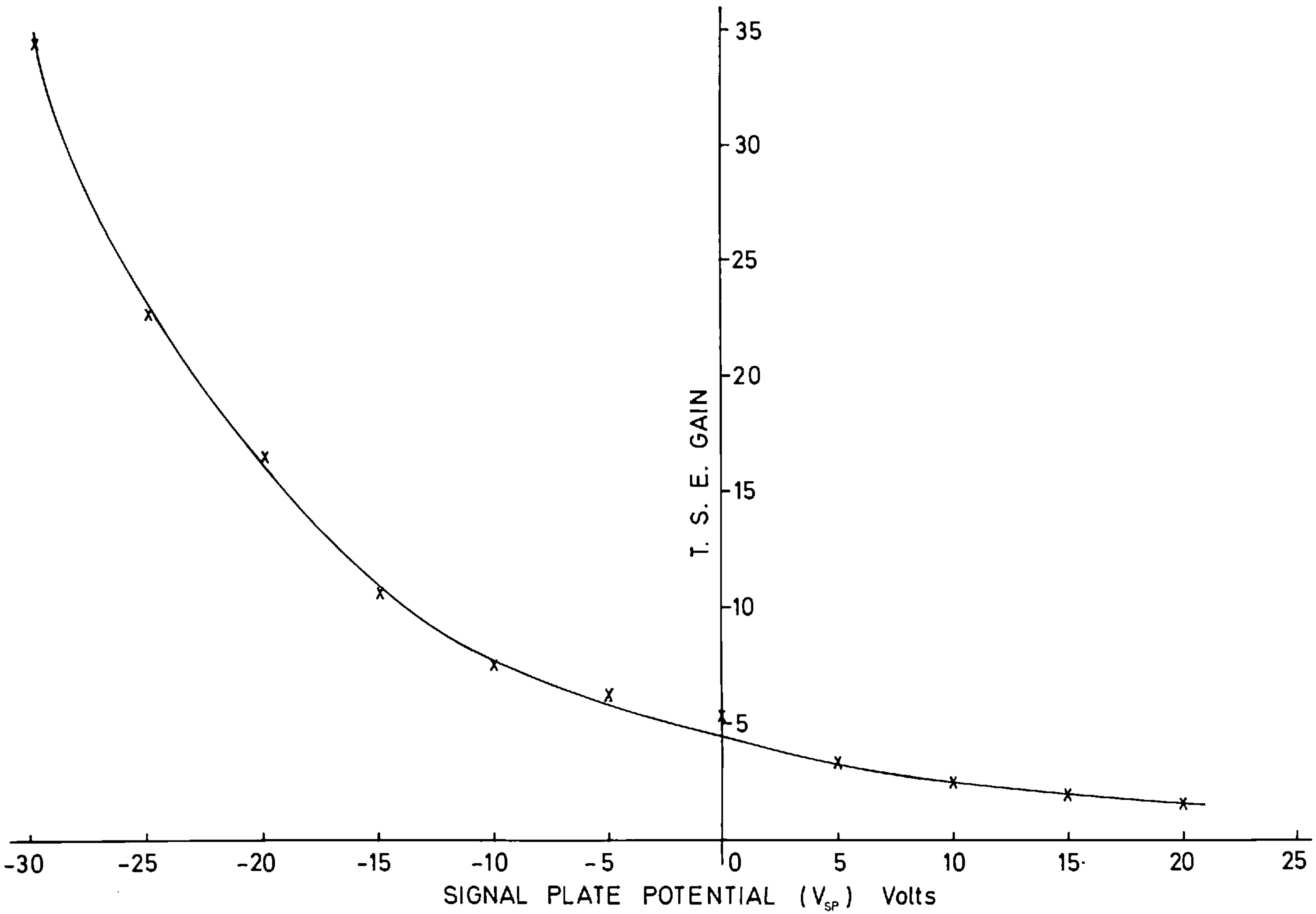

10.3 Secondary Electron Conduction.

While the curves in fig. 10.6 indicate that transmission secondary emission increases with decreasing signal plate potential, the total gain of the target was found to vary in the opposite way with signal plate potential. This was evidence for the existence of an additional mechanism, contributing to the signal generating process, which in some ways, appeared to be similar to the trans-target conduction effects, observed in tubes like the vidicon, (§ 6.6) and ebicon (§ 6.8), but no appreciable lag was observed to accompany the process, (see below § 10.9), indicating that the process occurring was probably somewhat different to the solid-state conduction occurring in the earlier types of television camera.

This was also observed by the Westinghouse workers(63), who designated the process occurring in the spongy layer, Secondary Electron Conduction, (S.E.C.), and ascribed the phenomenon to secondary electrons, excited within the layer, migrating through the vacuum pores in the spongy potassium chloride under the influence of the internal field, existing in the layer.

The author measured the S.E.C. gain of the target, using the set-up illustrated in fig. 10.7. The tube was set up to generate a picture of a steady light patch, and the current flowing into the signal plate was measured on the electrometer. Since the time constant of the electrometer was much greater than one frame period, the contribution due to the effect of T.S.E. was not observed as this was cancelled by a charging current, flowing to the target from earth to replace the transmitted secondaries. The current registered on the electrometer was thus the sum of the S.E.C. current, delivered to the target by the scanning beam, and the primary photo-current. By separately measuring the primary photo-current, the contribution to gain arising from S.E.C. was calculated.

The results of this experiment are illustrated in figs. 10.8 and 10.9, which show the variation of S.E.C. gain with primary electron energy and signal plate potential respectively, as the other parameter is kept constant.

10.4 Beam electron conduction.

The author suggests that an additional contribution to signal generation may arise through a fraction of the scanning beam electrons entering, positively charged regions of an exposed

FIG. 10.7 MEASUREMENT OF CONTRIBUTION TO SIGNAL GENERATION ARISING FROM S.E.C.

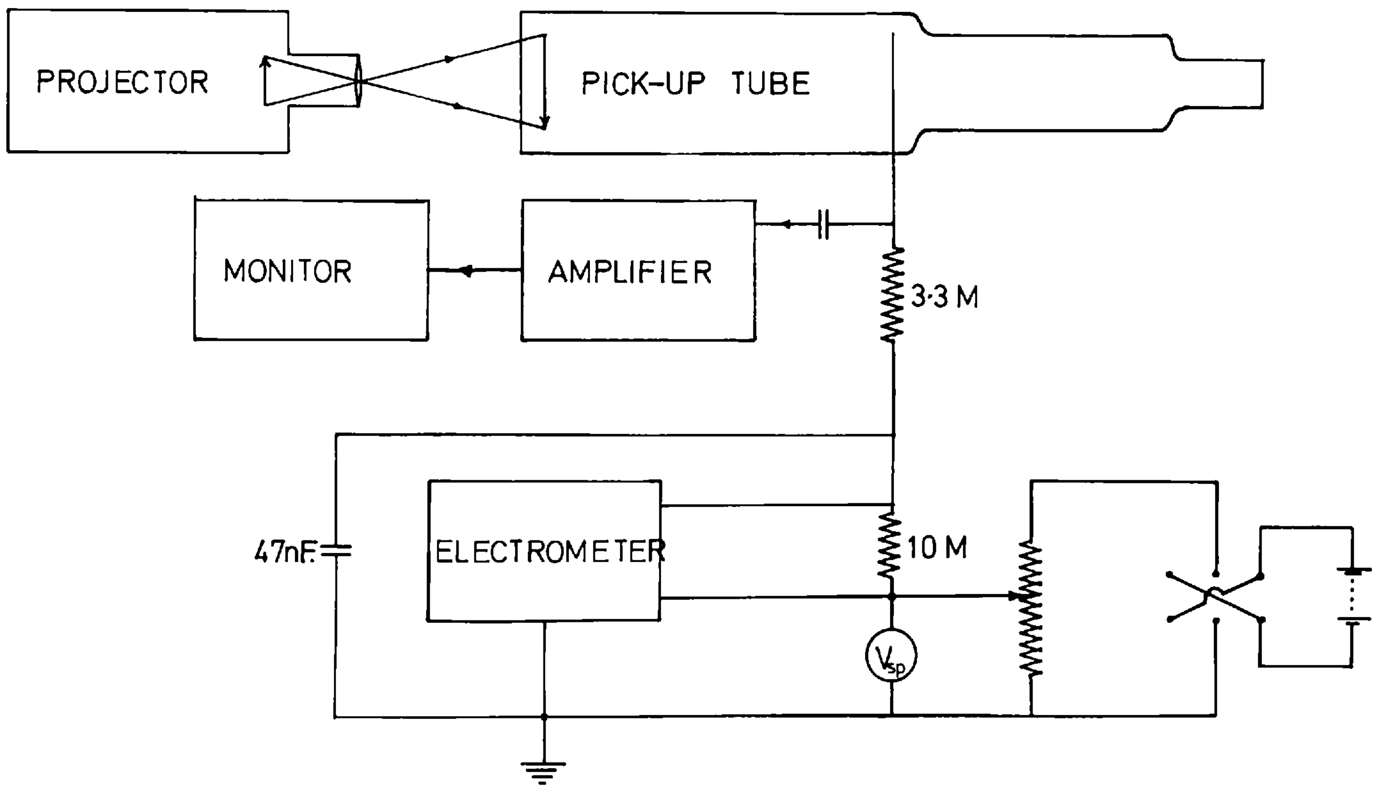

FIG.10.8 S. E. C. GAIN OF A TARGET AS A FUNCTION OF PRIMARY PHOTOELECTRON ENERGY FOR VARIOUS SIGNAL PLATE POTENTIALS.

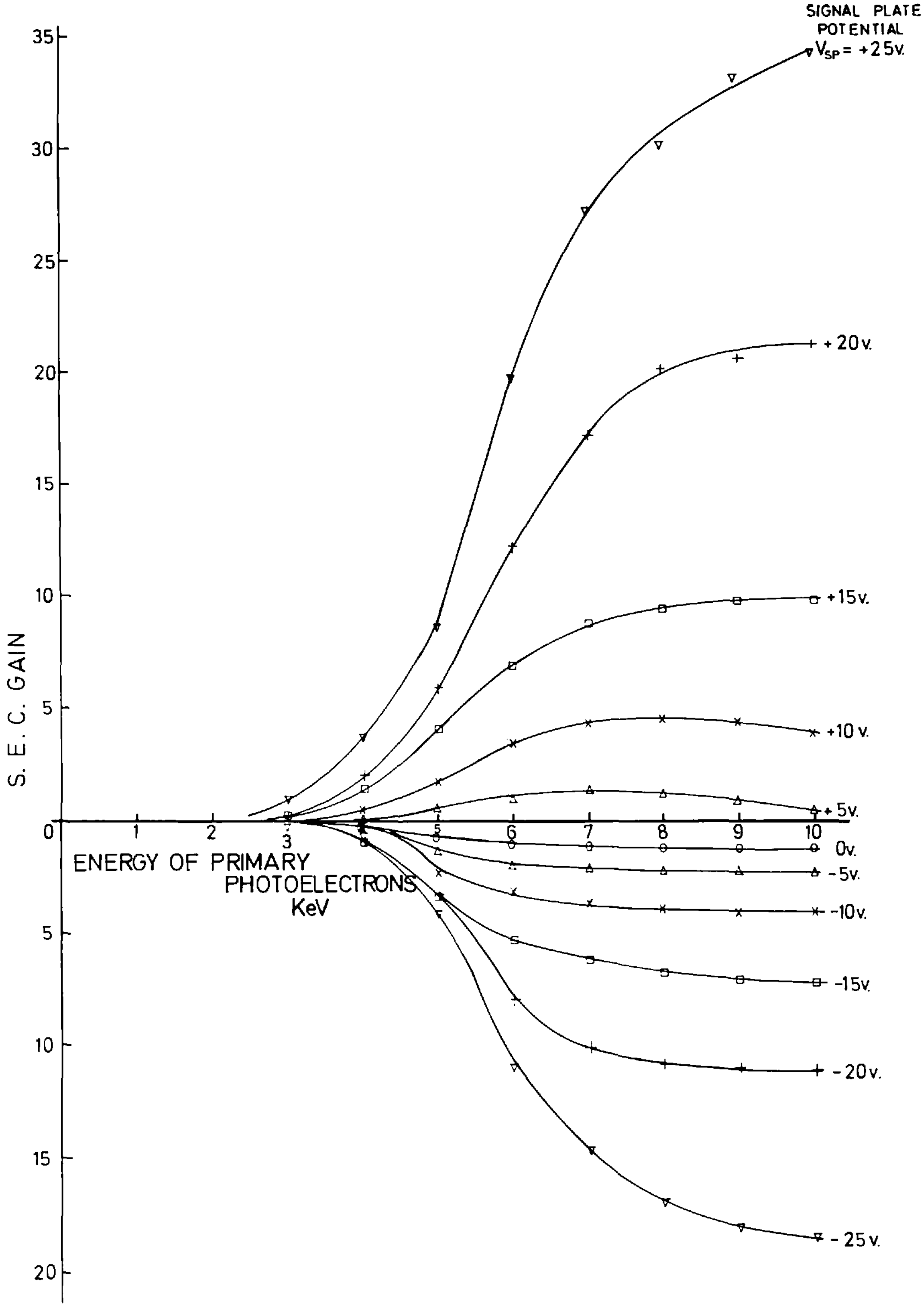

FIG. 10.9 S. E. C. GAIN OF A TARGET AS A FUNCTION OF SIGNAL PLATE POTENTIAL FOR 7KeV PRIMARY PHOTOELECTRONS

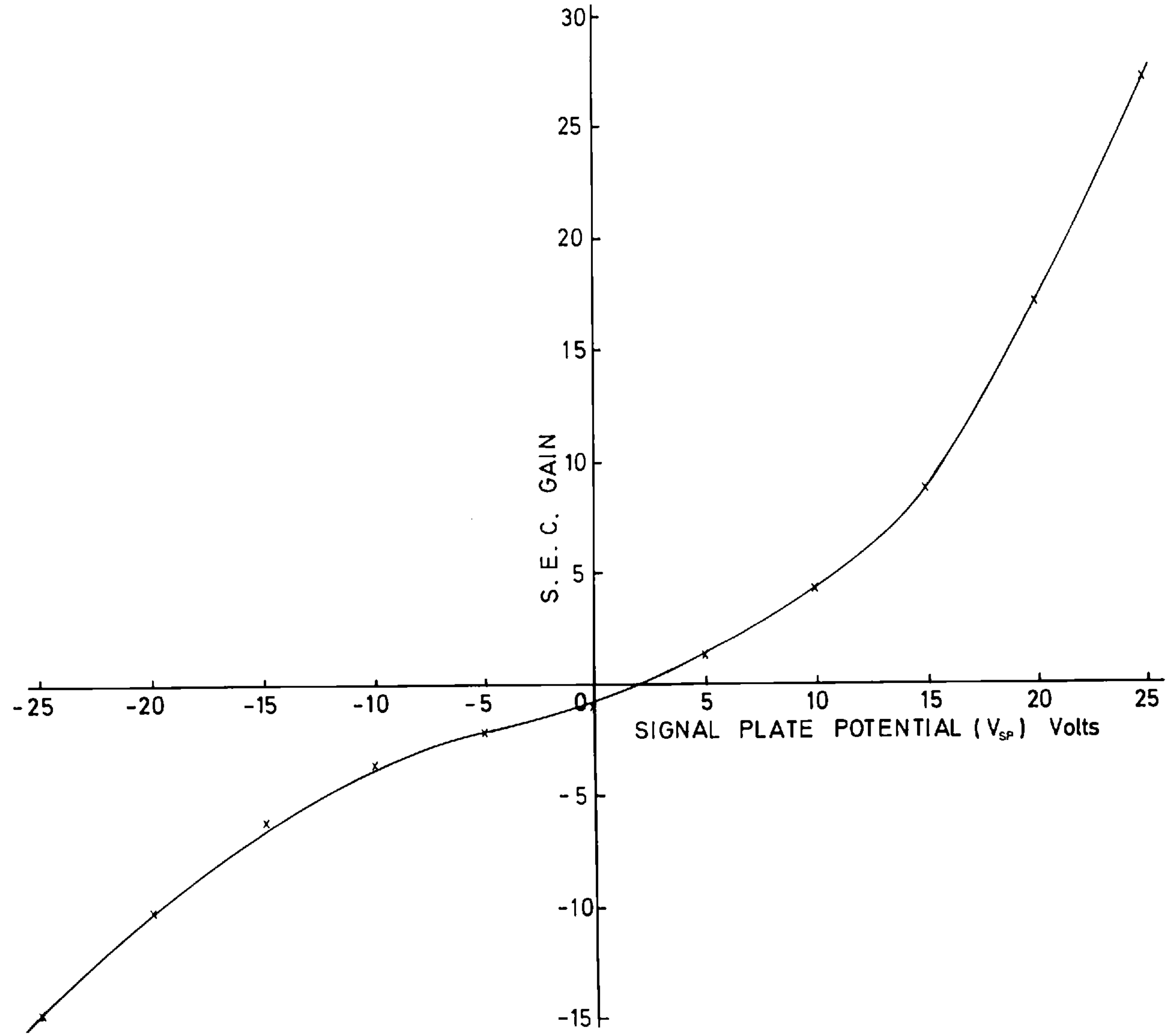

target, to move under the influence of the internal field, right to the signal plate. This process, which the author has termed, beam electron conduction, (B.E.C.) accounts for a number of phenomena observed in the tube. For example, the curve shown in fig. 10.9 exhibits an asymetry which can be explained by the fact that the measurements of S.E.C., described in §10.3 included any contribution to the signal, arising from this B.E.C. mechanism. While any signal contribution, arising from true S.E.C. would be expected to be constant for any fixed field gradient, and therefore, just to change sign as the layer polarity is reversed, B.E.C. will only contribute to the signal, when the signal plate is held positive.

It has also been noticed that an upper limit of 60 volts is set on the maximum signal plate potential that can be applied, since at higher signal plate potentials, scanning beam electrons will be accepted by the signal plate, even in the absence of primary photo-electrons.

Thirdly, the B.E.C. mechanism helps to account for the spongy potassium chloride target, possessing an effective storage capacity, much larger than that which would be expected from the electrostatic capacity, calculated from geometric considerations. Target capacity is discussed below (§ 10.9).

Figs 10.10, 10.11 and 10.12 illustrate diagramatically, the processes believed to occur during signal generation.

10.5 The total charge gain of a spongy potassium chloride target.

The curve given in fig. 10.13 illustrates the variation in the total charge gain of a spongy potassium chloride layer, with signal plate potential, showing the contributions arising from the T.S.E. and S.E.C. (embracing B.E.C.) mechanisms. The measurements were made for 7 keV primaries, and the layer measured exhibited a higher gain than those studied to obtain the results illustrated in figs 10.6 and 10.9. Recently, layers have been made with gains as high as 200, when operated with V_{sp} at 20 volts.

It is difficult to account for the variations in target properties, for layers prepared by apparently identical methods. A possible source of the variations could lie in the humidity of the atmospheres to which the layers were exposed, a parameter which may have been inadequately controlled in tube construction until very recently. The layers used to be removed from their storage desiccator, after the dry box in which assembly was to

FIG. 10.10 MECHANISM OF SIGNAL GENERATION IN DIFFUSE KCl LAYER OF CAMERA (1)

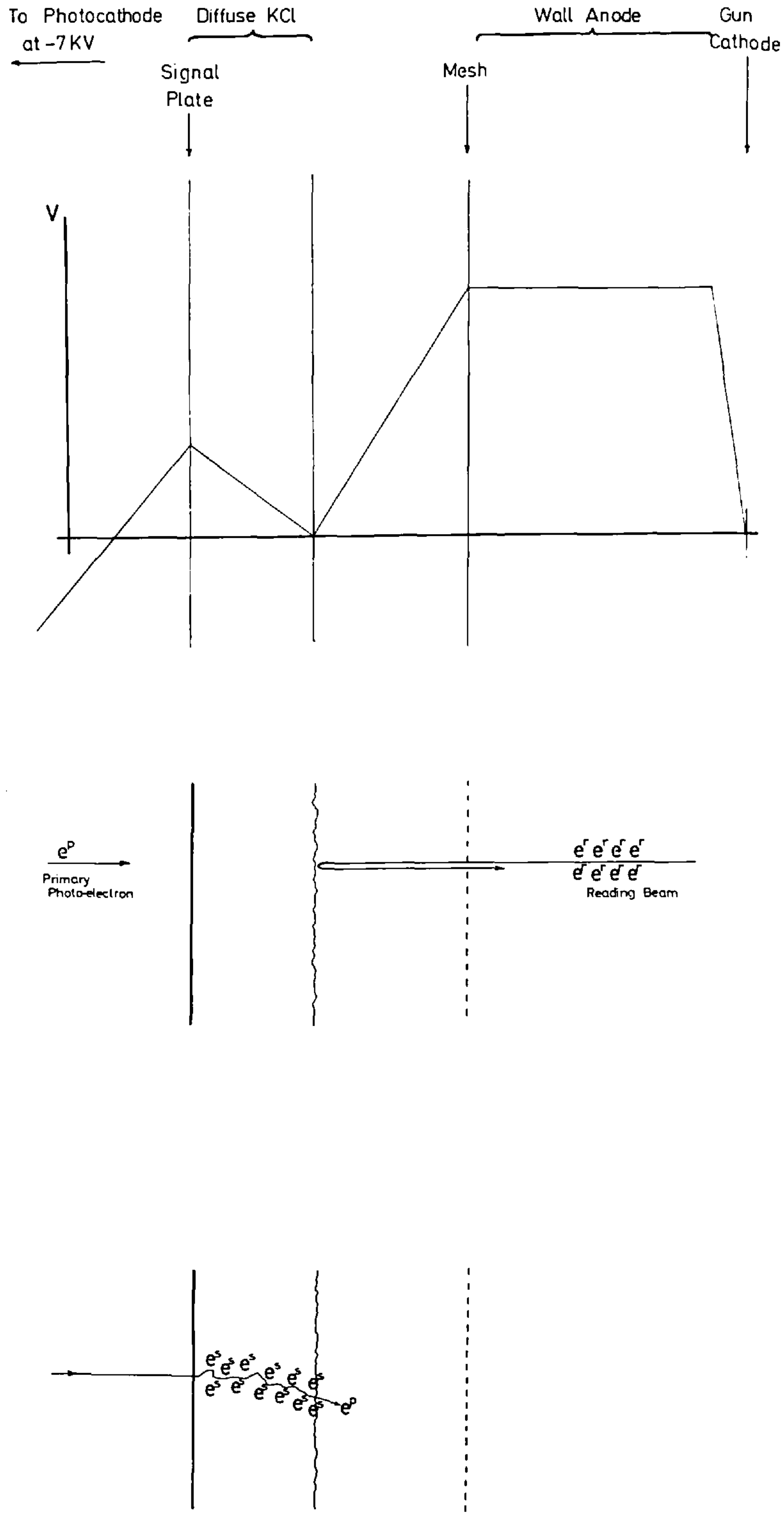

Potential distribution existing in tube prior to exposure.
The target surface is at gun cathode potential

Condition existing before primary photo-electrons e^p reach target.
The reading electrons e^r scanning the target encounter a potential barrier and return to the gun.

Primary photoelectron e^p entering layer excites many secondary electrons e^s.

FIG. 10.11 MECHANISM OF SIGNAL GENERATION IN DIFFUSE KCl LAYER OF CAMERA (2)

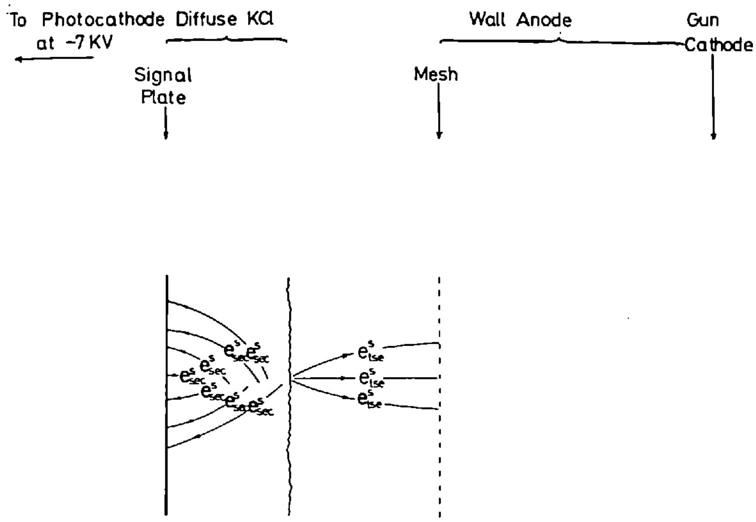

Motion of excited secondaries under influence of field in region of the layer.

Most of the electrons move under the influence of internal field in the layer to the signal plate (e^s_{sec}).

Some of the electrons leave the layer to be collected by the mesh (e^s_{tse})

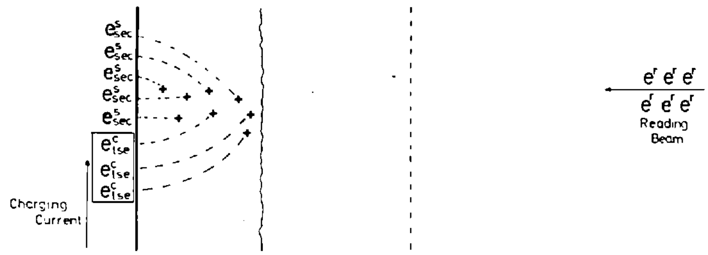

Charge distribution left in layer after exposure

The secondaries reaching the signal plate are held there by the +ve charges they leave in the KCl

+ve charges left by the electrons going to the mesh attract electrons from earth constituting a charging current in the signal lead. (e^c_{tse})

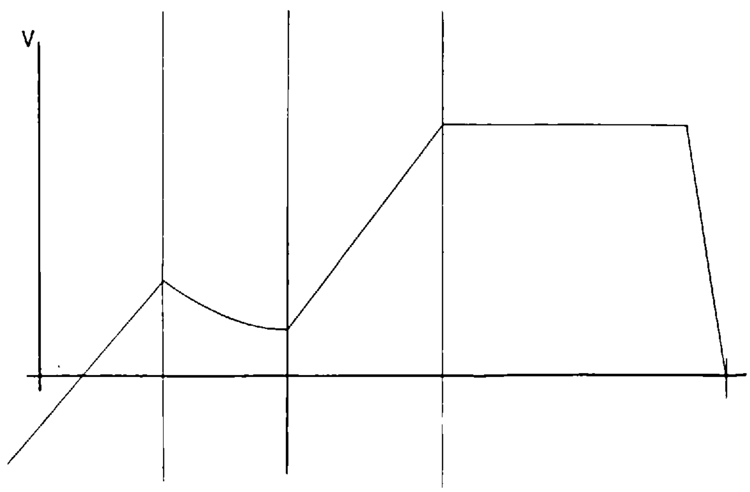

Potential distribution in tube after exposure.

The positively charged layer no longer presents a potential barrier preventing the scanning electrons from entering the layer.

FIG. 10.12 MECHANISM OF SIGNAL GENERATION IN DIFFUSE KCl LAYER OF CAMERA (3)

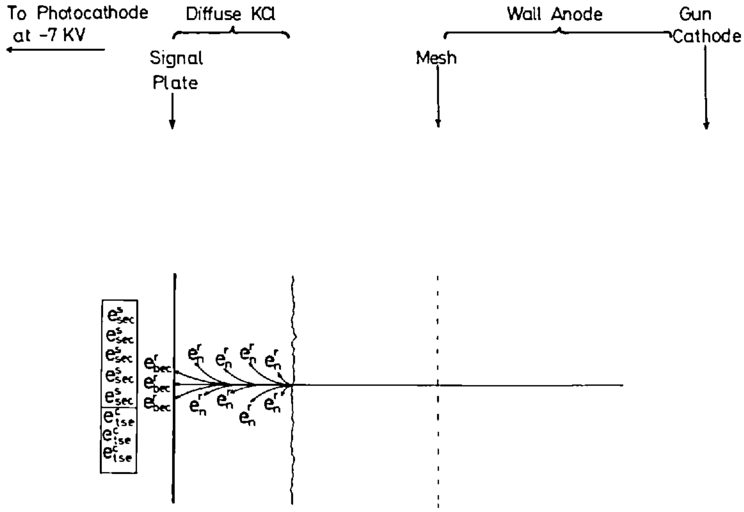

Processes occurring as exposed target is scanned.

The scanning electrons enter the layer

Some of them neutralize the +ve charge within the layer(e_n^r).

Others of them reach the signal plate (e_{bec}^r)

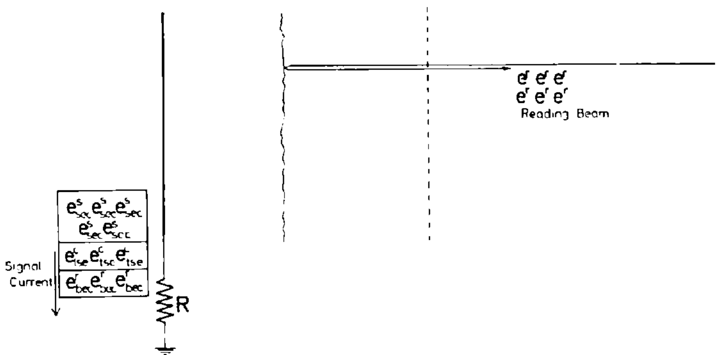

Condition existing immediately after scanning

As the +ve charge in the layer is neutralized, the potential of the surface is restored to gun cathode potential, preventing further electrons from landing The electron charges held on the signal plate are released (e_{sec}^s & e_{tse}^c). These together with the electrons landing direct on the signal plate from the scanning beam(e_{bec}^r) generate the video signal as they flow through R to earth.

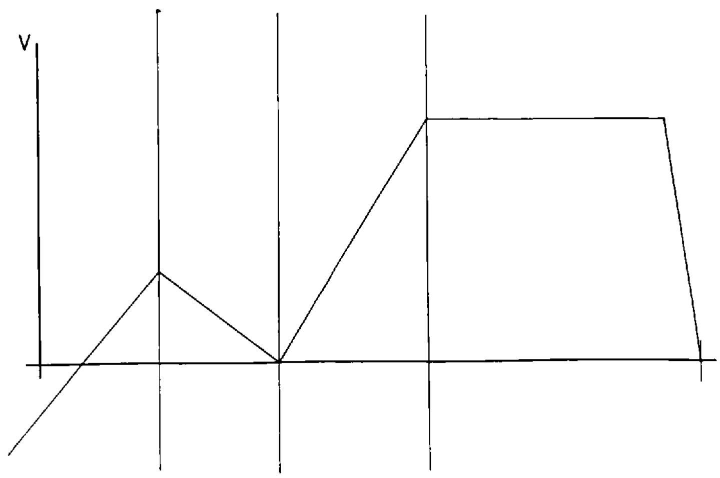

The potential distribution after scanning is restored to that existing before exposure.

FIG.10.13 THE VARIATION OF THE TOTAL CHARGE GAIN OF A LAYER WITH SIGNAL PLATE POTENTIAL, COMPILED FROM CURVES SHOWING THE CONTRIBUTIONS ARISING FROM THE T.S.E. AND S.E.C. MECHANISMS.

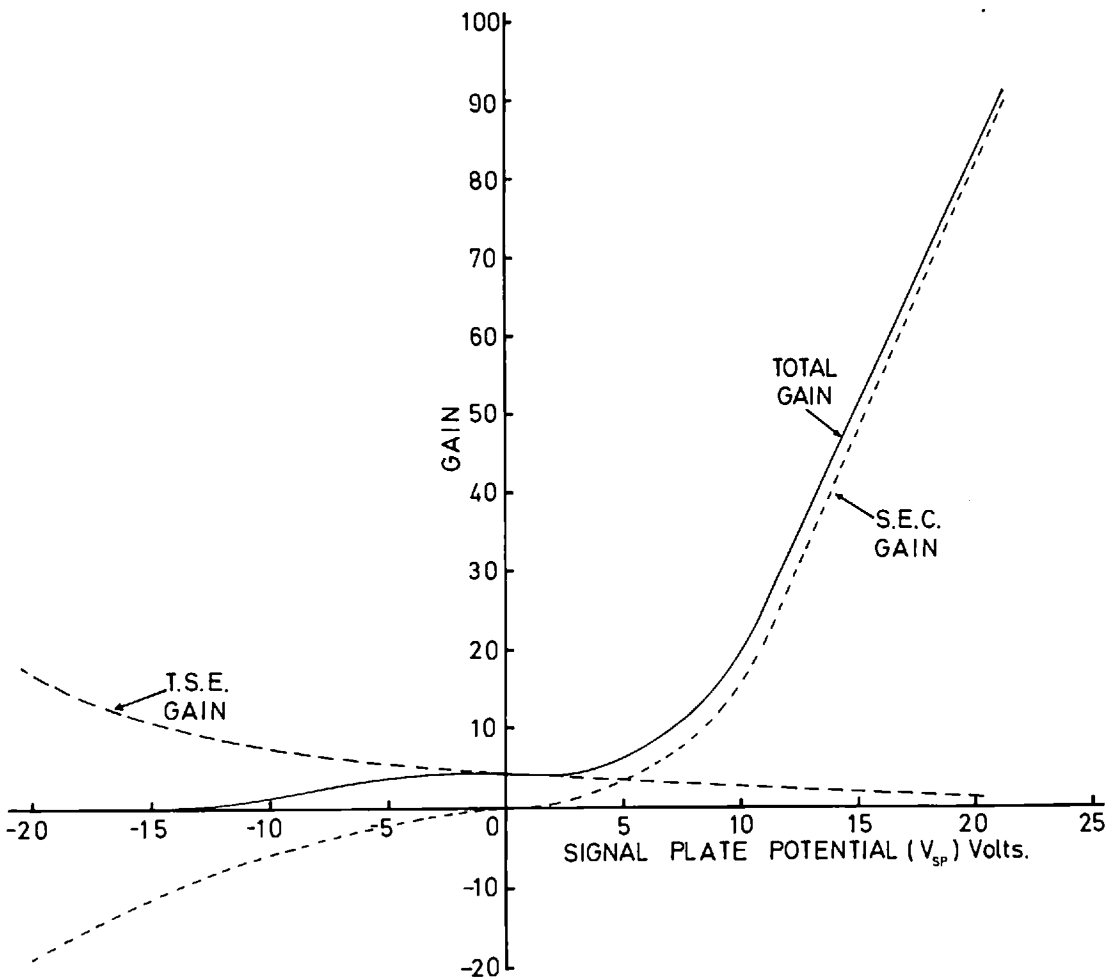

be carried out had been dried with fresh phosphorus pentoxide for about an hour. The fact that further phosphorus pentoxide, emptied into petrie dishes in the dry-box at this stage remained white and powdery, was taken as evidence that the chamber was sufficiently dry. However, a recently acquired humidity meter, manufactured by Shaw of Bradford, capable of monitoring dew points in the range - 20°C to - 50°C, has indicated that drying times of much longer than one hour, enable very much drier conditions to be realized. At time of writing, the author has insufficient evidence to make any conclusive statement as to how far, target performance may be improved by improving the dryness of the atmospheres to which the layers are exposed.

10.6 Signal transfer characteristics of the tube.

The variation in the video signal, generated by the tube with signal plate potential for four different values of light intensity is illustrated in fig. 10.14. These show that the gain of a spongy potassium chloride target is strongly dependent on the potential gradient across the layer. However, as stored charge builds up in a layer during exposure, the field gradient, and hence the layer gain will vary, resulting in the tube exhibiting a non-linear transfer characteristic. This is shown in

FIG. 10.14 THE VARIATION OF OUTPUT VIDEO SIGNAL WITH SIGNAL PLATE POTENTIAL FOR FOUR DIFFERENT LIGHT INTENSITIES

THE PARAMETER QUOTED ON EACH CURVE REPRESENTS THE TRANSMISSION OF A FILTER PLACED IN FRONT OF A LIGHT SOURCE OF FIXED INTENSITY

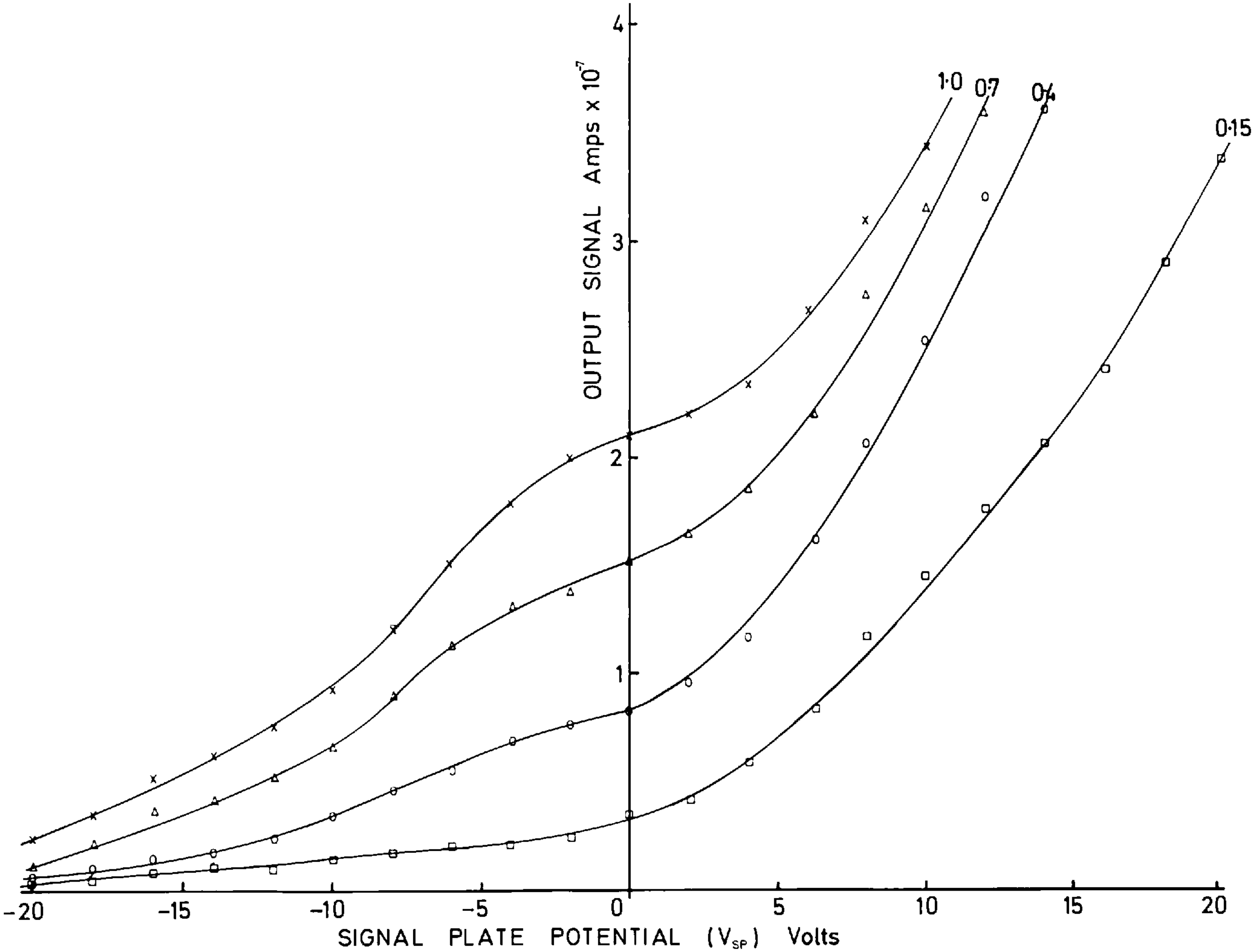

fig. 10.15, which gives transfer characteristics of the tube for various signal plate potentials.

For tubes run with positive signal plates, the build up of charge during exposure is such as to reduce the gain, so that the gamma is less than unity, while the converse is the case for tubes run with negative signal plates. The curves in fig. 10.15 do not obey a simple power law, so that a unique value of gamma cannot be associated with each value of signal plate potential.

10.7 Modulation transfer characteristic of the tube.

While the spongy potassium chloride target enables very high gains to be realized, this advantage is off-set by the relatively poor resolution the tube is capable of achieving. Early measurements of the modulation transfer characteristics were made, using photographic bar-test-patterns. These had to be micro-photometered, prior to use, to allow correction to be made for the non-opacity of the photographic black bars.

Later measurements of modulation transfer characteristic were made, using fully modulated test patterns, prepared by etching bar patterns in 0.001" copper foil, using photo-resist techniques[87]. A modulation transfer characteristic is shown

FIG. 10.15 TRANSFER CHARACTERISTICS OF THE TUBE FOR VARIOUS SIGNAL PLATE POTENTIALS

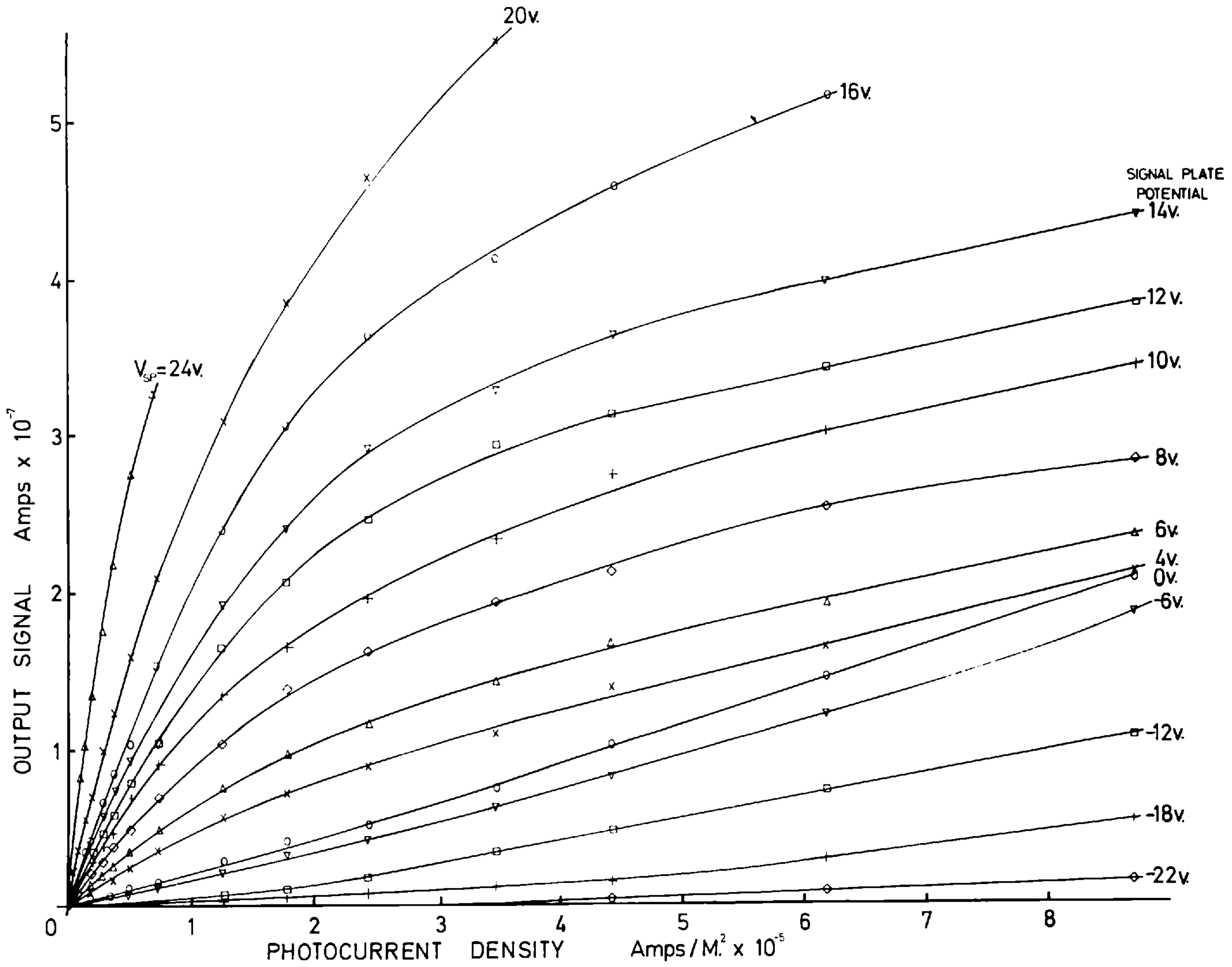

in fig. 10.16.

The various causes of loss of definition in television camera tubes were reviewed above (§ 5.3). It was shown on theoretical grounds that the image section, designed for the spongy potassium chloride layer tube was capable of realizing very high definitions (see appendix A.1), and was therefore, unlikely to account for the resolution limit, actually observed.

In order to confirm the adequacy of the electron optics of the image stage, and to investigate the effect of scanning field leakage, an image tube was constructed, identical to the image section of the camera tube, but the tube was terminated with a phosphor and an optically flat end window, (see fig. 10.17) instead of the spongy target and scanning gun. The tube was mounted in a solenoid, including a scanning yoke which occupied the same position, relative to the image section, as it would in a conventional camera tube. The system was focused on to a test pattern, using the same fields as those normally used in the camera tube. (V = 7 kV, B = 6.7 milli tesla), and the image formed on the phosphor was observed through a microscope (see fig. 10.18). The limiting resolution of the image, observed in the absence of scanning fields was 80 line pairs

FIG. 10.16 MODULATION TRANSFER CHARACTERISTIC OF TUBE

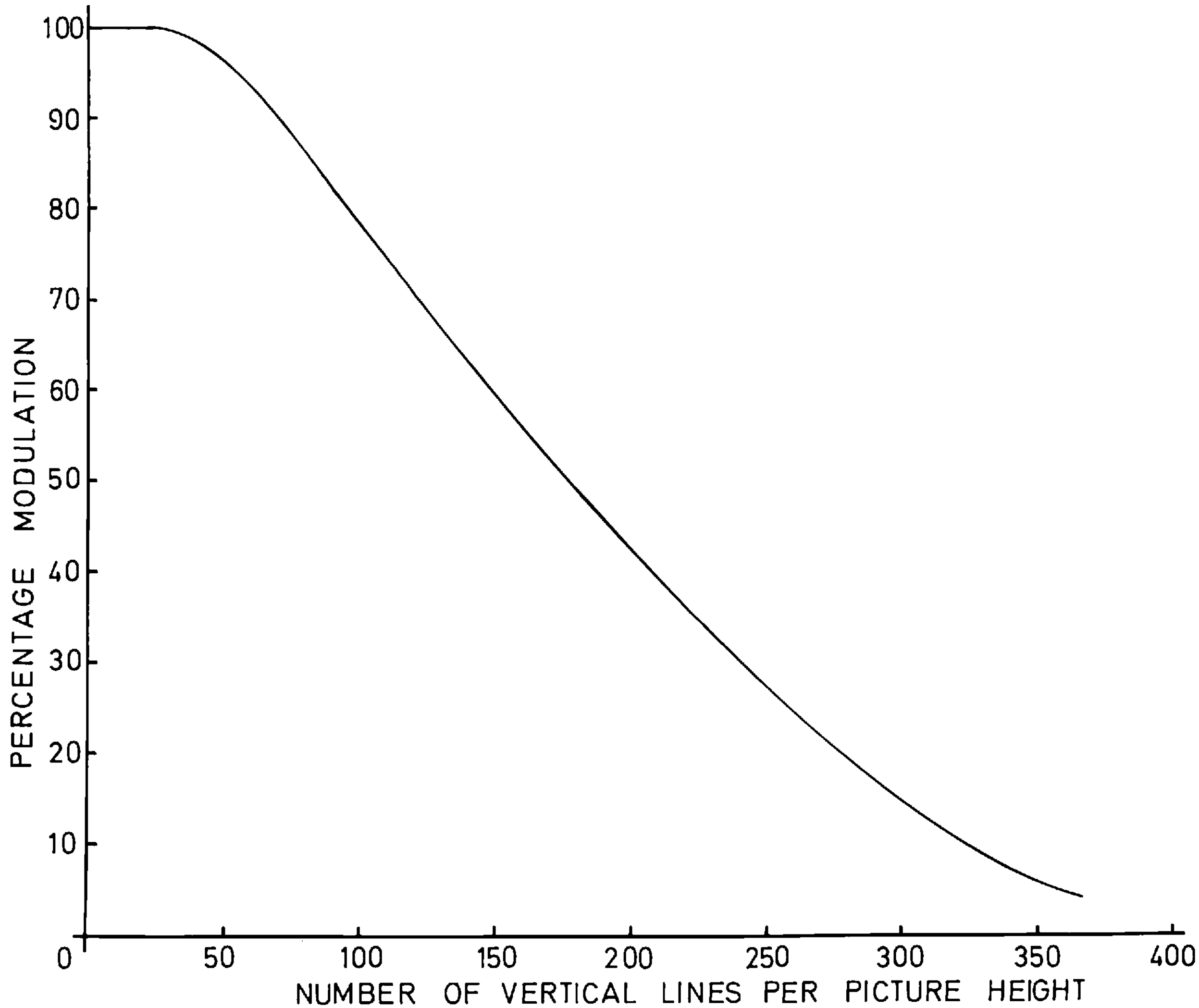

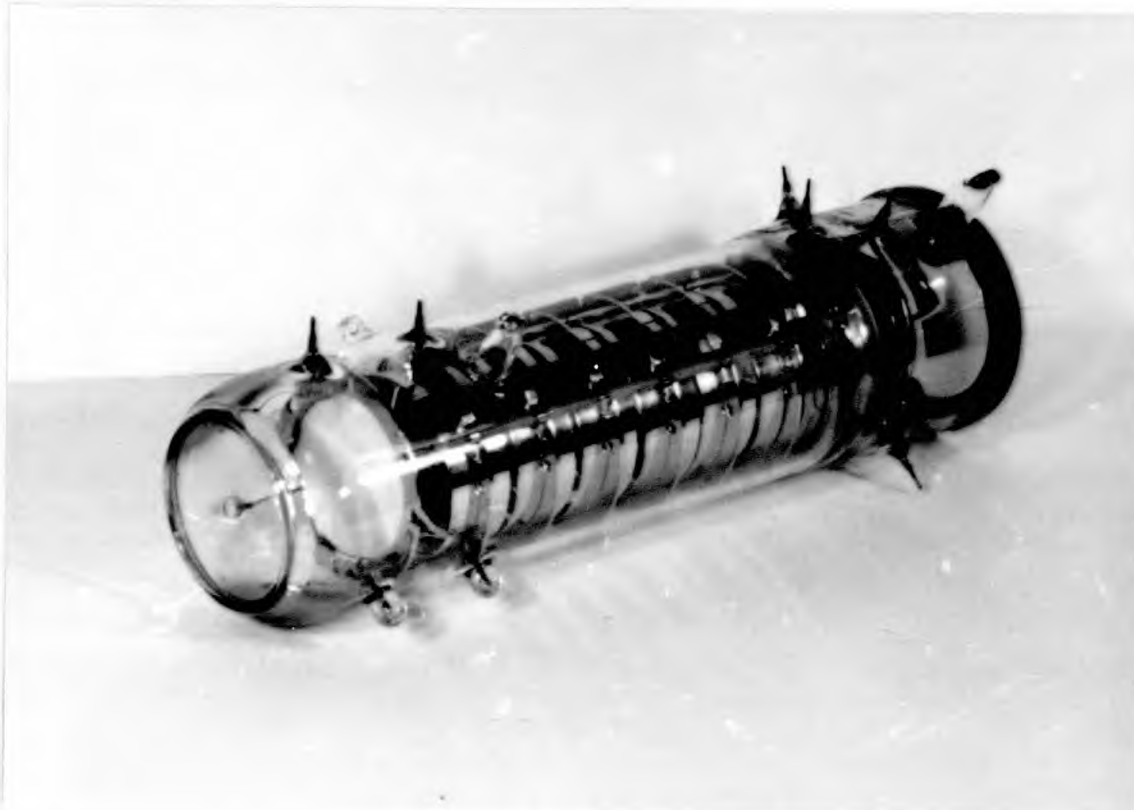

FIG.10.17 IMAGE TUBE CONSTRUCTED TO INVESTIGATE THE RESOLUTION OF THE CAMERA TUBE IMAGE SECTION

per mm. This approaches the resolution limit of the phosphor[1]. When the scanning fields were turned on, the definition was observed to drop to 50 line pairs per mm. Figs. 10.19 and 10.20 show the images observed with and without scanning fields. While this clearly demonstrated that scanning field leakage did degrade resolution in the image section, the definition observed on the image tube, even with applied scanning fields, was sufficiently better than that obtained in a storage tube, to exonerate the image section from being a source of definition loss.

It is not so easy to distinguish between resolution losses, caused either by target properties, or by a poorly focused scanning beam. Replacing the target with a metallic test pattern or a very thin target would not provide a conclusive test, as the change in surface potential of a standard target as it is discharged during a single frame, affects the focus of the low velocity scanning beam. However, evidence indicating the source of definition loss, was provided by observations on a tube, constructed with a target to ion-trap mesh spacing of somewhat less than 1 mm. While difficulties were experienced in focusing the gun section of this tube, without bringing the mesh into view at the edges of the picture, the

FIG. 10.18 OBSERVATION OF THE EFFECT OF SCANNING FIELDS ON THE RESOLUTION OF THE IMAGE STAGE

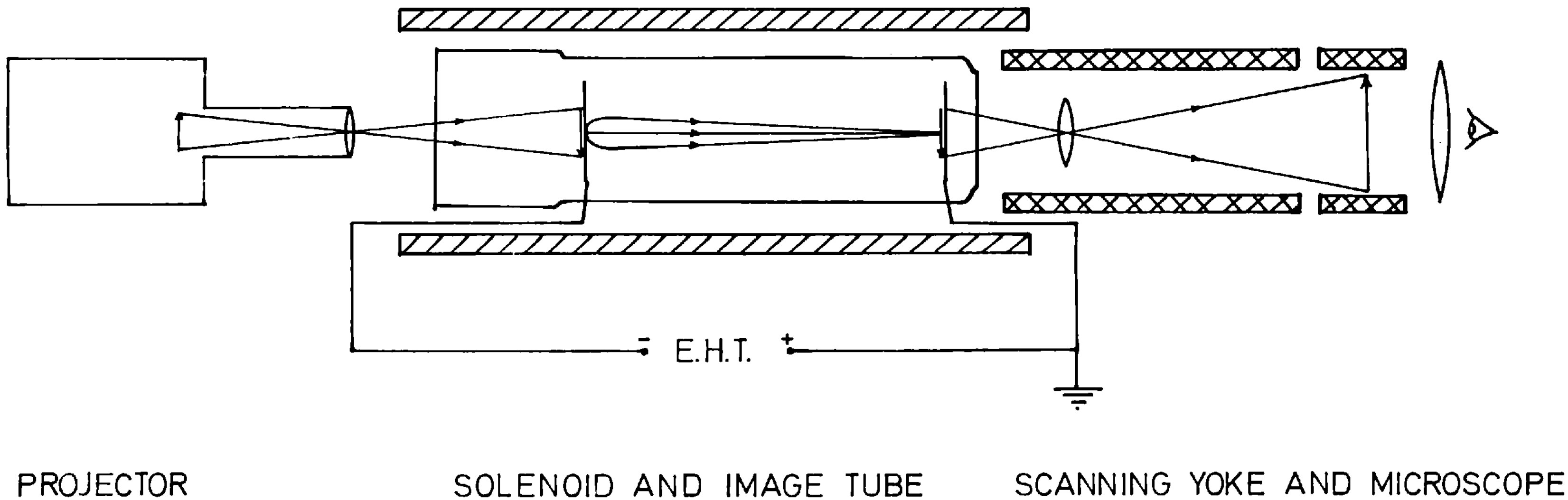

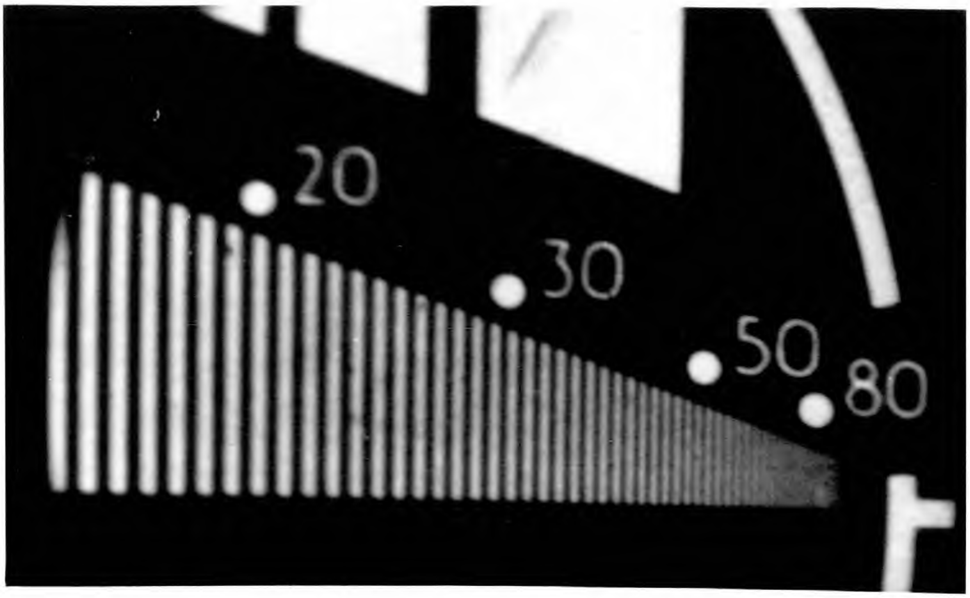

FIG.10.19 IMAGE ON PHOSPHOR WITHOUT APPLIED SCANNING FIELDS

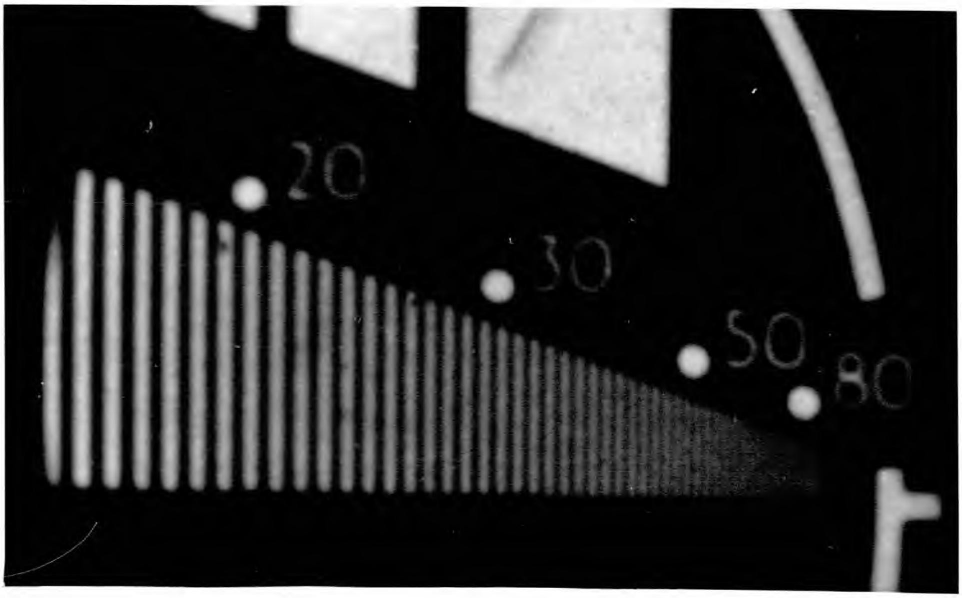

FIG.10.20 IMAGE ON PHOSPHOR WITH APPLIED SCANNING FIELDS

strong target to mesh field assisted in obtaining a finely focused scanning spot[100]. The picture, generated by this tube when the focus controls were set to give the best attainable gun definition was observed to momentarily brighten up every few seconds, this bright up being accompanied by an apparent jump of the picture. This effect was interpreted as arising from the scanning spot being sufficiently small to leave regions of undischarged target between scan lines. Charge was integrated in these interscan regions, until they reached a potential, high enough to pull the beam right on to themselves, generating the occasional bright and slightly shifted images. Image jumping could be prevented by slightly defocusing the gun section.

For image jumping to occur, the size of the scanning spot would have to be less than the separation of scan lines on the target (40 μm.). The limiting definition of 15 line pairs per mm., achieved on this tube, was however, no better than that obtained in tubes with larger target to mesh spacings, where it was not possible to operate them with such a finely focused spot. From this observation, it was concluded that processes occurring in the target were responsible for the resolution loss, rather than the loss being the result of a poorly defined scanning spot.

Since images may be stored for periods of several days without further loss in definition, charge leakage must clearly be ruled out as an explanation of the low resolution, and it would appear that primary photo-electrons must undergo considerable scattering in their passage through the 10 μ m. layer to produce a charge image, corresponding to a light point on the photo-cathode, greater than 40 μ m. in diameter. Layers of thicknesses, ranging between 5 μ m. and 20 μ m. all seem to exhibit the same resolution limit, and so far, measurements have not been made on layers outside this range.

Using the low velocity flood gun to stabilize unscanned regions of the target (see § 8.7), it was possible to zoom up an image, generated in the layer tester, to display pictures with definitions better than 20 line pairs per mm., this limit being set by the stencil in the layer tester. In order for this improved spatial definition to be observed, the primary current from the E.H.T. flood gun had to be increased from the level used for a fully scanned target. This primary current could be increased without causing overload, as zooming the picture had effectively increased the available scanning current per unit area of target surface, and in the author's opinion, the improvement in resolution was due to the apparently increased scanning current allowing the generation of signals, able to override the amplifier noise, from regions in the target corresponding to high, spatial definition. This supports the author's contention (§2.4) that the property, limiting resolution, commonly used in the literature to specify the performance on an image detecting device, is not a specially valuable concept, as it is not usually precisely defined in terms of a definite criterion.

10.8 Operation of the tube, using a high velocity scanning beam.

While it is well known that scanning with a high velocity beam introduces undesirable spurious signals, (§ 5.2 (a)), certain advantages may be derived from the use of high velocity scanning beams, since they are more easily focused than slow electrons, and target instability is obviated. The feasibility of this mode of operation was therefore tested by switching the signal plate potential from a voltage which could be adjusted relative to the gun cathode to one, adjustable relative to the ion trap mesh, which defined the new target surface stabilization potential. A photograph of the type of picture obtained is shown in fig. 10.21. The image could be zoomed at will, with no fear of instability occurring in the unscanned regions of the target, but this advantage was off-set by the poor quality of the pictures. No improvement in definition was observed over that obtained with a low velocity scanning beam, which is in agreement with the conclusion that the loss in definition was due to target properties, rather than to the scanning spot profile (§10.7). When operated in the high velocity mode, considerable spurious signals were generated by an effect, discussed above, (see §10.4) by which the scanning beam entered the target to reach the signal plate, even in unexposed regions of target. This effect was masked as far as possible in fig. 10.21, by means of the main amplifier lift control.

10.9 Target Capacity and Lag.

While undesirable discharge lag has been observed in camera tubes, incorporating thin ($\sim 5\,\mu$m.) spongy targets, operating at conventional frame rates, the thicker layers ($\sim 10\,\mu$m.) were found to be free from any serious lag. Qualitative assessments of lag were made by observing moving images with the camera tubes, or by magnetically deflecting

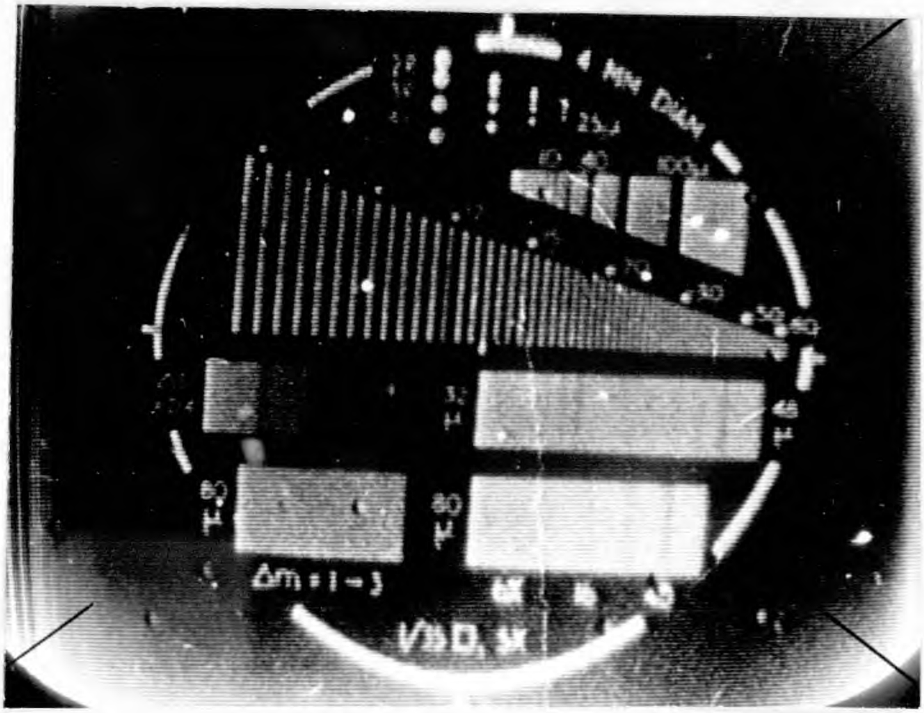

FIG.10.21 PICTURE GENERATED BY A TUBE WHEN OPERATED WITH A HIGH VELOCITY SCANNING BEAM . V_M = 270 volts . $V_{SP} = V_M + 5$ volts . DIAMETER OF TEST PATTERN IMAGE ON TARGET = 8 mm.

the primary electron beam in the layer tester. An arrangement used to monitor build up and decay lag is illustrated in fig. 10.22. Two Tectronix oscilloscopes were used for this experiment. Time base B, of a Tectronix 545 A oscilloscope (scope 1) was triggered by a line selector to monitor the video signal, corresponding to a selected line. A highlight from this line was selected by using the delay facility to trigger time base A at a suitable interval after the initiation of time base B. The scope allowed the selected highlight, corresponding to the period of time base A to be monitored as an intensified portion of the line trace. A gating pulse, corresponding to time base A, was used to brighten up a Tectronix 551 oscilloscope, (scope 2), whose time base was set to run at a rate of the order of one second. 'Scope 2 was set to monitor the D.C.level of the video signal which could be observed once per frame during the bright-up period. The display on 'Scope 2 thus enabled the build-up and decay of the signal to be monitored as the light source to which the tube was exposed, was turned on and off. Observations made for signal currents between 0.1 and 0.3 μA, and for signal plate potentials between -5 and +20 volts, indicated that the decay and build up processes

FIG. 10.22 EXPERIMENT TO MONITOR BUILD-UP AND DECAY LAG OF CAMERA TUBE

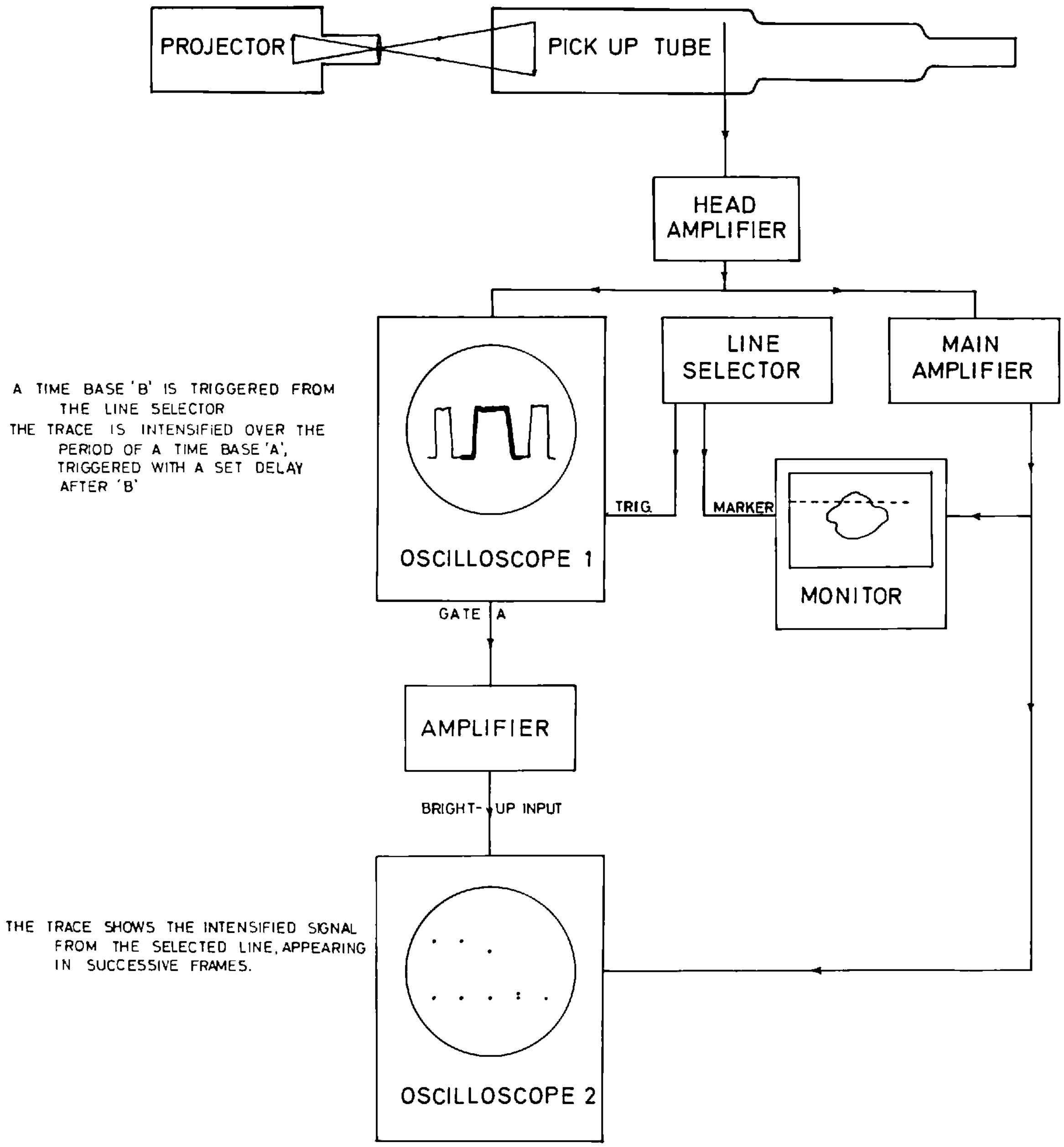

were completed, certainly within 2 frames.

The experiment described here, used a manually operated, tungsten filament lamp, which was of course, a very unsatisfactory light source for this experiment. Owing to the heavy demands on oscilloscopes in the department, the author has not reset-up the experiment, using a triggered light source to obtain more precise data on lag. It can be said however, that lag is within the limit required for entertainment applications.

While the target capacity is low enough to avoid discharge lag, it is high enough in a good target to enable peak white signals of 0.3 μA to be generated at conventional scan rates. This corresponds to a total target storage capacity of 7.5×10^{10} electrons. Now the electrostatic capacity of a 10 μm. thick layer, with dielectric constant unity, and area 20 mm by 15 mm. is 300 pF. 7.5×10^{10} electrons stored on this capacity would correspond to a potential rise of 25 volts. An experiment was carried out to measure the potential excursions actually experienced by the target surface.

First, the exposure required to charge the target to peak white was ascertained by observing on an oscilloscope, the transient signals generated as the scanning beam was switched on for one frame to discharge a target which had been exposed to a faint primary electron flux for varying periods. The unscanned target was then exposed for a period which would charge it to peak-white level, and the signal plate potential was retarded by a known amount before turning on the scanning beam for a single frame. The monitor was observed for any signal generated. The experiment was repeated with gradually increasing signal plate potential retardations, until the absence of any signal generation, indicated that the rise in target surface potential had been exactly compensated by the lowering of the signal plate voltage. This rather tedious experiment showed that a peak white signal corresponded to an 8 volt potential excursion of the target.

A more elegant experiment was carried out on the layer tester to confirm this result. A line, embracing a highlight, corresponding to a peak-white signal, generated by the test apparatus, was selected and monitored on an oscilloscope. The bias on the low velocity flood gun(see § 8.5) was then gradually reduced from a value, well above the scanning gun cathode potential, until the signal displayed on the oscilloscope started to drop, indicating that the flood gun cathode was at target highlight potential. The result obtained by this experiment was in agreement with the figure of 8 volts measured in devices without low velocity flood guns. The discrepancy between the measured and calculated values for the potential excursions experienced by a fully charged target, indicates that a model which assumes all the charge to be stored on the target surface is inadequate, and thus, provides evidence in support of the mechanisms of signal generation, described above (§s 10.2, 10.3 and 10.4). These postulate the storage of charge within the layer, and suggest a further increase in the effective capacity of the layer through the B.E.C. process.

For long term integration experiments, lag is unimportant, and slow speed read out would enable a much larger target capacity to be exploited with advantage. Work is at present in hand in the applied physics section of Imperial College to investigate techniques of manufacturing high gain, high capacity, spongy targets.

10.10 Target Overload.

The instability of the target against light overload was imentioned above, (§ 7.4 (d)). The cross-over potentials of targets have been measured by advancing the potential of the signal plate of an unscanned, discharged target by successively increasing potentials, until a point was reached where 'infra-black' signals were generated on turning on the scanning beam. This indicated that the target potential had been raised beyond its first cross-over point, and was operating under conditions of anode potential stabilization. First cross-over potential was found to occur at between 12 and 20 volts for various layers.

It anode potential stabilization conditions were established with the mesh held at much above 100 volts positive with respect to the signal plate, dielectric break-down of the layer occurred, leaving a punctured and permanently damaged target.

Areas of the target which have been overloaded and run under anode potential stabilization conditions have exhibited a temporary burn-in, these regions displaying enhanced sensitivity. Owing to the risk of layer damage however, uniform over-loading has not been exploited as a technique for super-sensitizing the layer..

The tendency of the target to revert to anode potential stabilization conditions represents a serious inherent defect in the target. Two methods of combatting this defect have been tried out so far, the use of a low velocity, flood-gun, biassed just below the first cross over potential (see §8.5) and the use of a stabilizer mesh. The flood gun does not give 100% protection against large overloads, but the stabilizer mesh provides an adequate safeguard. Technological difficulties do exist however, in mounting this mesh sufficiently close to the target to attain good definition, as the unbaked target is slack and floppy at the assembly stage, making it prone to touch against any closely spaced electrode. In the tube constructed in the applied physics section which incorporated a stabilizer mesh, spaced at a distance of 0.010" by mica washers, the target and the mesh actually touched during assembly, resulting in traces of potassium chloride adhering to the mesh. This resulted in the generation of poor quality although stable pictures by this particular tube.

10.11 The creation of colour centres in the target.

The demountable test apparatus described in chapter 8 is essentially a monoscope, and layers, removed from this after testing, were noted to exhibit a faint, pink pattern, corresponding to the test pattern, etched in the stencil. This was noticed most strongly in a layer that had been frequently overloaded during testing. The breakdown processes, occuring during overload, may be more significant in changing the structure of potassium chloride, than the phenomena, associated with normal signal generation, and on this evidence, it cannot be conclusively stated how effective are the 7 keV primary electrons in the creation of colour centres. It can be said that over a period of months, no significant change in target property occur, provided overloading is avoided. This shows that the normal flux of 7 keV photo-electrons, to which the target is exposed, does not seriously alter its structure.

CHAPTER 11

CONCLUSIONS

Spongy potassium chloride layers have been shown to possess many desirable properties which may be exploited with advantage when used as the targets of television camera tubes. In particular, the exceptional gain and insulation of these layers make them suitable for faint image detection by charge integration when incorporated in a suitably designed storage tube.

Figs. 11.1 and 11.2 show the quantum efficiency and image information recording efficiency of the spongy potassium chloride target tube as a function of image detail, concepts discussed at the beginning of this thesis (§s, 2.3 and 2.7). These curves were calculated for optimum amplifier bandwidth (see § 5.8) and assume a 20% quantum efficiency for the photo-cathode. Figures of 100 for target gain and 7×10^{10} electrons for the total storage capacity of the target were used, these being typical values, measured by the author. The modulation transfer characteristic shown in fig. 10.16 was used in making the calculations.

Figs. 11.1 and 11.2 may be compared with the corresponding curves, (figs 6.9 and 6.10), calculated by the author for estabilished camera tubes, reviewed earlier in this thesis (chap.6).

FIG. 11.1 EQUIVALENT QUANTUM EFFICIENCY AS A FUNCTION OF DETAIL FOR THE SPONGY KCl TARGET CAMERA OPERATED AT OPTIMUM SCAN RATES IN A 405 LINE SYSTEM

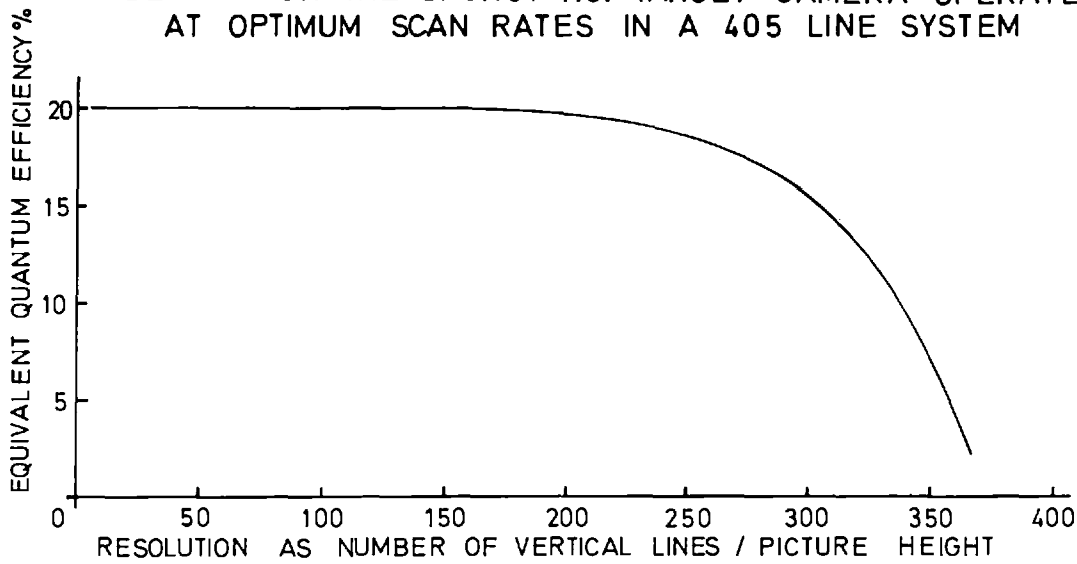

FIG. 11.2 IMAGE INFORMATION RECORDING EFFICIENCY AS A FUNCTION OF DETAIL FOR THE SPONGY KCl TARGET CAMERA OPERATED AT OPTIMUM SCAN RATES IN A 405 LINE SYSTEM

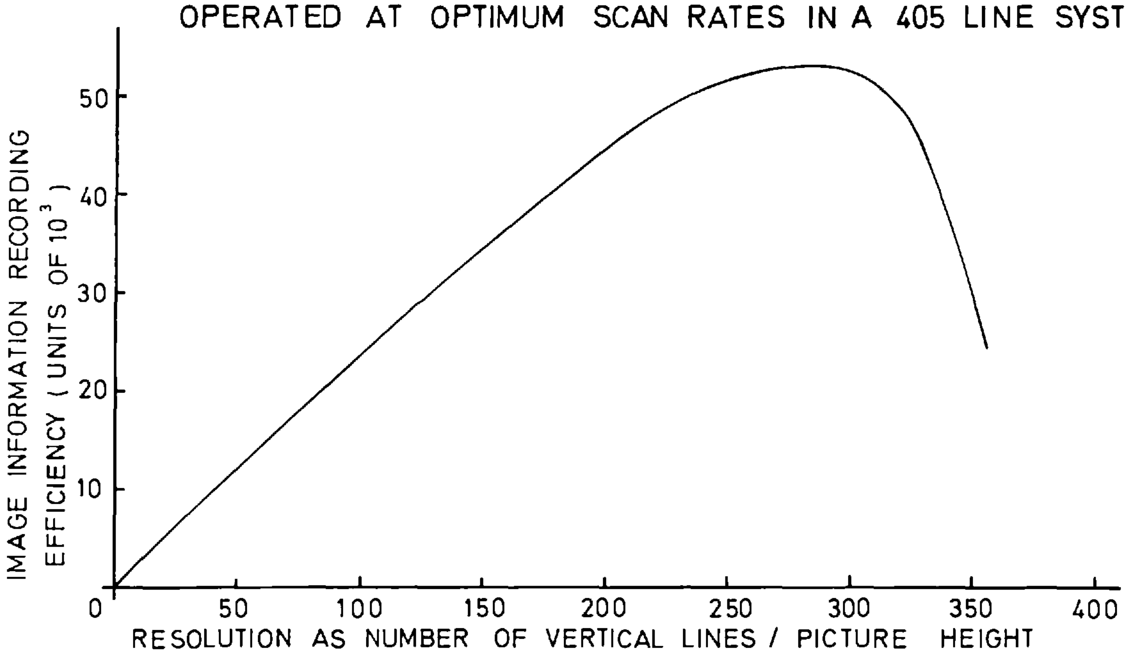

In its present state, the spongy target camera tube does not yet represent a camera, which universally supercedes all existing pick-up tubes. However, in the author's opinion, it is potentially capable of development to become a device, which besides its unique long term storage ability, could compete with image orthicons in the field of broadcasting. The major defect of the tube at present, arises from target properties which limit the ability of the tube to resolve fine detail. The targets used at present are less than one quarter the size of those used in the image orthicon or C.P.S. Emitron, and future technological development may enable tubes to be constructed, incorporating much larger spongy targets, so improving definition in terms of television lines. However, the author's experience in the preparation and handling of these spongy layers does not allow him to underestimate the problems associated with increasing their dimensions.

For cameras to be used exclusively for the detection of faint low-contrast static images, read out would be at slow rates. Improvement in the existing camera would therefore be realized if higher capacity spongy targets could be developed, provided that this was not achieved at the expense of target gain.

APPENDIX A.

A.1 Spatial destribution of photo-electrons in the image plane of an electron magnetically focused system.

Figs. A1.1 and A1.2 represent the motions of a photo-electron in the rotating meridional plage and in the advancing equatorial plane of a system focused by the action of uniform electrostatic and magnetic fields, E_e and B, applied normal to the photocathode. The electron is emitted from the photo-cathode with a velocity V_{em} at an angle, θ, to the normal. A target is located a distance ℓ from the cathode, at a potential V ($= E_e \ell$). In general, the electron will strike the target at a distance r from the axis of the system The value of r may be calculated as follows :-

Let V_T be the energy in volts, corresponding to a velocity Vem.

ω_c be the cyclotron frequency.

R_c be the radius of the electron orbit in the equatorial plane.

$$\omega_c = \frac{e}{m} B \qquad (A1.1)$$

$$R_c = \frac{1}{\omega_c} V_{em} \sin\theta \qquad (A1.2)$$

$$V_{em} = \sqrt{2 \frac{e}{m} V_T} \qquad (A1.3).$$

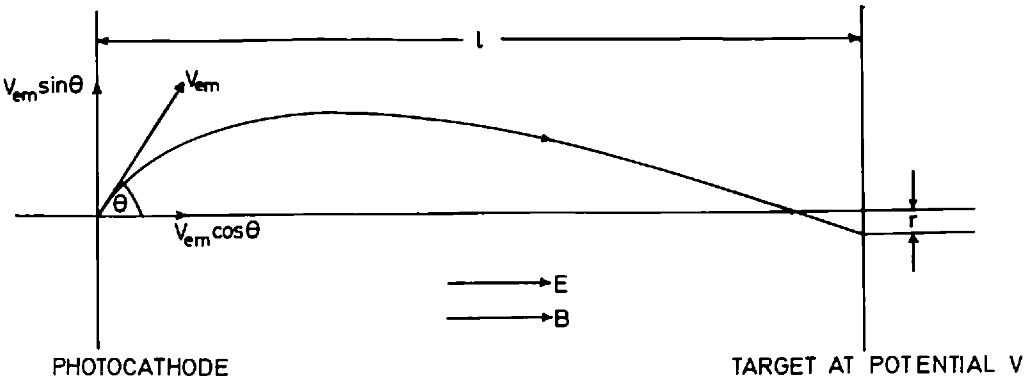

FIG.A1.1 ELECTRON MOTION IN ROTATING MERIDIONAL PLANE OF AN ELECTRO-MAGNETICALLY FOCUSED SYSTEM

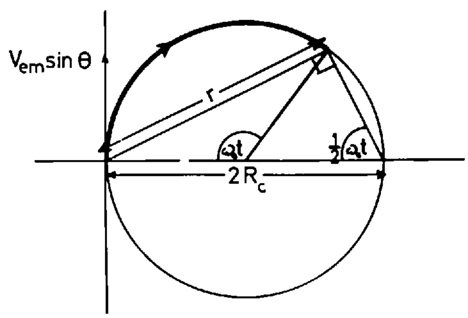

FIG.A1.2 ELECTRON MOTION IN ADVANCING EQUATORIAL PLANE OF AN ELECTRO-MAGNETICALLY FOCUSED SYSTEM

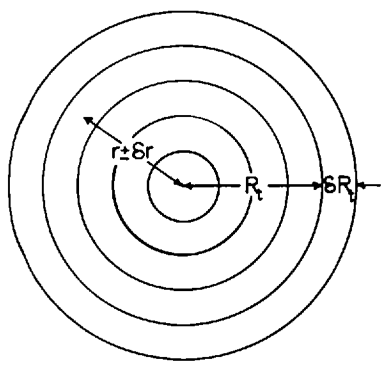

FIG. A1.3 IMAGE PLANE MARKED OUT INTO ANNULI FOR WHICH ARE SUMMED CONTRIBUTIONS TO THE ELECTRON DISTRIBUTION RESULTING FROM PHOTOELECTRONS LIBERATED FROM A POINT ON THE PHOTOCATHODE.

Since the electron is uniformly accelerated, the mean axial velocity of the electron, U_{mean} is given by :-

$$u_{mean} = \frac{1}{2}\left[V_{em}\cos\theta + \sqrt{2\frac{e}{m}[V+V_T]}\right]$$

$$= \sqrt{\frac{eV}{2m}}\left[\sqrt{\frac{V_T}{V}}\cos\theta + \left[1+\frac{V_T}{V}\right]^{\frac{1}{2}}\right] \qquad \text{from (A1.3)}$$

$$= \sqrt{\frac{eV}{2m}}\left[\sqrt{\frac{V_T}{V}}\cos\theta + 1 + \frac{1}{2}\frac{V_T}{V} + \;\ldots\ldots\right]$$

since

$$V \gg V_T \qquad \sqrt{\frac{V_T}{V}} \gg \frac{V_T}{V}$$

$$\therefore \quad u_{mean} \approx \sqrt{\frac{eV}{2m}}\left[1+\sqrt{\frac{V_T}{V}}\cos\theta\right] \tag{A1.4}$$

The time of flight, t , of the electron is given by

$$t = \frac{\ell}{u_{mean}}$$

$$= \frac{\ell}{\sqrt{\frac{eV}{2m}}\left[1+\sqrt{\frac{V_T}{V}}\cos\theta\right]}$$

$$\therefore \quad t = \frac{T_t}{\left[1 + \sqrt{\frac{V_T}{V}}\cos\theta\right]} \tag{A1.5}$$

where $$T_t = \ell\sqrt{\frac{2m}{eV}} \tag{A1.6}$$

Now from fig. A1.2, the diagram representing the electron motion in the advancing equatorial plane, it can be seen that r will be given by :-

$$r = 2 R_c \sin\left(\tfrac{1}{2}\omega_c t\right) \qquad (A1.7)$$

The radial aberration in the focal plane of the system under consideration is obtained by substituting in Eq. (A1.7), the values of R_c and t, given by Eqs. (A1.2), (A1.3) and (A1.5)

$$r = \frac{2}{\omega_c}\sqrt{2\frac{e}{m}V_r}\ \sin\theta\ \sin\left[\frac{\omega_c T_t}{2\left(1+\sqrt{\frac{V_r}{V}}\cos\theta\right)}\right] \qquad (A1.8)$$

A computor may be programmed to systematically scan through all angles of emission, θ, between 0 and $\frac{1}{2}\pi$ in steps of a specified increment, $\delta\theta$, and for each angle considered, a scan may be made through all energies of emission, V_r between 0 and V_r max, in specified increments of δV_r. For each combination of energy and angle of emission, the radial aberration, r, may be calculated, using eq (A1.8). The spread associated with the assessment of r at each stage, $\pm\ \delta r$, given by :-

$$\delta r = \frac{\partial r}{\partial \theta}\cdot\delta\theta + \frac{\partial r}{\partial V_T}\cdot\delta V_T$$

$$= \left\{ \frac{2}{\omega_c}\sqrt{2\frac{e}{m}V_T}\,\cos\theta\,\sin\left(\frac{\omega_c T_t}{2\left(1+\sqrt{\frac{V_T}{V}}\cos\theta\right)}\right) \right.$$
$$\left. +\sqrt{2\frac{e}{m}V_T}\,\sin\theta\left[\cos\left(\frac{\omega_c T_t}{2\left(1+\sqrt{\frac{V_T}{V}}\cos\theta\right)}\right)\right]\left[\frac{T_t}{\left(1+\sqrt{\frac{V_T}{V}}\cos\theta\right)^2}\right]2\sqrt{\frac{V_T}{V}}\sin\theta \right\}\delta\theta$$

$$+ \left\{ \frac{1}{\omega_c}\sqrt{2\frac{e}{mV_T}}\,\sin\theta\,\sin\left[\frac{\omega_c T_t}{2\left(1+\sqrt{\frac{V_T}{V}}\cos\theta\right)}\right] \right.$$
$$\left. +\sqrt{2\frac{e}{m}V_T}\,\sin\theta\left[\cos\left(\frac{\omega_c T_t}{2\left(1+\sqrt{\frac{V_T}{V}}\cos\theta\right)}\right)\right]\left[\frac{T_t}{\left(1+\sqrt{\frac{V_T}{V}}\cos\theta\right)^2}\right]\sqrt{\frac{1}{VV_T}}\cos\theta \right\}\delta V_T$$

Defining $\quad f(V_T,\theta) = \dfrac{1}{1+\sqrt{\frac{V_T}{V}}\cos\theta}$

$$\delta r = \left\{ \frac{2}{\omega_c}\sqrt{2\frac{e}{m}V_T}\,\cos\theta\,\sin\left(\tfrac{1}{2}\omega_c T_t\, f(V_T,\theta)\right) \right.$$
$$\left. +\sqrt{2\frac{e}{m}V_T}\,\sin\theta\,\cos\left(\tfrac{1}{2}\omega_c T_t\, f(V_T,\theta)\right)2T_t\sqrt{\frac{V_T}{V}}\cos\theta\,\overline{f(V_T,\theta)}^2 \right\}\delta\theta$$

$$+ \left\{ \frac{1}{\omega_c}\sqrt{2\frac{e}{mV_T}}\,\sin\theta\,\sin\left(\tfrac{1}{2}\omega_c T_t\, f(V_T,\theta)\right) \right.$$
$$\left. +\sqrt{2\frac{e}{m}V_T}\,\sin\theta\,\cos\left(\tfrac{1}{2}\omega_c T_t\, f(V_T,\theta)\right)T_t\sqrt{\frac{1}{VV_T}}\cos\theta\,\overline{f(V_T,\theta)}^2 \right\}\delta V_T$$

[A1.9]

Now the image plane under consideration may be marked off in annuli, centred on the Gaussian image, and of radii, R_t, which increase in equal steps of δR_t. (see fig. A1.3) δR_t is chosen to be at least an order of magnitude less than the maximum realizable value of r

Let n (θ) and n (V_T) represent the ordinates of the particular angular and energy distributions for the photo electrons in question.

For each value of θ and V_T successively selected as the computer proceeds on its scan, a value of r may be calculated using Eq. (A1.7). This identifies an annulus, for which :-

$$R_t \leq r < R_t + \delta R_t$$

into which ring fall $n(\theta)\,\delta\theta.\ n(V_T)\,\delta V_T$ photo-electrons. A progessive total of all such contributions may be stored in locations, reserved for each value of R_t, enabling a resultant electron density distribution to be printed out as the computor completes its scan. It is important that the values specified for $\delta\theta$ and δV_T should be sufficiently small, that the value of δr given by Eq. (A1.9) should be much less than δR_t.

This outlines the principles on which a programme was written to determine the electron distributions which may be obtained in the image plane of an electro-magnetically focussed system.

The programme was run on the Imperial College I.B.M. 7090 machine. The data used corresponded to the operating conditions of the camera tube, described in this thesis.

i.e. $B = 6.77$ milli tesla

$V = 7.000$ K volts

Electron distributions were obtained for a series of image planes, spaced at 0.1 mm intervals from

$\ell = 0.1300$ m. (the focal plane for electrons with zero axial velocity of emission).

to $\ell = 0.1322$ m.

A Lambertian angular distribution was assumed(75), and the energy distribution used was that measured by Shalabutoo et al.(162).

The specified increments in angle and energy of emission were

$\delta\theta = 0.01$ radians

$\delta V_T = 0.01$ volts

FIG. A1.4 DISTRIBUTION OF PHOTO-ELECTRONS AT DIFFERENT PLANES ALONG THE AXIS OF THE SYSTEM NEAR TO THE IDEAL FOCUS

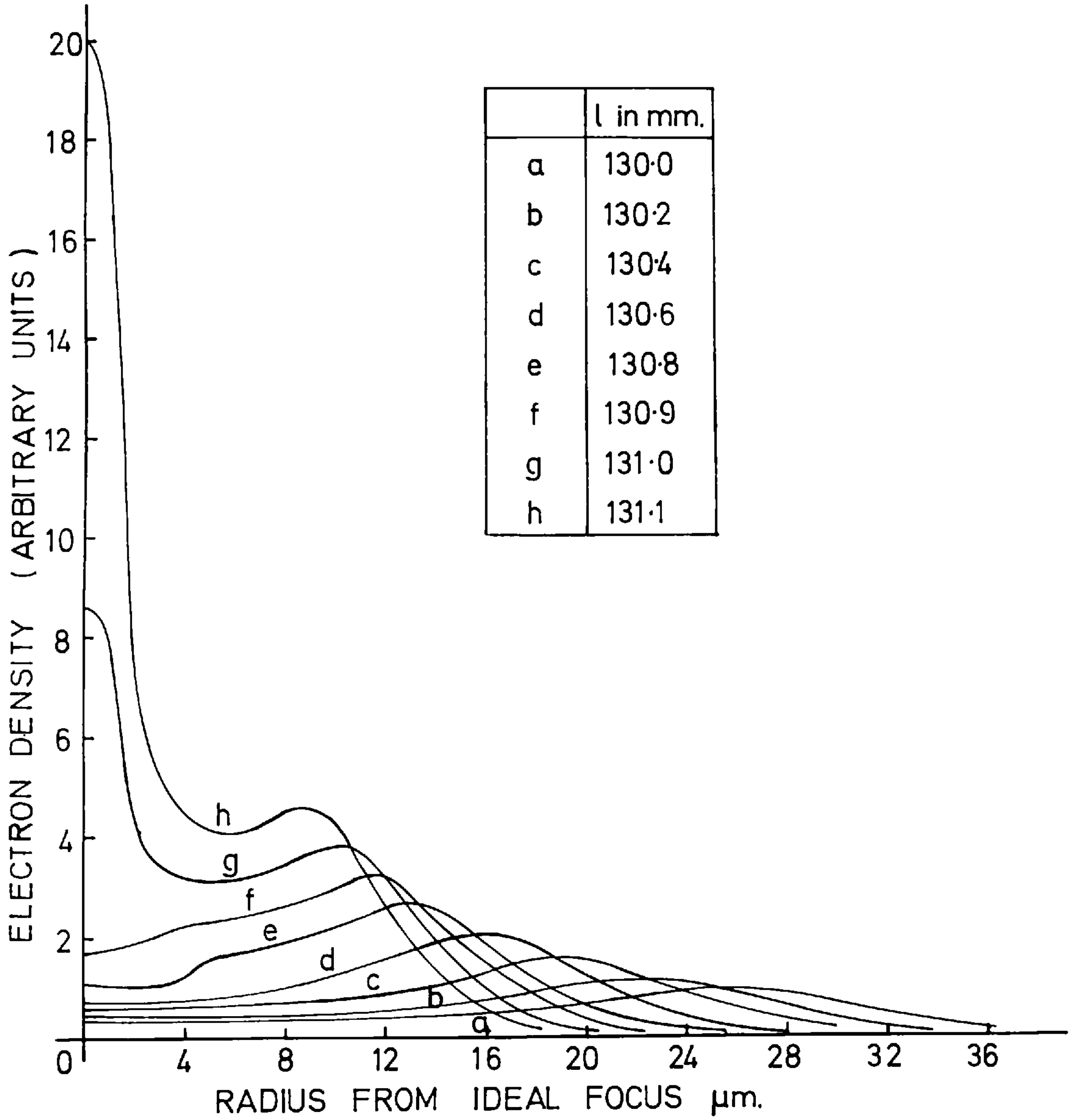

	l in mm.
a	130·0
b	130·2
c	130·4
d	130·6
e	130·8
f	130·9
g	131·0
h	131·1

FIG. A1.5 DISTRIBUTION OF PHOTO-ELECTRONS AT DIFFERENT PLANES ALONG THE AXIS OF THE SYSTEM NEAR TO THE IDEAL FOCUS

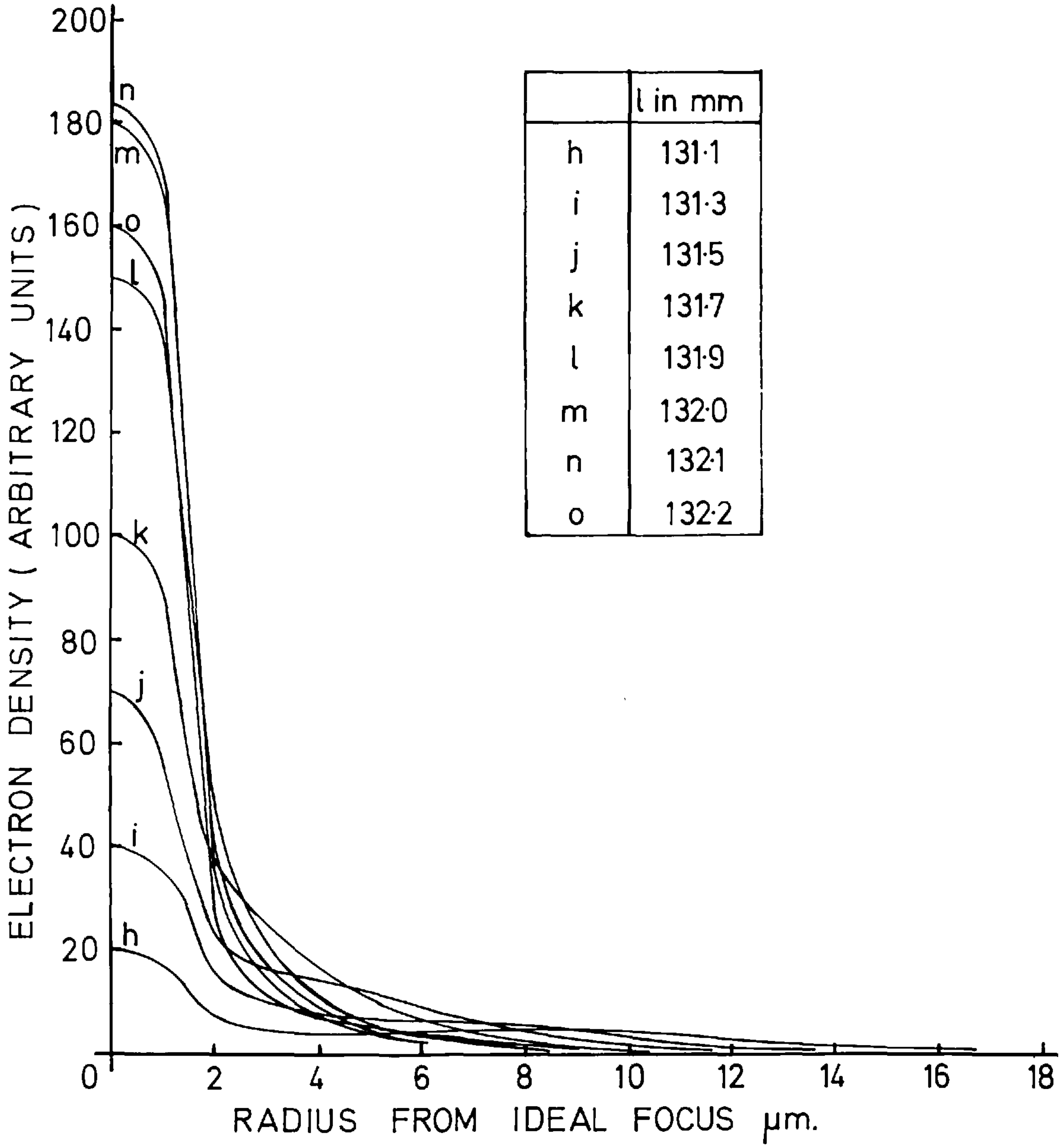

	l in mm
h	131·1
i	131·3
j	131·5
k	131·7
l	131·9
m	132·0
n	132·1
o	132·2

The distribution in the image plane was obtained by considering the electrons falling in rings bounded by circles of radii differing by $1\mu m$.

$$\text{i.e.} \quad \delta R_t = 10^{-6} \text{ m.}$$

The results obtained on running this programme are shown in figs. A1.4 and A1.5.

A.2 Degradation of signal occuring during the creation of a charge image in an insulating target by secondary emission.

Mandel[105] has shown that if a primary quantum gives rise to λ secondaries, where λ is a stochastic variate, ν incident particles, making independent interactions will give rise to μ secondaries so that :-

$$\overline{\Delta^2\mu} = \overline{\mu^2} - \overline{\mu}^2 \tag{A2.1}$$

$$\overline{\mu} = \overline{\nu}\,\overline{\lambda} \tag{A2.2}$$

$$\overline{\Delta^2\mu} = \overline{\lambda}^2\,\overline{\Delta^2\nu} + \overline{\nu}\,\overline{\Delta^2\lambda} \tag{A2.3}$$

These relationships hold for any probability distributions of ν and λ , and may be applied to the interactions occuring at the photo-cathode and storage surface of the system, illustrated in Fig 5.2

If the mean number of photons, falling on a cathode of sensitivity, σ for an individual photon, in a specified time interval is $\overline{P}$, we may use eq. (A2.2) to give the mean number of liberated photo-electrons, n_e

$$\overline{n_e} = \overline{P}\,\overline{\sigma} \tag{A2.4}$$

The distribution of P will be Poissonian[104], so that

$$\overline{\Delta^2 P} = \overline{P} \tag{A2.5}$$

It may be assumed that there is zero probability of more than one electron being emitted by an incident photon, so that the distribution $p(\sigma)$ of σ will be of the form

$$\begin{aligned} p(1) &= \overline{\sigma} \\ p(0) &= 1 - \overline{\sigma} \\ p(\sigma > 1) &= 0 \end{aligned}$$

Using eq. (A2.1)

$$\begin{aligned} \overline{\Delta^2 \sigma} &= \overline{\sigma^2} - \overline{\sigma}^2 \\ &= \sum_{\sigma=0}^{\infty} \sigma^2 p(\sigma) - \overline{\sigma}^2 \end{aligned}$$

$$\therefore \quad \overline{\Delta^2 \sigma} = \overline{\sigma} - \overline{\sigma}^2 \tag{A2.6}$$

Substituting (A2.5) and (A2.6) in (A2.3).

$$\overline{\Delta^2 n_e} = \overline{\sigma}^2\,\overline{P} + \overline{P}\left[\overline{\sigma} - \overline{\sigma}^2\right]$$

$$\overline{\Delta^2 n_e} = \overline{P}\,\overline{\sigma} \tag{A2.7}$$

Considering now the interaction at the storage surface, gain g_e (= δ - 1, where δ is the secondary emission coefficient), the mean numbers of emitted secondaries, $\overline{n_t}$ and stored electron charges, $\overline{n_s}$, will respectively be given from Eq. (A2.2) as

$$\overline{n_t} = \overline{\delta}\ \overline{n_e}$$
$$\overline{n_s} = \overline{g_e}\ \overline{n_e} = (\overline{\delta}-1)\overline{n_e}$$

From Eq. (A2.4), these become

$$\overline{n_t} = \overline{\delta}\ \overline{P}\ \overline{\sigma} \tag{A2.8}$$
$$\overline{n_s} = \overline{g_e}\,\overline{P}\,\overline{\sigma} = (\overline{\delta}-1)\overline{P}\,\overline{\sigma} \tag{A2.9}$$

From Eq. (A2.3), we may write for $\overline{\Delta^2 n_t}$ the mean square fluctuation in the transmitted secondaries

$$\overline{\Delta^2 n_t} = \overline{\delta}^2\ \overline{\Delta^2 n_e} + \overline{n_e}\ \overline{\Delta^2 \delta} \tag{A2.10}$$

Now the mean square fluctuation in the stored charge, $\overline{\Delta^2 n_s}$ will be given by the sum of the mean square fluctuations in the incident primary beam and the emitted secondaries. i.e.

$$\overline{\Delta^2 n_s} = \overline{\Delta^2 n_t} + \overline{\Delta^2 n_e}$$

from Eqs. (A2.4), (A2.7) and (A2.10), this becomes :-

$$\overline{\Delta^2 n_s} = \overline{\delta}^2\ \overline{P}\,\overline{\sigma} + \overline{P}\,\overline{\sigma}\,\overline{\Delta^2\delta} + \overline{P}\,\overline{\sigma}$$

$$\overline{\Delta^2 n_s} = \overline{P}\,\overline{\sigma}\left[\overline{\delta}^2 + 1 + \overline{\Delta^2\delta}\right] \tag{A2.11}$$

Eqs. (A2.9) and (A2.11) enable us to calculate an expression for $\left[\frac{N_s}{S}\right]$ the noise to signal ratio in the stored charge.

$$\left[\frac{N_s}{S}\right]^2 = \frac{\overline{\Delta^2 n_s}}{\overline{n_s}^2}$$

$$= \frac{\overline{P}\,\overline{\sigma}\left[\overline{\delta}^2 + 1 + \overline{\Delta^2\delta}\right]}{\left[(\overline{\delta}-1)\quad \overline{P}\,\overline{\sigma}\right]^2}$$

$$\left[\frac{N_s}{S}\right]^2 = \frac{\left[\overline{\delta}^2 + 1 + \overline{\Delta^2\delta}\right]}{(\overline{\delta}-1)^2\,\overline{P}\,\overline{\sigma}} \qquad \text{(A2.12)}$$

A knowledge of the statistics pertaining to the secondary emission process would enable further simplification of Eq. (A2.12)

<u>(a) Noiseless multiplication.</u>

For noiseless multiplication, i.e. δ is a constant,

$$\overline{\Delta^2\delta} = 0$$

Eq. (A2.12) then reduces to the following.

$$\left[\frac{N_s}{S}\right]^2 = \frac{\overline{\delta}^2 + 1}{(\overline{\delta}-1)^2\,\overline{P}\,\overline{\sigma}}$$

$$\left[\frac{N_s}{S}\right]^2 = \frac{1 + \frac{2\overline{\delta}}{(\overline{\delta}-1)^2}}{\overline{P}\,\overline{\sigma}} \qquad \text{(A2.13)}$$

For large $\overline{\delta}$

$$\left[\frac{N_s}{S}\right]^2 \approx \frac{1}{\overline{P}\,\overline{\sigma}} \qquad \text{(A2.14)}$$

Eqs. (A2.4) and (A2.9) enable us to write as alternative expressions

$$\left[\frac{N_s}{S}\right]^2 = \frac{1}{\overline{n_e}} = \frac{\overline{g_e}}{\overline{n_s}} \qquad \text{(A2.15)}$$

(b) Poissonian statistics of secondary emission.

If δ conforms to a Poissonian distribution

$$\overline{\Delta^2 \delta} = \overline{\delta}$$

Eq. (A2.12) then becomes

$$\left[\frac{N_s}{S}\right]^2 = \frac{\left[\overline{\delta}^2 + \overline{\delta} + 1\right]}{\left[\overline{\delta}-1\right]^2 \overline{P}\,\overline{\sigma}}$$

$$\left[\frac{N_s}{S}\right]^2 = \frac{1 + \frac{3\overline{\delta}}{(\overline{\delta}-1)^2}}{\overline{P}\,\overline{\sigma}} \qquad \text{(A2.16)}$$

For large $\overline{\delta}$ this approximates to the expressions given in Eqs. (A2.14) and (A2.15), derived for the case of noiseless multiplication.

(c) Exponential statistics of secondary emission.

Exponential statistics have been observed to apply for transmission secondary emission through thin solid potassium chloride dynodes[45].

For an exponential distribution,

$$\overline{\Delta^2 \delta} = \overline{\delta}^2$$

Eq. (A2.12) then becomes :-

$$\left[\frac{N_s}{S}\right]^2 = \frac{2\overline{\delta}^2 + 1}{(\overline{\delta}-1)^2\,\overline{P}\,\overline{\sigma}}$$

For large $\overline{\delta}$

$$\left[\frac{N_s}{S}\right]^2 \approx \frac{2}{\overline{P}\,\overline{\sigma}} \qquad \text{(A2.17)}$$

Eqs.(A2.4) and (A2.9) enable us to write as alternative expressions

$$\left[\frac{N_s}{S}\right]^2 = \frac{2}{n_e} = \frac{2\overline{g}_e}{n_s} \qquad \text{(A2.18)}$$

A3 Noise as a function of bandwidth (scanning speed) in a video amplifier.

The diagram shown in Fig. 5.3 represents the signal plate of storage tube target, coupled to the input of a head amplifier. The processes occurring, to generate the signal were described in § 5.6. From the relationships expressed by Eqs. (5.3) and (5.4), we may write for the signal current,

$$i_s = 2 M_m n_s e f_B \qquad (A3.1)$$

As this current flows through the input impedance Z of the head amplifier, a signal voltage V_i is developed at the grid of the first valve, given by :-

$$V_i = i_s \; Z \qquad (A3.2)$$

This is multiplied by the gain of the amplifier, $\frac{K}{Z}$, generating an output signal voltage, Vo, given by :-

$$V_o = \frac{K}{Z} \; V_i \qquad (A3.3)$$

Equations (A3.1), (A3.2) and (A3.3) combine to give for V_o :-

$$V_o = 2 K M_m n_s e f_B \qquad (A3.4)$$

Let us now consider the relative contributions, arising from the principal noise sources.

a. Johnson noise

The thermal or Johnson noise of grid resistor R may be regarded as arising from a source, generating a mean square noise voltage, $\overline{V_R^2}$ given by

$$\overline{V_R^2} = 4kTR\,df \qquad (A3.5)$$

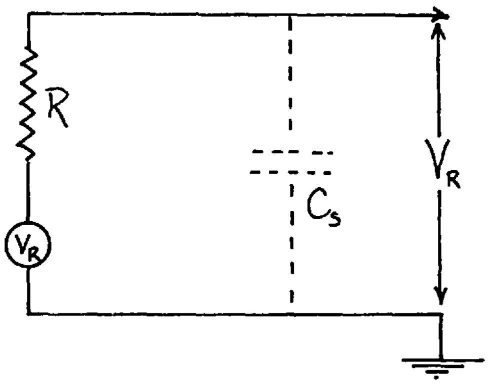

This is attenuated by the stray capacitance C_s, so that the actual mean square noise voltage, appearing at the grid of the head amplifier, $\overline{V_R'^2}$ is given by :-

$$\overline{V_R'^2} = \overline{V_R^2}\,\frac{\left|\frac{1}{j\omega C_s}\right|^2}{\left|R + \frac{1}{j\omega C_s}\right|^2}$$

$$\overline{V_R'^2} = \frac{\overline{V_R^2}}{R^2\omega^2C_s^2 + 1} \qquad (A3.6)$$

Substituting for $\overline{V_R^2}$ from (A3.5) we have :-

$$\overline{V_R^2} = \frac{4kTR\,df}{R^2\omega^2C_s^2 + 1}$$

$$\therefore \quad \overline{V_R^2} = \frac{4kTR\,df}{1+4\pi^2f^2C_s^2R^2} \qquad \text{(A3.7)}$$

This is amplified by a factor $\frac{K}{Z}$, so that on integrating over the amplifier band-width, we obtain for the thermal noise contribution, $\overline{V_{OR}^2}$ to the total mean square output noise voltage:-

$$\overline{V_{OR}^2} = \int_0^{f_B} \left|\frac{K}{Z}\right|^2 \cdot \frac{4kTR\,df}{1+4\pi^2f^2C_s^2R^2}$$

$$= \int_0^{f_B} K^2\left[\frac{1}{R^2} + 4\pi^2f^2C_s^2\right]\left[\frac{4kTR}{1+4\pi^2f^2C_s^2R^2}\right]df$$

$$= \int_0^{f_B} \frac{4K^2kTf_B}{R}$$

$$\therefore \quad \overline{V_{OR}^2} = \frac{4K^2kTf_B}{R} \qquad \text{(A3.8)}$$

The mean square noise to signal ratio due to Johnson noise $\left[\frac{N_R}{S}\right]^2$ is thus given from Eqs. (A3.4) and (A3.8) as

$$\left[\frac{N_R}{S}\right]^2 = \frac{\overline{V_{OR}^2}}{V_o^2}$$

$$= \frac{4K^2kTf_B}{4K^2M_m^2n_s^2e^2f_BR}$$

$$\therefore \quad \left[\frac{N_R}{S}\right]^2 = \frac{kT}{RM_m^2n_s^2e^2f_B} \qquad \text{(A3.9)}$$

b. Grid current shot noise.

The grid of the first valve of the head amplifier passes a certain amount of current whose fluctuations cannot be neglected.

Let i_g be the grid current, then :-

Mean square grid current fluctuations $= 2ei_g df$

These fluctuations are treated by the grid circuit and the amplifier in the same way as signal current, so that the grid current noise contribution to the mean square output noise voltage, $\overline{V_{OG}^2}$ is given by :-

$$\overline{V_{OG}^2} = \int_0^{f_B} [K]^2 \, 2ei_g \, df$$

$$\overline{V_{OG}^2} = 2K^2 e i_g f_B \qquad \text{(A3.10)}$$

The mean square noise to signal ratio $\left[\frac{N_G}{S}\right]^2$ arising from this source is thus given from Eqs. (A3.4) and (A3.10) by :-

$$\left[\frac{N_G}{S}\right]^2 = \frac{\overline{V_{OG}^2}}{V_0^2}$$

$$= \frac{2K^2 e i_g f_B}{4K^2 M_m^2 n_s^2 e^2 f_B^2}$$

$$\therefore \left[\frac{N_G}{S}\right]^2 = \frac{i_g}{2M_m^2 n_s^2 e f_B} \qquad \text{(A3.11)}$$

c. Anode current shot noise.

This may be calculated as the noise generated by the euivalent noise resistance, Re, introduced directly in series with the grid of the first valve. This generates a mean square noise voltage, $\overline{V_A^2}$ given by :-

$$\overline{V_A^2} = 4kTR_e df \tag{A3.12}$$

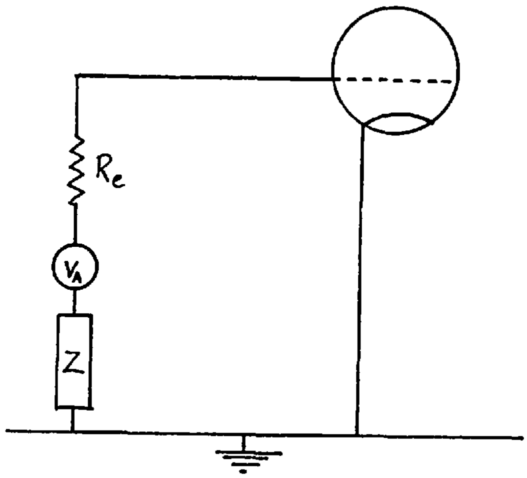

As this voltage is introduced directly on the grid, it is not attenuated by the capacity in the input circuit, as are the other noise contributions. Amplification by a factor $\frac{K}{Z}$ gives rise to an output mean square noise voltage, $\overline{V_{OA}^2}$ given by :-

$$\overline{V_{OA}^2} = \int_0^{f_B} \left[\frac{K}{Z}\right]^2 4kTR_e df$$

$$= \int_0^{f_B} K^2\left[\frac{1}{R^2} + 4\pi^2 f^2 C_s^2\right] \cdot 4kTR_e df$$

$$= \int_0^{f_B} \frac{K^2 4kTR_e (1 + 4\pi^2 f^2 C_s^2 R^2) df}{R^2}$$

$$\overline{V_{OA}^2} = \frac{4K^2kTR_e}{R^2}\left[f_B + \tfrac{4}{3}\pi^2R^2C_s^2f_B^3\right] \qquad (A3.13)$$

Eqs. (A3.4) and (A3.13) enable the mean square noise to signal ratio, arising from anode current shot noise $\left[\frac{N_A}{S}\right]^2$ to be expressed by :-

$$\left[\frac{N_A}{S}\right]^2 = \frac{\overline{V_{OA}^2}}{V_o^2}$$

$$= \frac{4K^2kTR_e}{4K^2M_m^2n_s^2e^2f_B^2R^2}\left[f_B + \tfrac{4}{3}\pi^2R^2C_s^2f_B^3\right]$$

$$\left[\frac{N_A}{S}\right]^2 = \frac{R_e}{R}\left[\frac{kT}{M_m^2n_s^2e^2f_BR}\right] + \frac{4\pi^2kTR_eC_s^2f_B}{3M_m^2n_s^2e^2} \qquad (A3.14)$$

Comparing this equation with (A3.9), it could be expressed in the form

$$\left[\frac{N_A}{S}\right]^2 = \left[\frac{R_e}{R}\right]\left[\frac{N_R}{S}\right]^2 + \frac{4\pi^2kTR_eC_s^2f_B}{3M_m^2n_s^2e^2} \qquad (A3.15)$$

Since large values of R (i.e. or orders higher than 10^6 ohms) are used to minimize the Johnson noise contribution, given by Eq (A3.9), and valves are selected with low values of Re (i.e. or order 10^2 ohms) to minimize the anode current shot noise contribution, given by Eq. (A3.14), it can be seen that the first term of Eq. (A3.15) will be smaller than the Johnson noise, and therefore, negligible when the overall noise, arising from all sources is computed. Eq. (A3.15) may therefore be used in the following simplified form :-

$$\left[\frac{N_A}{S}\right]^2 = \frac{4\pi^2 k T R_e C_s^2 f_B}{3 M_m^2 n_s^2 e^2} \qquad \text{(A3.16)}$$

A4. Signal to noise ratio that may be realized with return beam read-out of a stored charge image.

The operating principle of return beam read out for charge storage tubes is described in §5.9. Eq.(5.9) gives the signal current entering the multiplier, for a fully modulated signal, but taking into account the modulation transfer characteristic of the tube, the video signal, n_v may be expressed in terms of electrons per picture element by

$$n_v = M_m g_e P \sigma \tag{A4.1}$$

The noise inherent in the scanning beam in terms of electrons per picture element is $\sqrt{\overline{n_b}}$. Subtracting a precise quantity from this beam will in no way reduce the noise, so that if the scanning beam were to discharge a picture element in a noise free charge image, the noise present in the modulated return beam would still be $\sqrt{\overline{n_b}}$. In practice however, there will be a noise present in the stored charge image, given by Eq.(A2.11). The total mean square noise in the modulated return beam, will be given by adding the mean square beam noise and the mean square stored charge noise.

$$\overline{\Delta^2 n_b} = \overline{n_b} + M_m^2 \overline{P}\,\overline{\sigma}\left(\overline{\delta}^2 + 1 + \overline{\Delta^2 \delta}\right) \tag{A4.2}$$

The factor M_m arises from the modulation transfer characteristic, and is introduced to account for the filtering action of the camera tube, which attenuates stored charge noise, corresponding to high spatial frequencies, as well as attenuating the signal.

For Poissonian statistics of secondary emission,

$$\overline{\Delta^2 \delta} = \overline{\delta}$$

Eq. (A4.2) thus reduces to

$$\overline{\Delta^2 n_b} = \overline{n_b} + M_m^2 \, \overline{P} \, \overline{\sigma} \left[\overline{\delta}^2 + \overline{\delta} + 1 \right]$$

Working in terms of the gain of the target,

$$\overline{\Delta^2 n_b} = \overline{n_b} + M_m^2 \overline{P} \, \overline{\sigma} \left[\overline{g_e}^2 + 3(\overline{g_e} + 1) \right] \qquad \text{(A4.3)}$$

Using Eqs. (5.9), this may be alternatively expressed as:-

$$\overline{\Delta^2 n_b} = \overline{g_e} \, \overline{\sigma} \, \overline{P} \left[M_m^2 \left(\overline{g_e} + \frac{3(\overline{g_e} + 1)}{\overline{g_e}} \right) + \frac{1}{M_B} \right] \qquad \text{(A4.4)}$$

The mean square noise to signal ratio in the beam entering the multiplier, $\left[\frac{N_B}{S}\right]^2$ is obtained from Eqs. (A4.1) and (A4.4).

$$\left[\frac{N_B}{S}\right]^2 = \frac{\overline{g_e} + 3\,\frac{\overline{g_e} + 1}{\overline{g_e}} + \frac{1}{M_B M_m^2}}{\overline{g_e} \, \overline{P} \, \overline{\sigma}}$$

$$\approx \frac{\overline{g_e} + 3 + \frac{1}{M_B M_m^2}}{\overline{g_e} \, \overline{P} \, \overline{\sigma}} \qquad \text{(A4.5).}$$

Eqs. (A2.4) and (A2.8) enable us to write as alternative expressions

$$\left[\frac{N_B}{S}\right]^2 = \frac{\overline{g_e} + 3 + \frac{1}{\overline{M_B M_m^2}}}{\overline{g_e}\ \overline{n_e}} = \frac{\overline{g_e} + 3 + \frac{1}{\overline{M_B M_m^2}}}{\overline{n_s}} \qquad \text{(A4.6)}$$

If the secondary emission coefficient of the multiplier dynodes is δ' and the multiplication is governed by Poissonian statistics, the signal to noise ratio is further reduced by a factor $\sqrt{\frac{\delta' - 1}{\delta'}}$ but this is negligible for large δ'

A5. Signal to noise ratio that may be realized with isocon read out.

The processes involved in isocon read out are described in § 5.10. As the scanning beam discharges the elemental charges, n_s, stored on the target, Rs electrons per stored electron, are scattered in a non specular fashion so that $n_l\ (= R_s n_s)$ electron charges are available in the beam, returning towards the multiplier, to generate a video signal.

If we regard the n_s charges, held on the target elements as the primary particles, which independently interact with the scanning beam to produce the n_l daughter electrons, we may apply Mandel's formula (Eq. A2.3) to calculate the noise inherent in n_l

$$\overline{\Delta^2 n_l} = \overline{R_s}^2\, \overline{\Delta^2 n_s} + \overline{n_s}\, \overline{\Delta^2 R_s} \qquad \text{(A5.1)}$$

Eqs. (A2.9) and (A2.11) enable us to write,

$$\overline{\Delta^2 n_l} = \overline{R_s}\left[\overline{P}\,\overline{\sigma}\left(\overline{\delta}^2 + 1 + \overline{\Delta^2\delta}\right)\right] + \left(\overline{\delta} - 1\right)\overline{P}\,\overline{\sigma}\,\overline{\Delta^2 R_s} \qquad \text{(A5.2)}$$

Assuming that Poissonian statistics apply for both the secondary emission and for the scattering processes,

i.e. $\overline{\Delta^2\delta} = \overline{\delta}$ and $\overline{\Delta^2 R_s} = \overline{R_s}$

Eq. (A5.2) may be rewritten,

$$\overline{\Delta^2 n_l} = \overline{R_s}^2 \left[\overline{P}\,\overline{\sigma} \left(\overline{\delta}^2 + \overline{\delta} + 1 \right) \right] + \left(\overline{\delta} - 1 \right) \overline{P}\,\overline{\sigma}\,\overline{R_s}$$

$$\therefore \quad \overline{\Delta^2 n_l} = \left(\overline{\delta} - 1 \right) \overline{P}\,\overline{\sigma} \left[\overline{R_s}^2 \left[\left(\overline{\delta} - 1 \right) + \frac{3\,\overline{\delta}}{\overline{\delta} - 1} \right] + \overline{R_s} \right] \qquad \text{(A5.3)}$$

The scattered electrons enter a multiplier aperture, which accepts a fraction A, of the total number scattered. The probability distribution p(A) of A is of the form

$$p\,(1) = \overline{A}$$

$$p\,(0) = 1 - \overline{A}$$

$$p\,(A > 1) = 0$$

Using the same argument as that used to derive Eq.(A2.6), we may write :-

$$\overline{\Delta^2 A} = \overline{A} \left(1 - \overline{A} \right) \qquad \text{(A5.4)}$$

Invoking Mandel's formula, Eq. (A2.3), again to calculate the noise inherent in the scattered electrons carrying the video information which enters the multiplier, n_v ,we may write for $\overline{\Delta^2 n_v}$

$$\overline{\Delta^2 n_v} = \overline{A}^2\, \overline{\Delta^2 n_l} + \overline{n_l}\, \overline{\Delta^2 A} \qquad \text{(A5.5)}$$

Substituting Eqs. (5.11), (A2.9), (A5.3) and (A5.4) in Eq. (A5.5), we have :-

$$\overline{\Delta^2 n_v} = \overline{A}^2 \overline{g_e}\, \overline{P}\, \overline{\sigma} \left[\overline{R_s}^2 \left[(\overline{\delta}-1) + \frac{3\overline{\delta}}{\overline{\delta}-1} \right] + \overline{R_s} \right] + \overline{R_s}\, \overline{g_e}\, \overline{P}\, \overline{\sigma}\, \overline{A}(1-\overline{A})$$

$$= \overline{A}^2\, \overline{R_s}\, \overline{g_e}\, \overline{P}\, \overline{\sigma} \left[\overline{R_s} \left(\overline{\delta} - 1 + \frac{3\overline{\delta}}{\overline{\delta}-1} \right) + 1 + \frac{1}{\overline{A}} - 1 \right]$$

For large $\overline{\delta}$ $(= \overline{g_e} + 1)$ this becomes :-

$$\overline{\Delta^2 n_v} = \overline{A}^2\, \overline{R_s}\, \overline{g_e}\, \overline{P}\, \overline{\sigma} \left[\overline{R_s} \left(\overline{g_e} + 3 \right) + \frac{1}{\overline{A}} \right] \tag{A5.6}$$

Two additional factors must be taken into account in computing the mean square noise, $\overline{\Delta^2 n_b}$ in the total electron flux entering the multiplier.

First, there is a constant background noise, $\overline{B_n^2}$ arising from the small number of spurious electrons which can never be completely eliminated. A small background current persists in entering the multiplier aparture.

Also, account must be taken of the fast that noise, arising from components in the stored charge, corresponding to high spatial frequencies on the target surface, are filtered by a factor, equal to the modulation transfer characteristic of the camera, M_m. We may hence write for the mean square noise, $\overline{\Delta^2 n_b}$ at the input of the multiplier,

$$\overline{\Delta^2 n_b} = M_m^2 \, \overline{\Delta^2 n_Y} + \overline{B_n^2}$$

From Eq. (A5.6), we may write for this :-

$$\overline{\Delta^2 n_s} = M_m^2 \, \overline{A}^2 \, \overline{R_s} \, \overline{g_e} \, \overline{P} \, \overline{\sigma} \left[\overline{R_s} \left(\overline{g_e} + 3 \right) + \frac{1}{\overline{A}} \right] + \overline{B_n^2} \quad \text{(A5.7)}$$

The mean square noise to signal ratio at the input of the multiplier for isocon readout, $\left[\frac{N_I}{S}\right]^2$ is obtained from Eqs. (5. 13) and (A5.7), and is given by :-

$$\left[\frac{N_I}{S}\right]^2 = \frac{M_m^2 \, \overline{A} \, \overline{R_s} \, \overline{g_e} \, \overline{P} \, \overline{\sigma} \left[\overline{R_s} \left(\overline{g_e} + 3 \right) + \frac{1}{\overline{A}} \right] + \overline{B_n^2}}{M_m^2 \, \overline{A}^2 \, \overline{R_s}^2 \, \overline{g_e}^2 \, \overline{P}^2 \, \overline{\sigma}^2}$$

$$\left[\frac{N_I}{S}\right]^2 = \frac{\left(\overline{g_e} + 3 + \frac{1}{\overline{A} \, \overline{R_s}} \right)}{\overline{g_e} \, \overline{P} \, \overline{\sigma}} + \frac{\overline{B_n^2}}{M_m^2 \, \overline{A}^2 \, \overline{R_s}^2 \, \overline{g_e}^2 \, \overline{P}^2 \, \overline{\sigma}^2} \quad \text{(A5.8)}$$

Eqs. (A2.4) and (A2.9) enable us to write as alternative expressions

$$\left[\frac{N_I}{S}\right]^2 = \frac{\left(\overline{g_e} + 3 + \frac{1}{\overline{A} \, \overline{R_s}} \right)}{\overline{g_e} \, \overline{P} \, \overline{\sigma}} + \frac{\overline{B_n^2}}{M_m^2 \, \overline{A}^2 \, \overline{R_s}^2 \, \overline{g_e}^2 \, \overline{n_e}^2} \quad \text{(A5.9)}$$

$$\left[\frac{N_I}{S}\right]^2 = \frac{\left(\overline{g_e} + 3 + \frac{1}{\overline{A} \, \overline{R_s}} \right)}{\overline{g_e} \, \overline{P} \, \overline{\sigma}} + \frac{\overline{B_n^2}}{M_m^2 \, \overline{A}^2 \, \overline{R_s}^2 \, \overline{n_s}^2} \quad \text{(A5.10)}$$

A6 Skip distance of spurious electrons, emitted from the walls of an image tube.

(The following treatment is based on an analysis, given by Rosenbloom[153], in conjunction with whom the author performed the experimental work on signal background, described in § 7.3).

Figs. A6.1 and A6.2 represent the motions of spurious electrons, emitted from the wall of an image tube, in the advancing equatorial and rotating meridional planes. Since there are about two orders of magnitude difference in the radii of the tube and of the electron orbits, the glass wall of the tube can be treated as a plane surface.

On emission from the wall at an angle of ψ to the normal in the equatorial plane, the electron will move under the influence of the electrostatic and magnetic fields, E and B, for a time, t_s, until it restrikes the wall at a distance, s, further down the tube.

From fig. A6.1, it can be seen that :-

$$\omega_c t_s = \pi + 2\psi$$

$$t_s = \frac{\pi + 2\psi}{\omega_c} \qquad \text{(A6.1)}$$

Since the electron is uniformly accelerated along the tube, s will be given by :-

$$s = \sqrt{\frac{e}{2m}\frac{V}{l}\cdot s}\cdot t_s$$

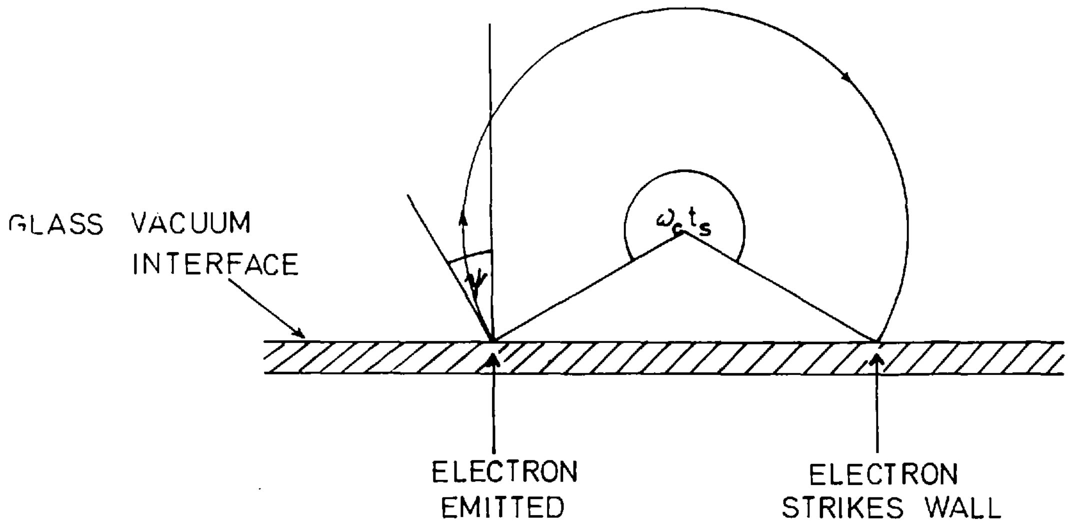

FIG. A6.1 MOTION OF SPURIOUS ELECTRON, EMITTED FROM WALL OF AN ELECTRO-MAGNETICALLY FOCUSED IMAGE TUBE, IN ADVANCING EQUATORIAL PLANE

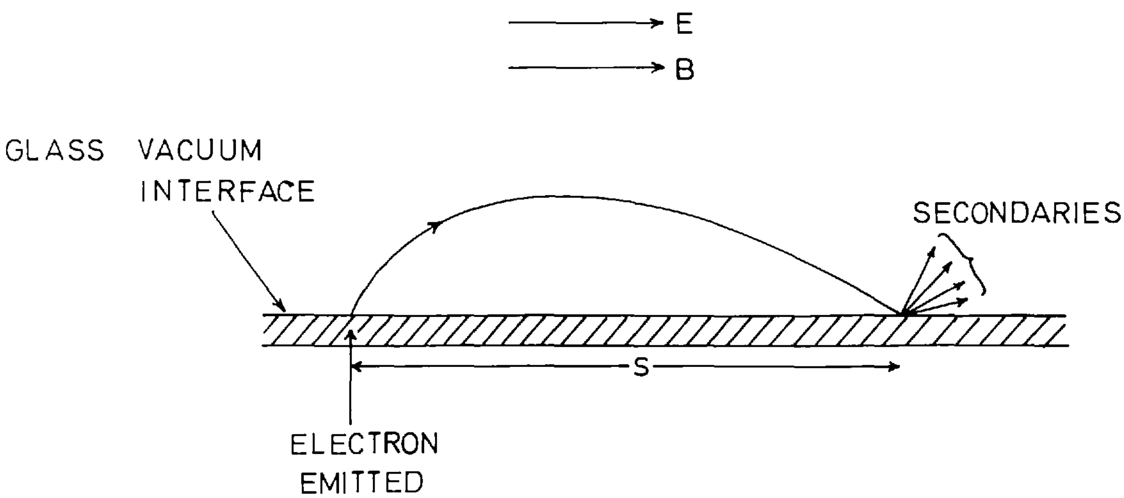

FIG. A6.2 MOTION OF A SPURIOUS ELECTRON, EMITTED FROM WALL OF AN ELECTRO-MAGNETICALLY FOCUSED IMAGE TUBE, IN ROTATING MERIDIONAL PLANE

From Eq. (A6.1), this becomes : -

$$s = \sqrt{\frac{e}{2m} \cdot \frac{V}{\ell} \cdot s} \quad \frac{(\pi + 2\psi)}{\omega_c}$$

$$s = \frac{1}{2} \frac{e}{m} \frac{V}{\ell} \cdot \frac{(\pi + 2\psi)^2}{\omega_c^2} \tag{A6.2}$$

(The symbols V, ℓ and ω_c have the same significance as defined in appendix A.1). Thus from Eq.(A1.1), Eq. (A6.2) may be expressed as

$$s = \frac{1}{2} \cdot \frac{m}{e} \cdot \frac{V}{B^2} \cdot \frac{(\pi + 2\psi)^2}{\ell} \tag{A6.3}$$

Let p (ψ) dψ be the probability that an electron is emitted at an angle between ψ and ψ+ dψ. Then we may write for the mean electron skip distance, $\bar{s}$,

$$\bar{s} = \frac{\int_{-\frac{\pi}{2}}^{\frac{\pi}{2}} p(\psi)\, s \, d\psi}{\int_{-\frac{\pi}{2}}^{\frac{\pi}{2}} p(\psi)\, d\psi}$$

$$\bar{s} = \frac{1}{2} \frac{m}{e} \frac{V}{B^2} \frac{1}{\ell} \frac{\int_{-\frac{\pi}{2}}^{\frac{\pi}{2}} (\pi + 2\psi)^2 p(\psi) d\psi}{\int_{-\frac{\pi}{2}}^{\frac{\pi}{2}} p(\psi) d\psi} \tag{A6.4}$$

We can consider two likely angular distributions.

<u>(a) Lambertian Emission</u>.

i.e. $\quad p(\psi)d\psi = K_F \cos\psi \, d\psi$

In this case

$$\frac{\int_{-\frac{\pi}{2}}^{\frac{\pi}{2}} (\pi + 2\psi)^2 \, p(\psi) \, d\psi}{\int_{-\frac{\pi}{2}}^{\frac{\pi}{2}} p(\psi) \, d\psi} = \frac{\int_{-\frac{\pi}{2}}^{\frac{\pi}{2}} (\pi + 2\psi)^2 \cos\psi \, d\psi}{\int_{-\frac{\pi}{2}}^{\frac{\pi}{2}} \cos\psi \, d\psi}$$

$$= 2(\pi^2 - 4)$$

<u>(b). All angles equally likely.</u>

i.e. $$p(\psi) d\psi = K_F \, d\psi$$

In this case

$$\frac{\int_{-\frac{\pi}{2}}^{\frac{\pi}{2}} (\pi + 2\psi)^2 \, p(\psi) \, d\psi}{\int_{-\frac{\pi}{2}}^{\frac{\pi}{2}} p(\psi) \, d\psi} = \frac{\int_{-\frac{\pi}{2}}^{\frac{\pi}{2}} (\pi + 2\psi)^2 \, d\psi}{\pi}$$

$$= \frac{4}{3}\pi^2$$

Substituting these results in Eq. (A6.4), tcgether with operating parameters corresponding to the prototype tube,

i. e. $$\ell = 0 \cdot 19 \text{ m.}$$

and $$\frac{V}{B^2} = 1 \cdot 17 \times 10^8 \text{ v. m}^4/\text{wb}^2$$

from the slope of the graph in fig 7.8,

We have

(a) For Lambertian emission $\overline{S}$ = 2.06 cm.

(b) For all angles of emission $\overline{S}$ = 2.32 cm. equally likely

These figures are close to the distance, (2 cm.), separating the platinum ring wall electrodes, fired into the glass in the prototype tube.

Reference Index

1. Airey, R.W., private communication.

2. Alexander, J.W.F., Burtt, R.B., Advances in Electronics and Electron Physics, Ed. McGee, J.D.Wilcock, W.L., and Mandel, L., 16, 235 - 245, (Academic Press, London and N.Y. 1962).

3. Allen, J.D., Advances in Electronics and Electron Physics, Ed. McGee, J.D., McMullan, D., and Kahan, E., 22 B, 849 - 864, (Academic Press, London and N.Y., 1966).

4. Amos, S.W., Birkinshaw, D.C., Television Engineering, 1, 194 - 212, (Iliffe, London, 1963).

5. Ansbacher, F., Ehrenberg, W., Proc. Phys. Soc., 64, 369, (1951).

6. Axon, P.E., Eur. Broadc. Un. Rev., Part A- Technical, No. 49, 2 - 7, (1958).

7. Banks, P.B., Turk, W.E., 14th Annual I.E.E.E.- G.B. Broadcast Symposium, 1 - 11, (1964).

8. Batey, P.H., Slark, N.A., A.E.E.P., 22A, 63 - 69, (1966).

9. Baum, W.A., Trans. Int. Ast. Un., 9, 681, (1955).

10. Baum, W.A., Advances in Electronics and Electron Physics, Ed. McGee, J.D.and Wilcock, W.L., 12, 1, (Academic Press, London and N.Y.1960).

11. Baum, W.A., A.E.E.P., 12, 200, (1960).

12. Baum, W.A., A.E.E.P., 16, 393 - 398, (1962).

13. Beyer, R.R., Goetze, G.W., A.E.E.P., 22A , 241 - 250, (1966).

14. Beyer, R.R., Green, M., Goetze, G.W., A.E.E.P., 22A, 251 - 260 (1966).

15. Beurle, R.L., Slark, N.A., A.E.E.P., 12, 247 - 261, (1960).

16. Beurle, R.L., Wreathall, W.M., A.E.E.P., 16, 333 - 335, (1962).

17. Beurle, R.L., Proc. I.E.E., 110, 1350 - 1364, (1963).

18. Binnie, D.M. Jane, M., Newth, J.A., Potter, D.C., Walters, J., Nuc. Inst. and Methods, 20, 221, (1963).

19. Blake, J., Burtt, R.B., A.E.E.P., 16, 213, (1962).

20. Boyer, L.A., Flory, L.E., Morgan, J.M., Pike, W.S., Journ. Soc. Mot. Pic. and T. V. Engrs., 74, 760, (1965).

21. Boerio, A.H., Beyer, R.R., Goetze, G.W., A.E.E.P., 22A, 229 - 239, (1966).

22. Braddick, H.J.J., The Physics of Experimental Method, p. 17, (Chapman and Hall, London 1954).

23. Cope, A.D., Image Intensifier Symposium, N.A.S.A., U.S.A.E.R.D.L., Fort Belvoir, Va., p 43 - 49 (1961).

24. Cope, A.D., Bruce, W., R.C.A. Review, 26, 242 - 261. (1965).

25. Cope, A.D., Luedicke, E., A.E.E.P., 22A, 175 - 187, (1966).

26. Davies, G.P., A.E.E.P., 16, 119, (1962).

27. Davis, R.J., A.E.E.P., 22B, 875 - 883, (1966).

28. Dawe, A.C., Television Soc. Journal, 10, 166 - 171, (1963).

29. Dawe, A.C., E. M. I. London Symposium, Camera Tubes, 3, (1964).

30. Day, H.R., Hannam, J., Wargo, P., Trans. I.R.E., E.D.7, 78 - 83, (1960).

31. De Haan, E. F., International Television Conference, I.E.E., Conference Report Series, No.5, 65-67, (1962).

32. De Haan, E.F., van der Drift, A., Schampers, P.P.M., Philips Tech. Rev., 25, 136-138, (1964).

33. ibid., p. 143 - 145.

34. ibid., p. 133 - 151.

35. Dennison, E.W., A.E.E.P., 22A, 435 - 439, (1966).

36. De Vore, H.B., Proc. I.R.E., 36, 335 - 345, (1948).

37. De Witt, J.H., Image Intensifier Symposium, N.A.S.A., U.S.A.E.R.D.L., Fort Belvoir, Va., p. 187 - 192 (1961).

38. De Witt, J.H., A.E.E.P., 16, 419 - 429, (1962).

39. Ditchburn, R.W., Light, p.78, (Blackie, London and Glasgow, (1952).

40. Doughty, D.D., A.E.E.P., 22A, 261-270, (1966).

41. Dresner, J., R.C.A., Review, 22, 305 - 324, (1961).

42. Duchesne, M., A.E.E.P., 16, 27, (1962).

43. Eastman Kodak Co., Modulation Transfer Data for Kodak Films, Ed. Eastman Kodak Co., Rochester 4, N.Y. (1962).

44. Edwardson, S.M., B.B.C. Research Report, No. T - 100/3, (1963).

45. Emberson, D.L., Todkill, A., Wilcock, W.L., A.E.E.P., 16, 127, (1962).

46. Emberson, D.L., Trans. I.R.E., N.S. - 9, 115, (1962).

47. Emberson, D.L. Ph.D. Thesis, Univ. of London, p. 28-30 (1961).

48. E.M.I., High Resolution Vidicon - Type 9677, Data Sheet.

49. English Electric Valve Data - 8540 Image Orthicon, (1964).

50. Enstone, C.A.G., Ph. D. Thesis, Univ. of London, (1959).

51. Eskart, F., Ann. Phys., 14, 98 (1954).

52. Fellget, P., Monthly Notices of the Royal Astr. Soc., 118, 398 (1958).

53. Fellget, P., The Present and Future of the Telescope of Moderate Size, Ed. Wood, F.B., p. 51, (Univ. of Pennsylvania Press, 1958).

54. Fix, H., Habermann, W., Rundfunk - Tech. Mitti, 3, 76, (1959).

55. Flory, L.E., Pike, W.S., Morgan, J.M., Boyer, L.A., A.E.E.P., 22B, 885 - 902, (1966).

56. Gebel, R.K.H., Devol, L., A.E.E.P., 12, 195-201 (1960).

57. Gibbons, D.J., A.E.E.P., 12, 203 - 218, (1960).

58. Gildemeister, O., Geise, R., A.E.E.P. 16, 113, (1962).

59. Goetz, G.W., A.E.E.P., 16, 145 (1962).

60 Goetze, G.W., Boerio, A.H., Electron Devices Meeting, Washington D.C. (Oct. 1963, unpublished but reported in Electronics, Nov. 1963 and Trans. I.E.E.E., Jan 1964).

61. Goetze, G.W., Boerio, A.H., Green, M., J.Appl.Phys., 35, 482, (1964).

62. ibid., p. 489.

63. Goetze, G.W., Boerio, A.H., Proc. I.E.E.E., 52, 1007 - 1012 (1964).

64. Goetze, G.W., A.E.E.P., 22A, 219 - 226, (1966).

65. Harris, L., J. Opt. Soc. Amer., 45, 27, (1955).

66. Hass, G., J. Opt. Soc. Amer., 39, 532, (1949).

67. Heimann, W., A.E.E.P., 12, 240-244, (1960).

68. Heimann, W., Kunze, C., A.E.E.P., 16, 217-225,(1962).

69. Hendry, E.D., Turk, W.E., J.S.M.P.T.E., 69, 88, (1960).

70. Herrmann, G., Wagener, S., The Oxide Coated Cathode, 1, 55-64, 2, 151-181, 255, (Chapman and Hall, London, 1951).

71. Hiltner, W.A., The Pres. and Fut. of Teles. of Mod. size, Ed. Wood, F.B., p.11, (Univ. of Pennsylvania Press, 1958).

72. Hiltner, W.A., Niklas, W.F., A.E.E.P., 16, 25,(1962).

73. Hynek, J.A., Barton, G., Aikens, R., Powers, W., A.E.E.P., 16, 412, (1962).

74. Iams, H., Morton, G.A., Zworykin, V.K., Proc. I.R.E., 27, 541 - 547, (1939).

75. Ives, H.E., Olpin, A.R., Johnsrud, A.L., Phys. Rev., 32, 57 - 80, (1928).

76. James, I.J.P., Proc. I.E.E., 99, 802, (1952).

77. Joint discussion on photo-electric image tubes and their astronomical applications, Trans. I.A. U., 9, 673, (1957).

78. Jones, R.C., Photogr. Sci. and Eng., 2, 57, (1958)

79. Khan, M.A.A., Ph. D. Thesis, Univ. of London, (1961).

80. ibid., p.77-85.

81. ibid., p. 73.

82. ibid., p. 74 - 76.

83. ibid., p. 95 - 97.

84. Khogali, A., Ph. D. Thesis, Univ. of London p.53 (1964).

85. ibid, p. 154.

86. Knoll, M., Kazan, B., Storage Tubes, p.18, (Wiley, N.Y., Chapman and Hall, London 1952).

87. Kodak Ltd., Photosensitive Resist Techniques, Ed. Kodak Ltd., London (1965).

88. Kron, G.E., A.E.E.P., 16, 25, (1962).

89. Lallemand, A., Com. Rend. Acad. Sci., Paris, 203, 243, (1936).

90. Lallemand, A., The Pres. and Fut. of Teles. of Mod. size, Ed. Wood, F.B., p 25, (Univ. of Pennsylvania Press, 1958).

91. Lallemand, A., Duchesne, M., Wlerick, G., A.E.E.P., 12, 5, (1960).

92. Lallemand, A., A.E.E.P., 16, 1, (1962).

93. Lallemand, A., A.E.E.P., 22A, 1 - 9, (1966).

94. Livingstone, W.C., Image Intensifier Symposium, N.A.S.A., U.S.A.E.R.D.L., Fort Belvoir, Va., p. 171., (1961).

95. ibid., p. 167-172.

96. Livingstone, W.C., A.E.E.P., 16, 444 - 445, (1962).

97. Livingstone, W.C., J.S.M.P.T.E., 72, 777 - 778, (1963).

98. Lubszynski, H.G., Brit. Pat. No. 457493 (1935).

99. Lubszynski, H.G., J.Sci. Inst., 34, 83 - 84, (1957).

100. Lubszynski, H.G. Taylor, S., Wardley, J., J.Brit. I.R.E., 20, 332 (1960).

101. ibid, p 326.

102. Lubszynski, H.G., Wardley, J., International Television Conference, I.E.E. Conference Report Series, No.5., 59-63 (1962).

103. Malling, L.R., Allen, J.D., A.E.E.P., 22B, 835 - 847, (1966).

104. Mandel, L., Proc. Phys. Soc. (Lond.), 71, 1037, (1958).

105. Mandel, L., Brit. J. Appl. Phys. 10, 233, (1959)

106. Marschka, F.D., Image Intensifier Symposium, N.A.S.A., U.S.A.E.R.D.L., Fort Belvoir, Va., p. 51 - 54 (1961).

107. McGee, J.D., Proc. I.E.E., 97, 377 - 392, (1950).

108. ibid., 384.

109. McGee, J.D., Jour. Roy. Soc. Arts., No.4869, 343, (1952).

110. ibid, p 344.

111. McGee, J.D., Jour. I.E.E., 8, 502 - 510, (1955)

112. McGee, J.D., Arch. Elektr. Ubert., 9, 355, (1955).

113. McGee, J.D., Jour. Television Soc., 8, 55 (1956).

114. McGee, J.D., Proceedings of a Symposium on Astronomical Optics and Related Subjects, Ed, Kopal, Z., p 205, (North - Holland Publishing Co., Amsterdam, 1956).

115. McGee, J.D., Image Intensifier Symposium, N.A.S.A., U.S.A.E.R.D.L., Fort Belvoir, Va.,(1958).

116. McGee, J.D., The Pres. and Fut. of Teles. of Mod. size, Ed. Wood, F.B., p.33 - 37. (Univ. of Pennsylvania Press, 1958).

117. McGee, J.D., Reports on Progress in Physics, 24, 173, (1961).

118. ibid., p 179 - 180

119. McGee, J.D., Airey, R.W., Wheeler, B.E., A.E.E.P., 16, 61, (1962).

120. McGee, J.D., Wheeler, B.E., A.E.E.P. 16, 47, (1962).

121. McGee, J.D., Astronomical Techniques, "Stars and Stellar Systems", Ed. Hiltner, W.A., 2, 302 - 329, (Univ. of Chicago Press, 1962).

122. McGee, J.D., International Television Conference, I.E.E. Conference Report Series, No. 5.,36-54,(1963).

123. ibid., p. 38.

124. McGee, J.D., Airey, R.W., Aslam, M., Powell, J.R., Catchpole, C.E., A.E.E.P., 22A, 113 - 126, (1966).

125. McGee, J.D., Khogali, A., Ganson, A., Baum, W.A., A.E.E.P., 22A, 11 - 30, (1966).

126. Meltzer, B., Holmes, P.L., Brit. J. Appl. Phys., 9, 139 - 143, (1958).

127. Mende, I.B., Ph. D. Thesis, Univ. of London, (1965).

128. ibid., p. 90 - 96.

129. Mende, S.B., Khan, A.A., Twiddy, N.D., Int. J. Elect., 19, 361 - 386, (1965).

130. Miyashiro, S., Nakagama, Y., A.E.E.P. 16, 171, (1962).

131. Morton, G.A., Trans. I.A.U., 9, 679, (1955).

132. Morton, G.A., Ruedy, J.E., A.E.E.P., 12, 183 - 193, (1960).

133. Morton, G.A., Image Intensifier Symposium, N.A.S.A., U.S.A.E.R.D.L., For Belvoir, Va., p. 81. (1961).

134. Nozawa, Y., A.E.E.P., 22B, 865 - 873, (1966).

135. Orvin, L.J., Brit. Pat. No. 445156, (1934).

136. Papp, G., Trans. I.R.E., N.S. - 9, 91, (1962).

137. Parton, J.S., Moody, J.C., Image Intensifier Symposium, N.A.S.A., U.S.A.E.R.D.L., Fort Belvoir, Va., p. 85 - 91, (1961).

138. Philips Gloeilampenfabrieken, Brit. Pat. No. 326200, (1928).

139. Pogson, N.R., Radcliffe Observations, 15, 295, (1854).

140. Randall, R.P., Diploma Thesis, Imperial College, p 38 - 43, (1959).

141. Randall, R.P., A.E.E.P., 12, 219 - 234, (1960).

142. Randall, R.P., A.E.E.P., 22A, 87 - 99, (1966).

143. Reed, C.R.G., Sanders, J.B., B.B.C. Research Report, No. T - 100, p. 21 - 24, (1963).

144. Rose, A., Iams, H., Proc. I.R.E., 27, 552, (1939).

145. Rose, A., Jour. Soc. Mot. Pic. Engrs., 47, 289, (1946).

146. Rose, A., Weimer, P.K., Law, H.B., Proc. I.R.E., 34, 424, (1946).

147. Rose, A., J. Opt. Soc. Amer., 38, 196, (1948).

148. Rose, A., Advances in Electronics and Electron Physics, Ed. Marton, L., 1, 131, (Academic Press, London and N.Y., 1948).

149. ibid., p.138.

150. Rosenbloom, M.E., Ph.D. Thesis, Univ. of London. (1965)

151. ibid., p. 31 - 54.

152. ibid., p. 62.

153. ibid., p. 209 - 213.

154. Sadashige, K., J.S.M.P.T.E., 73, 202, (1964).

155. Schade, O.H., R.C.A. Review, 9, 13, (1948).

156. ibid., p. 34.

157. Schade, O.H., J.S.M.P.T.E., 61, 135 - 133, (1953).

158. Schade, O.H., Applied Optics, 3, 17, (1964).

159. Schagen, P., Philips Research Report, 6, 135 - 153, (1951).

160. Schneeberger, R. J., Skorinko, G., Doughty, D.D. Feibelman, W.A., Image Intensifier Symposium, N.A.S.A., U.S.A.E.R.D.L., Fort Belvoir, Va, 27 - 34, (1961).

161. Schneeberger, R.J., Skorinko, G., Doughty, D.D., Feibelman, W.A., A.E.E.P., 16, 235 - 245, (1962).

162. Shalabatoo, I.K., Maslennikova, N.S., Soviet Physics, Technical Physics, 1, 1137, (1957).

163. Slark, N.A., Ph. D.Thesis, Univ. of London, (1961).

164. ibid., p. 101.

165. ibid., p. 64 - 69.

166. Slark, N.A., Woolgar, A.J. Trans. I.R.E., N.S. - 9, 115, (1962).

167. Slark, N.A., Woolgar, A.J., A.E.E.P., 16, 141, (1962).

168. Smithells, C.J., Metals Reference Book, 1, 254 - 60, (Butterworths, London 1955).

169. Sommer, A.H., Rev. Sci. Inst., 26, 725, (1955).

170. Stoudenheimer, R.G., A.E.E.P., 12, 41, (1960).

171. Taylor, S., A.E.E.P., 12, 263-274, (1960).

172. Theile, R., Townsend, F.H., Proc. I.R.E., 40 146, (1952).

173. Theile, R., A.E.E.P., 12, 277 - 290, (1960).

174. Theodorou, D.G., A.E.E.P., 22A, 477 - 489, (1966).

175. Towler, G.O., Private communication.

176. Tsukkerman, I.I., Electron Optics in Television, p.156, (Pergamon Press, Oxford, London, New York, Paris, 1961).

177. Vine, B.H., Janes, R.B., Veith, F.S., R.C.A., Review, 13, 7, (1952).

178. Wachtel, M.M., Doughty, D.D., Anderson, A.E., A.E.E.P., 12, 59, (1960).

179. Wachtel, M.M., Doughty, D.D., Goetze, G.W., Anderson, A.E., Sternglass, E.J., Rev. Sci. Inst., 31, 576, (1960).

180. Walkenhorst, W., Zeitschr. f. techn. Physic., 22, 14 - 21, (1941).

181. Wardley, J., A.E.E.P., 16, 227 - 233, (1962).

182. Wardley, J., A.E.E.P., 22A, 211 - 217, (1966).

183. Webley, R.S., Lubszynski, H.G., Lodge, J.A., Proc. I.E.E., 102, 402 - 406, (1955).

184. Weimer, P.K., R.C.A., Review, 10, 366 - 386, (1949).

185. Weimer, P.K., Forgue, S.V., Goodrich, R.R., Electronics, 23, 70 - 73, (1950).

186. Weimer, P.K., Advances in Electronics and Electron Physics, Ed. Marton, L., 13, 387 - 436, (Academic Press, London and N.Y. 1960).

187. ibid., p 412.

188. Wheeler, B.E., Ph.D. Thesis, Univ. of London, (1961).

189. White, E.L.C., Harker, M.G., Proc. I.E.E., 97, 408, (1950).

190. Wilcock, W.L., Emberson, D.L., Weekley, B., Trans. I.R.E., N.S. - 7, 126, (1960).

191. Woodhead, A.W., Taylor, D.G., Schagen, P., A.E.E.P., 16, 105, (1962).

192. Zacharov, B., Dowden, S., A.E.E.P., 12, 31, (1960).

193. Zacharov, B. O., Ph.D. Thesis, Univ. of London, (1960).

194. Zavoiskii, E.K., Smolkin, G.E., Plakhov, A. G., Butslow, M.M., Dokl. Akad. Nank. S.S.S.R., 100, 241, (1955).

195. Zworykin, V.K., Morton, G.A., Television, p. 320 - 332, (Wiley, N.Y., Chapman and Hall, London 1954).

List of Symbols.

A. fraction of useful electrons, scattered from the target of a tube operated in the isocon mode which are able to enter the electron multiplier.

A_r. aspect ratio (width / height) of a picture.

B. magnetic field.

B_n. R. M.S. background noise, expressed in terms of electrons per picture element, which arises from spurious electrons entering the multiplier aperture of an image isocon.

C. contrast of a highlight against background.

C_M. contrast of a star of magnitude M. against sky background.

C^i_{min} minimum contrast, inherently detectable in an image made up of a photon flux of P photons per picture element.

C^o_{min}. minimum contrast which may be definitely discerned by an image detecting device storing up to q events per picture element.

C_s. stray capacity, shunting input resistance of head amplifier.

E. equivalent quantum efficiency of an image detector.

E_e. electrostatic field.

E_o. equivalent quantum efficiency of an image detector, at a low spatial frequency, where the efficiency is at a maximum.

e. electronic charge.

e^c_{tse} charging current electron, drawn up to signal plate from earth as e^s_{tse} is emitted to the mesh.

e^p. energetic primary photo-electron, incident on target.

e^r electron in reading beam.

e^r_{bec} 'beam electron conduction' electron, i.e. a reading beam electron, able to traverse right across the target layer to land on the signal plate.

e^r_n reading beam electron, used to neutralize positive charges, stored within target.

e^s secondary electron, excited within target.

e^s_{sec} 'secondary electron conduction' electron.

e^s_{tse} 'transmitted secondary electron'.

$^e/m$. specific electronic charge.

F. image information recording efficiency, a figure of merit for an image detecting device.

f_b bandwidth of head amplifier.

g_e factor by which n_e photo-electrons are multiplied in the process of storing them as n_s electron charges on the target of a storage tube.

g_p factor by which P photons are multiplied in the process of recording the photon flux as q static events in an image detector.

h_i number of discernible half tones, i.e. definitely discernible brightness differences, accomodated by a photon flux of a given maximum number of photons.

h_o	the dynamic range of an image detector, i.e. the maximum number of half-tones which may be definitely discerned at the output of the detector.
$I_{max.}$	signal level at the output of an image detector, used to observe a regular, fully modulated bar pattern object, in a region corresponding to the whites.
$I_{min.}$	signal level at the output of an image detector, used to observe a regular, fully modulated bar pattern object in a region, corresponding to the blacks.
$I_{N.}$	intensity of a star of magnitude N.
$i_{b.}$	current in scanning electron beam.
$i_{g.}$	grid current of first valve of head amplifier.
i_s	signal current.
j.	$\sqrt{-\ 1}$
K.	constant by which the input admittance of a head amplifier is multiplied, to give a figure for the gain which the amplifier is designed to exhibit.
$K_{c.}$	coefficient of certainty, the factor by which the difference in the number of events observed in separate picture elements must exceed the root mean square noise fluctuation, to be considered significant.
K_F	arbitrary constant.
k.	Boltzmann's constant.
l.	distance between target and photocathode.
M.	stellar magnitude.
$M_{B.}$	fractional depth to which a scanning beam is modulated, as it discharges a picture element.

M_m modulation of a signal corresponding to a spatial frequency of m television lines.

m. definition of an image, expressed in terms of equivalent number of television lines.

N_n. root mean square background noise of an image detector, expressed in terms of an equivalent number of stored static events per picture element.

n. number of separate resolvable units into which an image may be divided.

n_b. number of electrons available in a scanning beam to discharge a picture element.

n_e. number of electrons, liberated from a photocathode by the action of P photons.

n_f. total number of electrons, entering the multiplier in an image isocon, per picture element.

n_i. number of electrons, non-specularly scattered from a picture element on a target, as it is scanned by an electron beam.

n_s. number of electron charges, stored on the target of a storage tube by interactions initiated by P primary photons.

n_t. number of secondary electrons, emitted from the target of a storage tube by interactions initiated by P primary photons.

n_v. video signal, expressed in terms of electrons per picture element.

$n(\theta)d\theta$ number of electrons, emitted from a photocathode in directions, between θ and $\theta + d\theta$ to the normal.

$n(V_T)dV_T$.   number of electrons, emitted from a photocathode with energies between V_T and $V_T + dV_T$.

P.   number of photons falling on a picture element of an image in a given observation time, T_e.

P'.   number of photons, falling on a single picture element, in a time, T_e, observed as a highlight in an array of randomly illuminated picture elements.

P_h.   a number of photons, capable of accommodating h discernible half-tones, i.e. there are h photon fluxes, less than P_h which represent steps of definitely detectable difference in light level.

p.   number of units of perceptible detail into which a television picture may be divided, across a frame.

$p(X)dX$ probablity that a parameter, associated with the variable X should lie between X and X + dX.

Q.   the total storage capacity of an image detector, i.e. the total number of events which the detector may store.

q.   the number of events stored in a picture element of an image detector by the action of P photons.

q_h.   a number of events, stored in a picture element of an image detector, capable of accomodating h half-tones.

q_{h_o} elemental storage capacity of an image detector, i.e. the maximum number of events which may be stored per picture element of an image detector.

R.   grid resistance at input of head amplifier.

R_c.   radius of electron orbit in advancing equatorial plane of an electron optical system.

R_e	equivalent noise resistance of input valve of head amplifier.
R_s	electron scattering coefficient of an isocon storage target.
R_t.	radius of annulus, marked off from Gaussian focus in image plane of electron optical system.
r.	distance from ideal focus at which a photo-electron strikes target.
S/N_A	contribution to signal to noise ratio, arising from anode current shot noise of first valve of head amplifier.
S/N_B	signal to noise ratio that may be realized in a camera tube, using return beam multiplier read-out.
S/N_G	contribution to signal to noise ratio arising from grid current shot noise of first valve of head amplifier.
S/N_I	signal to noise ratio that may be realized in a camera tube, using isocon read-out.
S/N_R	contribution to signal to noise ratio, arising from Johnson noise in input resistor of head amplifier.
S/N_s.	signal to noise ratio of the stored charge image of a storage tube.
S_i/N_i	signal to noise ratio associated with an input photon flux.
S_o/N_o	signal to noise ratio at the output of an image detector.
s.	electron skin distance along the wall of an image tube.
T	absolute temperature.
T_e.	exposure time.

T_t. defined by expression

t. transit time of electron moving from a photocathode to a target.

t_s. time of flight of a spurious background electron, emitted from the wall of an image tube, as it skips a distance, s along the wall.

u_{mean}. mean axial velocity of an electron moving between a photocathode and a target in a uniform electrostatic field.

V. potential of target with respect to photocathode.

V_i input signal voltage, developed at grid of first valve of head amplifier.

V_M mesh potential.

V_o signal output voltage from head amplifier.

V_{0A} r. m. s. noise voltage, appearing at output of head amplifier, due to anode current shot noise of first valve.

V_{0G} r. m. s. noise voltage, appearing at output of head amplifier, due to grid current shot noise of first valve.

V_{0R} r. m. s. noise voltage, appearing at output of head amplifier, due to V_R.

V_R. r. m. s. noise voltage, appearing at grid of first valve of head amplifier, due to v_R.

V_{SP}. signal plate potential.

V_T. potential in volts corresponding to an electron velocity of v_{em}.

v_A. an r. m. s. noise voltage, on the grid of the first valve of a head amplifier which would be equivalent to the anode current shot noise of the valve.

v_{em}. velocity with which an electron is emitted from a photo-cathode.

v_R. r. m. s. thermal noise e. m. f. generated in resistance, R, at a temperature, T.

Z. input impedance of head amplifier.

ΔT dwell time of a scanning beam on a picture element.

$\overline{\Delta X}$ r. m. s. fluctuation associated with quantity, represented by X.

$\overline{\Delta^2 X}$ mean square fluctuation associated with quantity represented by X.

δ secondary emission coefficient.

δX increment in quantity, represented by X.

ε permittivity.

ε_0 permittivity of free space.

θ angle to the normal at which a photo-electron is emitted from a photo-cathode.

λ number of secondary quanta, generated by a single primary quantum in a general interaction.

μ number of secondary quanta, generated by ν primary quanta in a general interaction.

ν number of incident quanta considered to be involvled in a general interaction.

ρ resistivity.

σ quantum efficiency of a photo-cathode.

τ time constant of image orthicon target.

ψ angle of emission in equatorial plane of spurious electrons emitted from wall of tube.

ω pulsatance of electrical signal.

ω_c electron cyclotron frequency.

ACKNOWLEDGEMENTS

The author would like to record his gratitude for the interest and facilities afforded by Professor J.D.McGee, in whose department this work was carried out, and to express his appreciation of the advice, suggestions and encouragement received from Dr. N.D.Twiddy who supervized the early part of the project and Dr. D. McMullan who directed the latter part of the work.

The author is also grateful of his invaluable association with Dr. S.B.Mende and Dr. M.E.Rosenbloom, in collaboration with whom, this project was started.

A special word of thanks is due too, to those whose technical assistance made this work possible, to Mr. J.Westlake for his skill, patience and initiative in tube assembly and processing, to Mr. W. T. Simpson for his work on the demountable vacuum systems, to Mr. A. Lewkowicz for his work on the electronics, to Messrs. W. Goodway and J. Beisiegel who were responsible for the glassblowing, and to Mr. B. Weekley who made the layers for the prototype tube.

The author would also like to thank Mr. G. Towler for his contribution to the latter part of the work.

Finally, the author would like to thank Mrs. V. White and Mrs. R. Rahim for typing this thesis and Mr. M. Wallace for photographing the diagrams.

The author was supported financially during the period of this research by a studentship and a research assistantship, awarded by the Science Research Council.

(*Reprinted from Nature, Vol.* 201, *No.* 4921, *pp.* 801–802, *February* 22, 1964)

A NEW TELEVISION CAMERA, INTENDED FOR SCIENTIFIC APPLICATIONS, HAVING A VERY HIGH SENSITIVITY AND GOOD STORAGE PROPERTIES

By R. S. FILBY, S. B. MENDE, M. E. ROSENBLOOM and DR. N. D. TWIDDY

Department of Physics, Imperial College of Science and Technology, London, S.W.7

THERE are considerable advantages to be obtained by using a specially designed television camera for the detection of faint optical images. These advantages arise from the greater quantum sensitivity and the absence of reciprocity failure in the photoelectric effect compared with photography, and because the output is in the form of an electric signal, ideally suited for transmission or computer applications.

The obvious fields of application are astronomy, space research and medical physics and, in the astronomical field, the use of the technique to extend the range of existing astronomical telescopes was first proposed by McGee[1]. Several attempts have been made to use television cameras in astronomy[2], but these have not been sufficiently successful so far to merit wide use of the technique.

In space research a suitable electronic camera would permit long exposures to visible or other radiation to be made, the picture being stored until it is convenient to transmit it to base by slow read out.

Existing television camera tubes are unsuitable because of their inability to store for periods longer than a few seconds. What is required is a television camera of high sensitivity capable of integrating a weak light input over a long period, of storing this integrated picture for an appreciable time without deterioration and finally the picture should be read out in a single television frame period.

A tube which seems to offer all the required features has been developed; it has sensitivity which compares very favourably with the best television camera tubes at present available, it is capable of storing a charge image for several hours without deterioration, its charge storage capacity can be adjusted in manufacture to suit the proposed application, and it does not exhibit appreciable persistence of image or 'lag' which is an undesirable feature of television camera tubes having too large a target capacity or using photoconductive layers.

The construction of the tube is shown in Fig. 1. The light input is focused on to a transparent photocathode (1). The photoelectron image so produced is then accelerated and focused by means of a uniform electric field provided by the metallic rings (2), and a uniform magnetic field produced by the long solenoid (3). These photoelectrons are accelerated to energies of the order of 5–7 keV and strike a special target (4).

The novel feature of the tube is the use of a target consisting of a thin conducting signal plate on which is deposited, on the side away from the photocathode, a spongy layer of highly insulating material. A cross-section through this target is shown in Fig. 2. It consists of a layer of aluminium oxide about 500 Å thick which serves as a support membrane for a signal plate of aluminium of similar thickness. On this signal plate is deposited a spongy layer of potassium chloride. The spongy layer is produced by evaporating the insulator in the presence of an inert gas so that atoms aggregate before reaching the target and form a spongy layer of much lower density and lower dielectric constant than the solid material. In a typical tube the spongy layer density may be of the order of 3 per cent of the solid and the layer thickness 5–10μ. The technique is similar to that developed by Goetze[3] for the preparation of films for transmission secondary emission image intensifiers.

Since the density of this layer is very low, electrons with energies of the order of 5 kV are able to penetrate it and build up a positive charge by transmission secondary emission. The secondary electrons are collected by the positive mesh (5).

In view of the relatively large thickness of the spongy layer, the capacitance between the surface of the layer

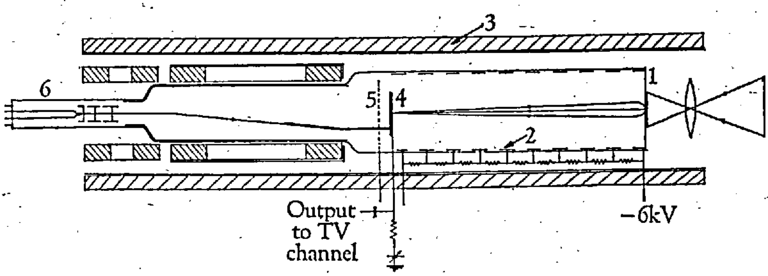

Fig. 1. New television signal generating tube. The optical input is imaged at the photocathode (1). The photoelectrons are imaged at the target (4) which is scanned on its reverse side by a low-velocity electron beam from the electron gun (6)

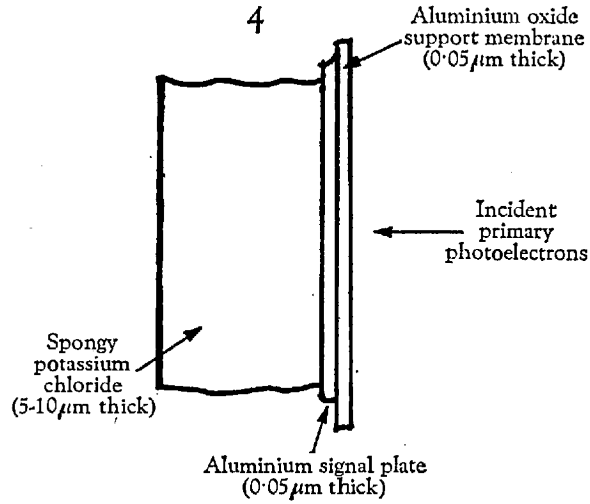

Fig. 2. Section through target (4)

and the conducting signal plate will be low compared with a tube using a solid layer. Therefore the undesirable capacitative 'lag' occurring in such tubes is avoided.

The capacity could be controlled during the formation of the layer by varying either, or both, the density and the thickness to achieve the ideal charge storage capacity for a given tube application.

The positive charge image can be retained on such layers for hours without deterioration and can be read out by scanning the layer surface orthogonally with a low-velocity electron beam from the gun (6). In the present tube the signal is obtained from the conducting signal plate. It could, however, also be obtained by collecting the return beam after it has scanned the insulating side of the target, in which case it would be advantageous to multiply the return beam by means of an electron multiplier as in the image orthicon. This amplification would result in a signal-to-noise ratio which would be determined mainly by the shot noise of the scanning beam and be independent of amplifier noise. The signal-to-noise ratio would, however, be better than that of an image orthicon because, unlike the image orthicon, there is no mesh in front of the target to intercept the primary electrons. Also the charge gain in the spongy layer is 7 compared with the image orthicon's gain of 5. However, the major improvement arises from the much larger charge storage capacity of the new tube. It is convenient to make this about 1,000–2,000 pF, that is, at least ten times the capacity of the image orthicon target[4].

However, even without this refinement, the performance of the tube is impressive. The experimental tube has a target capacity and signal extraction arrangement similar to a C.P.S. Emitron camera tube so that it was convenient to compare these cameras using identical head amplifiers. It was found that the new tube produced an output peak white signal seven times larger than the C.P.S. Emitron for the same light input and photocathode sensitivity. The experimental tube was operated to give a secondary emission gain of about 7 in this test and thus this result was to be expected since the C.P.S. Emitron has no secondary emission multiplication.

The tube has a limiting resolution of 13 line pairs/mm. The resolution is at present limited partly because the present reading section is identical to that of the C.P.S. Emitron and was designed to scan a larger target than that in the present tube, and partly due to the interaction between the primary electrons in the image section and the scanning fields, due to inadequate screening. In later versions it is proposed to use a scanning system designed for a vidicon camera which should improve the resolution.

In the image orthicon, the unavoidable penetration of the scanning field into the image section results in a loss of resolution, but this effect should be much smaller in our tube since the image-electron energies in the image section will be at least an order of magnitude larger.

If a potential difference is maintained across the spongy dielectric layer, then use may be made of electron bombardment induced conductivity to supplement the multi-

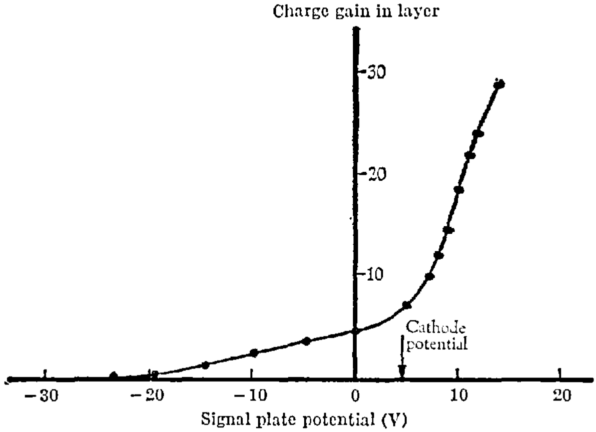

Fig. 3. The variation of the charge gain in the spongy target layer, with signal plate potential. The gain is 7 for zero volts across the layer (signal plate potential = cathode potential)

plication in the layer. The insulating surface of the layer is cathode potential stabilized and thus the potential difference across the layer may be conveniently varied by changing the signal plate potential. The variation of multiplication with signal plate potential is shown in Fig. 3. Satisfactory performance is obtained with relatively low voltages giving a multiplication of about seven, but, with the present layers, increasing the voltage across the layer to obtain gains of 20 or more results in the appearance of white spots due to pinholes in the layer. Under these conditions the tube is not suitable for television pictures or star fields, but would still be usable for scientific applications involving the detection of objects much larger than picture point size.

The output signal current is proportional to the input illumination, that is, the gamma (γ) is unity. When operated as a television camera, the tube is capable of withstanding light input overloads of 8 times the input corresponding to peak white signal before the target tends to anode potential stabilize. This may not be adequate for some television work. In a scientific application involving a long exposure to detect faint objects in the presence of bright ones, the rise of potential on the layer due to the bright sources can be limited by keeping the mesh at a potential below the first secondary emission crossover potential.

The device may, of course, be used for the detection of infra-red, ultra-violet, and X-radiation by replacing the existing photocathode by a photocathode or phosphor/photocathode sandwich sensitive to these radiations together with a suitable end-window.

[1] McGee, J. D., *J. Roy. Soc. Arts*, C, 329 (1952); *Astronomical Optics*, edit., by Kopal, Z., 205 (1956).

[2] Randall, R. P., *Adv. Electronics and Electron Phys.*, **12**, 219 (1960). Gebel, R. K. H., and Devol, Lee, *ibid.*, **12**, 195 (1960). Hynek, J. A., Barton, G., Aikens, R., and Powers, W., *ibid.*, **16**, 409 (1962). De Witt, jun., J. H., *ibid.*, **16**, 419 (1962). Livingston, W. C., *ibid.*, **16**, 431 (1962). Dennison, E. W., *ibid.*, **16**, 447 (1962). Gebel, R. K. H., *ibid.*, **16**, 451 (1962).

[3] Goetze, G. W., *Adv. Electronics and Electron Phys.*, **16**, 145 (1962).

[4] McGee, J. D., *I.E.E. Intern. Television Conf.*, 36 (1962).

Printed in Great Britain by Fisher, Knight & Co., Ltd., St. Albans.

Reprinted from
INTERNATIONAL JOURNAL OF ELECTRONICS, Vol. 19, No. 4, p. 387, October 1965

The Detection of Faint Optical Images by Charge Integration†

II. A New Television Camera, intended for Scientific Applications, having a very High Sensitivity and Good Storage Properties

By R. S. FILBY, S. B. MENDE and N. D. TWIDDY‡
Department of Physics, Imperial College of Science and Technology, London, S.W.7

[Received August 11, 1965]

ABSTRACT

The performance of a new photoelectric storage tube, capable of long term integration of faint optical images, is described. The device employs a low density potassium chloride layer as a storage target, in which considerable charge multiplication can be achieved.

§ 1. INTRODUCTION

IN an earlier paper (Filby *et al.* 1964) we reported briefly the development of a new type of television camera employing a low density potassium chloride layer as a storage target. The purpose of the present paper is to report further measurements on this device.

In this Department we have been concerned for some years with the development of photoelectronic storage devices intended for the detection of faint images of low contrast. Much of the effort has been devoted to a television signal generating tube in which both exposing and reading out operations were performed from the same side of a dielectric storage layer by a flying spot scanning technique. The performance of this device has been described in a companion paper (Mende *et al.* 1965) to be referred to as Part I. Although this device can achieve relatively high equivalent quantum efficiencies, its resolution is inadequate for many applications and this is largely due to the flying spot scanning feature.

Therefore it was decided to attempt the development of a television storage tube in which the exposing and reading out operations were performed on opposite sides of a storage target and to employ an electron gun to provide the low velocity reading beam. The device would have much in common with an image orthicon or an ebicon, consisting of an image section for exposing the target and this target would be read on its reverse side by a scanning electron beam. Clearly the heart of the problem was to find a suitable target material. The storage target must have

† Communicated by the Authors.
‡ Now at the Department of Physics, University of York, Heslington, York.

extremely high resistivity since integration and storage periods of the order of hours were envisaged; electrons of moderate energy should be able to produce positive charge build up on the scanned surface of the target preferably with appreciable charge multiplication.

A potentially suitable target material was being developed in another section of this Department for transmission secondary emission (T.S.E.) image intensifiers. Following the lead of Goetze in the United States, M. E. Rosenbloom and W. L. Wilcock at Imperial College had developed a technique for depositing low density spongy layers of potassium chloride and these were being investigated as possible dynode structures for T.S.E. image intensifiers. Rosenbloom had found that charge distributions could be retained on these layers for periods of several days and it seemed probable that the low density layers would provide the other features required of a satisfactory target material.

Experimental tubes were therefore constructed and showed the new layer to possess most of the required properties of an ideal storage target. In brief, the layer could store charge pictures for many hours; the charges could be built up by electrons with energies 5–10 kev and the charge gain in the layer could be varied readily from very low values up to well over 100 times simply by changing the potential difference across the layer. This is a particularly useful feature since the detector can thus be operated with high equivalent quantum efficiency for the detection of both high and low contrast images (see Part I, fig. 3). Furthermore, layers could be made with the right order of storage capacity and they did not exhibit appreciable persistance of image or 'lag'. Goetze and Boerio have reported a similar tube development at Westinghouse (Goetze and Boerio 1963, 1964) which they have named the S.E.C. vidicon.

§ 2. The Tube and its Construction

A photograph of the tube is given in fig. 1 and a schematic diagram is shown in fig. 2. The light input is focused on to the transparent photocathode (1). The photoelectron image so produced is then accelerated in the electric field produced by the metallic cylinders and annuli (2), and focused by the uniform magnetic field produced by the long solenoid (3). These photoelectrons are accelerated to an energy of 7 kev and strike the target (4) where they give rise to appreciable secondary emission, the low energy secondary electrons being ejected into the inter-particle space in the spongy layer. By a mechanism to be discussed below the secondary emission results in a positive charge being left in the target so that a positive charge picture is built up and retained in the target. This stored positive charge picture can be readily removed by scanning the layer orthogonally with a low velocity electron beam from the electron gun (6) to re-stabilize the surface to a uniform potential. This results in a signal current flowing from the metallic signal plate which forms part of the layer so that the output is in the form of a television signal. In the tube shown

Fig. 1

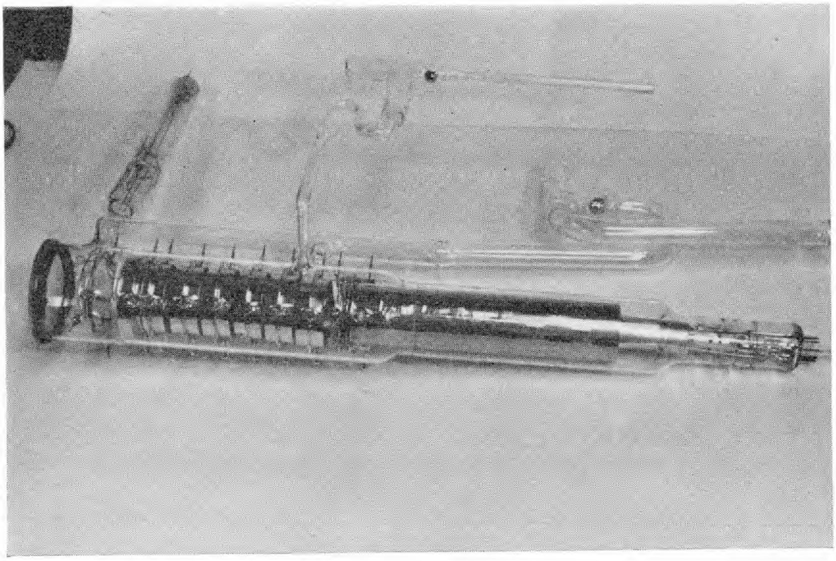

The television camera tube, photographed prior to processing, showing side arms and pumping stem.

Fig. 2

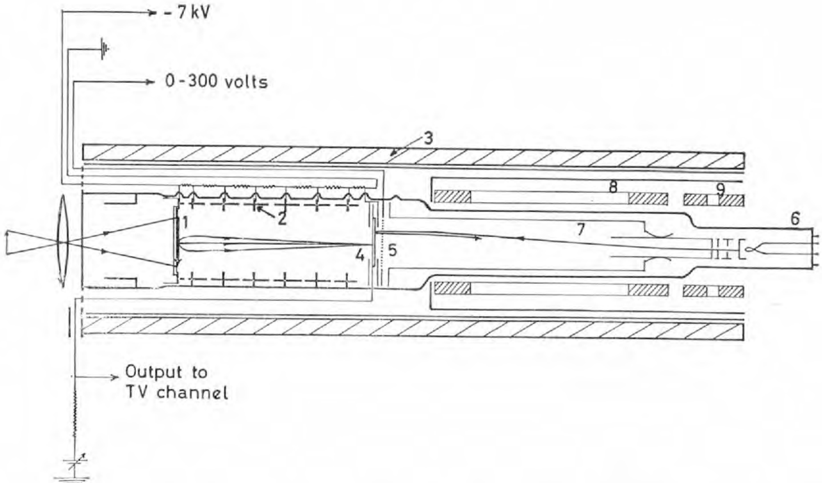

The television signal generation tube. The optical input is imaged at the photocathode (1). The photoelectrons are imaged at the target (4) which is scanned on its reverse side by a low-velocity electron beam from the electron gun (6).

the cylinders and annuli (2) shield the photoelectrons from electrostatic charges on the walls which would otherwise cause some distortion of picture geometry and they also prevent stray electrons from striking the walls and significantly increasing the background (McGee 1961). The compartment at the front of the tube is used only for processing the photocathode (S9 or S20) and prevents the entry of alkali vapours into the remainder of the tube which would result in increased background (McGee 1956).

The reading section of the tube contains the electron gun (6), the wall anode (7), which is normally held at 300 v, and a separately connected mesh whose potential may be adjusted to be a few volts more positive than

Fig. 3

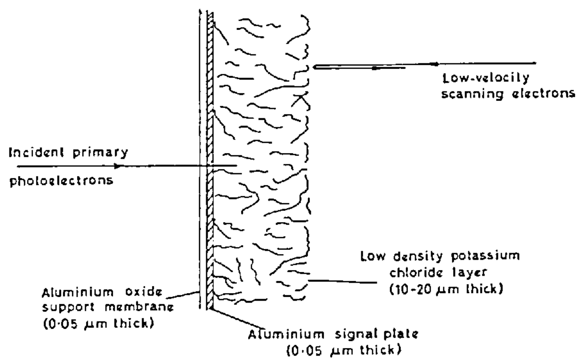

Section through the target.

the wall anode to give optimum focusing and beam landing conditions (Lubszynski and Wardley 1962). The electron beam is deflected magnetically by means of the scan coils (8). The d.c. magnetic field produced by the solenoid (3) has a value of between 40 and 80 gauss and results in several focusing loops. In order to use the same field to focus the 7 kev primaries it is necessary to make the image stage fairly long giving an overall tube length of 49 cm.

A section through the target (4) is shown in fig. 3. The aluminium oxide membrane ($\sim 0{\cdot}05\,\mu$m thick) supports a thin evaporated aluminium signal plate ($\sim 0{\cdot}05\,\mu$m thick). The spongy potassium chloride layer (~ 10–$20\,\mu$m thick) is deposited on top of this.

§ 3. The Manufacture of the Target

The thin aluminium oxide support membranes are prepared by anodizing 0·001 in. thick aluminium foil, the surplus aluminium being etched away in an acid bath. The films are mounted on lime soda glass rings with potassium silicate solution and the film stretched by heating in air to 250 °c since the expansion coefficient of soda glass is about three times that of aluminium oxide. This results in a slightly wrinkled film on cooling which is capable of taking up any strain which occurs during the annealing processes of the subsequent layers (aluminium and potassium chloride) which are evaporated onto the film.

Aluminium is evaporated in a conventional vacuum evaporation plant to a thickness ~ 500 Å by monitoring to observe a drop in transmission to 1%. The KCl evaporation is carried out in a dry argon atmosphere at a pressure of 2 mm Hg with the film specimens being rotated at about 1 rev/sec by an induction motor, the whole evaporation taking about 10 min. The light transmission is monitored until this falls to 75%. When the tube is subsequently baked to 200°C before processing the target membrane tightens and remains taut on cooling.

An electron micrograph of the spongy KCl is given in fig. 4.

Fig. 4

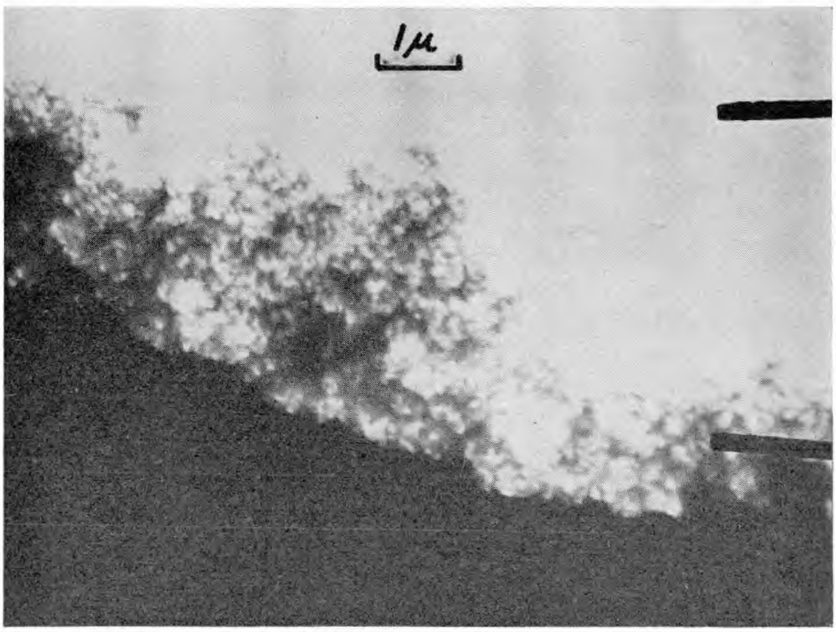

Electron micrograph showing a low density deposit of potassium chloride evaporated onto a mesh.

It was hoped that the tube would have the following advantages over the photocathode scanned storage tube described in Part I.

1. Adequate scanning beam currents would be available which would permit the discharge of the target in a single scan, even at normal television scan rates.
2. The fluctuations in the scanning beam would be small.

3. Because of the high degree of collimation of the electrons from the gun, the low velocity beam can be very well focused.
4. Reading beam electrons reflected from the target are unable to return to the target because they are collected by the mesh, or wall anode, held at a high positive potential.
5. This also applies to the secondary electrons which emerge from the layer in the writing process thus avoiding secondary electron redistribution effects.
6. There is no mesh to intercept the primary electrons.
7. A practical advantage of the proposed tube is that there is no need to switch the electrode potentials, or insert a mirror when changing from writing to reading and the tube can be operated continuously as a television camera. This greatly simplifies the focusing and adjustment of the tube.

§ 4. The Mechanism in the Layer

Primary electrons enter the layer resulting in a large number of secondary electrons being created and ejected into the inter-particle space with low energy. They come under the influence of the field present in or immediately outside the layer due to the potentials on the signal plate and mesh (5). A proportion of these secondary electrons will be collected either by the signal plate or by the mesh (5) which is held near wall anode potential (+300 v). With the potentials and geometry normally employed the external collecting field due to the mesh is ~ 200 v/mm while that across the layer can have any value from zero to ± 2000 v/mm (e.g. ± 40 v across a 0·020 mm layer). Although there is no fundamental difference it is convenient to make a distinction between the currents to these two electrodes because they are easily distinguished experimentally. The flow of the secondary electrons to the target signal plate takes place in the interparticle space in the layer rather than in the conduction band of the solid and this has been termed secondary electron conduction (S.E.C.) by Goetze and Boerio (1963, 1964). We shall follow their lead in this. The secondaries which leave the target layer and are collected by the mesh (5), held at +300 v, may be classified as transmitted secondary electrons (T.S.E.).

The authors suggest a third factor contributing to the high gain of the layer, namely the direct landing of the beam electrons on the signal plate while the beam is accepted by the layer. This process can take place only when the layer is charged positive. As the electrons in the scanning beam discharge the layer to gun cathode potential, the layer screens the positive signal plate from the scanning beam and all the scanning electrons are returned towards the gun. Such an effect would be expected to take place, because the mechanism of the S.E.C. process requires that low velocity secondary electrons, excited within the layer should be able to traverse the layer under the influence of the internal field to reach the signal plate. The positive charges left within the layer are neutralized by the scanning electrons, which must therefore penetrate deeply into the layer. It follows that a fraction of these low velocity scanning electrons will also be able to reach the signal plate as they come under the influence of the field within the layer.

This mechanism is fundamentally different from S.E.C. or T.S.E. signal generation because, instead of the beam discharging previously produced positive charges, the instantaneous potential on the storage surface modulates the amount of beam landing on the signal plate. The layer thus acts somewhat as the control grid in an amplifying valve. Following the example of the term S.E.C., this process may be described as B.E.C., beam electron conduction.

The measured values of S.E.C. are derived from contributions due to true S.E.C. (migration of secondary electrons across the layer during exposure) and B.E.C. (migration of beam electrons across the layer during scanning), but they are not readily distinguishable experimentally. It is therefore convenient to retain the term S.E.C. to embrace both contributions.

§ 5. The Charge Gain of the Tube

Goertze *et al.* (1964) have made detailed investigations of the secondary emitting properties of low density films. However their published work was principally concerned with applications in image intensifiers in which the exit surface of the layer is not stabilised by an electron beam but can rise to quite high potentials.

Fig. 5

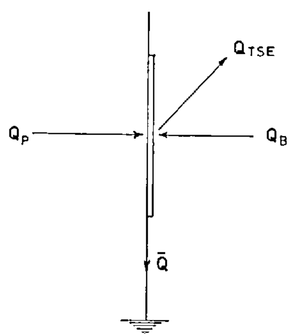

Charges flowing to and from the target contributing to the signal generating process which takes place during each frame.

We have measured the charge gain in the layer and shall distinguish between T.S.E. gain and S.E.C. gain, the latter includes the B.E.C. process. These two separate contributions to the total gain may be readily determined experimentally and account for the shape of the observed total gain characteristic.

If the photocathode of the tube is illuminated and the target scanned continuously by the reading beam, the resulting number of primary electrons per picture element per frame time can be represented by the charge Q_P which on entering the target results in the release of a charge Q_{TSE} to the mesh by transmission secondary emission and ultimately a charge Q_{SEC} to the signal plate by both secondary electron conduction and beam electron condition. If the positive charges built up by these processes are removed by scanning continuously with the electron beam, the charge landing from the beam Q_B will be the sum of these two charges. Therefore

$$Q_B = Q_{TSE} + Q_{SEC} \tag{1}$$

and thus the total charge gain of the tube is given by:

$$\frac{Q_B}{Q_P} = \frac{Q_{TSE}}{Q_P} + \frac{Q_{SEC}}{Q_P} \quad \text{from (1)}$$

i.e. $$G_{\text{Total}} = G_{TSE} + G_{SEC}.$$

The total charge taken up by the signal plate lead is $\bar{Q}$ which is the algebraic sum of the signal charge Q_B, primary charge Q_P and the transmitted secondary emission charge Q_{TSE}, i.e.

$$\bar{Q} = Q_B + Q_P - Q_{TSE},$$

substituting for Q_B from (1):

$$\bar{Q} = Q_{TSE} + Q_{SEC} + Q_P - Q_{TSE},$$

$$\bar{Q} = Q_{SEC} + Q_P,$$

dividing by Q_P:

$$\frac{\bar{Q}_P}{Q_P} = \frac{Q_{SEC}}{Q_P} + 1 = G_{SEC} + 1,$$

so G_{SEC} can be obtained from measurements of $\bar{Q}$ and Q_P.

The variation of S.E.C. gain versus target signal plate potential V_{SP} is shown in fig. 6 for primary electrons of 7 kev energy. When there is no field across the layer ($V_{SP}=0$) the S.E.C. gain is zero. With the signal plate positive, the charge gain increases rapidly with the collecting field across the layer, reaching a value of 120 when $V_{SP} = +25$ v. If the signal plate is made negative the field is such that the transmission secondary emission is enhanced by the field in the layer but the total charge gain is low since the secondary electron conduction taking place now opposes the positive charge build up in the layer.

The way in which the S.E.C. gain varies with primary photoelectron energy is shown in fig. 7 for a range of signal plate potentials V_{SP}. It should be mentioned however that the particular layer studied to produce this family of curves had only a moderate S.E.C. gain.

The T.S.E. gain is measured by a pulse method. A light pulse having a duration of a few microseconds is generated every frame by a cathode ray tube having a short persistence P16 phosphor. The light is focused

Fig. 6

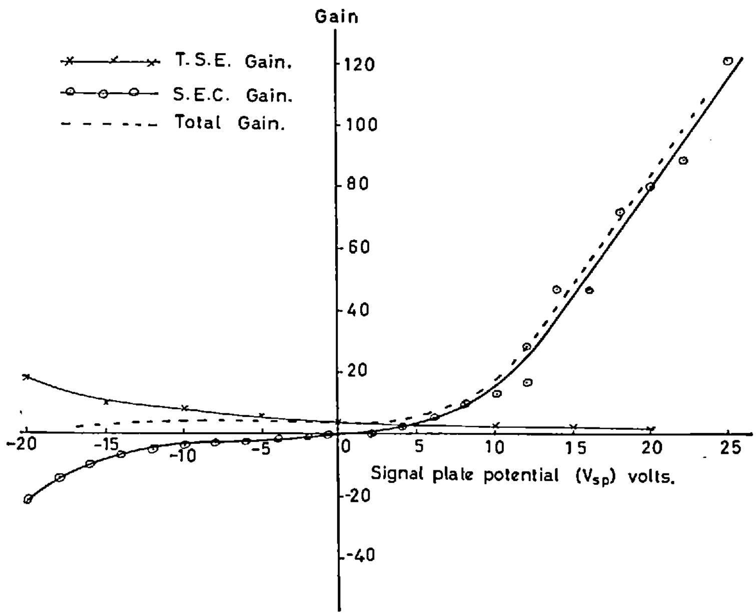

The variation of the total charge gain of the layer with signal plate potential, compiled from curves showing the contributions arising from the T.S.E. and S.E.C. mechanisms.

onto the photocathode of the tube. The resulting charging current pulse in the signal plate lead can be measured on an oscilloscope and is the difference between the primary current and the transmission secondary electron current:

$$I_{\mathrm{SP}} = I_{\mathrm{TSE}} - I_{\mathrm{P}},$$

so that if the primary current I_{P} is measured, usually by reducing the primary energy until transmission secondary emission is negligible, the T.S.E. gain can be calculated. The results of such measurements are shown in fig. 8. The T.S.E. gain decreases monotonically with increasing signal plate potential and has its lowest value when the S.E.C. gain is a maximum. If the target signal plate potential is zero the gain in the layer will be solely due to T.S.E. and has a value between 4 and 5. The tube is normally operated with appreciable positive potentials on the signal plate and under these conditions the S.E.C. gain far exceeds that due to T.S.E. This is clearly illustrated in fig. 6, where the two gain curves for the same layer have been combined into a single total gain curve. This curve closely follows the S.E.C. curve at high positive potentials, crosses the T.S.E. curve at zero potential, remains fairly constant over a range of negative potentials and finally, at high negative potentials has very low values since in this region the T.S.E. and S.E.C. gains are of opposite sense.

The variation of T.S.E. gain with primary electron energy has been investigated and is shown in fig. 9. T.S.E. clearly commences at about 4 kev and for negative signal plate potentials reaches a maximum between 7 and 8 kev.

The output video signal is of course proportional to the total gain of the tube and typical measurements of this signal current versus the target signal plate potential are shown in fig. 10 for four different light intensities.

Fig. 7

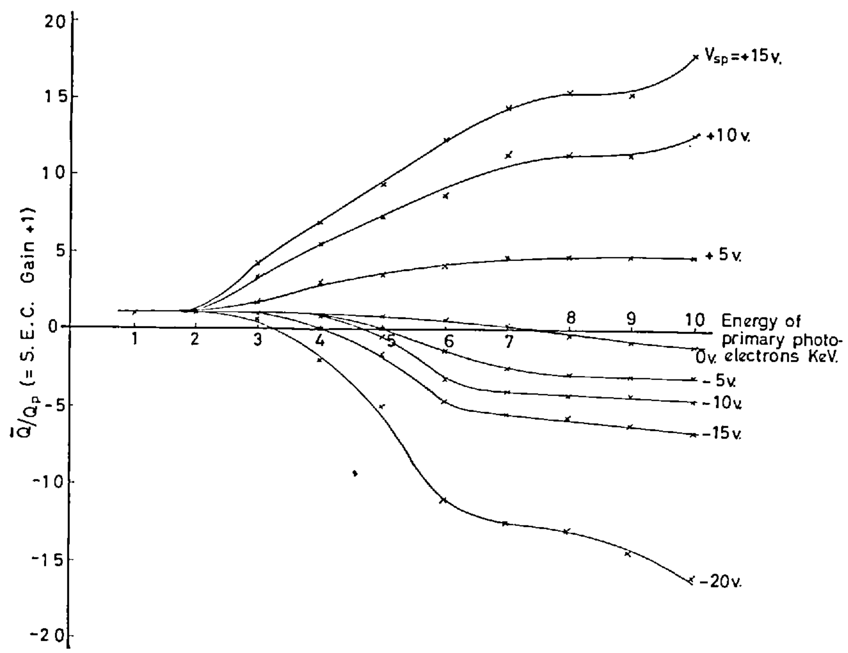

The variation of S.E.C. gain with primary photoelectron energy for various signal plate potentials.

These curves are similar to that obtained earlier in fig. 6 by adding the S.E.C. and T.S.E. gain curves, and around zero signal plate potential points of inflexion can be seen where S.E.C. is no longer the dominant process.

Fig. 8

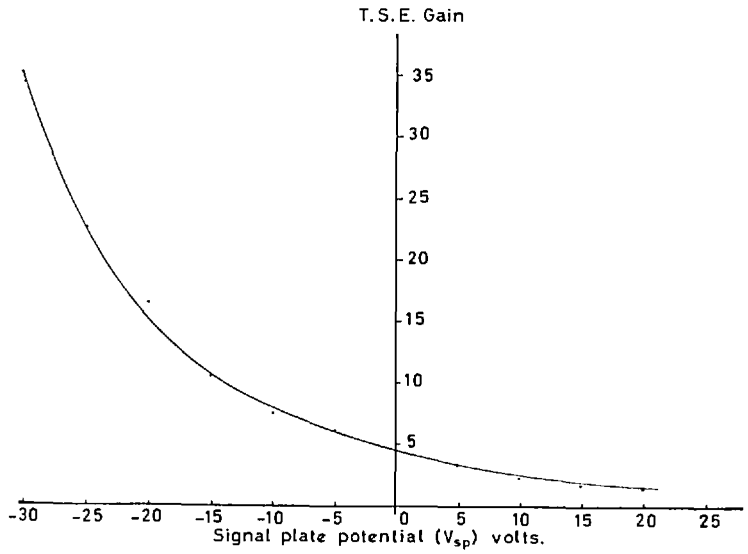

The variation of T.S.E. gain with signal plate potential for 7 kev primary photoelectrons.

Fig. 9

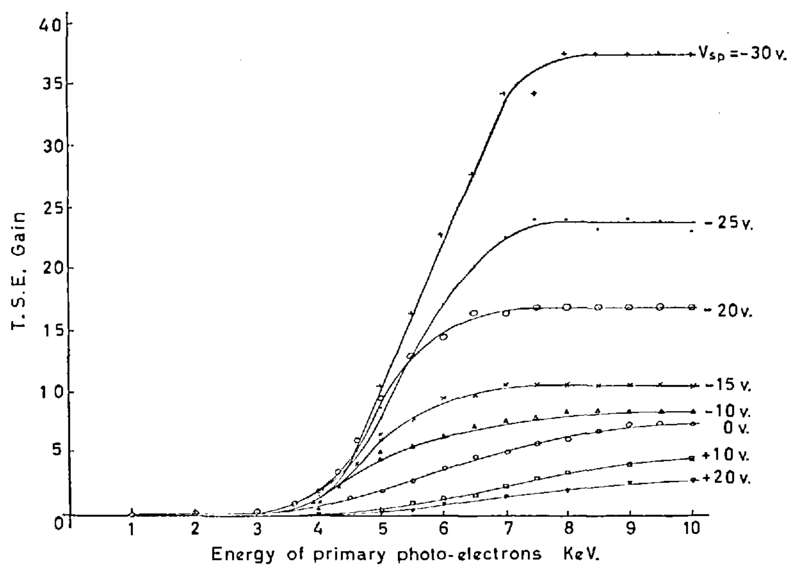

The variation of T.S.E. gain with primary photoelectron energy for various signal plate potentials.

Fig. 10

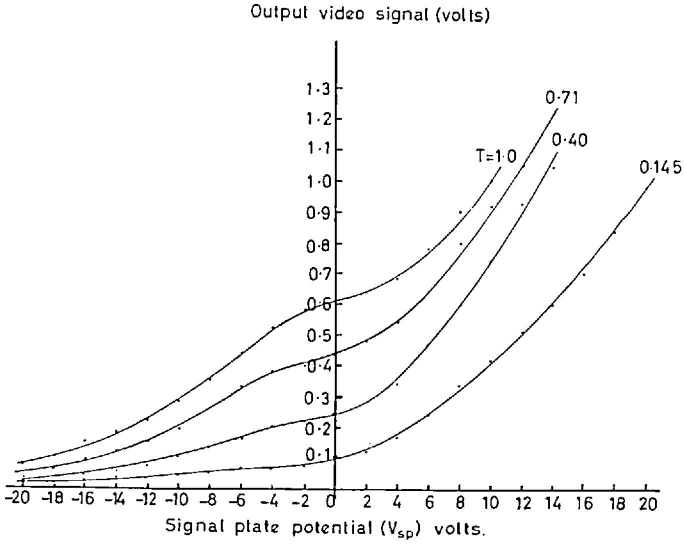

The variation of output signal with signal plate potential for four different light intensities. The parameter quoted on each curve represents the transmission of a filter placed in front of a light source of fixed intensity.

Fig. 11

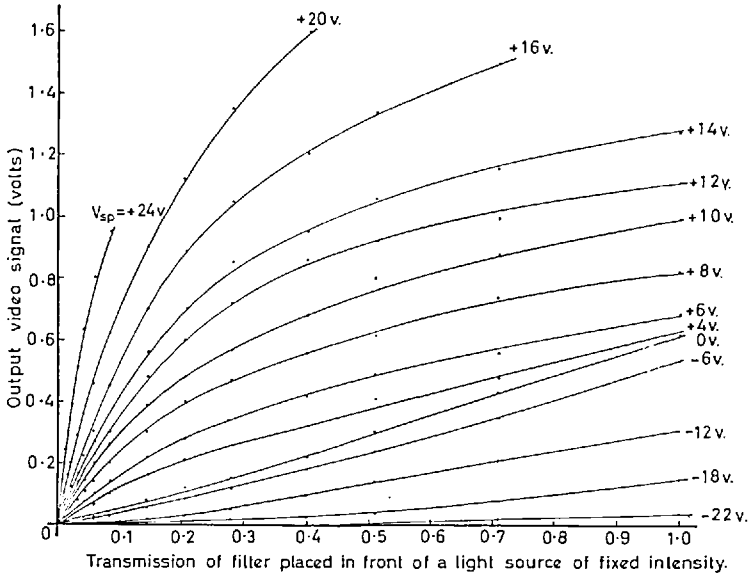

Transfer characteristic of the tube for various signal plate potentials.

§ 6. The Transfer Characteristics

The charge gain occurring in the layer is highly dependent on the potential difference across it. Now, as the stored charge on the layer builds up to the maximum value corresponding to the peak white signal, the potential across the layer will change by several volts and this change is such as to reduce the field across the layer. This in general reduces the charge gain as the charge integration continues resulting in a non-linear input–output transfer characteristic with a decreasing slope.

This is clearly shown in fig. 11 which shows the transfer characteristics for a large range of target signal plate potentials V_{SP}. The decreasing slope is evident for all positive values of V_{SP}. However, for values of V_{SP} between ± 2 v the characteristic is linear (gamma = unity). This is because in this region the curve of charge gain versus V_{SP} has a plateau (see fig. 6). For more strongly negative values of V_{SP} there is some tendency for the slope of the transfer characteristic to increase with input (see fig. 11).

§ 7. Light Input Overload

In normal operation the positive charge picture is removed by scanning with a low velocity electron beam which stabilizes the surface at cathode potential. If however the charge built up on the surface is excessive, due to say light input overload, the scanning electrons will be attracted more strongly to the surface gaining sufficient energy to give rise to appreciable secondary emission. If at this energy the secondary emission coefficient exceeds unity, the surface will not fall to the cathode potential but instead will rise towards the mesh potential. This results in a 'blacker than black' signal from the regions effected. More serious however is the fact that a very high field develops in the layer, electrical breakdown occurs and the layer is punctured. These pinholes can be seen in the layer and appear on the monitor screen as white spots (see fig. 12) since the scanning electron beam can 'see' the positive backing plate exposed in these regions. Therefore the electron beam lands on these regions, resulting in a strong white picture signal.

This is clearly a very serious defect of the device as a televison camera. It could be overcome by inserting a stabilising mesh just in front of the target surface, held at a few volts positive to the cathode, as was used in the stabilized C.P.S. Emitron (McGee 1955). The mesh would have to be very close to the target surface to avoid loss of definition in the reading section (Lubszynski and Wardley 1962).

It may be possible that the target could be made self-stabilizing by depositing on the exit surface a very thin layer of a substance having a $\delta\max < 1$ or a high secondary emission crossover potential, e.g. many metals.

When the device is used as a single exposure storage tube, the exposure can be made with the mesh potential lowered so that the potential rise in the overload region is limited. If an overload does occur it is necessary to prevent a further potential rise on reading. This can be achieved by keeping the mesh potential below the first crossover potential while scanning. If in addition the cathode potential is raised by 10 v any over-loaded areas would be stabilized on scanning without removing the wanted picture charge. The tube operating potentials can then be returned to the normal values and the stored picture read out.

Fig. 12

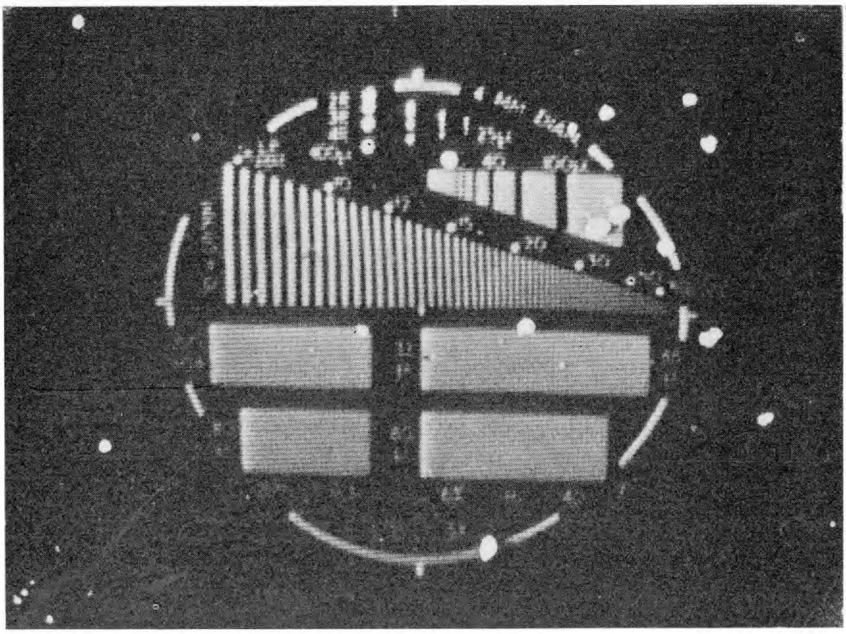

Photograph of test pattern generated by a tube whose target had become punctured as a result of overloading. $V_{SP}=10$ v. Diameter of test pattern image on target $=8$ mm.

§ 8. Resolution

The limiting resolution of the tube so far achieved is 15 line pairs/mm which with the present target size of 20×15 mm corresponds to 600 vertical T.V. lines. This is much less than can be explained in terms of scattering in the target which is only 10–20 μm thick while the picture element size (405 line system) is 33 μm.

The resolution may be degraded by the electron optics of the image stage, by interactions between the primary photoelectrons and the scanning fields, by the target layer or by the reading system. The first two were shown to be unimportant by the construction of an image section identical to that in the complete tube except that the layer was replaced by a phosphor. This image intensifier, operated at 7 kv, had a resolution of better than 30 line pairs/mm and no deterioration was observed when the scanning fields were applied.

The limitations therefore occur either in the layer or in the reading process. The vidicon gun used is capable of very high resolution but in our application the electron transit time is much longer than in a vidicon so that the performance will be inferior. However, we feel that a further important factor limiting the resolution is the comparatively large potential variations (~ 8 v) which exist in the layer which would be sufficient to deflect or defocus the low energy reading beam. This must be regarded as tentative and we are trying to estimate the relative importance of these factors.

§ 9. The Storage Capacity and Discharge Lag

The tube provides a peak white signal of $0{\cdot}3\,\mu$A which corresponds, for a 405 line system, to about 3×10^5 electrons per picture element. This represents a storage capacity of 1000 pF on the assumption of a potential rise of 8 v. However, the electrostatic capacitance of a $20\,\mu$m thick layer with dielectric constant of unity and area 20×15 mm is only 150 pF. This shows that a model which assumes that the charge is stored only on the surface of the layer cannot fully account for the signal generated by the tube and suggests both the storage of charge inside the layer and the beam electron conduction (B.E.C.) process proposed above.

The stored positive charge is very readily discharged by the scanning electron beam. When operated as a television camera, the persistence of picture or lag is very low comparing favourably with other television cameras.

§ 10. Signal Shot Noise

If the tube is operated with a charge gain of 100, the equivalent quantum efficiency for storage and read out is high. From Part 1:

$$E = \frac{1}{k + [N_n^2/\bar{g}^2\bar{p}]} \doteqdot \frac{1}{k} \text{ for } g = 100 \text{ and } \mathrm{N}_n = 10^3 \text{ e/p.e.}$$

This implies that the amplifier noise is negligible and the signal to noise on read out is equal to the shot noise in the number of photoelectrons divided by k where k is a factor depending upon the statistics of multiplication; i.e.

$$S_0/N_0 = \frac{\bar{P}}{k}.$$

Since the effective storage capacity of the tube per picture element is 3×10^5 electrons the number of photoelectrons $\bar{P}$ will be 3000. The most favourable statistics of multiplication correspond to $k = 1$ and therefore the signal to r.m.s. noise ratio in the output cannot exceed $\sqrt{(3000)} = 55$. This implies that at high gain the noise in the white areas should exceed that in the black parts of the picture but this is not in fact observed. Two factors will certainly contribute to this state of affairs. Firstly, the noise appearing in the whites will be dependent upon the ability of the tube to resolve the fluctuations in the stored charge, i.e. the resolution of the scanning side, so the fluctuations will be attenuated unless the resolution is perfect. Secondly, when the tube is operated at high gain, the transfer characteristic has a pronounced saturation which will tend to ' crush ' the shot noise in the whites. This situation is not fully understood and the problem is being investigated.

Fig. 13

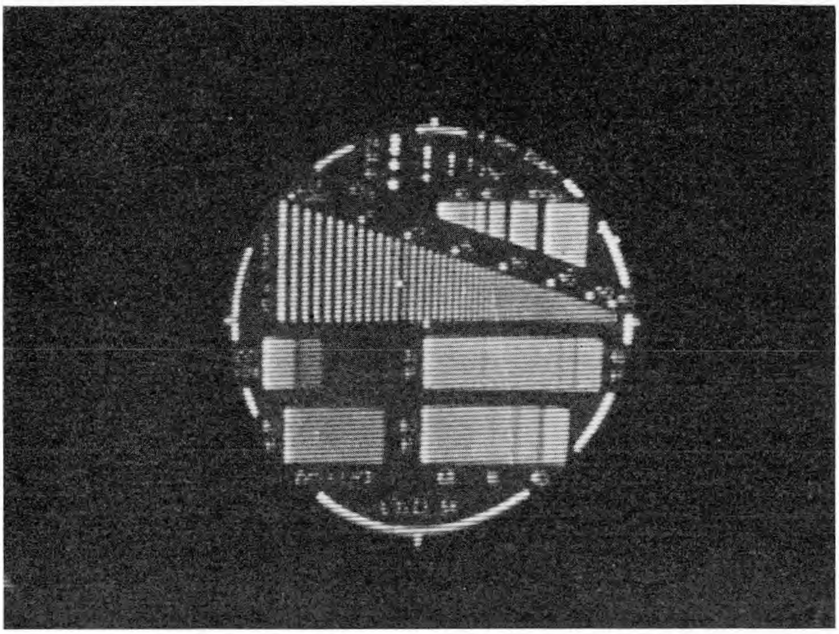

Photograph of a test pattern generated by a tube, run with $V_{SP}=10$ v. Diameter of test pattern image on target = 8 mm.

§ 11. Conclusions

In order to overcome the limitations of the photocathode scanned tube a new type of charge storage tube has been developed. This incorporates the advantages of electron gun scanning and should eliminate the secondary electron redistribution effect which rendered the photocathode scanned storage tube unable to detect low contrast images of fine resolution.

It was found in practice that the new target was not only capable of long term retention and integration of the photoelectronic charge but that it is also capable of high charge multiplication in the layer, producing many stored electronic charges per incident primary. This gain makes the detection of faint optical images of high and low contrast very efficient with this tube.

As a detector of faint optical images the tube is a very versatile device incorporating the convenience of electrical read out which is essential in many experiments concerning space astronomy, or observation in which the data is to be handled electronically.

Acknowledgments

The authors wish to thank Professor J. D. McGee for his interest and support and to acknowledge the considerable help of Mr. M. E. Rosenbloom in the construction and testing of the first experimental tubes. The authors are indebted to Mr. J. Westlake for assembling and processing the tubes and to Mr. W. I. Simpson for mechanical assistance. Acknowledgments are also due to the Department of Scientific and Industrial Research for financial support.

References

Filby, R. S., Mende, S. B., Rosenbloom, M. E., and Twiddy, N. D., 1964, *Nature, Lond.*, **201,** 801.

Goetze, G. W., 1962, *Advanc. Electrons*, **16,** 145.

Goetze, G. W., and Boerio, A. H., 1963, I.E.E.E. Electron Devices Meeting Oct. 31, 1963. (Unpublished); 1964, *Proc. I.E.E.E.*, **52,** 1009.

Goetze, G. W., Boerio, A. H., and Green, 1964, *J. appl. Phys.*, **35,** 482.

Lubszynski, H. G., and Wardley, J., 1962, IEE Conference Report No., 5.61.

McGee, J. D., 1955, *Arch. elektr. Übertr.*, **9,** 355 ; 1956, *The Present and Future of the Telescope of Moderate Size*, 1961, *Rep. Prog. Phys.*, **24,** 167.

Mende, S. B., Khan, A. A., and Twiddy, N. D., 1965, Part I. *Int. J. Electron.*, **19,** 361.

REPRODUCED FROM
ADVANCES IN ELECTRONICS AND ELECTRON PHYSICS VOLUME 22
PHOTO-ELECTRONIC IMAGE DEVICES, THIRD SYMPOSIUM
PUBLISHED BY ACADEMIC PRESS

A Television Camera-tube Using a Low Density Potassium Chloride Target

R. S. FILBY, S. B. MENDE† and N. D. TWIDDY‡

Applied Physics Department, Imperial College
University of London, England

Introduction

During the past two years, work has been in progress at Imperial College to construct and assess storage tubes with low-density potassium chloride targets. These spongy potassium chloride layers are very similar to those first developed by Goetze of Westinghouse.[1] A programme of research to study the properties of these layers was

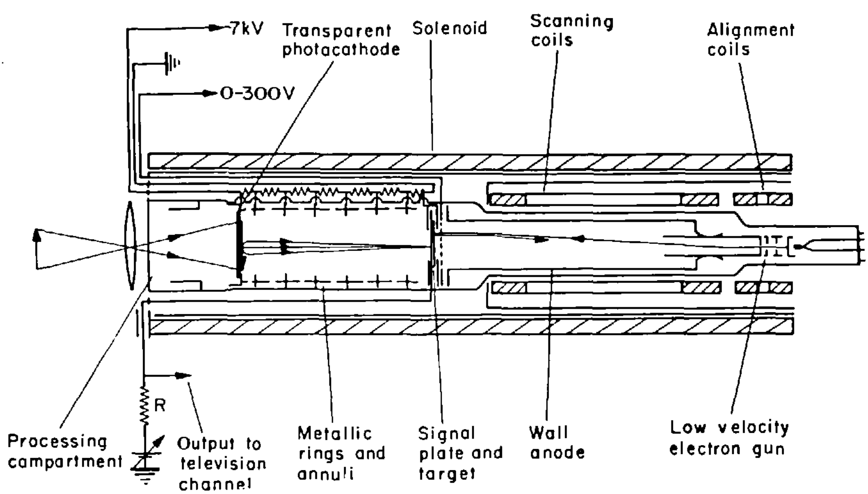

FIG. 1. Television camera tube using spongy potassium chloride target.

undertaken at Imperial College by Rosenbloom,[2] working under Wilcock. These low-density potassium chloride layers were being investigated to ascertain their suitability for use in transmission secondary emission image intensifiers. However, it was as a result of a report given by Rosenbloom on the outcome of his study that the work described in this

† Now at Rice University, Texas, U.S.A.
‡ Now at University of York, England.

paper was initiated. The high secondary emission yield and the insulation properties of these potassium chloride layers indicated that they might find application as targets in television camera-tubes or in charge storage tubes. A camera-tube was consequently constructed incorporating such a target layer. The structure of the tube is illustrated schematically in Fig. 1. Although developed independently, [3, 4] this tube has many similarities with the S.E.C. camera-tube of Westinghouse.[5, 6]

Electrons from the photocathode are accelerated through 7 kV, and electromagnetically focused onto the target, where secondaries are excited. The secondaries are collected by positive electrodes adjacent to the target by mechanisms described in detail below, leaving a positive charge pattern in the insulating potassium chloride layer. The target is then scanned by a low velocity electron beam, discharging the target. The current flowing into the signal-plate is modulated by the positive charge image stored in the layer during exposure, and thus a video signal is developed across the signal resistor R.

Theoretical Considerations Underlying the Application of Storage Tubes

One application of storage tubes is the detection of faint images of low contrast. If a faint image is superimposed on a background, the limit of detection of the faint image is set by the statistical fluctuation of the photons from the background. In order to distinguish the image, it is necessary to store a large number of quanta, so that the wanted image emerges distinctly from the random fluctuations. An efficient detector is therefore required to record this large number of quanta without the addition of further noise. The ability of a detector to do this is represented by its equivalent quantum efficiency E. This may be defined by

$$E = \frac{\text{mean square signal-to-noise ratio in output}}{\text{mean square signal-to-noise ratio in input}}. \tag{1}$$

In general, E will be a function of the mean number of quanta to be detected.

The quantum efficiency of a photocathode is relatively high and if this is to be exploited in a photoelectric device, it is important that the processing of the photoelectrons should not introduce any further noise. Then the overall quantum efficiency of the device will also be high.

The noise introduced by the amplifier in a television channel will depend upon bandwidth, input valve, and load resistor. For example, a television camera-tube generating a signal for a system with a 3 Mc/s bandwidth, (405 lines at 25 frames/sec), in which the input valve is an E.M.I. R 5559, with a 2·7-MΩ load resistor, it may be shown that the r.m.s. noise signal in the amplifier is equivalent to $n = 2 \times 10^3$ electrons per picture element per frame.

To calculate the total noise in the output signal, the mean square shot noise in the charge stored in the target must be added to the amplifier noise. If the target has a gain g, and a picture element is charged by the action of P primary photoelectrons, then the number N of electronic charges stored per picture element is given by

$$N = g\,P. \tag{2}$$

Now in general, g and P will exhibit statistical fluctuations, and it is therefore more convenient to consider the mean gain of the target, $\bar{g}$, and the mean number of photons per picture element $\bar{P}$. Mandel[7] has shown that a relationship analogous to Eq. (2) holds to give the mean number of stored electronic charges per picture element

$$\bar{N} = \bar{g}\,\bar{P}. \tag{3}$$

Mandel[7] has also shown that the mean square fluctuations $\overline{\Delta^2 N}$ about the mean $\bar{N}$ is given by

$$\begin{aligned}\overline{\Delta^2 N} &= \bar{g}^2\,\overline{\Delta^2 P} + \bar{P}\,\overline{\Delta^2 g}\\ &= \bar{g}^2\,\overline{\Delta^2 P} + \bar{P}\,(\overline{g^2} - \bar{g}^2)\\ &= \bar{g}^2\,(\overline{\Delta^2 P} - \bar{P}) + \overline{g^2}\,\bar{P}.\end{aligned} \tag{4}$$

For primary photoelectrons obeying Poissonian statistics

$$\overline{\Delta^2 P} = \bar{P}, \tag{5}$$

and thus Eq. (4) simplifies to

$$\overline{\Delta^2 N} = \overline{g^2}\,\bar{P}. \tag{6}$$

The total mean square noise in the output arising from amplifier and stored charge shot noise is therefore

$$n^2 + \overline{\Delta^2 N} = n^2 + \overline{g^2}\,\bar{P}. \tag{7}$$

Hence from Eqs. (3) and (7),

$$\text{mean square signal-to-noise ratio in output} = \frac{(\bar{g}\,\bar{P})^2}{n^2 + \overline{g^2}\,\bar{P}}. \tag{8}$$

Equation (5) gives

$$\text{mean square signal-to-noise ratio in input} = \bar{P}, \tag{9}$$

and Eqs. (8) and (9) enable us to write for the equivalent quantum efficiency defined in Eq. (1)

$$E = \frac{\bar{g}^2 P}{n^2 + \overline{g^2} P}$$

$$= \frac{1}{\dfrac{n^2}{\bar{g}^2 P} + \dfrac{\overline{g^2}}{\bar{g}^2}}. \tag{10}$$

Defining a factor K by

$$K = \frac{\overline{g^2}}{\bar{g}^2}, \tag{11}$$

and using Eq. (3), Eq. (10) may be expressed as

$$E = \frac{1}{K + \dfrac{n^2}{g\bar{N}}}. \tag{12}$$

The factor K depends on the statistics of multiplication. It may be shown to be 2 for exponential statistics and to be nearly unity for Poissonian statistics when the gain is appreciable, i.e. to approach the condition existing when the gain is noiseless (for noiseless gain $\overline{g^2} = \bar{g}^2$ so that from Eq. (11), $K = 1$).

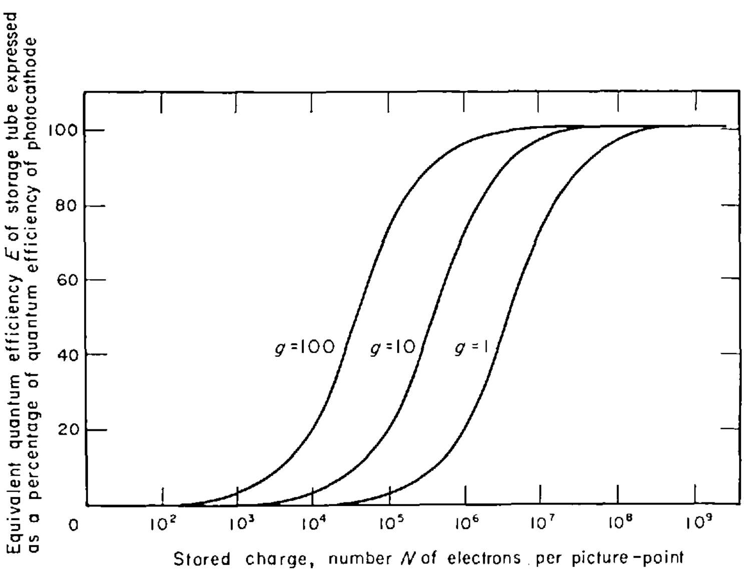

FIG. 2. Equivalent quantum efficiency E of a storage tube as a function of the stored charge N electrons per picture point for various gains g, for a system with a background noise of 2000 electrons per picture point due to amplifier noise.

Equation (12), representing the efficiency with which primary photoelectrons are recorded in the storage tube, gives the factor by which the inherent quantum efficiency of the photocathode is reduced in signal processing. This is illustrated by the curves in Fig. 2, where equivalent quantum efficiency E is plotted as a function of stored charge N for multiplications g of 1, 10 and 100 in the layer. These curves were calculated from Eq. (12) with $K = 1$, and they therefore represent the result to be expected with noiseless multiplication. The curves corresponding to gains g of 10 and 100 deviate only slightly from the result which holds for Poissonian multiplication.

From these curves, it can be seen that a storage tube with a capacity in excess of 10^5 electrons per picture element and a gain of the order of 10 to 100, can make full use of the photocathode efficiency in the detection of low contrast images.

Design Considerations

Experiments have shown that the insulation of the diffuse potassium chloride layer is sufficiently good to enable an image to be stored on the

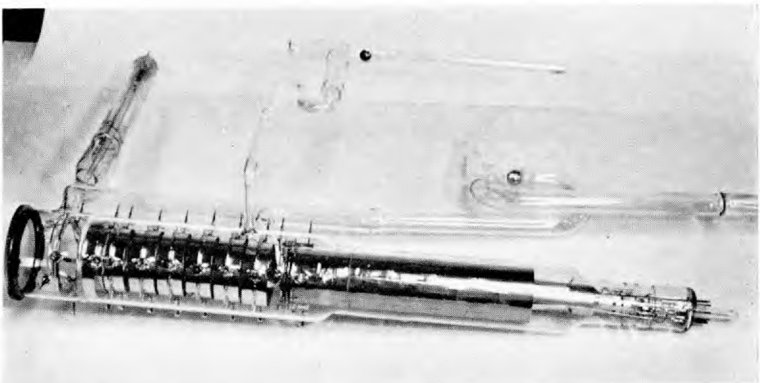

Fig. 3. The television camera-tube prior to processing.

target for several days, without apparent loss in definition. In order to exploit this property in the detection of faint images, the tube should be exposed to the object under observation for long periods. This enables a charge image to be integrated on the target, which may then be read off. It was therefore necessary to design the image section of the tube to minimize background, which is integrated along with the useful signal. In the tubes constructed so far, useful integration times of up to one hour have been achieved at room temperature by taking the following precautions against background.

The cathode is processed in a separate compartment (see Fig. 1) to eliminate alkali-metal vapours from the working section of the tube. This avoids the creation of surfaces with low work-function, which can contribute to background by thermal and secondary emission. The cathode may be reversed after the tube has been sealed off the pump by means of a device described by McGee[8] and Slark.[9]

Electron multiplication along the walls of the tube is prevented by a series of annuli, acting as baffles[10] (see Fig. 1). These are mounted on open tungsten pins, sealed into the glass, and enable a uniform electrostatic field to be applied along the image section. Adverse effects arising from the accumulation of charges on the glass walls of the tube are obviated by screening the walls with metallic rings, mounted on the annuli (see Fig. 1).

Figure 3 is a photograph of the tube before processing and shows the antimony evaporator, a gas inlet side-arm, and the pumping stem. The separate processing compartment and the metallic rings and annuli in the image section can be clearly seen.

Preparation of the Target

The potassium chloride layer is supported by a thin aluminium oxide film. This alumina film is prepared electrolytically and is mounted on

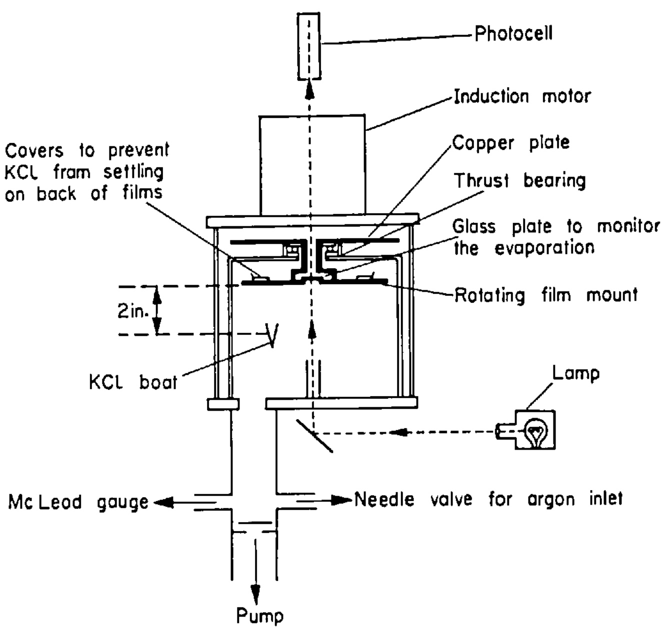

FIG. 4. Evaporation apparatus used in the preparation of spongy potassium chloride targets.

a platinized soda-glass ring. Soda glass has a slightly larger expansion coefficient than alumina, so that heating the mounted film to 250°C pre-stretches the layer, compensating for shrinkage which occurs during subsequent processing. Films which were not pre-stretched in this way were found to become excessively taut on baking after the aluminium and potassium chloride evaporated layers had been deposited, and ruptured very easily.

The evaporations are carried out in the demountable vacuum system shown in Fig. 4. A conducting layer of aluminium is evaporated onto the stretched film, followed by a spongy layer of potassium chloride. Four films are evaporated simultaneously. The aluminized films are held 2 in. above the boat from which the potassium chloride is evaporated and to ensure uniformity, the platform on which they are mounted is rotated during evaporation by means of an induction motor. The evaporation is carried out in an atmosphere of argon at a pressure of 2 torr and is monitored by noting the optical transmission of a monitor plate, mounted on the axis of the rotating system. The evaporation is continued until a 25% drop in transmission is observed and is controlled to take about ten minutes. The target is very sensitive to moisture and is assembled into the tube in a dry box.

Structure of the Target

A cross-section through the target is illustrated in Fig. 5. The thickness of the potassium chloride deposit has been measured by breaking the glass plates used to monitor the evaporation and examining the

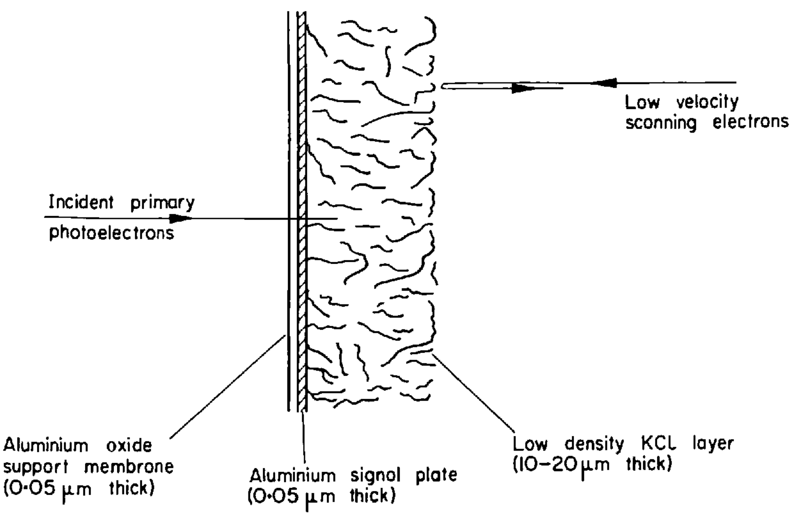

FIG. 5. Section through the target layer.

cross-section under a microscope. Layers prepared under apparently identical conditions have been found to range from 10 to 20 μm in thickness.

The electron micrograph shown in Fig. 6 gives an insight into the

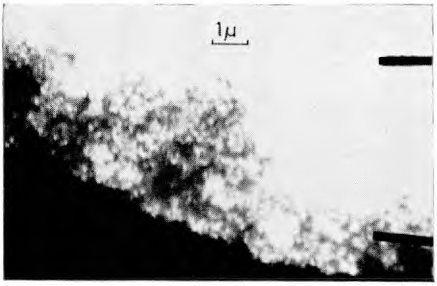

FIG. 6. Electron micrograph showing a low density deposit of potassium chloride evaporated onto a mesh.

structure of low-density potassium chloride layers. As the evaporated potassium chloride molecules are cooled by the argon atmosphere, they coalesce and settle in diffuse strands on the substrate.

EFFECT OF FIELD GRADIENT IN THE LAYER ON TARGET PROPERTIES

Measurements have been made on the targets to determine their properties and to investigate the mechanisms of signal generation. The gain of the target is found to depend very strongly on the potential gradient across it. Since the front surface is effectively stabilized at gun-cathode potential by the action of the low-velocity scanning beam, the gradient across the layer may be varied by altering the signal-plate potential. The sensitivity increases with increasing signal-plate potential, as for a conventional vidicon. This is illustrated in Fig. 7, which shows the variation of video signal with signal-plate potential for four different light intensities.

The increase of video signal with field gradient across the layer would lead one to predict a departure from unity gamma, since the gain of the layer will vary during exposure, as the potential gradient changes with the build-up of positive charge.

The transfer characteristics shown in Fig. 8 exhibit the expected non-linearity. The curves indicate a gamma of less than unity with the signal-plate positive, when the build-up of stored charge in the potassium chloride reduces the field gradient across the layer. Conversely, the gamma is greater than one, when the tube is run with the signal-plate negative with respect to the gun cathode. As the graphs shown in Fig. 8 do not obey a simple power law, unique values of gamma can-

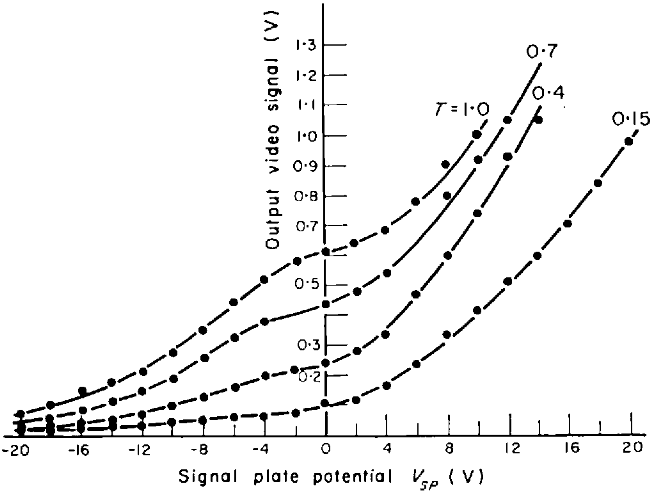

FIG. 7. The variation of output video signal with signal-plate potential for 4 different light intensities. The parameter T represents the transmission of a filter placed in front of the light source of fixed intensity.

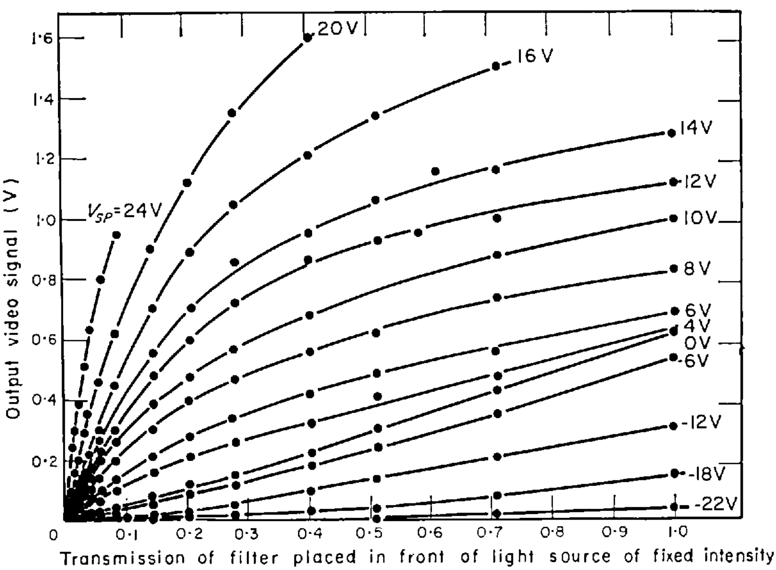

FIG. 8. Transfer characteristics of the tubes for various signal plate potentials.

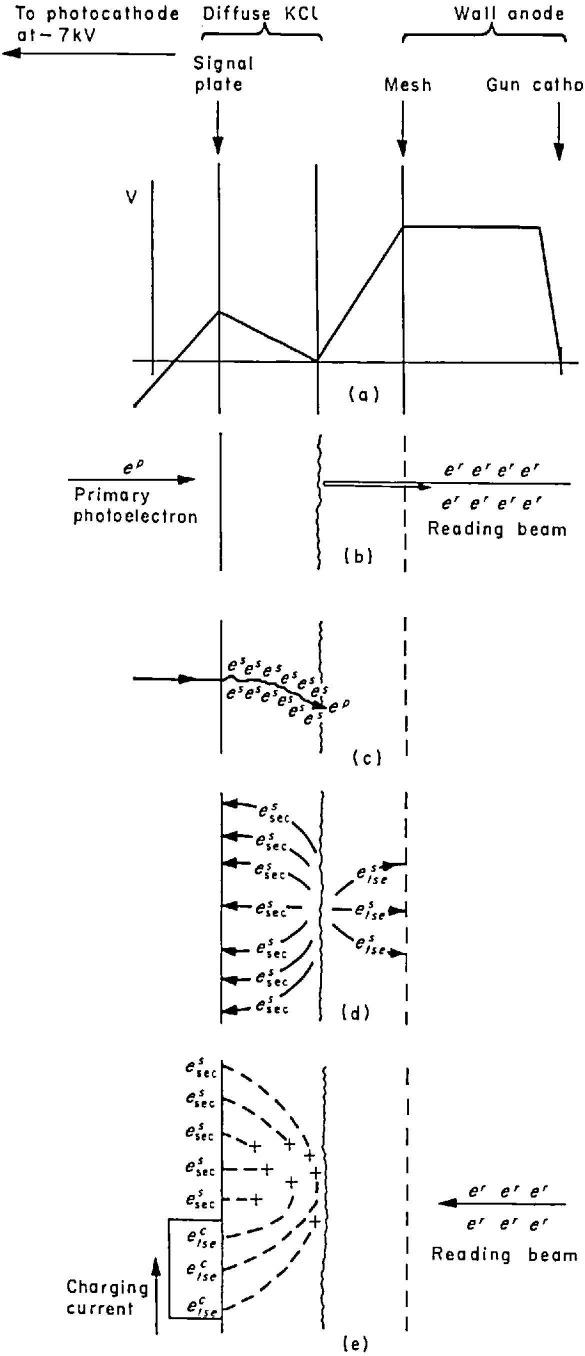

Potential distribution existing in tube prior to exposure. The target surface is at gun cathode potential.

Condition existing before primary photo-electrons e^p reach target. The reading electrons e^r scanning the target encounter a potential barrier and return to the gun.

Primary photo-electron e^p entering layer excites many secondary electrons e^s.

Motion of excited secondaries under influence of field in region of the layer. Most of the electrons move under the influence of internal field in the layer to the signal plate (e^s_{sec}). Some of the electrons leave the layer to be collected by the mesh (e^s_{lse}).

Charge distribution left in layer after exposure. The secondaries reaching the signal plate are held there by the +ve charges they leave in the KCl. +ve charges left by the electrons going to the mesh attract electrons from earth constituting a charging current in the signal lead (e^c_{lse}).

FIG. 9. Mechanism of signal generation in spongy potassium chloride layer.

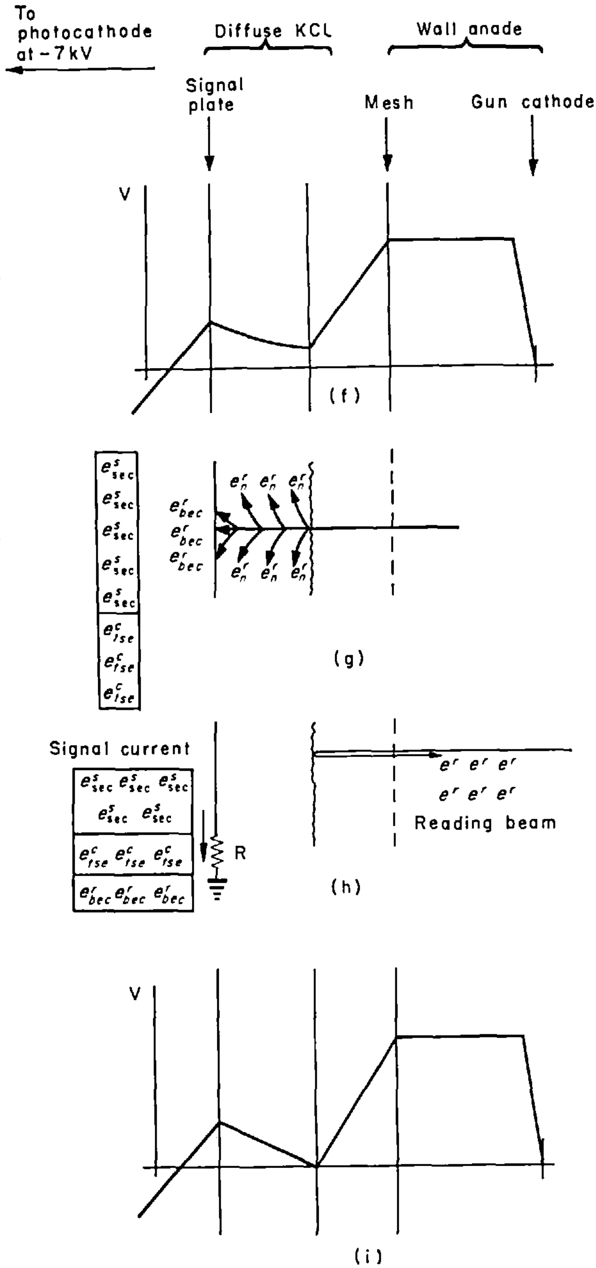

Potential distribution in tube after ex-
sure. The positively charged layer no
nger presents a potential barrier pre-
nting the scanning electrons from entering
e layer.

Processes occurring as exposed target is
anned. The scanning electrons enter the
'er. Some of them neutralize the +ve
arge within the layer (e^r_n). Others of
em reach the signal-plate (e^r_{bec}).

Condition existing immediately after
anning. As the +ve charge in the layer is
utralized, the potential of the surface is
stored to gun cathode potential, prevent-
g further electrons from landing. The elec-
on charges held on the signal-plate are
leased (e^s_{sec}) and (e^c_{tse}). These together
ith the electrons landing direct on the
;nal-plate from the scanning beam (e^r_{bec})
nerate the video signal as they flow through
to earth.

The potential distribution after scanning
restored to that existing before exposure.

FIG. 9. Continued.

not be associated with the various signal-plate potentials corresponding to each of these curves.

Mechanism of Signal Generation

Signal generation may be considered to be effected through the contributions of three processes. (a) Transmission secondary emission (TSE) describes the effect by which excited secondaries leave the layer to be collected by the adjacent mesh, held at around +300 V. (b) Many of the secondary electrons excited in the layer will have insufficient energy to escape from the exit surface of the potassium chloride and these will migrate back towards the signal-plate under the influence of the internal field in the layer. Following the practice of the Westinghouse workers this process will be termed secondary electron conduction (SEC). As very little is known about the mean free path of these electrons, moving within the spongy potassium chloride, it is difficult to assess what fraction of them is used in neutralizing positive charges, created within the layer, closer to the signal-plate. (c) A third significant contribution to signal generation may arise from scanning electrons landing directly on the signal-plate. This can occur, because, with the build-up of positive charge in the potassium chloride during exposure, the signal-plate will no longer be effectively screened from the scanning beam. Slow electrons, entering into the layer from the scanning beam should behave in the same way as SEC electrons. A percentage of these electrons originating from the scanning beam might thus be expected to migrate to the signal-plate without being used up in neutralizing charges stored within the insulator. The authors have termed this process beam electron conduction (BEC).

A series of diagrams to illustrate these processes, believed to occur during signal generation, is given in Fig. 9.

It is difficult to distinguish experimentally between the SEC and BEC modes of signal generation and, therefore, to assess quantitatively the relative contribution of each of these electron conduction mechanisms to the signal generated. There is much evidence however, to support the postulation of BEC.

First, it has been found that 60 V is the maximum signal-plate potential that can be applied, since for potentials in excess of this, beam electrons will begin to be accepted by the signal-plate, even in the absence of positive charges created in the layer by primary photoelectrons. As the signal-plate potential is raised further, it becomes impossible to stabilize the target at gun-cathode potential and the tube generates a continuous white signal showing that under these conditions of tube operation, large numbers of scanning electrons can migrate across the potassium chloride layer to be accepted by the signal-plate.

Secondly, BEC helps to account for an effective target capacitance several times larger than the electrostatic capacitance calculated from geometric considerations.

Thirdly, it also helps to account for an asymmetry observed in the contributions to signal generation due to electron conduction effects in the layer as the signal-plate potential, and hence the field gradient in the layer, is reversed. True SEC should just change sign with this reversal of field polarity across the layer, but the BEC effect can only occur for positive signal-plate potentials.

Measurement of Effects Contributing to Signal Generation

Although true SEC and BEC prove difficult to isolate and measure independently, TSE can be readily measured since this gives rise to a

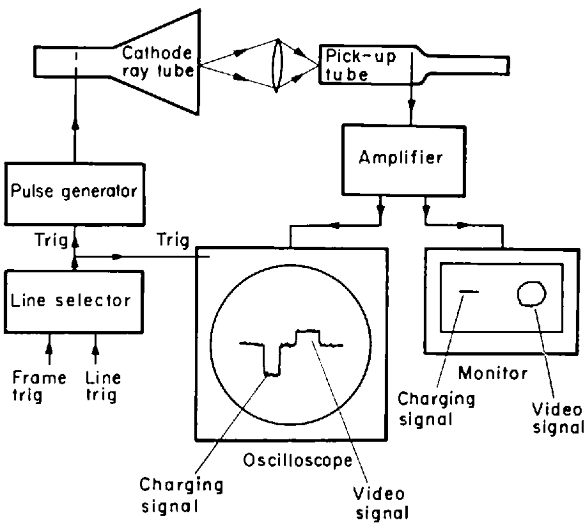

Fig. 10. Pulsed light experiment to measure the contribution to signal generation arising from TSE. The line selector is used to provide trigger pulses for the oscilloscope and pulse generator, once per frame, at a pre-selected line. On triggering, the pulse generator introduces a delay of 20 μsec before switching on the cathode-ray tube for a 20 μsec period. The oscilloscope monitors the line from the video signal which embraces the charging signal produced by the light pulse.

charging current during exposure. The arrangement used to measure the TSE gain of the target, while its exit surface was being scanned to maintain it at gun-cathode potential, is shown in Fig. 10.

A cathode-ray tube with a short persistence phosphor (P·16), is triggered once each frame to provide a light pulse of duration 10–20 μsec. A black signal, corresponding to the instant of pulsing is observed on the monitor. When the video signal, corresponding to the line including the charging pulse is selected and monitored on the oscilloscope, this negative going charging signal appears together with the conventional positive going television signal which produces the picture of the light patch. For ease of measurement, the position of the light patch and the time of pulsing are adjusted so that the two signals do not interfere and appear spatially separated on the oscilloscope, as shown in Fig. 10.

The height of the charging current pulse is measured and then the accelerating potential on the image section is reduced. This is accompanied by the disappearance of the conventional television signal and

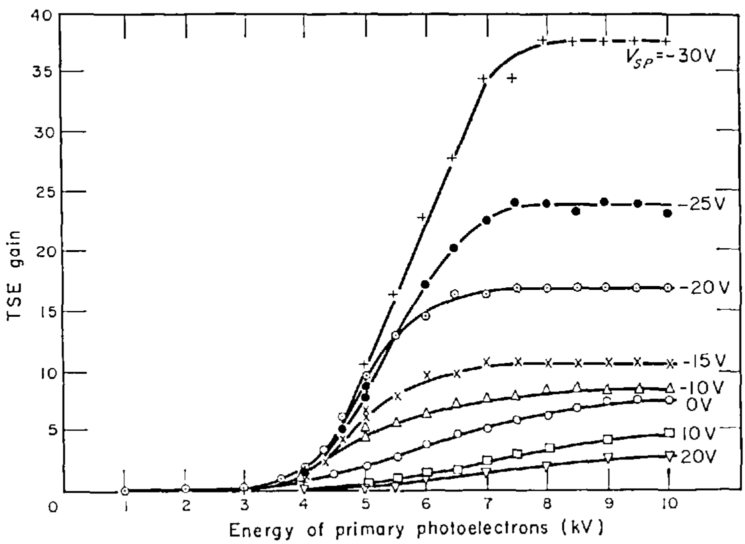

FIG. 11. The variation of TSE gain with primary photoelectron energy for various signal plate potentials.

the reversal of the sign of the charging current pulse which reaches a flat maximum over a range of low primary electron energies. The magnitude of this flat maximum is taken as a measure of the primary photocurrent. Thus, from these charging current pulse-height measurements, the TSE contribution to gain may be obtained.

The variation of TSE gain with primary photoelectron energy for various signal-plate potentials, is illustrated in Fig. 11. These curves start to rise steeply for primary electron energies between 3 and 4 keV and the transmission secondary emission appears to saturate for primary energies in excess of 7 keV. One of the curves in Fig. 12 shows the variation of TSE gain with signal-plate potential for 7 keV primary photoelectrons. As would be expected, this curve exhibits a negative slope, since transmission secondary emission is favoured by a field gradient which accelerates electrons towards the exit surface.

Since the SEC and BEC processes are not readily distinguished experimentally, the term SEC will be retained to embrace both effects.

The contribution to signal generation arising from SEC (including BEC) has been measured by observing on a galvanometer the mean current flowing into the signal-plate while the tube is generating a picture of a steady light patch. The time constant of the galvanometer is much greater than a frame period and therefore the contribution arising from the TSE effect is not observed, as this is cancelled by the

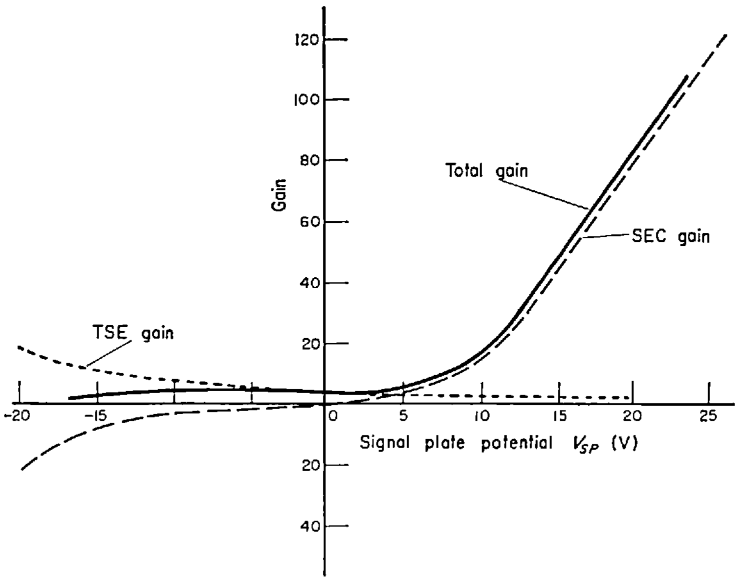

FIG. 12. The variation of the total charge-gain of the layer with signal-plate potential, compiled from curves showing the contributions arising from the TSE and SEC mechanisms.

charging current. The galvanometer thus gives the SEC contribution to the signal, subject to a small correction for the primary photocurrent.

The variation of total SEC gain with signal-plate potential for 7 keV electrons is represented by the curve drawn with dashes in Fig. 12. The asymmetry has been interpreted as arising from the BEC contribution which occurs only for positive signal-plate potentials.

The continuous curve in Fig. 12 shows the variation of the total charge gain of the tube with signal-plate potential. It has been plotted as the sum of two curves representing the separate contributions arising from the TSE and the SEC effects.

Limitations of Storage Tubes with Potassium Chloride Target Layers

Two defects in this storage tube for which possible remedies are being currently investigated are the tendency of the target to become damaged if overloaded by exposure to too high a light intensity and the relatively poor resolution capability of the tube. A photograph of a resolution pattern generated by the tube is shown in Fig. 13. The

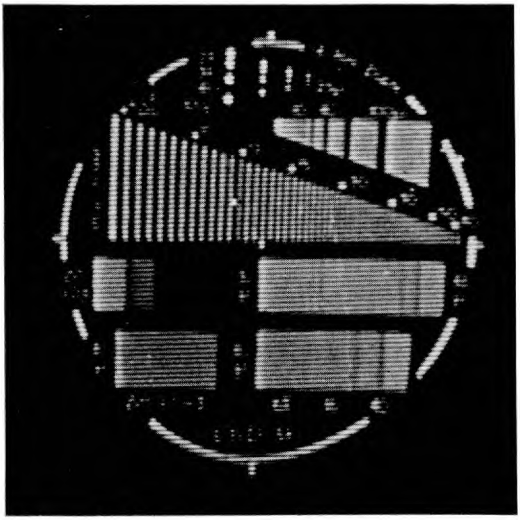

Fig. 13. Photograph of a test pattern generated by a tube run with $V_{SP} = 10$ V. Diameter of test pattern image on target = 8 mm.

limiting resolution of the tubes constructed so far has been 15 lp/mm which, with the present target, corresponds to only 600 vertical television lines.

It should be possible to avoid the tendency of the target to charge beyond the first cross-over potential at high illumination levels by the well known method of introducing a stabilizing mesh held at a low potential.[11] To investigate possible causes of low resolution, an image section was constructed, terminated with a phosphor in place of the target, and the resolution checked. The resolution achieved was better than 30 lp/mm, and no deterioration was observed when scanning fields were applied, indicating that cross-talk between the scanning fields and the image section did not account for the observed loss in resolution.

It is unlikely that scattering in the target accounts for serious loss in resolution, since this is likely to be comparable with the target thickness of 10–20 μm which is less than 33 μm, the size of a picture element in a 405-line raster scanned on these experimental tubes.

The large potential excursions of the target, i.e. a peak white signal corresponds to an 8-V potential rise, may explain the inferior resolution of the target, but no definite conclusions have so far been reached and work is in hand to investigate the source of definition loss.

Conclusion

If future work succeeds in overcoming the two defects of the tube mentioned above, the excellent performance of the camera in other respects, that is, its sensitivity, its exceptional integration and storage properties, its low lag, and its easily variable gain, would make this tube a very versatile device.

Acknowledgments

The authors would like to express their gratitude for the interest and advice of Prof. J. D. McGee in whose department this work was carried out. The authors would also like to record their thanks to Mr. J. Westlake for the skill and care with which he has assembled and processed the tubes and to Mr. W. Simpson for his work on the demountable vacuum system in which the layers were prepared.

One of the authors (R.S.F.) is indebted to the Science Research Council for a maintenance grant, and another (S.B.M.) to the Committee of Vice-Chancellors and Principals of the United Kingdom.

References

1. Goetze, G. W., *In* "Advances in Electronics and Electron Physics", ed. by J. D. McGee, W. L. Wilcock and L. Mandel, Vol. 16, p. 145. Academic Press, New York (1960).
2. Rosenbloom, M. E., Ph.D. Thesis, University of London (1965).
3. Filby, R. S. Mende, S. B., Rosenbloom, M. E. and Twiddy, N. D., *Nature* **201**, 801 (1964).
4. Filby, R. S., Mende, S. B. and Twiddy, N. D., *Internat. J. Electronics* **19**, 387 (1965).
5. Goetze, G. W. and Boerio, A. H., I.E.E.E. Electron Devices Meeting (unpublished) October 1963.
6. Goetze, G. W. and Boerio, A. H., *Proc. Inst. Elect. Electronic Engrs* **52**, 1009 (1964).
7. Mandel, L., *Brit. J. Appl. Phys.* **10**, 233 (1959).
8. McGee, J. D., "The Present and Future of the Telescope of Moderate Size", p. 31. University of Pennsylvania Press (1956).
9. Slark, N. A., Ph.D. Thesis, University of London, p. 64 (1958).
10. Zacharov, O., Ph.D. Thesis, University of London, p. 123 (1960).
11. McGee, J. D., *Arch. elektr. Übertragung* **9**, 355 (1955).

Discussion

B. W. MANLEY: What is the measured target capacitance?

R. S. FILBY: A peak white signal corresponds to about 3×10^5 electrons per picture point and this is accompanied by a rise in target potential of 8 V. This means that the effective target capacitance is 1200 pF, which is considerably larger than the capacitance calculated from geometric considerations. The dimensions of the layer are 20 mm $\times$ 15 mm $\times$ 10 μm in thickness. If it were assumed that all the stored charge resides on the scanned surface of the layer, these dimensions give a target capacitance of about 200 pF.

T. REICHEL: Did you try to evaporate the potassium chloride layer in a discharge in an argon atmosphere in order to obtain low density layers of uniform thickness? I have obtained good results with this method.

R. S. FILBY: No, to achieve uniformity, the platform on which the substrates were mounted was rotated during evaporation, but thank you for this suggestion. This appears to be a technique which we might adopt with advantage.